GSK-3α/β IN ENDOPLASMIC RETICULUM STRESS AND ATHEROSCLEROSIS

THE ROLE OF GLYCOGEN SYNTHASE KINASE-3α/β IN ENDOPLASMIC RETICULUM STRESS AND ATHEROSCLEROSIS

BY:

CAMERON STUART MCALPINE, B.SC. (HONOURS)

A Thesis Submitted to the School of Graduate Studies in Partial Fulfilment of the Requirements for the Degree Doctor of Philosophy

McMaster University

DOCTOR OF PHILOSOPHY (2015)	McMaster University
(Medical Sciences)	Hamilton, Ontario, Canada
TITLE:	The role of glycogen synthase kinase-3α/β in endoplasmic reticulum stress and atherosclerosis
AUTHOR:	Cameron Stuart McAlpine, B.Sc. (Honours) (Acadia University)
SUPERVISOR:	Geoff H. Werstuck, B.Sc., Ph.D.
NUMBER OF PAGES:	xvii, 223

ABSTRACT

Atherosclerosis is a multifactorial inflammatory disease of the arterial wall and its clinical manifestations, including myocardial infarction and stroke, are the leading causes of death in western societies. Recent data has suggested that disruption of protein homeostasis in a cell's endoplasmic reticulum (ER), a condition known as ER stress, is associated with the progression of atherosclerosis. Furthermore, signaling by the serine/threonine kinase glycogen synthase kinase (GSK)-3α/β mediates pro-atherogenic processes. This thesis examines the role of ER stress and GSK3α/β signaling in atherosclerosis.

Initially, three apolipoprotein-E deficient ($ApoE^{-/-}$) mouse models of accelerated atherosclerosis were established. Relative to $ApoE^{-/-}$ mice fed a chow diet, pro-atherogenic conditions promoted hepatic steatosis, atherosclerosis, ER stress and GSK3β activity. A subset of mice from each group were given the GSK3α/β inhibitor valproate. Valproate supplementation suppressed hepatic steatosis, atherosclerosis and GSK3β activity in each mouse model without altering ER stress levels. This study revealed a role for ER stress and GSK3α/β in multiple murine models of atherosclerosis.

Next, we investigated ER stress and GSK3α/β signaling in macrophage foam cell formation. In macrophages, ER stress induced GSK3α/β activity in a protein kinase R-like endoplasmic reticulum kinase (PERK) dependent manor. GSK3α/β inhibition attenuated ER stress induced lipid accumulation and the expression of distal components of the PERK pathway. Overexpression of constitutively active GSK3β induced foam cell formation. In mice, valproate supplementation attenuated PERK signaling in peritoneal macrophages and macrophages within atherosclerotic lesions. Together, these results point to GSK3α/β being a downstream component of the PERK

pathway and that PERK-GSK3α/β signaling mediates ER stress induced foam cell formation.

Lastly, we investigated the tissue and homolog specific functions of GSK3α and GSK3β in atherosclerosis. In high fat diet (HFD) fed low-density lipoprotein receptor deficient ($LDLR^{-/-}$) mice, deletion of GSK3α or GSK3β in hepatocytes did not alter liver lipid content or atherosclerosis. Myeloid cell deletion of GSK3α, but not GSK3β, attenuated HFD induced atherosclerosis. Mechanistically, deletion of GSK3α in macrophages promotes the anti-atherogenic M2 macrophage phenotype by modulating signal transducer and activator of transcription (STAT)-3 and STAT6 phosphorylation and activation.

Together, the data presented in this thesis suggest; 1) GSK3α/β inhibition attenuates atherosclerosis in multiple mouse models, 2) PERK-GSK3α/β signaling regulates macrophage foam cell formation and 3) myeloid cell GSK3α mediates atherosclerosis and macrophage phenotype.

AKNOWLEDGEMENTS

Completing my PhD would not have been possible without the love, support and encouragement from countless people. First and foremost I'd like to acknowledge and thank my supervisor, Geoff. His guidance, mentorship and friendship made my graduate school experience enjoyable and rewarding. Geoff motivated and inspired me to pursue research and to ask the right questions. It is thanks to his leadership that all this work was possible. I'd also like to thank all the past and present members of the Werstuck lab, of which there are too many to name here. You made the long hours in the lab fun and entertaining.

I'd also like to thank my family for all their love and support. To Sarah, my bride-to-be, for all her love and solace after hard days in the lab. And finally, to Mom and Dad for their continued encouragement and support through all these years. Thank you!

TABLE OF CONTENTS

LIST OF FIGURES

Chapter 6: General Discussion

LIST OF TABLES

LIST OF ABREVIATIONS

ABCA1	ATP-binding cassette transporter member 1
ABCG1	ATP-binding cassette sub-family G member 1
AcLDL	Acetylated low-density lipoprotein
Ad	Adenovirus
AGE	Advanced glycation endproduct
Alb	Albumin
APC	Axin, adenomatous polyposis coli
ApoE	Apolipoprotein-E
ARE	Antioxidant response element
Arg1	Arginasae-1
ANOVA	Analysis of variance
ATF	Activating transcription factor
BMDM	Bone marrow derived macrophage
BSA	Bovine serum albumin
bZIP	Basic leucine zipper
C	Control
CCL	Chemokine ligand
CCR	Chemokine receptor
CD	Cluster of differentiation
cDC	Classical dendritic cell
CHOP	C/EBP- homologous protein
CK1	Casein kinase 1
CLPC	Common lymphoid progenitor cell
CMPC	Common myeloid progenitor cell
CREB	Cyclic AMP response element-binding protein
CVD	Cardiovascular disease
DAPI	4',6-Diamidino-2-phenylindole
DC	Dendritic cell
DMEM	Dubecco's modified eagle medium

DMSO	Dimethyl sulfoxide
DNA	Deoxyribonucleic acid
DTT	Dithiothreitol
EDTA	Ethylenediaminetetraacetic acid
eIF2	Eukaryotic initiation factor-2
ELISA	Enzyme-linked immunosorbent assay
ER	Endoplasmic reticulum
ERAD	Endoplasmic reticulum associated degradation
ERK	Extracellular signal-regulated kinase
FABP4	Fatty acid binding protein-4
FBS	Fetal bovine serum
FAS	Fatty acid synthase
Fl	Floxed
GFAT	Glutamine:fructose-6-phosphate amino-transferase
GLN	Glucosamine
GRP	Glucose related protein
GSK3	Glycogen synthase kinase-3
HBP	Hexosamine biosynthesis pathway
HDAC	Histone deacetylases
HDL	High-density lipoprotein
HF	High fat
HFD	High fat diet
HG	Hyperglycemia
HH	Hyperhomocysteinemia
HMGCoA	3-Hydroxy-3-methylglutaryl-coenzyme A
HRP	Horseradish peroxidase
HSC	Hematopoietic stem cell
IFNγR	Interferon-γ receptor
IGF	insulin-like growth factor
IL	Interleukin
INF	Interferon
IRE1	Inositol-requiring enzyme-1

IRES	Internal ribosome entry sites
IRS	Insulin receptor substrates
JNK	c-Jun N-terminal kinase
KDEL	Lysine-aspartic acid-glutamic acid-leucine
Lαfl/fl	$LDLR^{-/-}$GSK3α floxed
Lβfl/fl	$LDLR^{-/-}$GSK3β floxed
LDLR	low-density lipoprotein receptor
LEF	Lymphoid enhancer factor
LLαKO	$LDLR^{-/-}$ liver-specific GSK3α knockout
LLβKO	$LDLR^{-/-}$ liver-specific GSK3β knockout
LMαKO	$LDLR^{-/-}$ myeloid-specific GSK3α knockout
LMβKO	$LDLR^{-/-}$ myeloid-specific GSK3β knockout
LPL	Lipoprotein lipase
LPS	Lipopolysaccharide
LyzM	Lysozyme M
MCP	Monocyte chemoattractant protein
MCSF	Macrophage colony-stimulating factor
MEF	Mouse embryonic fibroblasts
Mer	Mouse estrogen receptor
Mgl2	Macrophage galactose-type lectin -2
MHC	Major histocompatibility complex
MMP	Matrix metalloprotease
MOI	Multiplicity of infection
NaCl	Sodium chloride
NaF	Sodium Floride
NF-κB	Nuclear Factor κB
NK	Natural killer
NO	Nitric oxide
Nrf	Nuclear factor-like
PA	Palmitic acid
PAGE	Polyacrylamide gel electrophoresis
4PBA	4-Phenylbutyric acid

PBS	Phosphate buffered saline
PCR	Polymerase chain reaction
pDC	Plasmacytoid dendritic cell
PDI	Protein disulphide isomerase
PERK	Protein kinase R-like endoplasmic reticulum kinase
Pgc1	Peroxisome proliferator-activated receptor gama coactivator-1
pGS-2	Phospho-glycogen synthase peptide-2
PI3K	Phosphatidyl-inositide3-dependent-kinase
PKB	Protein kinase B
PKC	Protein kinase C
PMA	Phorbol-12-myristate-13-acetate
PMSF	Phenylmethanesulfonylfluoride
PP1	Protein phosphatase-1
PYK2	Protein tyrosine kinase-2
RAGE	Receptor for advanced glycation endproduct
RNA	Ribonucleic Acid
ROS	Reactive oxygen species
S1P	Site-1 protease
S2P	Site-2 protease
SDS	Sodium dodecyl sulfate
siRNA	Small interfering RNA
SR-A	Scavenger receptor class A
SR-B1	Scavenger receptor class B1
SREBP2	Sterol element binding protein-2
STAT	Signal transducer and activator of transcription
STZ	Streptozotocin
TCF	T-cell factor
TGF	Transforming growth factor
Thaps	Thapsigargin
TLR	Toll-like receptor
TNF	Tumor necrosis factor
TRAF2	TNF receptor-associated factor-2

UPR	Unfolded protein response
VCAM	Vascular cell adhesion molecule
VLDL	Very low-density lipoprotein
VPA	Valproate
VSMC	Vascular smooth muscle cell

CHAPTER 1: General Introduction

1.1 FOREWORD

Portions of this general introduction are a direct representation of two review articles published in *Cardiovascular and Hematological Disorders: Drug Targets*. The manuscripts were written by Cameron McAlpine in collaboration with Dr. Geoff Werstuck. The complete references are as follows:

McAlpine CS, Bowes AJ, Werstuck GH. Diabetes, hyperglycemia and accelerated atherosclerosis: Evidence supporting a role for endoplasmic reticulum (ER) stress signaling. *Cardiovascular and Hematological Disorders: Drug Targets.* 2010;10:151-157. ©2010 Bentham Science

McAlpine CS, Werstuck GH. The development and progression of atherosclerosis: Evidence supporting a role for endoplasmic reticulum stress signaling. *Cardiovascular and Hematological Disorders: Drug Targets.* 2013;13:158-164. ©2013 Bentham Science

1.2 ATHEROSCLEROSIS

Burden

Diseases resulting in damage to the heart, coronary blood vessels or peripheral blood vessels are collectively referred to as cardiovascular disease (CVD). CVD is the leading cause of death globally, accounting for 17.3 million or 30% of deaths worldwide in 2008.[1] CVD rates, however, are not proportional across socioeconomic groups as 80% of CVD deaths occur in low and middle income nations.[1] Due to the growing prevalence of diabetes and obesity, CVD is expected to result in 23.3 million deaths per year by 2030.[1] Annually, CVD costs the Canadian economy over $22 billion including $7.6 billion in direct costs to the Canadian health care system.[2]

Risk factors

CVD is a complex and multifactorial disease that is associated with a number of risk factors. CVD risk factors include dyslipidemia (low-density lipoprotein (LDL) ≥4.1 mmol/L and high-density lipoprotein (HDL) ≤1.0 mmol/L), hypercholesterolemia (total cholesterol ≥6.2 mmol/L), hypertension (blood pressure ≥140/90 mmHg), diabetes (fasting blood glucose ≥7.0 mmol/L) and obesity (body mass index ≥30).[3] Collectively, these risk factors comprise the "metabolic syndrome", a condition of energy and metabolic imbalance. Clinically, an individual is diagnosed with metabolic syndrome if they present with three or more of these risk factors and this translates to a 40 fold increased risk of developing CVD.[3] Other CVD risk factors include smoking, genetics and environmental toxins.[3-5] Interestingly, this diverse group of risk factors gives rise to a similar disease pathology, possibly due to a state of chronic inflammation being the underlying stimulus for CVD development.[6-8] The molecular and cellular mechanisms by which this diverse array of risk factors promotes CVD is poorly understood.

Pathophysiology

The underlying pathology of the CVD is atherosclerosis, an inflammatory disease characterized by leukocyte and lipid accumulation in arterial walls (Figure 1.1).[8, 9] Atherosclerotic lesions typically appear at sites of endothelial insult or injury in regions of the artery that contain bifurcations, branches or inner curvatures which disrupt linear blood flow. A number of risk factors promote endothelial injury including hypercholesterolemia, dyslipidemia, obesity, hyperglycemia, insulin resistance and hypertension. Endothelial cells respond to injury by; i) increasing the expression of adhesion proteins at the cell surface, such as vascular cell adhesion molecule (VCAM)-1

and P-selectin, which mediate the attachment of leukocytes and, ii) releasing factors, including monocyte chemoattractant protein (MCP)-1 and matrix metalloprotease (MMP)-9, that accentuate monocyte diapedesis into the sub-endothelial layer of the vessel wall.[10-13] Once in the vessel wall, intimal monocytes are induced to differentiate into macrophages by macrophage colony-stimulating factor (MCSF).[14] LDL and modified LDL particles that have entered the intima are taken up by macrophage endocytosis, a process mediated by scavenger receptors such as scavenger receptor class A (SR-A) and CD36. The uptake of lipoprotein particles leads to the development of lipid-engorged macrophages, called foam cells, which are found at all stages of lesion development. Initially, the accumulation of macrophage foam cells in the intima of the artery wall form what is known as a “fatty streak”.

Fatty streaks are generally thought to be clinically benign and, in most instances, the process of atherogenesis will be arrested at this stage. For reasons that are not completely understood however, the inflammatory response is dramatically amplified and/or improperly resolved which promotes the evolution of fatty streaks into advanced atherosclerotic lesions.[15] Lesion advancement is characterized by an expansion in the inflammatory cell population through the accumulation and infiltration of monocytes, CD4+ T cells, natural killer (NK) cells, neutrophils and mast cells.[16-19] In advanced lesions monocyte infiltration is reduced and the myeloid cell population expands through macrophage proliferation.[20] This increased inflammatory state is initiated by cytokine, growth factor and chemokine secretion by leukocytes including interleukin (IL)-1β, tumor necrosis factor (TNF)-α, interferon (INF)-γ and chemokine ligand (CCL)-2.[19, 21] Cytokines also induce the migration of vascular smooth muscle cells (VSMCs) from the tunica media into the intima.[19] VSMC synthesize and secrete extracellular matrix proteins,

including collagen, which form a protective, stabilizing, fibrous cap over the lesion. As the lesion expands it can become vascularized, a process that may facilitate cellular infiltration and enhance lesion growth.[22]

Lipid engorged foam cells ultimately undergo apoptosis leading to the formation of a growing acellular region of the lesion, known as the necrotic core. Necrosis and cellular apoptosis is a key feature of unstable or vulnerable lesions which are prone to rupture. Other factors contributing to lesion destabilization are collagenases, including macrophage/foam cell secreted MMPs-1, -8, -9 and -13, which disrupt the integrity of the fibrous cap.[23] Concurrent to the action of MMPs, pro-inflammatory cytokines, released by foam cells and T cells, reduce the production of collagen by VSMCs.[24] Together, these effects can lead to the thinning and overall destabilization of the cap which, as a result, becomes predisposed to rupture. When lesion rupture occurs, circulating blood comes into contact with lipids, cellular debris and tissue factor within the necrotic core, initiating platelet adherence and thrombosis.[25] The rapidly forming thrombus can occlude a coronary artery and block blood flow near the site of the rupture, causing myocardial infarction, or detach and travel to the vessels of the brain and cause a stroke.

Figure 1.1. Progression of an atherosclerotic lesion. Early fatty streaks are characterized by macrophage and modified lipid particles in the subendothelial space. Lesions progress due to an increased inflammatory response and the migration of collagen secreting vascular smooth muscle cells (VSMCs) above the lesion, forming the fibrous cap. Thinning of the fibrous cap leads to lesion instability and may result in rupture and thrombus formation occluding the vessel.

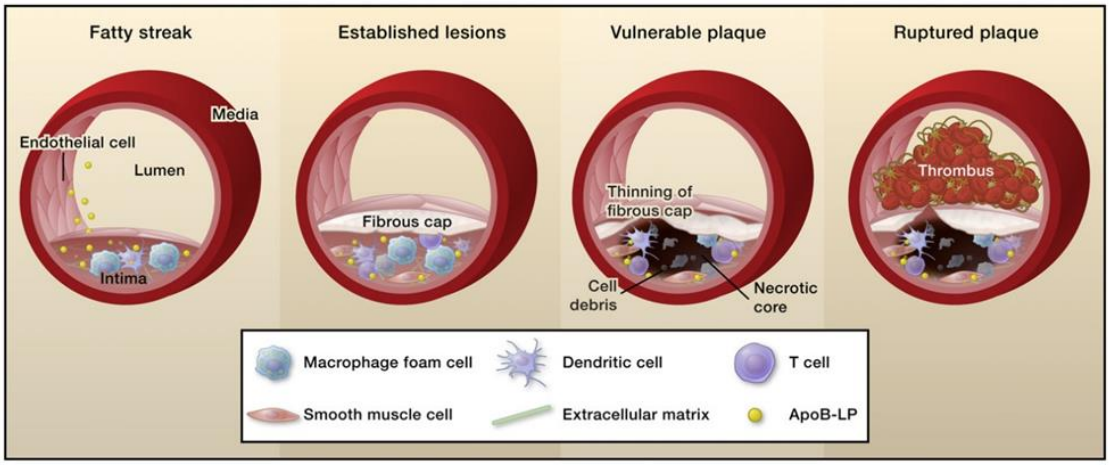

Reprinted with permission from:

Moore KJ, Tabas I. Macrophages in the pathogenesis of atherosclerosis. *Cell* 2011;145:341-355.©2011 Elsevier Inc.

License number: 3593191213522

1.3 ENDOPLASMIC RETICULUM STRESS

The unfolded protein response

In eukaryotic cells the endoplasmic reticulum (ER) is the site of protein folding and modification. Formation of disulphide bonds, secondary and tertiary structure, dimerization and glycosylation are all necessary modifications for proper protein function. If a protein is not properly folded or modified, ER associated degradation (ERAD) is triggered which results in ubiquitination and degradation of the protein.[26] Under normal conditions, the ER is able to maintain homeostasis between folded and misfolded proteins. However, if the processing capacity of the ER is overwhelmed or impaired and misfolded proteins accumulate, the unfolded protein response (UPR) is initiated (Figure 1.2). The UPR comprises three signaling cascades regulated by the ER trans-membrane proteins: inositol-requiring enzyme (IRE)-1, activating transcription factor (ATF)-6 and protein kinase R-like endoplasmic reticulum kinase (PERK).

Inositol-requiring enzyme (IRE)-1

IRE1 signaling is conserved across all eukaryotic cells and was first identified in yeast.[27] Under homeostatic conditions the ER lumen domain of IRE1 is associated with the ER resident chaperone glucose-related protein (GRP)78 (also known as BiP). Due to the hydrophobic gradient created by exposed hydrophobic residues of unfolded proteins, GRP78 dissociates from IRE1, allowing it to auto-phosphorylate and activate its RNase domain.[28] Active IRE1 cleaves and facilitates the alternative splicing of the mRNA transcript encoding the basic leucine zipper (bZIP) transcription factor XBP-1 promoting its translation. XBP-1 binds to X-box promoter elements and enhances the expression of chaperones and foldases including GRP78, GRP94 and protein disulphide isomerase

(PDI). XBP-1 also initiates lipogenesis to expand the ER membrane increasing its protein folding capacity.[28]

Activating transcription factor (ATF)-6

Similar to IRE1 activation, the presence of unfolded proteins induces GRP78 dissociation from the ER domain of ATF6 enabling its translocation to the Golgi. Once at the Golgi, site-1 proteases (S1Ps) and site-2 proteases (S2Ps) cleave ATF6 releasing its N-terminal bZIP domain. The ATF6 bZIP domain binds to, and promotes, the expression of cAMP response elements (CREs) and ER stress response elements (ERSE)-I and II. [28] This results in the upregulation of genes involved in protein folding (including GRP78 and GRP94) and lipid metabolism (such as sterol element binding protein (SREBP)-2).[28]

Protein kinase R-like endoplasmic reticulum kinase (PERK)

As with IRE1 and ATF6 activation, the presence of unfolded proteins prompts GRP78 dissociation from PERK enabling its dimerization, autophosphorylation and activation. PERK phosphorylates nuclear factor-like (Nrf)-2 causing its nuclear localization where it promotes the transcription of genes containing antioxidant response elements (AREs). PERK also phosphorylates eukaryotic initiation factor (eIF)-2 at Ser51 of its alpha subunit preventing exchange of eIF2-GDP to eIF2-GTP, which is required for mRNA cap recognition and the proper binding of met-tRNAs.[28] This attenuates general translation. Paradoxically, P-Ser51-eIF2α also enhances the expression of activating transcription factor (ATF)-4 by utilizing internal ribosome entry sites (IRES).[29] ATF4 promotes the expression of the pro-apoptotic factor C/EBP homologous protein (CHOP), nuclear factor (NF)-κB as well as genes involved in amino acid metabolism.[28] PERK

signaling has a negative feedback mechanism in which ATF4 enhances the expression of the phosphatase GADD34 which dephosphorylates eIF2α.[28]

The *in vivo* relevance and physiological role of ER stress and UPR signaling is often viewed in the context of the "multiple hit" hypothesis.[30, 31] This concept stipulates that initially, ER stress results in the upregulation of adaptive and pro-survival pathways such as the expression of chaperones, translation attenuation and autophagy, as an attempt to recover from the stress.[30, 31] The induction of distal, maladaptive, apoptotic and inflammatory mechanisms, coinciding with the suppression of pro-survival pathways, is induced by a second "hit" which can include a second stressor, such as elevated cholesterol levels, or persistent and chronic UPR activation.[30, 31] The physiological relevance of ER stress signaling is further complicated by cross talk between the three UPR pathways.[32, 33]

Figure 1.2. The unfolded protein response. The unfolded protein response (UPR) is initiated by the accumulation of misfolded proteins. Signaling through the inositol-requiring enzyme (IRE)-1, protein kinase R-like endoplasmic reticulum kinase (PERK) and activating transcription factor (ATF)-6 pathways leads to the inhibition of translation, the production of chaperones and the degradation of misfolded proteins. If ER stress persists, inflammatory and apoptotic pathways can be initiated.

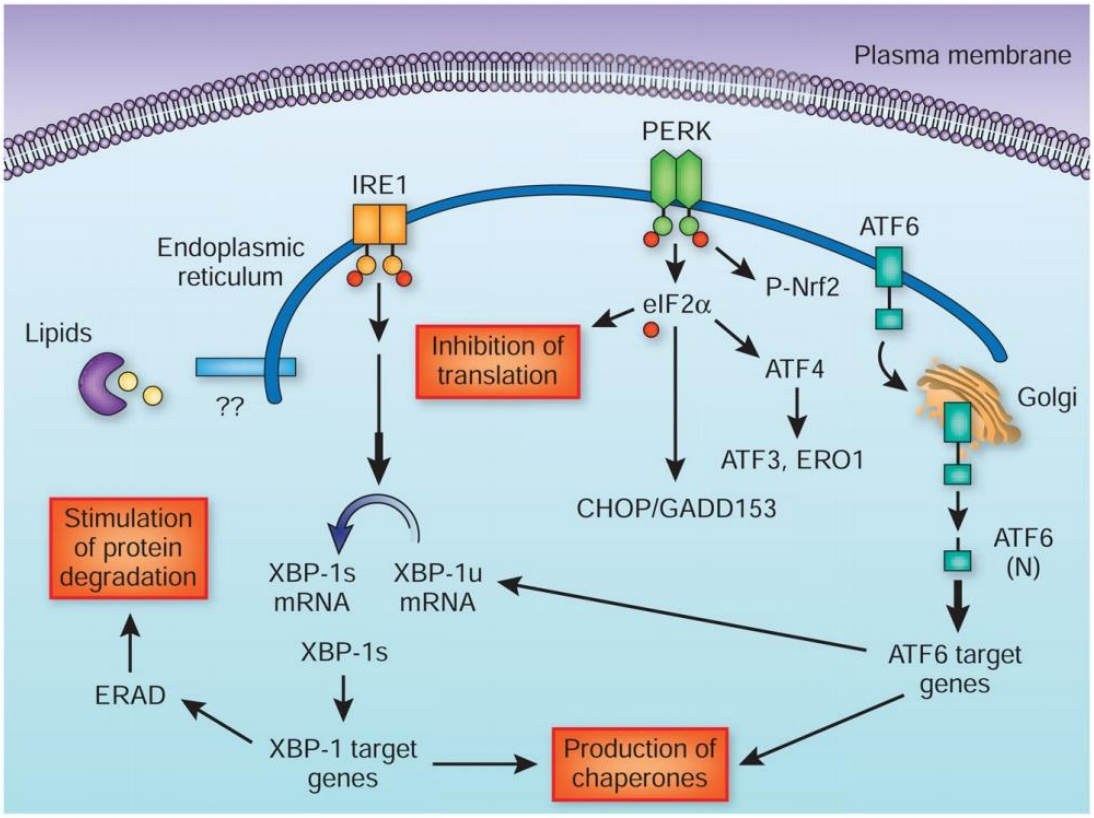

Reprinted with permission from:

Hotamisligil GS. Endoplasmic reticulum stress and atherosclerosis. *Nat Med.* 2010;16:396-399 ©2010 Nature Publishing Group

License number: 3593190316837

Cardiovascular risk factors and ER stress

There is increasing experimental evidence in support of a direct and causative role for ER stress in atherosclerosis.[34-36] Several independent cardiovascular risk factors, including hyperglycemia[37], hyperhomocysteinemia[38], obesity[39], cigarette smoke[40], air pollutants[41], and elevated levels of unesterified cholesterol[42] or palmitate[43], have been associated with increased ER stress, suggesting that this pathway may represent a common or unifying mechanism of accelerated atherosclerotic lesion development.[44, 45]

The mechanism by which dyslipidemia disrupts ER homeostasis is not fully understood but appears to depend upon cell type and the lipid in question.[28, 46-48] Elevated intracellular levels of unestified cholesterol promote its shuttling from the plasma membrane to the ER membrane.[49] The consequence is an increased ratio of cholesterol to phospholipid, which is normally very low in the ER membrane. This results in altered membrane fluidity affecting the function of integral membrane proteins that are involved in signal transduction, including those directly involved in UPR activation.[50] The altered ER membrane composition may also impair the functioning of calcium pumps.[50, 51] Disrupted ER Ca^{2+} homeostasis is a potent inducer of ER stress and both unesterified cholesterol and palmitate have independently been shown to deplete ER Ca^{2+} stores.[43, 50, 51]

There is a large amount of experimental data linking elevated concentrations of glucose to atherogenesis. Hyperglycemia promotes intracellular glucose metabolism leading to the overproduction of superoxide anion by the mitochondrial electron transport chain. Reactive oxygen species (ROS) can promote pro-atherogenic processes through the activation of protein kinase C (PKC), the modification of LDL particles, and the enhanced formation of a heterogenous group of compounds called advanced glycation

endproducts (AGEs). AGEs can bind to RAGE (receptor for AGE), found on macrophages, endothelial cells and smooth muscle cells, and this interaction triggers the production of intracellular reactive oxidative species that initiate an inflammatory response and promote atherosclerosis.[52-57] While there is very good pre-clinical evidence supporting a causative role for oxidative stress/AGEs in atherogenesis, virtually every large well-controlled clinical trial has failed to show a cardiovascular benefit in diabetic patients receiving anti-oxidant treatments.[58, 59] Together, these findings suggest that additional pathways may play a role in diabetes/hyperglycemia associated atherosclerosis.

Elevated glucose levels can induce ER stress by increasing flux through the hexosamine biosynthesis pathway (HBP).[60, 61] The rate limiting step of the HBP is mediated by the enzyme glutamine:fructose-6-phosphate amino-transferase (GFAT) which converts fructose-6-phosphate into glucosamine-6-phosphate. In cultured cells, exposure to glucosamine or over expression of GFAT promotes ER stress, lipid accumulation and inflammation.[61, 62] Importantly, supplementation of mice with glucosamine induces ER stress and accelerates atherosclerosis.[37, 61, 63] Together, these studies suggest glucose induced flux through the HBP and the resultant induction of ER stress may be a mechanism by which hyperglycemia accelerates atherosclerosis.

ER stress in early atherosclerosis

Elevated levels of ER stress are observed in all cell types at every stage of lesion development.[64] Suppression of ER stress with the chemical chaperone 4-phenylbutyric acid (4PBA) attenuates hepatic steatosis, reduces LDL secretion and improves glucose tolerance.[47, 65, 66] Importantly, 4PBA attenuates atherosclerosis in low-density lipoprotein

receptor deficient ($LDLR^{-/-}$) and apolipoprotein-E deficient ($ApoE^{-/-}$) mice.[66, 67] Prior to lesion formation, the UPR is activated in endothelial cells isolated from atherosclerosis-prone, but not athero-protected regions of the vessel wall.[68] One possible early effect of ER stress in the pre-atherosclerotic endothelium is to increase local inflammation. ER stress inducing agents, including glucosamine and unesterified cholesterol, increase the activity of NF-κB, the transcription factor that regulates inflammatory gene expression, leading to the upregulation of inflammatory cytokines including TNFα and IL-6.[37, 69, 70] Mechanistically, activated IRE-1 associates with the adaptor molecule TNF receptor-associated factor (TRAF)-2 and signals through downstream kinases to activate host defense proteins including NF-κB and c-Jun.[71, 72] As with endothelial cells, diagnostic markers of ER stress are elevated in macrophages and macrophage foam cells which compose the fatty streak.[64] In this manner, the ER stress response mechanism can play a central role in the pro-inflammatory response to endothelial injury that initiates atherosclerosis.

ER stress in lesion progression

ER stress may also activate/dysregulate metabolic pathways that are directly involved in the growth of atherosclerotic lesions. It is well established that ER stress inducing agents, including lipids, can promote lipid accumulation in both vascular macrophages and hepatic cell types, through the activation of SREBPs.[73, 74] SREBPs are transcription factors that control the expression of enzymes involved in cholesterol and triglyceride biosynthesis and uptake.[75, 76] Interestingly, SREBPs are activated by the same proteolytic mechanism as the ER stress sensor ATF6.

The amplification of inflammation seen in atherosclerosis progression is partly driven by ER stress. ER stress impairs the adaptive immune response by attenuating major histocompatibility complex (MHC) class I protein processing and expression.[77, 78] Moreover, lipid induced ER stress prevents the proper activation and polarization of T cells and NK cells.[79] Another emerging mechanism of atherosclerotic lesion progression is macrophage proliferation. *In situ* macrophage proliferation within the vessel wall gives rise to the majority of macrophages in established lesions and this process may be influenced by ER stress.[20, 80] Induction of ER stress in macrophages by hyperglycemia, elevated lipid levels or dysregulation of calcium stores promotes proliferation.[20, 81, 82]

ER stress in the advanced atherosclerotic lesion

Macrophage/foam cell apoptosis is characteristic of complex and advanced lesions. Engulfment of toxic lipid particles by macrophages may be beneficial in early lesions but leads to ER stress and apoptosis at later stages.[83] In advanced lesions macrophage apoptosis promotes lesion instability and rupture. Tabas and colleagues have shown that loading macrophages with unesterified cholesterol results in activation of the UPR, increases CHOP expression and induces apoptosis.[84-86] These findings are further supported by the observation that both $ApoE^{-/-}$ and $LDLR^{-/-}$ mice lacking CHOP have significantly less plaque apoptosis and necrosis, in addition to reduced lesion areas.[87]

1.4 GLYCOGEN SYNTHASE KINASE 3α/β

Structure, function and regulation

Glycogen Synthase Kinase (GSK)-3α and β are homologous serine/threonine kinases central to many cellular signaling pathways (Figure 1.3). GSK3α and β are encoded on separate genes; *gsk3*α is located on mouse chromosome 7 and human chromosome 9 while *gsk3*β is located on mouse chromosome 16 and human chromosome 9.[88] GSK3α (51kDa) is 4kDa larger than GSK3β (47KDa) due to an N-terminus glycine-rich extension, which may play a role in its nuclear localization.[89] The proteins are highly homologous (98%) within the kinase domain however, they share only 36% amino acid sequence similarity at their C-terminal. GSK3α and β homologs have been found in all species studied and are highly conserved between species – humans and flies share 90% sequence similarity.[90] A minor splice variant of GSK3β, GSK3β2, has been described. GSK3β2 contains a 13 residue insert in its kinase domain, has a lower activity than GSK3β and is localized primarily to neuronal cell bodies.[91] Despite their structural similarity, GSK3α and GSK3β have both redundant and unique functionality. For example, in Wnt signaling (discussed below) both homologs display similar propensities towards β-catenin phosphorylation.[92] However, GSK3α and GSK3β also have unique roles; GSK3α$^{-/-}$ mice are viable with no overt phenotype while GSK3β deficient mice die during mid-gestation [E13.5-16.5] due to hypertrophic cardiomyopathy.[93-95] The GSK3α homolog is unable to rescue this phenotype.

GSK3α/β substrates have the consensus sequence Ser/Thr-X-X-X-Ser/Thr-P, where the first (N-terminal) Ser/Thr is GSK3α/β's target residue and the last (C-terminal) Ser/Thr is the priming residue. The phosphorylated priming residue binds to a positively charged pocket adjacent to the active site, which contains the residues Lys205, Arg96

and Arg180.[88, 90] Binding of a primed substrate to this pocket orientates the substrate in the proper configuration resulting in a 500- to 1000-fold increase in kinase activity.[90] Inhibition of GSK3α and β is achieved by phosphorylation at the serine residues 21 and 9, respectively, which create competitive pseudosubstrates for the priming pocket. A number of kinases can act on GSK3α/β at these serine residues including protein kinase B (PKB/AKT), p38MAPK and p90rsk along with phosphatases such as protein phosphatase-1 (PP1).[96-99] As with other kinases, GSK3α and β can be phosphorylated at tyrosine residues within their activation loops (T-loops) increasing the space available for substrate binding and thus increasing kinase activity.[90] Within the T-loop, GSK3α can be phosphorylated at Tyr279 and GSK3β at Tyr216. Phosphorylation at these sites is accomplished by autophosphorylation as well as by kinases such as ZAK1, extracellular signal-regulated kinase (ERK)-1/2 and protein tyrosine kinase (PYK)-2.[100-102] GSK3α/β's tyrosine residues can also be dephosphorylated by the phosphatase PtpA.[103] Although not as well characterized, GSK3α/β can be phosphorylated at a number of other residues which may impact its activity.[104, 105] GSK3α/β function can also be regulated by protein-protein interaction, such as complex and scaffold association during Wnt signaling (discussed below),or by sub-cellular localization.[88, 106] GSK3α/β protein has been detected in most cellular organelles including cytoplasm, nuclei and mitochondria.[88] In particular, the level of nuclear GSK3α/β is dynamic and dependent on cell cycle, apoptotic state and its association with FRAT, which enhances its nuclear localization.[107-109]

Figure 1.3. Glycogen synthase kinase-3α/β. Mammalian glycogen synthase kinase (GSK)-3α and GSK3β with common serine and tyrosine phosphorylation sites indicated. GSK3α's glycine rich N-terminal domain is indicated in blue and the kinase domains are indicated in red.

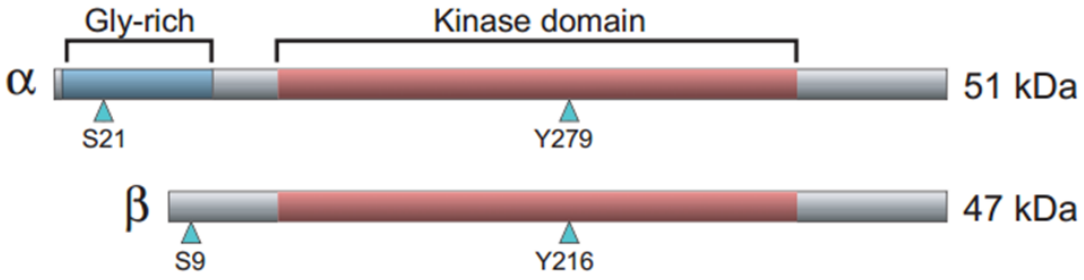

Cellular signaling

A role for GSK3α/β has been suggested in such diverse cellular processes as transcription factor regulation, cellular structure, polarity, survival, metabolism and circadian rhythm.[88] To date, over 100 substrates have been described as targets of GSK3α and/or GSK3β.[110]

Insulin signaling

As early as 1978 GSK3α/β was suggested to be a target of the insulin signaling pathway.[111] Binding of insulin to the insulin receptor stimulates phosphorylation of the insulin receptor substrates (IRS) 1 and 2. Active IRS1/2 recruit phosphatidyl-inositide3-dependent-kinase (PI3K) which activates AKT by phosphorylation at Thr308 and Ser473. AKT subsequently phosphorylates GSK3α/β at its inhibitory serine residues. Inactive GSK3α/β is no longer able to phosphorylate and inhibit glycogen synthase, a well characterized GSK3α/β substrate, resulting in increased glucose storage through glycogen synthesis.

Wnt signaling

Canonical Wnt signaling regulates cell growth, survival and differentiation.[112] In unstimulated cells, GSK3α/β phosphorylates β-catenin at Thr41, Ser 37 and Ser 33 marking it for ubiquitylation and degradation by proteasomes. Binding of a Wnt ligand to the Frizzled receptor, however, induces the formation of a complex comprising of the scaffold protein axin, adenomatous polyposis coli (APC), casein kinase 1 (CK1) and the kinase Dishevelled which phosphorylates and inactivates GSK3α/β. This leads to the accumulation of β-catenin which binds to members of the T-cell factor (TCF) and

lymphoid enhancer factor (LEF) family of DNA binding proteins promoting the transcription of TCF/LEF target genes.

Mitogen Activated Protein Kinase (MAPK) signaling

GSK3α/β is involved in the regulation of the transcription factors c-Jun and c-Myc.[113] GSK3α/β activates c-Jun N-terminal Kinase (JNK) which phosphorylates c-Jun proximal to its DNA binding domain at Thr239, Ser243 and Ser249 inhibiting its ability to bind to DNA.[114] Similarly, GSK3α/β activates ERK1/2 (also known as p44/p42 mitogen-activated kinase) which phosphorylates c-Myc at Ser62 stabilizing the transcription factor.[115] Interestingly, GSK3α/β also phosphorylates c-Myc directly at Thr58 promoting its degradation.[114]

GSK3α/β and ER stress

A role for GSK3α/β in ER stress signaling and the UPR has been suggested but is poorly understood.[116, 117] Initial work from our group has demonstrated that genetic deficiency or pharmacological inhibition of GSK3α/β attenuates ER stress induced lipid accumulation and apoptosis in cultured mouse embryonic fibroblasts (MEFs).[73] Scinivasan *et al.* have demonstrated that pancreatic islet β-cells transfected with siRNA directed against GSK3β are resistant to ER stress induced apoptosis.[118] Moreover, treatment of cultured cells with thapsigargin, an inhibitor of ER calcium ATPases, increases GSK3β activity through reduced Ser9 phosphorylation resulting in capsase 3 expression and apoptosis.[116] Finally, GSK3α/β may be involved in regulating the expression of cellular chaperones.[73, 119-121] Together, these studies suggest GSK3α/β is a target of ER stress signaling and that ER stress increases GSK3α/β activity. The

molecular mechanisms by which ER stress and the UPR signal to GSK3α/β have not been elucidated. Specifically, the role of individual UPR pathways (PERK, IRE1 or ATF6) in the regulation of GSK3α/β is unknown.

GSK3α/β and atherosclerosis

Evidence suggests GSK3α/β signaling regulates a number of metabolic processes which are implicated in atherogenesis. In cell culture models, GSK3α/β mediates components of the inflammatory, lipid accumulation and apoptotic pathways, hallmark features of atherosclerosis.[73, 122] GSK3α$^{-/-}$ MEFs, GSK3β$^{-/-}$ MEFs or MEFs exposed to the GSK3α/β inhibitor valproate are resistant to ER stress-induced lipid accumulation.[73, 123] Further, GSK3α/β is an important mediator of the inflammatory process. GSK3α/β is required for NF-κB expression and the nuclear translocation of its p65 subunit.[95] In cultured human monocytes, toll-like receptor (TLR)-4 stimulation attenuates GSK3β activation in a PI3K/AKT dependent fashion and inhibition of GSK3α/β suppresses inflammatory cytokine production in response to bacterial infection.[124] These affects appear to be due to GSK3α/β's ability to modulate the activity and expression of cyclic AMP response element-binding protein (CREB).[124] Downstream of TLR stimulation, GSK3α/β has also been implicated in the regulation and phosphorylation of signal transducer and activator of transcription (STAT) transcription factors, critical mediators of the inflammatory process.[125, 126] There is limited *in vivo* evidence implicating GSK3α/β in atherosclerosis. Recently, our group demonstrated that atherosclerosis is attenuated by valproate, a non-specific GSK3α/β inhibitor, in hyperglycemic ApoE$^{-/-}$ mice.[123]

All together, these studies implicate GSK3α/β signaling in the atherosclerotic processes, however, a number of questions remain. First, the role of GSK3α/β in multiple mouse models of accelerated atherosclerosis has not been investigated. Moreover, no GSK3α/β inhibitor is able to distinguish between its two homologs, therefore, the homolog specific functions of GSK3α and GSK3β in atherosclerosis are unknown. Finally, the uses of inhibitors impose systemic attenuation of GSK3α/β activity, therefore the tissue specific functions of GSK3α/β in atherogenesis are unknown.

1.5 MYELOID CELLS

Myeloid cell biology

Leukocytes are mediators of the immune and inflammatory systems. In the bone marrow, all blood cells, including leukocytes, derive from hematopoietic stem cells (HSCs) which differentiate along specific linages. Differentiation of HSCs into common lymphoid progenitor cells (CLPCs) is the first committed step in the production of lymphocytes including T cells, B cells and NK cells. Conversely, differentiation of HSCs into common myeloid progenitor cells (CMPCs) is the first committed step in myeloid cell differentiation. CMPCs can differentiate further into megakaryocytes, erythrocytes, mast cells or myoblasts. Myoblasts give rise to myeloid cells, granular leukocytes, which include basophils, neutrophils, eosinophils and monocytes.

Monocytes are released from the bone marrow, circulate in the blood and are key effector cells of the inflammatory response. The cell surface of monocytes is equipped with chemoattractant and adhesion molecule receptors which facilitate their migration and movement. Mouse monocytes can be segregated based on expression of the glycoprotein Ly6C. Ly6C^{lo} monocytes patrol tissues searching for sites of damage and

attenuate inflammation.[127, 128] Ly6C^{hi} monocytes are actively recruited to sites of damage and promote inflammation.[127, 128]

During inflammation, Ly6C^{hi} monocytes infiltrate tissue and give rise to both macrophages and dendritic cells (DCs). DCs are divided into two subtypes – classical DCs (cDCs) and plasmacytoid DCs (pDCs). cDCs are phagocytic antigen presenting cells that secrete cytokines while pDCs are specialized to fight viral infection. Macrophages are mononuclear phagocytic, endocytic and secretory cells that maintain tissue homeostasis. Macrophages are the first line of the innate immune defense - they migrate towards sites of inflammation to clear debris, including pathogens and apoptotic material, and initiate tissue repair. While most macrophages differentiate from monocytes, an embryonically-derived resident macrophage population exists in most tissues including heart, lung and liver.

Like monocytes and DCs, macrophages can be divided into a number of phenotypic subtypes along a broad spectrum of differentiation states (Figure 1.4). Classical M1 macrophages arise when exposed to products of Th1 cells such as TNFα and IFNγ or microbial products such as lipopolysaccharide (LPS).[129] M1 macrophages perpetuate the inflammatory response by secreting pro-inflammatory cytokines and chemokines.[130] Alternative M2 macrophages, elicited by the Th2 cell products IL-4 or IL-13, are immunoregulatory, reparative and secrete anti-inflammatory cytokines including IL-10.[130] M1 and M2 macrophages are recruited by different chemotactic mechanisms.[131, 132] CCL19 and CCL21 bind to chemokine receptor (CCR)-7 on the surface of M1 macrophages to induce their migration.[131] In M2 polarized cells, however, CCR7 is cytosolic and not expressed at the cell surface, therefore M2 macrophages do not respond to CCL19 or CCL21. [131] The metabolic programs of M1 and M2

macrophages differ as M1 macrophages utilize glycolysis for energy production resulting in nitric oxide (NO) and ROS secretion along with extracellular acidification.[133, 134] M2 macrophages, on the other hand, rely on fatty acid oxidation and mitochondrial biosynthesis which results in arginase, proline and collagen production.[133, 134]

A number of other macrophage subtypes have been identified. Exposing macrophages to oxidized phospholipids polarizes them towards the Mox phenotype. Mox cells are less phagocytic and display increased expression of redox regulating genes.[135] An important role for macrophages in iron metabolism has recently emerged. MHb macrophages are stimulated by hemoglobin and display an increased capacity for erythrocyte phagocytosis.[136] After hemoglobin degradation, MHb macrophage secrete high levels of the iron containing heme group which is phagocytosed by unstimulated macrophages and polarizes them towards the Mhem phenotype.[135] These iron loaded macrophages have increased cholesterol efflux capacity, are resistant to oxidative stress and localize to areas of neovascularization.[135] Finally, M4 macrophages, induced by the platelet derived chemokine CSCL4, display increased metalloproteinase activity and reduced iron processing.[137] The physiological role of these macrophage subtypes in disease is poorly understood.

Figure 1.4. Macrophage subtypes in atherosclerotic lesions. Macrophage subtypes detected in human (H) and mouse (M) atherosclerotic lesions and their suggested impact on lesion development.

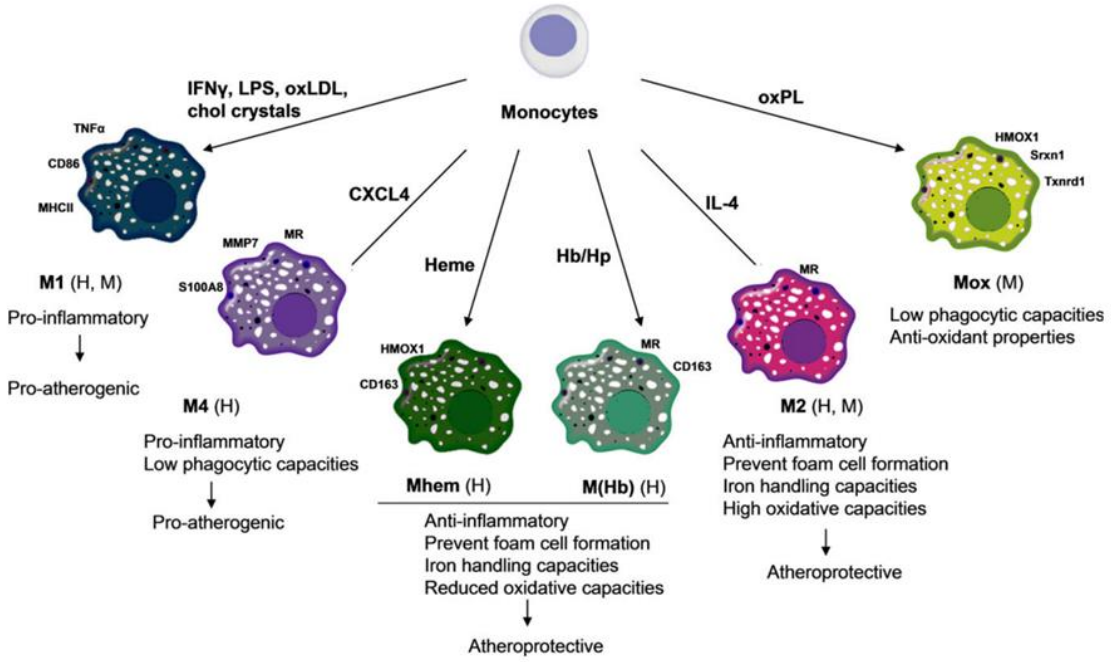

Reprinted with permission from:

Colin S, Chinetti-Gbaguidi G, Staels S. Macrophage phenotypes in atherosclerosis. *Immunol Rev.* 2014;262:153-166. ©2014 John Wiley and Sons

License number: 3593200496288

Myeloid cells in atherosclerosis

Myeloid lineage cells make up the majority of an atherosclerotic lesion's cellular bulk and monocyte number is predictive of disease severity.[138, 139] Hypercholesterolemia and dyslipidemia promote hematopoiesis in the bone marrow and release of monocytes from splenic reservoirs.[10, 140, 141] Once in the circulation, Ly6C^{hi} monocytes are recruited to the vessel wall via CCL2-CCR2 and form fatty streaks more readily than Ly6C^{lo} monocytes.[10, 142] In the intima, virtually all monocytes differentiate into macrophages and begin to uptake modified lipids.[143] Lipid cytotoxicity is the predominant cause of macrophage apoptosis within atherosclerotic lesions.[36, 144] In advanced lesions, macrophage foam cells undergo proliferation, potentially as a mechanism to cope with lipid cytotoxicity and prevent apoptosis.[20]

To date, only M1, M2 and Mox macrophages have been identified in murine atherosclerotic lesions while M1, M2, M4, Mhem and MHb macrophages have been identified in human lesions. [135] The contribution of each macrophage phenotype to atherosclerosis progression is poorly understood.[143] While both M1 and M2 macrophages have the propensity to ingest lipids and become foam cells, they appear to localize to different areas of the lesion.[145] M1 macrophages are the predominant macrophage subtype in rupture prone areas of the lesion including surrounding the necrotic core.[146] In contrast, M2 macrophages localize to stable, IL-4 and cell rich portions of lesion, away from the necrotic core.[147] Functionally, M2 macrophages efferocytose debris and apoptotic material within atherosclerotic lesions, attenuate inflammation and are less likely to undergo apoptosis.[130, 145] In animal models, the deficiency of IL-13 in LDLR$^{-/-}$ mice promotes polarization of macrophages to the M1 phenotype and exacerbates atherosclerosis.[148] Conversely, deletion of STAT1, a key

promoter of the M1 program, attenuates atherosclerosis.[149, 150] Moreover, regression of atherosclerotic lesions is associated with macrophages switching from an M1 to an M2 phenotype.[151, 152] Despite the importance of macrophage phenotypes to the progression and regression of atherosclerosis the molecular signaling networks that regulate macrophage polarization and phenotype are poorly understood.

1.6 RESEARCH GOAL

Over the past decade significant advances in our understanding of the molecular and cellular mechanisms of atherosclerosis have been made. Despite this, few specific and targeted anti-atherogenic therapeutics have been developed and clinical management of CVD remains largely restricted to lifestyle modifications and mechanical reopening of arteries. While these are important and worthy clinical goals, the development of innovative and targeted treatments will greatly decrease disease burden. With this aim in mind, this thesis sought to elucidate novel molecular and cellular mechanisms of atherogenesis that could be targeted therapeutically. Specifically, this work investigated the relationship between GSK3α/β, ER stress and myeloid cell function in atherosclerotic lesion development.

CHAPTER 2: General Hypothesis and Objectives

2.1 GENERAL HYPOTHESIS

We hypothesize that cardiovascular risk factors, including dyslipidemia and hyperglycemia, promote the accelerated development of atherosclerosis by a mechanism that involves ER stress-induced activation of GSK3α and/or β resulting in the induction of pro-atherogenic processes including lipid accumulation and inflammation.

2.2 GENERAL OBJECTIVES

The objectives of these studies are to:

1) Determine the role of ER stress and GSK3α/β signaling in multiple mouse models of experimental atherosclerosis
2) Delineate the molecular mechanisms of ER stress – GSK3α/β signaling in the context of atherosclerosis
3) Investigate the tissue and homolog specific functions of GSK3α and GSK3β in atherosclerosis

CHAPTER 3: Endoplasmic Reticulum Stress and Glycogen Synthase Kinase-3β Activation in Apolipoprotein E-Deficient Mouse Models of Accelerated Atherosclerosis

Cameron S. McAlpine,[1,3] Anna J. Bowes,[2,3] Mohammad I. Khan,[3]

Yuanyuan Shi,[3] and Geoff H. Werstuck[1,2,3]

Departments of [1]Medicine and [2]Biochemistry and Biomedical Sciences, and the

[3]Thrombosis and Atherosclerosis Research Institute, McMaster University

Hamilton, Ontario, Canada

3.1 FOREWORD

This study investigates the role of ER stress and GSK3α/β in atherosclerosis. We demonstrate increased ER stress, GSK3β activity and lesion size in three mouse models of experimental atherosclerosis. Supplementing mice with the GSK3α/β inhibitor valproate attenuates GSK3β activity and atherosclerosis but does not alter ER stress levels.

This work was published in *Arteriosclerosis Thrombosis and Vascular Biology*, volume 32, pages 82-91, January 2012. The experiments in this study were conducted by Cameron McAlpine with assistance from the co-authors. The manuscript was written by Cameron McAlpine in collaboration with Dr. Geoff Werstuck. The content of Chapter 3 is a direct representation of this publication. The complete reference is as follows: McAlpine CS, Bowes AJ, Khan MI, Shi Y, Werstuck GH. Endoplasmic reticulum stress and glycogen synthase kinase-3β activation in apolipoprotein E-deficient mouse models of accelerated atherosclerosis. *Arteriosclerosis Thrombosis and Vascular Biology*. 2012;32:82-91.

3.2 ABSTRACT

Objective

To examine the role of ER stress signaling and the contribution of GSK3β activation in hyperglycemic, hyperhomocysteinemic, and high fat fed ApoE-deficient ($ApoE^{-/-}$) mouse models of accelerated atherosclerosis.

Approach and Results

Female $ApoE^{-/-}$ mice received multiple low dose injections of streptozotocin (40μg/kg) to induce hyperglycemia, methionine-supplemented drinking water (0.5% w/v) to induce hyperhomocysteinemia, or a high fat (21% milk fat + 0.2% cholesterol) diet to induce relative dyslipidemia. A subset of mice from each group were supplemented with sodium valproate (625 mg/kg), a compound with GSK3 inhibitory activity. At 15 and 24 weeks of age markers of ER stress, lipid accumulation, GSK3β phosphorylation, and GSK3β activity were analyzed in liver and aorta. Atherosclerotic lesions were examined and quantified. Hyperglycemia, hyperhomocysteinemia and high fat diet significantly enhanced ER stress, GSK3β activity and also increased hepatic steatosis and atherosclerotic lesion volume compared to controls. Valproate-supplementation blocked GSK3β activation without altering ER stress levels and attenuated the development of atherosclerosis and the accumulation of hepatic lipids in each of the models examined. The mechanism by which GSK3β activity is regulated in these models likely involves alterations in phosphorylation at serine-9 and tyrosine-216.

Conclusions

These findings support the existence of a common mechanism of accelerated atherosclerosis involving ER stress signaling through activation of GSK3β. Furthermore

our results suggest that atherosclerosis can be attenuated by modulating GSK3β phosphorylation.

3.3 INTRODUCTION

Atherosclerosis is a disease of the arterial wall that is characterized by inflammation and lipid accumulation.[1] It is the underlying cause of cerebro- and cardiovascular disease that together account for approximately one third of the annual mortality in westernized societies.[1, 2] Risk factors for cardiovascular disease include diabetes mellitus, hypertension, dyslipidemia, hyperhomocysteinemia, abdominal obesity, smoking, and physical inactivity.[3, 4] However the underlying cellular and molecular pathways that link specific risk factors to accelerated development of atherosclerosis remain unclear. Understanding of the mechanisms that promote atherogenesis will be a major step toward the development of novel and effective anti-atherosclerotic therapies.

Endoplasmic reticulum (ER) stress is defined as a condition in which the protein processing capacity of the endoplasmic reticulum is exceeded by nascent proteins resulting in the accumulation of unfolded and/or mis-folded proteins. The unfolded protein response (UPR) is a cellular self-defense mechanism that alleviates ER stress by limiting *de novo* protein synthesis, enhancing protein folding capacity, through the up-regulation of specific ER chaperones including GRP78, GRP94, and calreticulin, and increasing the degradation of irreversibly mis-folded proteins.[5, 6] If the UPR is insufficient to restore ER homeostasis, pro-apoptotic signaling factors, such as C/EBP homologous protein (CHOP), can initiate programmed cell death.

Accumulating evidence supports a causative role for ER stress in the development and/or progression of atherosclerosis. First, several independent cardiovascular risk factors, including hyperglycemia[7], hyperhomocysteinemia[8], obesity[9], cigarette smoke[10] and elevated levels of unesterified cholesterol[11] or palmitate[12, 13], have been associated with activation of the UPR. Secondly, recent evidence shows that the UPR is specifically activated in atherosclerosis-susceptible regions of the arterial wall, prior to lesion development.[7, 14] Finally, ER stress-inducing agents can activate/dysregulate metabolic pathways that are directly involved in the development of atherosclerotic lesions. Specifically, we have shown that conditions of ER stress promote lipid accumulation by activating the sterol regulatory element binding proteins (SREBPs), which are transcription factors that control lipid biosynthesis and uptake.[8, 15] ER stress-inducing agents also activate NF-κB, the transcription factor responsible for promoting inflammatory gene expression.[16] In addition, ER stress can activate caspases and promote apoptosis of endothelial cells, macrophages and other cell types.[17] Together, lipid accumulation, inflammation and endothelial/macrophage/foam cell apoptosis are hallmark features of atherosclerosis.

The molecular pathways by which ER stress and/or the UPR activate pro-atherogenic responses are not known. One potential factor that is involved in ER stress signaling is glycogen synthase kinase (GSK)-3α/β, a kinase involved in many metabolic pathways.[18] Conditions of ER stress have been shown to increase the activity of GSK3β in cultured cells. Furthermore, GSK3α/β has been shown to play a role in the activation of NF-κB both in *vivo* and *in vitro.*[19, 20] Recently we have found that dietary supplementation with valproate, a small branch chain fatty acid with GSK3 inhibitory properties[21], can attenuate accelerated atherosclerosis in a STZ-induced hyperglycemic

ApoE$^{-/-}$ mouse model.[22] These were the first reports to implicate GSK3 in the development of atherosclerosis. Here we investigate the potential role of ER stress and GSK3 in other models of accelerated atherosclerosis including hyperhomocysteinemic and high fat fed mice. In addition, we examine the specific effects of valproate-supplementation on vascular and hepatic ER stress and GSK3β activity levels in mice. Finally, we examine the mechanisms by which these pro- and anti-atherogenic stimuli regulate kinase activity in these different mouse models.

3.4 METHODS

Mouse models

Five week old female apolipoprotein E deficient (ApoE$^{-/-}$)(B6.129P2-ApoE^{tm1Unc}) mice, purchased from Jackson Labs (stock number 002050), were placed on a defined chow diet (Harlan Teklad, TD92078) and randomly divided into four groups (n=24/group). To induce hyperglycemia, one group was injected intraperitoneally with 10 injections of STZ (40 mg/kg/day) as previously described.[23] To induce hyperhomocysteinemia, L-methionine (0.5%, w/v) was added to drinking water. To induce relative dyslipidemia, mice were fed a high fat diet containing 21% milk fat and 0.2% cholesterol (Harlan Teklad, TD97363). The final group remained on the standard chow diet. After one week, half of the mice in each group were switched to diet supplemented with 625 mg/kg sodium valproate (standard plus valproate (TD02165) or high fat plus valproate (TD06228)). All mice had unrestricted access to both food and water throughout the study. Mice were sacrificed at 15 (HG, HH) or 24 (HF) weeks of age and blood and tissues were collected for further analysis. The McMaster University Animal Research Ethics Board approved all procedures.

Plasma analysis

Non-fasting whole blood glucose levels were measured using a DEX glucometer (Bayer). Plasma glucose and lipid levels were determined in non-fasted mice using the colorimetric diagnostic kits for total cholesterol and glucose purchased from Thermal DMA Inc. Plasma valproate concentrations were determined using an AxSYM system (Abbott Laboratories). Plasma homocysteine levels were determined using IMx system (Abbott Diagnostics). Plasma lipoproteins were separated by fast protein liquid chromatography, and total cholesterol was measured in each fraction.

Immunohistochemical analysis

Mice were euthanized, vasculature was flushed with 1X PBS and perfusion-fixed with 10% neutral buffered formalin. Liver and heart, including the aortic root, were removed and embedded in paraffin. Serial sections (4 μm) of aortic root were collected on pre-coated glass slides for measurement of lesion size (hematoxylin and eosin staining) or immunohistochemical staining.[24] The Vectastain ABC System was used for immunohistochemical analysis. Sections were stained with primary antibodies and appropriate biotinylated secondary antibodies and visualized using Nova Red. Sections were counterstained with hematoxylin. Serial sections were stained with pre-immune IgG, in place of primary antibodies, to control for non-specific staining. Images were captured with an Olympus microscope and a 12.5 Mega pixel DP71 digital camera. Phospho-Y216-GSK3β antibody was purchased from BD Transductions (Cat#612312), phospho-S9-GSK3β antibody was purchased from Cell Signaling (Cat#93235) and total GSK3β antibody was purchased from BD Transductions (Cat#610202). Anti-KDEL

antibody was purchased from Assay Designs (Cat#SPA-827) and anti-CHOP antibody was purchased from Santa Cruz (Cat#sc-575).

Immunoblot analysis

Total protein lysates were solubilized in GSK3 buffer containing; 50 mmol/L Tris HCl pH 8.0, 150 mmol/L NaCl, 5 mmol/L EDTA, 50 mmol/L NaF, 1% Triton X, 10 mmol/L DTT, 1 mmol/L benzamidine, 1 mmol/L PMSF and PhosSTOP Phosphatase Inhibitor (Roche). Protein lysates were diluted in SDS-PAGE gel loading buffer, resolved by SDS-PAGE and transferred to nitrocellulose membranes. After incubation with the appropriate primary and horseradish peroxidase (HRP)-conjugated secondary antibodies (Life Technologies), membranes were developed using the Immobilon Western chemiluminescent HRP substrate (Millipore).

Anti-KDEL (GRP78/94) antibody was purchased from Assay Designs (Cat#SPA-827), PDI antibody was also purchased from Assay Designs (Cat#SPA-891) and α-Actin Antibody was purchased from Sigma-Aldrich (Cat#A3854). Phospho-Y216-GSK3β antibody was purchased from BD Transductions (Cat#612312), phospho-S9-GSK3β antibody was purchased from Cell Signaling (Cat#93235) and total GSK3β antibody was purchased from BD Transductions (Cat#610202).

GSK3β activity assay

GSK3β was immunoprecipitated from 900 μg total mouse liver protein in GSK3 buffer using a monoclonal antibody specific for GSK3β (BD Transductions Cat#610202) and Ultra Link immobilized Protein A Plus (Pierce). Kinase activity was measured by monitoring the incorporation of ^{32}P onto phospho-glycogen synthase peptide-2 (pGS-2,

Upstate Biotech). Briefly, immunoprecipitated GSK3β was combined with 15 μmol/L p-GS-2 and 0.5 μCi/μl [γ^{32}P]-ATP in a reaction mixture containing 20 mmol/L MOPS, 50 μmol/L EDTA, 0.25 mmol/L Mg acetate, 5 mmol/L $MgCl_2$, 5 mmol/L β-glycerol phosphate, 1 mmol/L EGTA, 0.25 mmol/L Na_3VO_4, 0.25 mmol/L DTT and 35 μmol/L ATP in a total volume of 40 μL. After 60 min at room temperature samples were placed on ice, then spotted onto Whatman P81 phosphocellulose paper and washed 3X with 0.75% *o*-phosphoric acid and once with acetone. ^{32}P incorporation onto the substrate was determined by scintillation counting and total counts minus background are reported.

Lipid staining

Liver cryosections, 7 μm thick, were collected on slides and fixed in formal calcium for 30 minutes. Neutral lipids were visualized using Oil red O as described previously.[8] Relative amounts of lipid staining were quantified using Image J 1.35 Software. For *en face* staining, descending aortas were collected and periadventitial tissue was removed. Clean aortas were washed in 70% ethanol, stained with 0.5% Sudan IV for 15 minutes, destained with 80% ethanol and rinsed with dH_2O. After longitudinal dissection, stained aortas were mounted *en face* and the images were visualized and captured using a Leica surgical microscope and DC300 digital camera using IM50 software.

Cell culture

HepG2 cells were cultured in Dubecco's Modified Eagle Medium (DMEM, Invitrogen) with 10% Fetal Bovine Serum (FBS) at 37°C and 5% CO_2. Cells were treated

with 8μg/ml tunicamycin or 250μM BSA-coupled palmitic acid for 8 hours. Oil Red O stain was applied to cells and, after washing with PBS and 60% ethanol, the cells were fixed in 2.5% paraformaldehyde. Images were captured with an Olympus microscope and a 12.5 Mega pixel DP71 digital camera. Intensity of staining was quantified using Image J software.

Statistical analysis

Results are presented as the mean ± standard deviation. Student's t-test was used to assess differences between experimental groups and controls. Probability values of <0.05 were considered statistically significant.

3.5 RESULTS

Mouse models of accelerated atherosclerosis

We directly compared the effects of chronic hyperglycemia, hyperhomocysteinemia or high fat diet on ER stress levels, GSK3β and accelerated atherosclerosis in ApoE$^{-/-}$ mice (Table 3.1). Hyperglycemia was induced with multiple low dose injections of STZ (40mg/kg body weight) in 5 week old ApoE$^{-/-}$ mice. At 15 weeks of age, non-fasting blood glucose levels had increased to 23.2±5.6 mmol/L compared to 10.5±2.0 mmol/L in controls (P<0.05). Hyperhomocysteinemia was induced by adding 0.5% methionine (w/v) to the drinking water starting at 5 weeks of age. In the methionine-supplemented group, plasma homocysteine levels increased to 14.1±4.0 μmol/L compared to 4.6±0.8 μmol/L in controls (P<0.05). ApoE$^{-/-}$ mice fed a high fat diet containing 21% milk fat and 0.2% cholesterol had a significant increase in total plasma cholesterol (25.0±3.6 mmol/L vs 14.8±2.7 mmol/L in controls, P<0.05) and blood glucose

(11.2±0.9 mmol/L vs 8.5±0.3 mmol/L in controls, $P<0.05$). Subsets of mice from each group were fed diets supplemented with 625 mg/kg sodium valproate. Valproate has been shown to inhibit GSK3β activity both *in vitro* and *in vivo* (21,22,25,26).

Plasma valproate concentration in supplemented mice was 33-54 μmol/L with the exception of the high fat diet mice in which it was significantly lower (7 μmol/L). The reason for this is not clear; however it is possible that conditions of severe dyslipidemia may affect valproate uptake, clearance, or detection. Plasma homocysteine levels were lower in hyperglycemic mice compared to the normoglycemic treatment groups. This effect may result from insulin deficiency and has been previously noted in both animal models and young patients with diabetes mellitus[27, 28] Valproate-supplementation did not significantly affect blood glucose or plasma homocysteine concentrations in any of the groups (Table 3.1). In hyperglycemic and hyperhomocysteinemic mice, total plasma cholesterol and plasma lipid profiles were similar to those of control mice (Table 3.1 and Supplementary Figure I). As expected high fat diet was associated with increased total plasma cholesterol relative to standard chow fed controls. Valproate-supplementation did not affect plasma lipid profiles in hyperglycemic or hyperhomocysteinemic mice and was associated with a slight, non-significant decrease in very low-density lipoprotein (VLDL) and LDL sized particles in high fat fed mice.

Table 3.1. Metabolic parameters in ApoE$^{-/-}$ mice

	Experimental Group								
	control 15 wk	control +V	HG	HG +V	HH	HH +V	control 24 wk	HF	HF +V
body weight (g)	20.9±1.8	20.9±1.1	19.5±0.6	20.1±1.6	21.4±1.2	20.6±0.3	23.5±0.7	23.4±0.9	23.0±0.5
lesion volume ($10^{-3}mm^3$)	3.80±0.55	3.21±0.56	8.62±1.23*	4.98±0.76†	7.83±0.99*	5.26±0.50†	87.5±1.90	208±9.0*	187±8.0†
Plasma									
valproate (µmol/L)	0	37.5±14.9	0	33.7±6.2	0	54.2±11.3	0	0	7.3±5.4
glucose (mmol/L)	10.5±2.0	9.4±2.6	23.2±5.6‡	27. 0±0.9‡	10.6±0.8	7.9±3.9	8.5±0.3	11.2±0.9*	10.3±0.5*
homocysteine (µmol/L)	4.6±0.8	5.2±0.8	1.9±1.8	1.2±0.5	14.1±4.0‡	21.2 ±2.9§	4.1±1.8	1.7±1.4	1.9±1.0
cholesterol (mmol/L)	11.6±2.1	13.1±3.7	12.7±3.1	13.5±3.5	15.1±0.6	14.0±1.1	14.8±2.7	25.0±3.6*	19.4±1.8

n = 9-16/treatment group for each measurement

*P<0.05 relative to control mice fed the non-supplemented (control) diet.

†P<0.05 relative to the same group fed control diet

‡P<0.05 relative to control mice fed the same diet

The effects of valproate-supplementation on accelerated atherosclerosis

Both hyperglycemia and hyperhomocysteinemia significantly increased mean atherosclerotic lesion volume at the aortic root of 15 week old female ApoE$^{-/-}$ mice (Figure 3.1 and Table 3.1). Mice fed valproate-supplemented diets had significantly reduced cross sectional lesion area and total mean lesion volume than the mice fed control diet (4.98±0.76 versus 8.62±1.23 x 10^{-3} mm^3, P<0.05 in hyperglycaemic mice, and 5.26±0.50 versus 7.83±0.99 x 10^{-3} mm^3, P<0.05 in hyperhomocysteinemic mice). Twenty-four week old mice fed high fat diet had significantly larger lesion volume compared to the mice fed control diet (208±9 versus 87.5±1.9 x 10^{-3} mm^3, P<0.05) and the littermates fed the high fat diet supplemented with valproate had significantly reduced atherosclerotic lesion volume (187±8 versus 208±9 x 10^{-3} mm^3, P<0.05) (Figure 3.1 and Table 3.1).

Atherosclerotic lesions from each group were further characterized by measuring necrotic area. Plaque necrosis, defined as acellular regions of the lesion, was quantified and is presented relative to total lesion volume. Hyperglycemic, hyperhomocysteinemic and high fat fed mice had significantly increased levels of necrosis within lesion areas relative to controls (Figure 3.1C). With valproate-supplementation, the proportion of necrosis was significantly reduced in all models (Figure 3.1C).

Atherosclerotic lesion areas were determined in descending aortas by staining *en face* with Sudan IV. Few lesions were found in the descending aortas of 15 week old control, hyperglycemic, or hyperhomocysteinemic ApoE$^{-/-}$ mice (data not shown). At 24 weeks of age, however, there was detectable lesion development along the entire aorta. High fat feeding increased atherosclerotic lesion areas approximately 3 fold relative to age-matched controls (Supplementary Figure II). Similar to the effects observed at the

aortic sinus, valproate-supplementation significantly reduced lesion area in the descending aorta (Supplementary Figure II).

Figure 3.1. The effect of valproate supplementation on accelerated atherosclerosis. A) Representative hematoxylin and eosin stained cross sections of the aortic sinus from 15 week old control (C), hyperglycemic (HG), hyperhomocysteinemic (HH) or 24 week old high fat diet fed (HF) female $ApoE^{-/-}$ mice. Arrows indicate atherosclerotic lesions. **B)** Quantification of atherosclerotic lesion area in the ascending aorta. **C)** Necrotic area within plaque as a percentage of total plaque size. $^{*}P<0.05$ relative to control mice fed the non-supplemented (control) diet. # $P<0.05$ relative to the same group fed control diet, n=9-10/group **(A and B)**, n=4-5/group **(C)**.

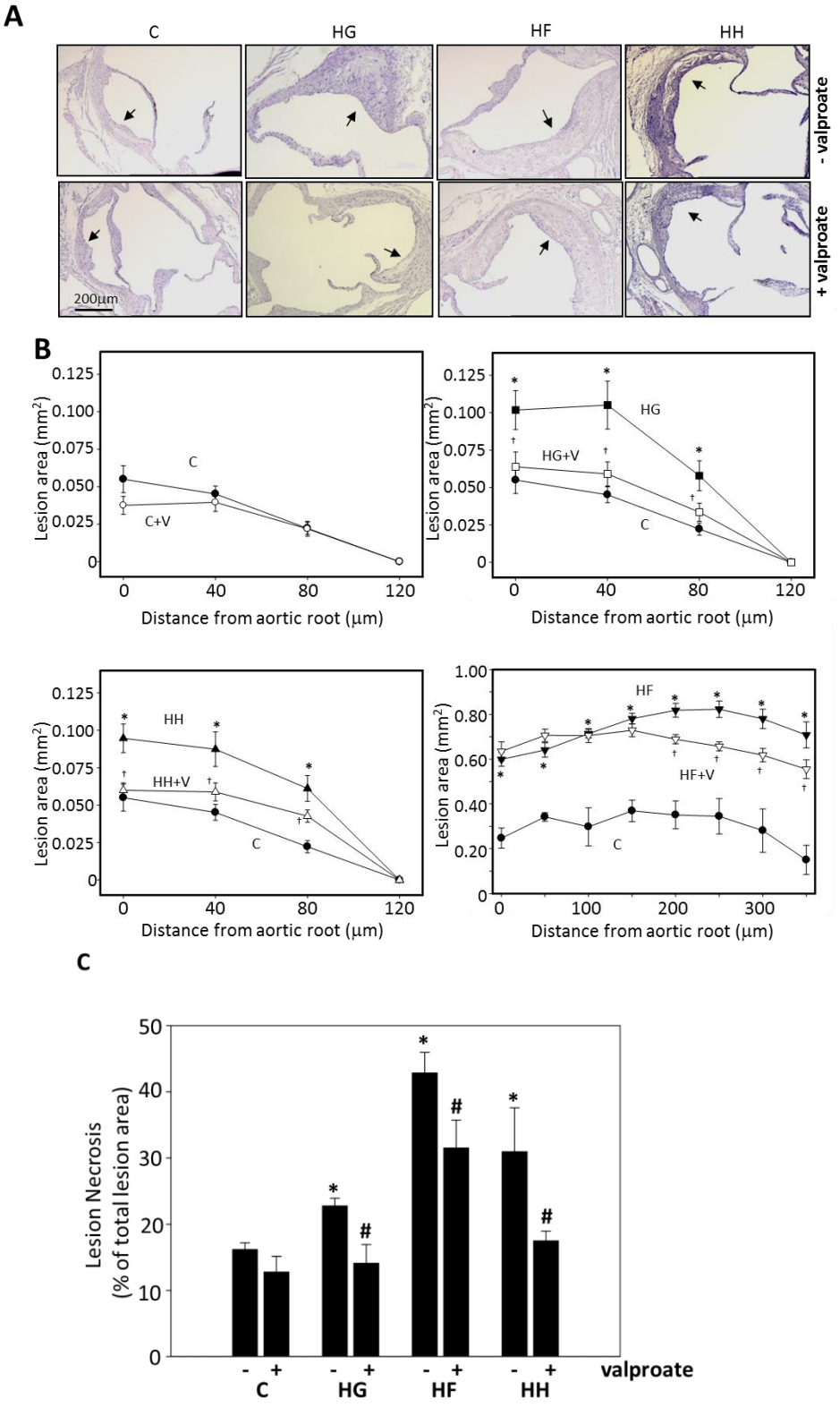
A
C
HG
HF
HH
- valproate
+ valproate
200µm
B
Lesion area (mm²)
Distance from aortic root (µm)
C
HG
HG+V
HH
HH+V
HF
HF+V
C
Lesion Necrosis
(% of total lesion area)
valproate
C
HG
HF
HH

Hepatic and aortic ER stress levels

Immunohistochemical and immunoblot analyses were used to evaluate ER stress levels in the different experimental groups. Consistent with previous observations[8, 23], hyperglycemia, hyperhomocysteinemia and high fat feeding were each associated with increased ER stress response protein expression. Immunoblot analysis of hepatic GRP78, GRP94 and PDI protein levels show significantly elevated levels of all ER stress markers in each of the mouse models (Figure 3.2A and B). Aortic immunohistochemical analysis demonstrated increased expression of GRP78/94 and CHOP by probing with anti-KDEL and anti-CHOP antibodies respectively (Figure 3.2C and D). Valproate-supplementation did not significantly alter the intensity or staining pattern of the ER stress response proteins nor did it significantly affect the levels of ER stress markers in any of the models and tissues examined.

Figure 3.2. ER stress levels in hyperglycemic, hyperhomocysteinemic and high fat fed ApoE$^{-/-}$ mice. A) Equal amounts of total liver lysate protein from C, HG. HF, or HH ApoE$^{-/-}$ mice, plus or minus valproate-supplementation, were resolved by SDS PAGE and probed for diagnostic ER stress markers, GRP78, GRP94 and PDI. **B)** Immunoblots were quantified by densitometry. All protein levels were normalized to β actin and plotted relative to the control. **C)** Representative aortic sections immunostained with an anti-KDEL antibody recognizing GRP78 and GRP94 (upper panels) or an antibody against CHOP (lower panels). Arrows indicate positively stained cells. **D)** Quantification of the number of positively stained cells per lesion relative to non-supplemented control mice. *P<0.05 relative to the corresponding control, n=6-8/group.

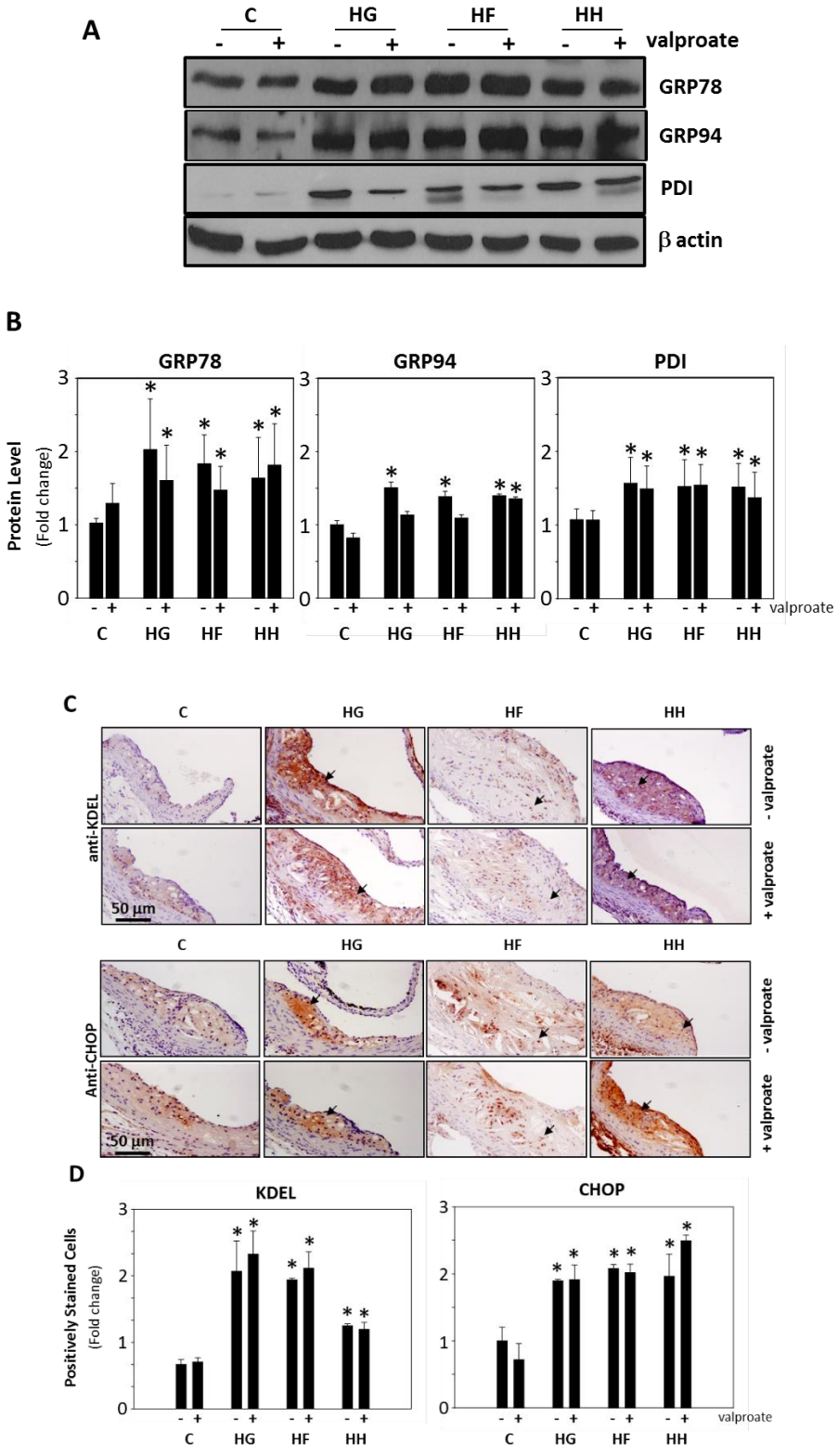
A
C
HG
HF
HH
valproate
GRP78
GRP94
PDI
β actin
B
GRP78
GRP94
PDI
Protein Level
(Fold change)
valproate
C
HG
HF
HH
C
anti-KDEL
Anti-CHOP
- valproate
+ valproate
50 μm
D
KDEL
CHOP
Positively Stained Cells
(Fold change)

Lipid accumulation and the effects of valproate-supplementation

Diabetes mellitus, severe hyperhomocysteinemia and high fat diet have each been associated with the accumulation of hepatic lipids leading to non-alcoholic fatty liver.[8, 29] Conditions of ER stress have been shown to promote lipid accumulation in specific cell types, including hepatocytes, by dysregulating SREBP-controlled cholesterol and triglyceride biosynthesis and/or uptake.[30] We quantified the relative hepatic neutral lipid levels in our hyperglycemic, hyperhomocysteinemic and high fat fed ApoE$^{-/-}$ mice by Oil Red O staining of frozen liver sections (Figure 3.3A). Results show a significant accumulation of hepatic lipid in each of the models, relative to controls. In hyperglycemic and hyperhomocysteinemic mice, valproate-supplementation significantly reduced lipid concentrations to levels observed in the age matched control mice. High fat fed mice showed no significant change in hepatic lipid levels when supplemented with valproate (Figure 3.3B).

The role of GSK3β in ER stress-induced lipid accumulation

To begin to examine the specific role of GSK3β in lipid accumulation, HepG2 cells were cultured in the presence of ER stress inducing agents, tunicamycin (8μg/mL) or palmitic acid (250 μM). Consistent with previous findings, conditions of ER stress were associated with significant intracellular lipid accumulation as determined by Oil Red O staining (Supplementary Figure III). Pretreatment of cells with 5 mM valproate, or 200 μM of a specific GSK3 inhibitor, GSK3 Inhibitor II, attenuated lipid accumulation. This finding indicates that GSK3α/β activity is required for ER stress-induced lipid accumulation and is consistent with our hypothesis that ER stress signals through GSK3β and that valproate blocks ER stress-induced GSK3β activity.

Figure 3.3. Hepatic lipid accumulation and the effect of valproate supplementation. **A)** Representative sections of liver from C, HG, HH or HF ApoE$^{-/-}$ mice, fed control diet or valproate-supplemented diet, as indicated, were stained with Oil Red O. **B)** Quantification of Oil Red O staining in liver sections. $^{*}P<0.05$ relative to control mice fed the non-supplemented diet. $^{\#}P<0.05$ relative to the same group fed non-supplemented diet, n=12/group.

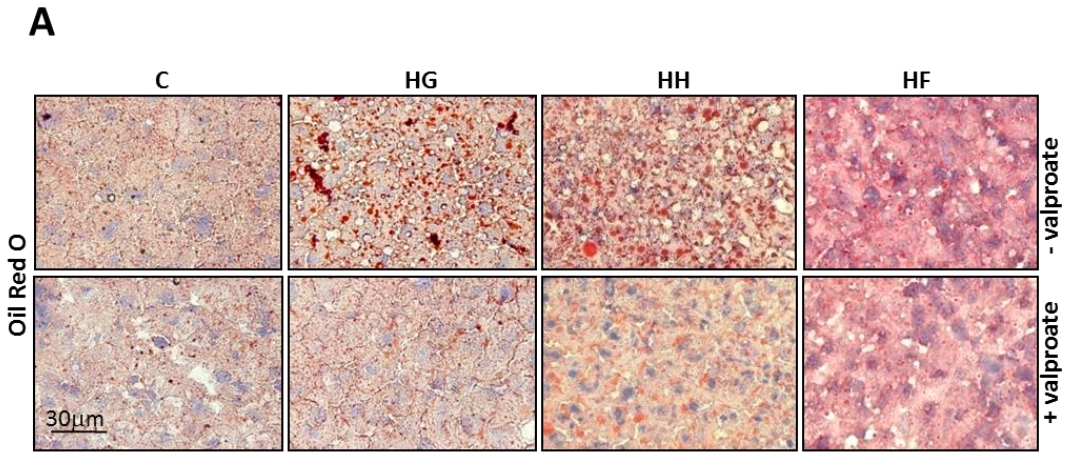
A
C
HG
HH
HF
Oil Red O
- valproate
+ valproate
30μm

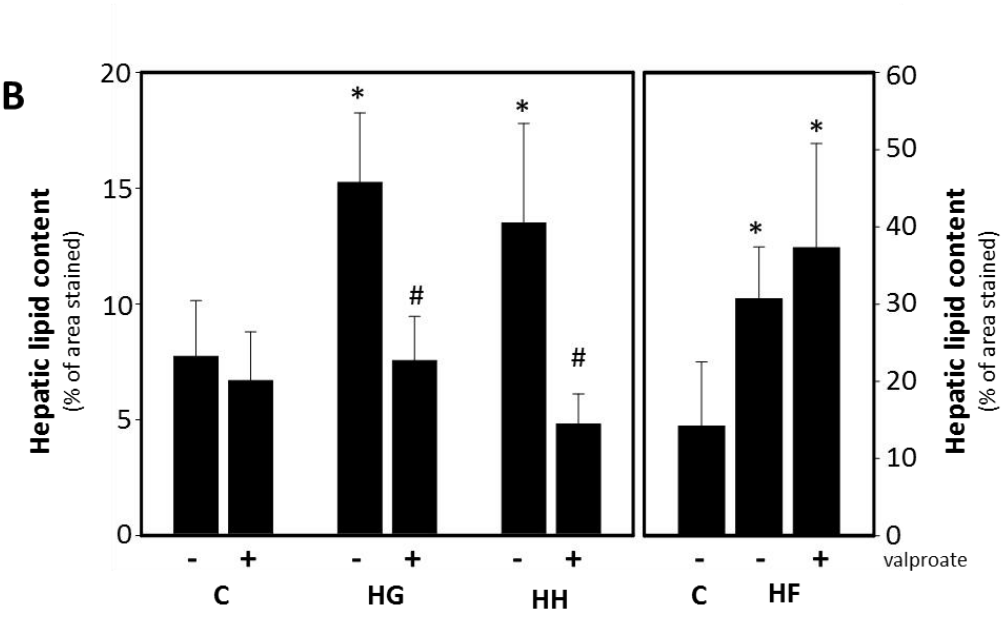
B
Hepatic lipid content
(% of area stained)
Hepatic lipid content
(% of area stained)
valproate
C
HG
HH
C
HF

GSK3β regulation in mouse models of accelerated atherosclerosis

In order to determine the relative effects of hyperglycemia, hyperhomocysteinemia and high fat diet on hepatic GSK3β activity we immunoprecipitated total GSK3β from homogenized liver lysates and monitored its ability to incorporate ^{32}P into a phospho-primed glycogen synthase peptide (p-GS2) substrate. We found that conditions/treatments that increased ER stress levels and accelerated atherosclerosis were associated with significantly enhanced GSK3β activity (Figure 3.4A). Dietary supplementation with valproate attenuated activation of GSK3β in hyperglycemic, hyperhomocysteinemic and high fat fed mice, but had no effect on basal level GSK3β activity in control mice.

GSK3β can be regulated by post-translational phosphorylation of specific tyrosine and serine residues that can enhance (phospho-Y^{216}) or inhibit (phospho-S^{9}) GSK3β kinase activity.[31, 32] We investigated the phosphorylation status of GSK3β by immunoblot analysis of protein isolated from mouse liver using antibodies specific for total GSK3β, phospho-S^{9}-GSK3β or phospho-Y^{216} GSK3β. Phosphorylated GSK3β levels were normalized to total GSK3β for each treatment group. Our results show that conditions of hyperglycemia, hyperhomocysteinemia and high fat feeding do not significantly affect total GSK3β or phospho-S^{9}-GSK3β levels (Figure 3.4B and C). Dietary supplementation with valproate did significantly increase the relative levels of phosphorylation on S^{9} in each of the treatment groups. This finding is consistent with the observed attenuation of GSK3β activity in liver lysates from valproate-supplemented mice (Figure 3.4A). Hyperglycemia, hyperhomocysteinemia and high fat feeding were associated with increased levels of phospho-Y^{216}-GSK3β relative to the control groups. Dietary supplementation with valproate appeared to reduce Y^{216} phosphorylation to

basal levels in the treatment groups and had no effect on Y^{216} phosphorylation in the control group. Together these results suggest that GSK3β activity is regulated, at least in part, by ER stress and valproate-induced changes in phosphorylation patterns.

Immunohistochemical staining was performed on fixed cross sections of aortic root to determine if the correlation between ER stress and the activation of GSK3β observed in the liver was also present in the developing atherosclerotic lesion. Sections stained with an antibody specific for phospho-S^{9}-GSK3β showed increased staining in the vessel wall of mice fed a valproate-supplemented diet relative to mice fed a non-supplemented standard diet (Figure 3.5A). The presence of hyperglycemia, hyperhomocysteinemia, or relative dyslipidemia was associated with increased levels of phospho-Y^{216}-GSK3β (Figure 3.5B). Mice receiving valproate-supplementation had decreased phospho-Y^{216} staining relative to non-supplemented controls. Generally, staining was most intense in the macrophage foam cells within the atherosclerotic lesion. Total GSK3β protein levels were not significantly affected by any of the treatments (data not shown)**.** These results suggest that GSK3β, in the liver and the atherosclerotic lesion, are regulated in a similar manner in response to pro-atherosclerotic stimuli and valproate-supplementation.

Figure 3.4. Hepatic GSK3β activity and phosphorylation in hyperglycemic, hyperhomocysteinemic and high fat diet fed mice. A) GSK3β was immunoprecipitated from total protein lysates prepared from the livers of C, HG, HF and HH mice plus or minus valproate-supplementation, as indicated. GSK3β kinase activity was determined by monitoring ^{32}P incorporation onto a phopho-primed glycogen synthase derived peptide (pGS2). Activities are presented relative to un-supplemented control. **B)** Immunoblot analysis of total protein isolated from C, HG, HF or HH liver, in the presence or absence of valproate-supplementation, as indicated. Total protein lysates were resolved by SDS-PAGE, transferred to nitrocellulose membranes, and immunostained with antibodies specific for phospho-S^{9}-GSK3β, phopho-Y^{216}-GSK3β, total GSK3β, or β actin, as indicated. **C)** All protein levels were quantified by densitometry, phospho-S^{9}-GSK3β and phopho-Y^{216}-GSK3β were normalized to total GSK3β and presented relative to the levels found in non-supplemented control liver. *P<0.05 relative to non-supplemented control. #P<0.05 relative to non-supplemented mice from the same treatment group, n=6-8/group.

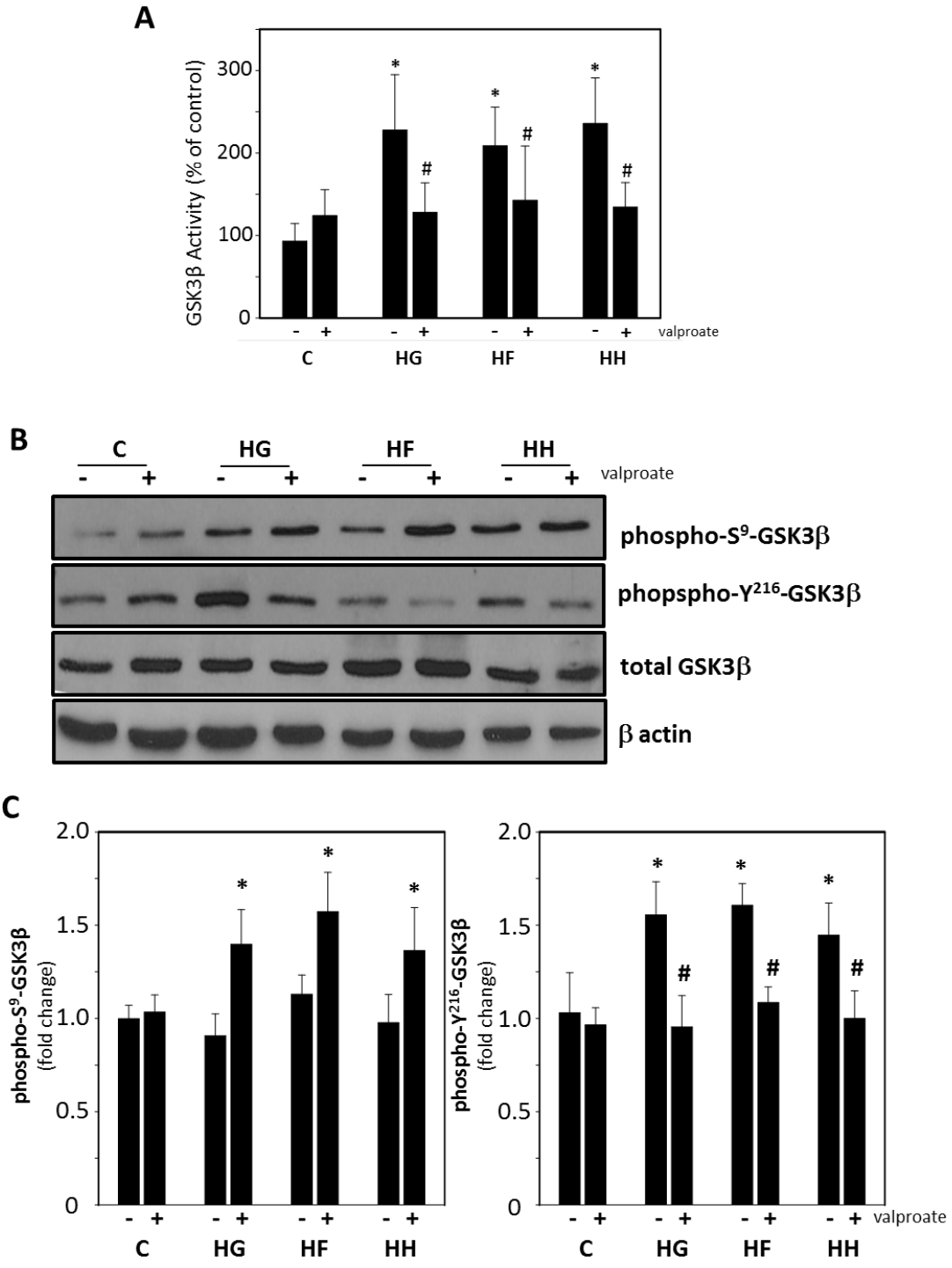
A
GSK3β Activity (% of control)
300
200
100
0
*
#
- + - + - + - +
valproate
C HG HF HH
B
C HG HF HH
- + - + - + - +
valproate
phospho-S9-GSK3β
phopspho-Y216-GSK3β
total GSK3β
β actin
C
phospho-S9-GSK3β (fold change)
phospho-Y216-GSK3β (fold change)
2.0
1.5
1.0
0.5
0
- + - + - + - +
valproate
C HG HF HH

Figure 3.5. Aortic GSK3β phosphorylation in hyperglycemic, hyperhomocysteinemic and high fat diet fed mice. Representative sections of aorta sinus from C, HG, HH, or HF ApoE$^{-/-}$ mice, with and without valproate supplementation as indicated, were immunostained with antibodies specific for **A)** phospho-S^{9}-GSK3β or **B)** phopho-Y^{216}-GSK3β. Arrows indicate positively stained cells. n=5-6/group.

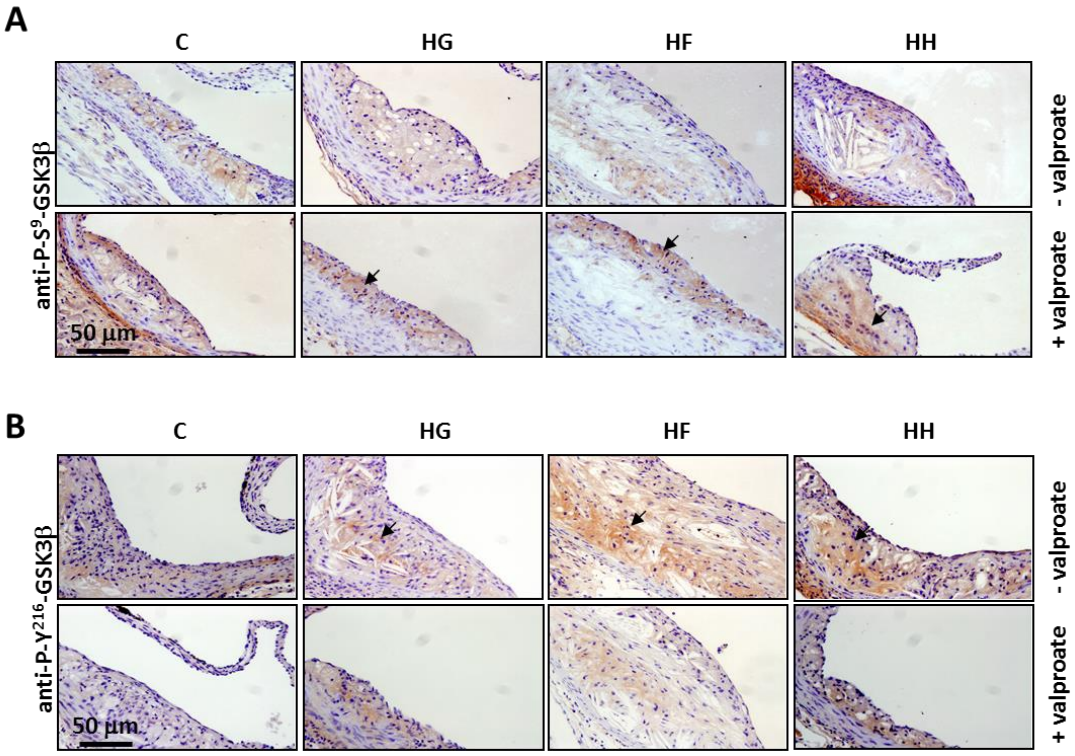
A
C
HG
HF
HH
anti-P-S9-GSK3β
- valproate
+ valproate
50 µm
B
C
HG
HF
HH
anti-P-Y216-GSK3β
- valproate
+ valproate
50 µm

3.6 DISCUSSION

A diverse, but finite, array of risk factors has been associated with the development of cardiovascular disease. These include dyslipidemia, smoking, stress, diabetes mellitus, hypertension, obesity and sedentary lifestyle.[3] Despite considerable advances, our understanding of the molecular mechanisms by which multiple risk factors actively promote atherosclerosis, the underlying cause of myocardial infarction, remains incomplete.

In this study we investigated the potential role of ER stress signaling and GSK3β activation in the development and progression of atherosclerosis induced by three established cardiovascular risk factors. We found elevated levels of diagnostic markers of ER stress and increased GSK3β activity in the livers and atherosclerotic lesions of hyperglycemic, hyperhomocysteinemic and high fat fed mice relative to age matched controls. There was a direct correlation between these changes and the accelerated development of atherosclerosis in each of the mouse models. Mice fed a diet supplemented with valproate exhibited similar ER stress levels as non-supplemented controls, but had attenuated GSK3β activity and significantly reduced atherosclerotic lesion volume. Together, these data support a role for ER stress-induced GSK3β activity in the accelerated development of hepatic steatosis and atherosclerosis in ApoE$^{-/-}$ mice and identify GSK3β as a potential target for anti-atherogenic interventions.

Elevated levels of ER stress have previously been observed in mouse models of hyperglycemia [7], hyperhomocysteinemia[8] and obesity[9]. The molecular mechanisms by which these conditions promote ER stress and/or activate the UPR are not fully understood. In cultured cells, both low and high concentrations of glucose have been associated with ER stress and the glucose metabolite, glucosamine, is an especially

potent ER stress-inducing agent.[23, 33] Alterations in intracellular glucose concentration may disrupt ER homeostasis by interfering with the N-linked glycosylation of proteins, a major factor in proper protein folding, however there is little direct evidence for this at the present time. Elevated concentrations of homocysteine are associated with ER stress and induction of the UPR in cultured cells as well as in animal models of hyperhomocysteinemia.[8, 34] It has been suggested that the free thiol of homocysteine can interfere with disulfide bond formation - an essential event in the proper folding of many proteins in the ER.[35] There is also evidence that elevated homocysteine concentration disrupts Ca^{2+} homeostasis in the ER.[36] The mechanism by which high fat feeding and/or the resulting dyslipidemia may promote ER stress is not completely understood. Specific lipids, including palmitate and unesterified cholesterol, have been shown to induce the UPR in cultured cells perhaps by directly altering the consistency and function of the ER membrane.[37, 38] More recently, other factors and conditions associated with cardiovascular risk have been shown to promote ER stress, including cigarette smoke and obesity.[9, 10] The association of multiple risk factors with ER stress suggests that activation of ER stress response pathways play a central role in accelerated atherosclerosis. Therefore it is important to investigate how ER stress activates pro-atherogenic mechanisms.

The UPR intersects directly and indirectly with many different stress-signaling pathways. There is increasing evidence of the ability of ER stress to signal through GSK3.[18, 39, 40] GSK3α and β are homologous, ubiquitously expressed, serine/threonine kinases that are involved in a variety of intracellular signaling pathways.[41] Dysregulation of GSK3 activity has been implicated in the development of cancer, Alzheimer's disease, bipolar disorder, cardiac myopathy and insulin resistance.[42] We have shown that GSK3-

deficient cultured mouse embryonic fibroblasts are protected from glucosamine-induced lipid accumulation and that this effect could be mimicked by pretreatment of wild type MEFs with valproate, or other compounds with GSK3 inhibitory properties.[22] Recently it has been shown that GSK3 inhibition attenuates ER stress-induced lipid-associated apoptosis in cultured hepatocytes.[43] These findings directly lead to the experiments described in this report that test the ability of valproate to attenuate accelerated atherosclerosis in ApoE$^{-/-}$ mouse models.

Intracellular control of GSK3βα/β activity is relatively complex and can be modulated through interactions with a number of different scaffold proteins (axin, APC) as well as intracellular localization.[44] Regulation appears to predominantly occur by phosphorylation and dephosphorylation of specific residues. GSK3β activity is inhibited by phosphorylation of an amino-terminal serine residue (S^9).[31] Most evidence suggests that Akt is responsible for phosphorylating S^9 of GSK3β however other kinases may also play a role.[45] Activation of GSK3β has been associated with phosphorylation of a specific tyrosine residue (Y^{216}).[46, 47] Lochhead *et al* (2006) have suggested that nascent GSK3β acts as a tyrosine kinase that auto-phosphorylates Y^{216} during a protein maturation process.[48] Other studies have shown that Y^{216} phosphorylation/dephosphorylation is used as a mechanism to activate/inhibit the mature GSK3β protein.[49] The hierarchal relationships of these multiple GSK3 regulatory pathways are still being deciphered.

Our findings suggest atherogenic risk factors induce ER stress that leads to the activation of GSK3β, in hepatocytes and macrophage foam cells within the atherosclerotic lesion. Our results suggest that conditions of ER stress activate GSK3β by increasing the relative phosphorylation of Y^{216}. Furthermore, we show that valproate, in addition to its ability to directly inhibit GSK3β[21], can also alter the phosphorylation

status of GSK3β. Specifically, *in vivo* treatment with valproate is associated with a relative increase in the phosphorylation of S^{9} and decreased phosphorylation of Y^{216}. The mechanisms by which this occurs have yet to be determined but likely involve the ability of valproate to interact with upstream kinases and/or phosphatases. Previous studies have suggested that valproate can affect GSK3β activity by inhibition of Akt.[26]

Valproate is a potent and commonly prescribed drug that acts both as an anti-convulsant in the treatment of epilepsy, and as a mood-stabilizer to control bipolar disorder.[50] A recently published pharmacoepidemiological study has shown that epileptic patients taking valproate have a significantly reduced risk of myocardial infarction.[51] Despite its wide use, the specific molecular mechanism(s) responsible for the clinical efficacy is not known. Exposure to millimolar concentration of valproate can induce a variety of cellular responses that may be responsible for its clinical effectiveness. In addition to its ability to inhibit GSK3, it has been reported that valproate potentiates GABA-mediated postsynaptic inhibition[52], depletes intracellular inositol concentrations[53], inhibits histone deacetylases (HDAC)[54] and induces the expression of cellular chaperones.[55, 56] Our data are consistent with a mechanism by which the anti-atherogenic effects of valproate are conferred by its ability to inhibit GSK3β activity. In support of this hypothesis, we show that valproate, and another more specific inhibitor of GSK3, attenuate ER stress-induced lipid accumulation in cultured cells. In addition, we have previously shown that valproate protects cultured cells from ER stress-induced apoptosis.[56] Together these findings may explain the reduction in total volume, and decreased necrotic area, of atherosclerotic lesions in valproate-supplemented mice. Further studies, perhaps using GSK3-deficient mice, will be required to further test the role of GSK3 in pro-atherogenic signaling pathways.

These studies identify a role for ER stress-GSK3 signaling in the progression and development of atherosclerosis. Furthermore, they suggest a mechanism by which pro- and anti-atherogenic signals are transmitted via alterations to the phosphorylation status of GSK3β. This is potentially an important step toward our overall understanding of the molecular and cellular mechanisms that lead to cardiovascular disease in that it may provide a new and unexplored class of targets for the development of anti-atherogenic drug therapeutics.

3.7 REFERENCES FOR CHAPTER 3

1. Ross R. Atherosclerosis – an inflammatory disease. *New Engl J Med.* 1999;340:115-126.
2. Glass CK, Witztum JL. Atherosclerosis – the road ahead. *Cell.* 2001;104:503-516.
3. Anand SS, Islam S, Rosengren A, Franzosi MG, Steyn K, Yusufali AH, Keltai M, Diaz R, Rangarajan S, Yusuf S; INTERHEART Investigators. Risk factors for myocardial infarction in women and men: insights from the INTERHEART study. *Eur Heart J*. 2008;29:932-940.
4. Lentz SR. Mechanisms of homocysteine-induced atherothrombosis. *J Thromb Haemost*. 2005;3:1646-1654.
5. Pahl HL. Signal transduction from the endoplasmic reticulum to the cell nucleus. *Physiol Rev.* 1999;79:683-701.
6. Kaufman RJ. Stress signaling from the lumen of the endoplasmic reticulum: coordination of gene transcriptional and translational controls. *Genes Dev.* 1999;13:1211-1233.
7. Khan MI, Pichna B, Shi YY, Bowes AJ, Werstuck GH. Endoplasmic Reticulum Stress plays a Causal Role in the Development of Atherosclerosis in a Hyperglycemic Mouse Model. *Antioxid Sig Res.* 2009;11:2289-2298.
8. Werstuck GH, Lentz SR, Dayal S, Shi Y, Hossain GS, Sood SK, Krisans SK, Austin RC. Homocysteine-induced endoplasmic reticulum stress causes dysregulation of the cholesterol and triglyceride biosynthetic pathways. *J Clin Invest.* 2001;107:1263-1273.
9. Özcan U, Cao Q, Yilmaz E, Lee A-H, Iwakoshi NN, Özdelen E, Tuncman G, Görgun C, Glimcher LH, Hotamisligil GS. Endoplasmic reticulum stress links obesity, insulin action, and type 2 diabetes. *Science.* 2004;306:457-461.
10. Kelsen SG, Duan X, Ji R, Perez O, Liu C, Merali S. Cigarette smoke induces an unfolded protein response in the human lung: a proteomic approach. *Am J Respir Cell Mol Biol.* 2008;38:541-550.
11. Li Y, Schwabe RF, Devries-Seimon T, Yao PM, Gerbod-Giannone MC, Tall AR, Davis RJ, Flavell R, Brenner DA,Tabas I. Free cholesterol-loaded macrophages

are an abundant source of TNF-alpha and IL-6. Model of NF-kappa B- and MAP kinase-dependent inflammation in advanced atherosclerosis. *J Biol Chem*. 2005;280:21763-21772.
12. Gwiazda KS, Yang TL, Lin Y, Johnson JD. Effects of palmitate on ER and cytosolic Ca2+ homeostasis in beta-cells. *Am J Physiol Endocrinol Metab*. 2009;296:E690-E701.
13. Karaskov E, Scott C, Zhang L, Teodoro T, Ravazzola M, Volchuk A. Chronic palmitate but not oleate exposure induces endoplasmic reticulum stress, which may contribute to INS-1 pancreatic beta-cell apoptosis. *Endocrinology.* 2006;147:3398-3407.
14. Civelek M, Manduchi E, Riley RJ, Stoeckert CJ Jr, Davies PF. Chronic Endoplasmic Reticulum Stress Activates Unfolded Protein Response in Arterial Endothelium in Regions of Susceptibility to Atherosclerosis. *Circ Res.* 2009;105:453-461.
15. Shimano H, Horton JD, Hammer RE, Shimomura I, Brown MS, Goldstein JL. Overproduction of cholesterol and fatty acids causes massive liver enlargement in transgenic mice expressing truncated SREBP-1a. *J Clin Invest.* 1996;98:1575-1584.
16. Jiang HY, Wek SA, McGrath BC, Scheumer D, Kaufman RJ, Cavener DR, Wek RC. Phosphorylation of the alpha subunit of eukaryotic initiation factor 2 is required for activation of NF-kappaB in response to diverse cellular stresses. *Mol Cell Biol*. 2003;23:5651-5663.
17. Zinszner H, Kuroda M, Wang XZ, Batchvarova N, Lightfoot RT, Remotti H, Stevens JL, Ron D. CHOP is implicated in programmed cell death in response to impaired function of the endoplasmic reticulum. *Genes Dev*. 1998;12:982-995.
18. Song L, De Sarno P, Jope RS. Central role of glycogen synthase kinase-3beta in endoplasmic reticulum stress-induced caspase-3 activation. *J Biol Chem.* 2002;277:44701-44708.
19. Hoeflich KP, Luo J, Rubie EA, Tsao MS, Jin O, Woodgett JR. Requirement for glycogen synthase kinase-3beta in cell survival and NF-kappaB activation. *Nature* 2000;406:86-90.
20. Demarchi F, Bertoli C, Sandy P, Schneider C. Glycogen synthase kinase-3 beta regulates NF-kappa B1/p105 stability. *J Biol Chem.* 2003;278:39583-39590.
21. Werstuck GH, Kim AJ, Brenstrum T, Ohnmacht SA, Panna E, Capretta A. Examining the correlations between GSK-3 inhibitory properties and anticonvulsant efficacy of valproate and valproate-related compounds. *Bioorg Med Chem Lett.* 2004;14:5465-5467.
22. Bowes A, Khan M, Shi Y, Robertson L, Werstuck G. Valproate attenuates accelerated atherosclerosis in hyperglycemic apoE-deficient mice: evidence in support of a role for endoplasmic reticulum stress and glycogen synthase kinase-3 in lesion development and hepatic steatosis. *Am J Pathol*. 2009;174::330-342.
23. Werstuck GH, Khan MI, Femia G, Kim AJ, Tedesco V, Trigatti B, Shi YY. Glucosamine-induced endoplasmic reticulum stress is associated with accelerated atherosclerosis in a hyperglycaemic mouse model. *Diabetes.* 2005;55:93-101.
24. Paigen B, Morrow A, Holmes PA, Mitchell D, Williams RA. Quantitative assessment of atherosclerotic lesions in mice. *Atherosclerosis.* 1987;68:231-240.

25. Chen G, Huang L-D, Jiang Y-M, Manji HK. The mood-stabilizing agent valproate inhibits the activity of glycogen synthase kinase-3. *J Neurochemistry.* 1999;72:1327-1330.
26. De Sarno P Li X, Jope RS. Regulation of Akt and glycogen synthase kinase-3 beta phosphorylation by sodium valproate and lithium. *Neuropharmacology. 2002;*43:1158-1164.
27. Jacobs RL, House JD, Brosnan ME, Brosnan JT. Effects of streptozotocin-induced diabetes and of insulin treatment on homocysteine metabolism in the rat. *Diabetes*. 1998; 47:1967-1970.
28. Cotellessa M, Minniti G, Cerone R, Prigione F, Calevo MG, Lorini R. Low total plasma homocysteine concentrations in patients with type 1 diabetes. *Diabetes Care*. 2001; 24:969-971.
29. Loria P, Lonardo A, Targher G. Is liver fat detrimental to vessels?: intersections in the pathogenesis of NAFLD and atherosclerosis. *Clin Sci (Lond)* 2008;115:1-12.
30. Lee JN, Ye J. Proteolytic activation of SREBP induced by cellular stress through the depletion of Insig-1. *J Biol Chem.* 2004;279:45257-45265.
31. Cross DA, Alessi DR, Cohen P, Andjelkovich M, Hemmings BA. Inhibition of glycogen synthase kinase-3 by insulin mediated by protein kinase B. *Nature* 1995;378:785-789.
32. Murai H, Okazaki M, Kikuchi A. Tyrosine dephosphorylation of glycogen synthase kinase-3 is involved in its extracellular signal-dependent inactivation. *FEBS Lett.* 1996;392:153-160.
33. Lee AS, Bell J, Ting J. Biochemical characterization of the 94- and 78-kilodalton glucose-regulated proteins in hamster fibroblasts. *J Biol Chem.* 1984;259:4616-4621.
34. Zhou J, Werstuck GH, deKoning ABL, Hossain GS, Sood SK, Shi YY, Moller J, Ritskes-Hoitinga M, Falk E, Austin RC. Association of multiple cellular stress pathways with accelerated atherosclerosis in hyperhomocysteinemic ApoE-deficient mice. *Circulation.* 2004;110**:**207-213.
35. Ron D. Hyperhomocysteinemia and function of the endoplasmic reticulum. *J Clin Invest*. 2001;107:1221-1222.
36. Dickhout JG, Sood SK, Austin RC. Role of endoplasmic reticulum calcium disequilibria in the mechanism of homocysteine-induced ER stress. *Antioxid Redox Signal.* 2007;9:1863-1873.
37. Karaskov E, Scott C, Zhang L, Teodoro T, Ravazzola M, Volchuk A. Chronic palmitate but not oleate exposure induces endoplasmic reticulum stress, which may contribute to INS-1 pancreatic beta-cell apoptosis. *Endocrinology.* 2006;147:3398-3407.
38. Li Y, Schwabe RF, DeVries-Seimon T, Yao PM, Gerbod-Giannone MC, Tall AR, Davis RJ, Flavell R, Brenner DA, Tabas I. Free cholesterol-loaded macrophages are an abundant source of tumor necrosis factor-alpha and interleukin-6: model of NF-kappaB- and map kinase-dependent inflammation in advanced atherosclerosis. *J Biol Chem.* 2005;280:21763-21772.
39. Baltzis D, Pluquet O, Papadakis AI, Kazemi S, Qu LK, Koromilas AE. The eIF2alpha kinases PERK and PKR activate glycogen synthase kinase 3 to promote the proteasomal degradation of p53. *J Biol Chem.* 2007;282:31675-31687.

40. Qu L, Huang S, Baltzis D, Rivas-Estilla AM, Pluquet O, Hatzoglou M, Koumenis C, Taya Y, Yoshimura A, Koromilas AE. Endoplasmic reticulum stress induces p53 cytoplasmic localization and prevents p53-dependent apoptosis by a pathway involving glycogen synthase kinase-3beta. *Genes Dev.* 2004;18:261-277.
41. Doble BW, Woodgett JR. GSK-3: tricks of the trade for a multi-tasking kinase. *J Cell Sci*. 2003;116:1175-1186.
42. Martinez A. Preclinical efficacy on GSK-3 inhibitors: towards a future generation of powerful drugs. *Med Res Rev.* 2008;28:773-796.
43. Ibrahim SH, Akazawa Y, Cazanave SC, Bronk SF, Elmi NA, Werneburg NW, Billadeau DD, Gores GJ. Glycogen synthase kinase-3 (GSK-3) inhibition attenuates hepatocyte lipoapoptosis. J Hepatol. 2010 [Epub ahead of print].
44. Ali A, Hoeflich KP, Woodgett JR. Glycogen Synthase Kinase-3: Properties, Functions, and Regulation. *Chem Rev*. 2001;101:2527-2540.
45. van Weeren PC, de Bruyn KM, de Vries-Smits AM, van Lint J, Burgering BM. Essential role for protein kinase B (PKB) in insulin-induced glycogen synthase kinase 3 inactivation. Characterization of dominant-negative mutant of PKB. *J Biol Chem*. 1998;273:13150-13156.
46. Murai H, Okazaki M, Kikuchi A. Tyrosine dephosphorylation of glycogen synthase kinase-3 is involved in its extracellular signal-dependent inactivation. *FEBS Lett.* 1996;392:153-160.
47. Buescher JL, Phiel CJ. A non-catalytic domain of glycogen synthase kinase-3 (GSK-3) is essential for activity. *J Biol Chem. 2010;*285:7957-7963.
48. Lochhead PA, Kinstrie R, Sibbet G, Rawjee T, Morrice N, Cleghon V. A chaperone-dependent GSK3β transitional intermediate mediates activation-loop autophosphorylation. *Mol Cell. 2006;*24:627-633.
49. Bhat RV, Shanley J, Correll MP, Fieles WE, Keith RA, Scott CW, Lee C-M. Regulation and localization of tyrosine^{216} of glycogen synthase kinase-3 in cellular and animal models of neuronal degeneration. *Proc Natl Acad Sci USA.* 2000;97:11074-11079.
50. Penry JK, Dean JC. The scope and use of valproate in epilepsy. J Clin Psych. 1989;50:17-22.
51. Olesen JB, Hansen PR, Abildstrøm SZ, Andersson C, Weeke P, Schmiegelow M, Erdal J, Torp-Pedersen C, Gislason GH. Valproate attenuates the risk of myocardial infarction in patients with epilepsy: a nationwide cohort study. *Pharmacoepidemiol Drug Saf.* 2010 [Epub ahead of print]
52. MacDonald RL, Bergey GK. Valproic acid augments GABA-mediated postsynaptic inhibition in cultured mammalian neurons. *Brain Res*. 1979;170:558-562.
53. Williams RSB, Cheng L, Mudge AW, Harwood AJ . A common mechanism of action for three mood-stabilizing drugs. *Nature*. 2002;417:292-295.
54. Phiel CJ, Zhang F, Huang EY, Guenther MG, Lazar MA, Klein PS. Histone deacetylase is a direct target of valproic acid, a potent anticonvulsant, mood stabilizer, and teratogen. *J Biol Chem*. 2001;276:36734-36741.
55. Wang J-F, Bown C, Young LT. Differential display PCR reveals novel targets for the mood-stabilizing drug valproate including the molecular chaperone GRP78. *Mol Pharm*. 1999;55:521-527.

56. Kim AJ, Shi YY, Austin RC, Werstuck GH. Valproate protects cells from endoplasmic reticulum stress-induced lipid accumulation and apoptosis by inhibiting glycogen synthase kinase 3. *J Cell Sci*. 2005;118:89-99.

CHAPTER 4: Protein Kinase R-Like Endoplasmic Reticulum Kinase and Glycogen Synthase Kinase-3α/β Regulate Foam Cell Formation

Cameron S. McAlpine[1,3] and Geoff H. Werstuck[1,2,3]

Departments of [1]Medicine, [2]Biochemistry and Biomedical Sciences and the [3]Thrombosis and Atherosclerosis Research Institute, McMaster University, Hamilton, Ontario, Canada

4.1 FOREWORD

This study investigates the role of the UPR and GSK3α/β in macrophage foam cell formation. We demonstrate that ER stress activates GSK3α/β in a PERK dependent manner and that GSK3α/β mediates the expression of downstream components of the PERK pathway. Moreover, ER stress induced foam cell formation is attenuated by GSK3α/β or PERK inhibition. Constitutive GSK3β activation promotes foam cell formation despite PERK inhibition. Finally, $ApoE^{-/-}$ mice supplemented with valproate have reduced CHOP expression in macrophages isolated from the peritoneal cavity and in macrophages within their atherosclerotic lesions.

This work was published in the *Journal of Lipid Research*, volume 55, pages 2320-2333, November 2014. The experiments in this study were conducted by Cameron McAlpine. The manuscript was written by Cameron McAlpine in collaboration with Dr. Geoff Werstuck. The contents of Chapter 4 are a direct representation of this publication. The complete reference is as follows:

McAlpine CS, Werstuck GH. Protein kinase R-like endoplasmic reticulum kase and glycogen synthase kinase-3α/β regulate foam cell formation. *Journal of Lipid Research.* 2014;55:2320-2333.

4.2 ABSTRACT

Objective

Evidence suggests a causative role for endoplasmic reticulum (ER) stress in the development of atherosclerosis. This study investigated the potential role of glycogen synthase kinase (GSK)-3α/β in pro-atherogenic ER stress signaling.

Approach and results

Thp1-derived macrophages were treated with the ER stress-inducing agents, glucosamine, thapsigargin or palmitate. Using small molecule inhibitors of specific unfolded protein response (UPR) signaling pathways, we found that PERK, but not IRE1 or ATF6, is required for the activation of GSK3α/β by ER stress. GSK3α/β inhibition or siRNA-directed knockdown attenuated ER stress-induced expression of distal components of the PERK pathway. Macrophage foam cells within atherosclerotic plaques and isolated macrophages from $ApoE^{-/-}$ mice fed a diet supplemented with the GSK3α/β inhibitor valproate had reduced levels of CHOP. GSK3α/β inhibition blocked ER stress-induced lipid accumulation and the up regulation of genes associated with lipid metabolism. In primary mouse macrophages PERK inhibition blocked ER stress induced lipid accumulation whereas constitutively active S9A-GSK3β promoted foam cell formation and CHOP expression, even in cells treated with a PERK inhibitor.

Conclusions

These findings suggest that ER stress-PERK- GSK3α/β signaling promotes pro-atherogenic macrophage lipid accumulation.

4.3 INTRODUCTION

Atherosclerosis is an inflammatory disease within the walls of medium and large arteries.[1] It is the leading cause of cerebrovascular and cardiovascular diseases which together account for a third of all deaths in western societies.[1, 2] Multiple risk factors contribute to the initiation and progression of atherosclerosis including diabetes mellitus, hypertension, obesity, dyslipidemia, a sedentary life style and smoking.[3] One of the hallmark features of every stage of atherogenesis, from the fatty streak to the complex plaque, is the presence of lipid-laden macrophages known as foam cells. Intimal macrophage/foam cells accumulate lipids from LDL and modified LDL particles and secrete a variety of inflammatory cytokines. In advanced plaques, foam cells undergo apoptosis thereby contributing to the formation of a highly thrombotic, lipid rich, necrotic core (reviewed by Moore and Tabas[4]). The molecular events that promote the initiation and development of atherosclerosis are poorly understood. A better understanding of the signaling networks which regulate foam cell formation and atherosclerotic plaque development may lead to the identification of novel therapeutic targets.

The endoplasmic reticulum (ER) is the organelle responsible for the proper folding, modification and processing of secretory, transmembrane and ER resident proteins. If the processing capacity of the ER is overwhelmed, unfolded or misfolded proteins begin to accumulate - a condition known as ER stress. The accumulation of misfolded proteins triggers the initiation of the Unfolded Protein Response (UPR) which is composed of three signaling cascades regulated by ER transmembrane proteins (reviewed Schroder and Kaufman[5]). The activation of PKR-like endoplasmic reticulum kinase (PERK), inositol requiring enzyme (IRE)-1, and activating transcription factor (ATF)-6 coordinate the attenuation of protein translation and the increased expression of

cellular chaperones, as the cell attempts to reattain ER homeostasis. If these early, adaptive mechanisms are not successful at alleviating the stress, downstream components of the UPR will initiate pro-apoptotic pathways to eliminate the cell.
ER stress and UPR activation have been associated with the progression and development of atherosclerotic plaques. Multiple cardiovascular risk factors including hyperglycemia[6, 7], hyperhomocysteinemia[7, 8], obesity[9], cigarette smoke[10], as well as elevated concentrations of unesterified cholesterol[11] or palmitic acid[12] have each been shown to induce ER stress. ER stress and the activation of the UPR have been observed in atherosclerosis-prone areas of the vessel wall prior to lesion development[13] as well as at all stages of plaque progression.[14] Furthermore, the alleviation of ER stress with a chemical chaperone reduces atherosclerotic plaque size in apolipoprotein E-deficient ($ApoE^{-/-}$) mice.[15] ER stress has also been associated with the dysregulation of lipid metabolism by disruption of sterol regulatory element binding proteins (SREBPs)[8, 16], the induction of inflammation by nuclear factor(NF)-κB upregulation[17, 18] and activation of pro-apoptotic process by induction of C/EBP homologous protein (CHOP) expression.[19, 20] However, the molecular mechanism(s) by which ER stress and the UPR activate these and other pro-atherogenic pathways remain unresolved.

Glycogen synthase kinase (GSK)-3 is a serine/threonine kinase involved in several different cell signaling pathways (reviewed by Doble and Woodgett[21]). There are two forms of GSK3 encoded on separate genes, a 51 KDa alpha form and a 47 KDa beta form. Regulation of GSK3α/β activity is predominantly, but not entirely, through phosphorylation. Phosphorylation at residue serine21 of alpha and serine9 of beta is indicative of inhibition while phosphorylation at tyrosine279 of alpha and tyrosine216 of beta is associated with kinase activation. GSK3α/β activity can also be regulated by

altering its subcellular localization.[22, 23] Although GSK3α and GSK3β share 90% homology within the kinase domain, the enzymes have been shown to have both distinct as well as common substrates.[24-26] Recent evidence suggests that GSK3α/β's role in cell metabolism extends to ER stress and the activation of pro-atherogenic pathways. In cultured cells, conditions of ER stress activate GSK3β.[27, 28] *In vivo* studies have also demonstrated a role for GSK3α/β in the regulation of NF-κB.[29] Furthermore, our group and others have shown that inhibition ofGSK3α/β is associated with attenuated atherosclerotic developmentand reduced hepatic steatosis in different mouse models.[7, 30,31] However, the mechanism(s) by which ER stress modulates GSK3α and/or β, and how GSK3α/β regulates pro-atherogenic processes, remain unresolved. In this study, we present evidence showing that ER stress-induced GSK3α/β does not regulate the adaptive components of UPR signaling, but instead acts as a modulator of distal, pro-apoptotic elements of the PERK signaling pathway. Moreover, we demonstrate that inhibition of PERK-GSK3α/β signaling attenuates macrophage lipid biosynthesis and uptake, lipid accumulation and foam cell formation induced by ER stress.

4.4 METHODS

Cell culture and treatments

Thp-1 human monocytes were cultured in Roswell Park Memorial Institute 1640 medium (Invitrogen) containing 10% fetal bovine serum at 37˚C and 5% CO_2. Monocytes were differentiated into macrophages by exposing the cells to 100nmol/L phorbol-12-myristate-13-acetate (PMA) for 72 hours. Thioglycolate elicited peritoneal macrophages were isolated from 8 week old female C57BL6 mice or ApoE$^{-/-}$ mice and cultured in DMEM (Life Technologies) containing 10% fetal bovine serum.

Cultured cells were treated with 1μmol/L thapsigargin, 5mmol/L glucosamine or 600μmol/L palmitic acid coupled with 4% bovine serum albumin for 18 hours. Enzymatic activity was inhibited by pre-treating the cells with indicated inhibitors and concentrations for 2 hours. GSK3α/β activity was inhibited with 4μmol/L CT99021 (Cayman Chemical cat#13122). PERK was inhibited with 3μmol/L GSK2606414 (Millipore cat#516535), IREI was inhibited with 6μmol/L IRE1 Inhibitor III (Millipore cat#412512), and ATF6 was inhibited with 250μmol/L 4-(2-aminoethyl)benzenesulfonyl fluoride hydrochloride (AEBSF, Sigma Aldrich cat#A8456). Adenovirus infections were performed 72 hours prior to the experiments using 10 MOI of either an empty adenovirus vector (Ad-CMV-Null) or adenovirus encoding constitutively active GSK3β (Ad-CMV-S9A-GSK3β). GSK3α/β siRNA was purchased from Cell Signaling (cat#6301) and all siRNA experiments were conducted using antibody-free media. 50nmol/L scramble (control) or GSK3α/β siRNA was transfected into cells using Lipofectamine (Invitrogen cat#11668-019) for 8 hours and then treated, as indicated, 24 hours later.

Real time PCR

Total RNA was isolated from cultured cells using an RNeasy mini kit (Qiagen). RNA was quantified by measuring the absorbance at 260nm and RNA purity was verified by calculating the ratio of the absorbance at 260 and 280nm (A_{260}/A_{280}). cDNA was reverse transcribed from 1μg of RNA using Superscript II Reverse Transcriptase (Invitrogen). Real-time PCR was performed on the StepOne Plus (Applied Biosystems) using iQ SYBR Green Supermix (Bio-Rad), 1μg cDNA and 500nM forward and reverse primers. See Supplementary Table I for primer sequences and amplified product size.

Immunoblot

Total protein lysates were solubilized in kinase buffer containing; 50mmol/L Tris HCl pH 8.0, 150mmol/L NaCl, 5mmol/L EDTA, 50mmol/L NaF, 1% Triton X100, 10mmol/L DTT, 1mmol/L benzamidine, 1mmol/L PMSF and PhosSTOP Phosphatase Inhibitor (Roche). Protein lysates (15µg) were diluted in SDS-PAGE gel loading buffer, resolved by SDS-PAGE and transferred to nitrocellulose membranes. Blots were probed with primary antibodies against phospho-S51-EIF2α antibody (Cell Signaling cat# 3398), KDEL (Assay Designs, cat#SPA-827), PDI (Assay Designs cat#SPA-891), CHOP (Santa Cruz Biotechnology cat# sc-7351), β catenin (Cell Signaling cat# 9581), GSK3α/β (Cell Signaling 5676) or β actin (Sigma-Aldrich cat#A3854). After incubation with the appropriate primary and horseradish peroxidase (HRP)-conjugated secondary antibodies (Life Technologies), membranes weredeveloped using the Immobilon Western chemiluminescent HRP substrate (Millipore). Protein band intensities were quantified and normalized to β-actin.

Animal models

Five week old female apolipoprotein E-deficient ($ApoE^{-/-}$)($B6.129P2\text{-}ApoE^{tm1Unc}$) mice (n=24), purchased from Jackson Labs (stock number 002050), were placed on a high fat diet containing 21% milk fat and 0.2% cholesterol (Harlan Teklad, TD97363). After one week, half of the mice (n=12) were switched to a HFD supplemented with 625 mg/kg sodium valproate while the other half of the mice (n=12) remained on unsupplemented HFD. All mice had unrestricted access to both food and water throughout the study. Mice were sacrificed at 24 weeks of age for atherosclerotic plaque analysis or 8 weeks of age for analysis of peritoneal macrophages and blood and tissues

were collected for further analysis. The McMaster University Animal Research Ethics Board approved all procedures.

Immunofluorescence

Mice were euthanized, vasculature was flushed with 1X PBS and perfusion-fixed with 10% neutral buffered formalin. Liver and heart, including the aortic root, were removed and embedded in paraffin. Serial sections (4 μm thick) of aortic root were collected on pre-coated glass slides. Sections were stained with primary antibodies against KDEL, CHOP (Santa Cruz cat#sc-575), or Mac3 (Becton Dickson Co. cat# 553322). Serial sections were stained with pre-immune IgG, in place of primary antibodies, to control for non-specific staining. Images were captured with an Olympus microscope and a 12.5 Mega pixel DP71 digital camera. Immunofluorescence was quantified using ImageJ 1.43 software. Briefly, 12 aortic sections from each animal (n=6 to 7 mice per treatment group), representing the entire length of the lesion, were stained and imaged. Staining intensity above background was determined over a fixed threshold. The staining intensity of the 12 aortic sections from each animal was averaged to provide a staining intensity for each animal. Data shown is average staining intensity for each animal within the group.

Kinase activity assay

Total GSK3α/β activity was determined from 250μg total cell protein. For isoform specific analysis, GSK3α or GSK3β were immunoprecipitated from 600 μg total cell protein in kinase buffer using a monoclonal antibody specific for GSK3β (BD Transductions cat#610202) or GSK3α (Cell Signaling cat#07-389) and Ultra Link

immobilized Protein A Plus (Pierce) (Supplementary Figure II). Kinase activity was measured by monitoring the incorporation of ^{32}P onto phospho-glycogen synthase peptide-2 (pGS-2, Upstate Biotech). Briefly, either cell lysate or immunoprecipitated GSK3α or β was combined with 15μmol/L p-GS-2 and 0.5μCi/μl [$\gamma^{32}P$]-ATP in a reaction mixture containing 20mmol/L MOPS, 50μmol/L EDTA, 0.25mmol/L Mg acetate, 5mmol/L $MgCl_2$, 5mmol/L β-glycerol phosphate, 1mmol/L EGTA, 0.25mmol/L Na_3VO_4, 0.2 mmol/L DTT and 35μmol/L ATP in a total volume of 40μL. As background controls, a subset of samples were incubated with 0.5μmol/L CT99021. After 60 min at room temperature samples were placed on ice, then spotted onto Whatman P81 phosphocellulose paper (GE Healthcare) and washed 3X with 0.75% *o*-phosphoric acid and once with acetone. ^{32}P incorporation onto the substrate was determined by scintillation counting and total counts minus background are reported.

Lipid analysis

Esterified and unesterified cholesterol levels were determined in macrophages using a Cholesterol Quantitation Kit (Sigma-Aldrich cat#MAK043) according to manufacturer's instructions (Supplementary Figure I). Briefly, lipids were extracted from $1X10^6$ cells with chloroform:isopropanol:IGEPAL CA-630 (7:11:0.1). Lipids were incubated with a cholesterol probe and either with (total cholesterol) or without (free cholesterol) cholesterol esterase for 60mins at 37˚C. Esterified cholesterol levels were determined by the difference between total and free cholesterol levels. The absorbance of the sample was determined at 570nm (A_{570}) and compared to a known standard (Supplementary Figure I). Protein concentrations were determined in the organic phase using a Bradford assay (Bio-Rad). Lipid uptake was determined by treating cells as

indicated and then supplementing media with Alexa fluor 488-AcLDL (7μg/ml) (Life Technologies) for 2 hours at 37˚C and 5% CO_2.To observe lipid droplets, cells were grown or differentiated onto glass cover slips and stained with Oil Red O (0.5% w/V) dissolved in isopropanol:PBS (4:3) followed by 4',6-diamidino-2-phenylindole (DAPI). Cover slips were mounted onto slides in Crystal-mount media. All images were captured using an Olympus microscope and a 12.5 megapixel DP71 digital camera. Oil Red O and Alexa fluor 488-AcLDL was quantified using ImageJ 1.43 software. Briefly, each biological experiment and treatment was conducted a minimum of 4 times. From each of these biological replicates a minimum of 5 images, each containing approximately 200 cells, was captured. Stained area over background as well as cell number was quantified. Data from each image of a biological replicate was combined providing an average stained area per cell with a minimum of 1000 cells. Data shown is average stained area per cell from at least 4 biological replicates (minimum 4000 cells).

Statistical analysis

All experiments are representative of at least 3 independent biological experiments. All data is expressed as mean±S.D. An unpaired Student *t* test or 1-way ANOVA test was used, as appropriate, to determine statistical significance. A value of $P<0.05$ was considered statistically significant.

4.5 RESULTS

GSK3α/β inhibition does not affect the adaptive UPR

Thp-1 human monocytic cells were differentiated into macrophages by exposure to 100nmol/LPMA for 72 hours. The small molecule GSK3α/β inhibitor CT99021 was

used to directly inhibit GSK3α/β activity.[32] To confirm inhibition, GSK3α and GSK3β were immunoprecipitated from Thp-1 macrophage lysates and kinase activity was determined in the presence or absence of 0.5μmol/L CT99021 (Supplementary Figure IIA).[33] GSK3α/β inhibition was verified indirectly by monitoring the accumulation of β-catenin in cells treated with 4μmol/L CT99021 (Supplementary Figure IIB). To determine the impact of GSK3α/β inhibition on ER stress induced chaperone expression, macrophages were pre-treated for 2 hours in the presence or absence of 4μmol/L CT99021 and then challenged with ER stress-inducing agents, including 1μmol/L thapsigargin (Thaps), 5mmol/L glucosamine (GLN), or 600μmol/L palmitic acid (PA), for 18 hours. Neither ER stress nor GSK3α/β inhibition reduced Thp-1 macrophage cell viability below 80% (Supplementary Figure III). Total RNA was isolated and quantitative real time PCR was performed. The expression levels of the cellular chaperones and foldases, glucose related protein (GRP) 78, GRP94, calreticulin as well as protein disulphide isomerase (PDI) were determined (Figure 4.1). These components of the adaptive ER stress response were significantly upregulated by Thaps, GLN and PA (Figure 4.1). GSK3α/β inhibition did not alter GRP78, GRP94, calreticulin or PDI expression (Figure 4.1). Consistent with these findings, siRNA-directed knockdown of GSK3α/β did not alter the ability of Thaps, GLN, or PA to increase GRP78 protein levels (Supplementary Figure IV A-C). These results suggest that GSK3α/β activity is not required for early, adaptive UPR signaling.

Figure 4.1. GSK3α/β inhibition does not affect the adaptive UPR. Thp-1 derived macrophages were cultured in the presence or absence of the ER stress-inducing agents thapsigargin (Thaps, 1μmol/L), glucosamine (GLN, 5mmol/L) or palmitic acid (PA, 600μmol/L) for 18 hours. To inhibit GSK3α/β activity cells were pre-treated for 2 hours with 4μmol/L CT99021, a specific GSK3α/β inhibitor. Using quantitative real time PCR the expression level of **A)** GRP78, **B)** GRP94, **C)** calreticulin and **D)** protein disulphide isomerase (PDI) were determined. n=3-4, *$p<0.05$ relative to untreated cells.

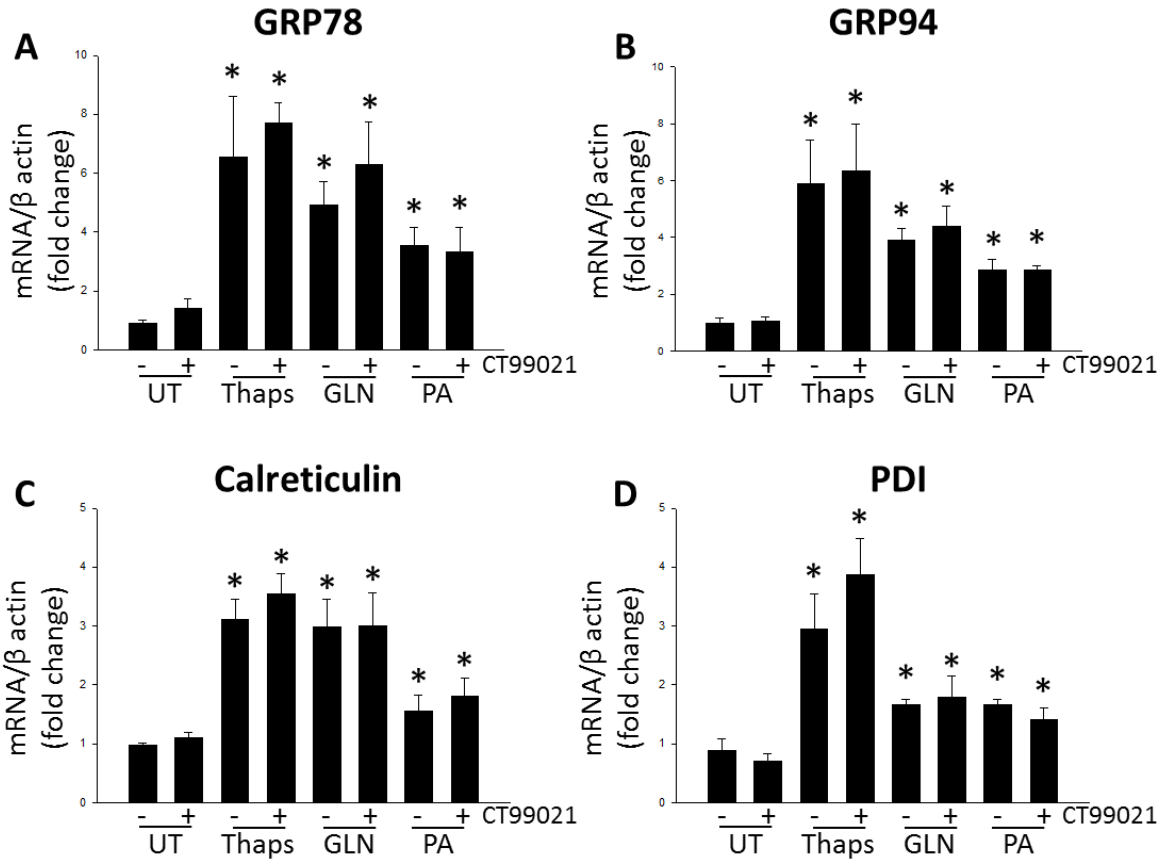
A
GRP78
mRNA/β actin (fold change)
B
GRP94
C
Calreticulin
D
PDI
- + - + - + - + CT99021
UT Thaps GLN PA

GSK3α/β is a target of the PERK signaling pathway

We next investigated the three branches of UPR and the potential role of GSK3α/β in each of these signaling pathways. Initially, the effect of ER stress on GSK3α/β activation was determined. ER stress-induced by Thaps, GLN and PA significantly increased GSK3α/β activity in Thp-1 macrophages (Figure 4.2A). Macrophages were then exposed to inhibitors of each of the three UPR signaling pathways. Inhibition of the PERK, but not IRE or ATF6, significantly attenuated ER stress-induced GSK3α/β activity (Figure 4.2A and Supplementary Figure V). Activated PERK phosphorylates the eukaryotic initiation factor (eIF)-2α at serine 51. This phosphorylation event results in the attenuation of general protein translation and the specific up regulation of activating transcription factor (ATF)-4 and CHOP. Immunoblot analysis of protein lysates from macrophages challenged with Thaps, GLN or PA shows the expected ER stress-induced phosphorylation of eIF2α, indicative of the activation of the PERK signaling pathway (Figure 4.2B and C). P-eIF2α levels were unaffected by GSK3α/β inhibition suggesting that GSK3α/β does not affect PERK activity directly. However, ER stress-induced CHOP and ATF4 expression were blocked by GSK3α/β inhibition and siRNA knockdown (Figure 4.2B, D-F, and Supplementary Figure IV A-D). These results indicate that GSK3α/β plays a role in the regulation of downstream components of the PERK branch of the UPR.

Figure 4.2. GSK3α/β is a distal target of the PERK signaling pathway. Thp-1 derived macrophages were treated with 1μmol/L thapsigargin (Thaps), 5 mmol/L glucosamine (GLN) or 600μmol/L palmitic acid (PA) in the presence or absence of small molecule inhibitors of PERK (GSK2606414, 3μmol/L), IREI (inh III, 6μmol/L) or ATF6 (AEBSF, 250μmol/L). **A)** GSK3α/β activity was determined in whole cell lysates. ER stress-induced GSK3α/β activity while PERK inhibition, but not IRE1 or ATF6 inhibition, attenuated ER stress-induced GSK3α/β activity (n=6-7). Thp-1 macrophages were treated with Thaps, GLN and PA in the presence or absence of the GSK3α/β inhibitor CT99021 (4μmol/L). **B)** Whole cell protein lysates were resolved by SDS-PAGE and probed with antibodies against total or phospho-S51-eIF2α or CHOP. Immunoblots were quantified by densitometry **(C and D)**. Total RNA was isolated from similarly treated cells and the expression level of **E)** ATF4 and **F)** CHOP were quantified by real time PCR. n=4, *$p<0.05$ relative to untreated cells, #$p<0.05$ relative to cells of the same treatment without CT99021.

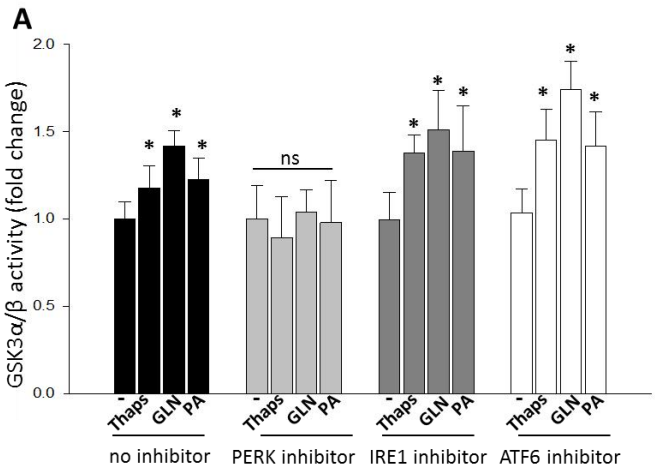
A
GSK3α/β activity (fold change)
2.0
1.5
1.0
0.5
0.0
ns
- Thaps GLN PA
no inhibitor
PERK inhibitor
IRE1 inhibitor
ATF6 inhibitor

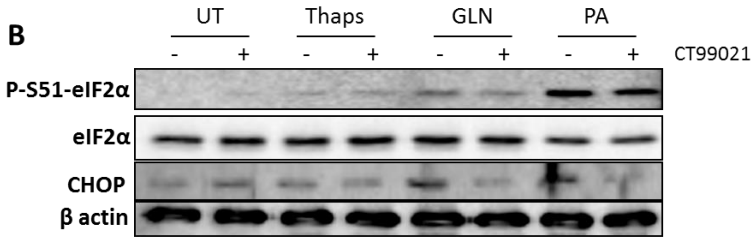
B
UT
Thaps
GLN
PA
- + - + - + - +
CT99021
P-S51-eIF2α
eIF2α
CHOP
β actin

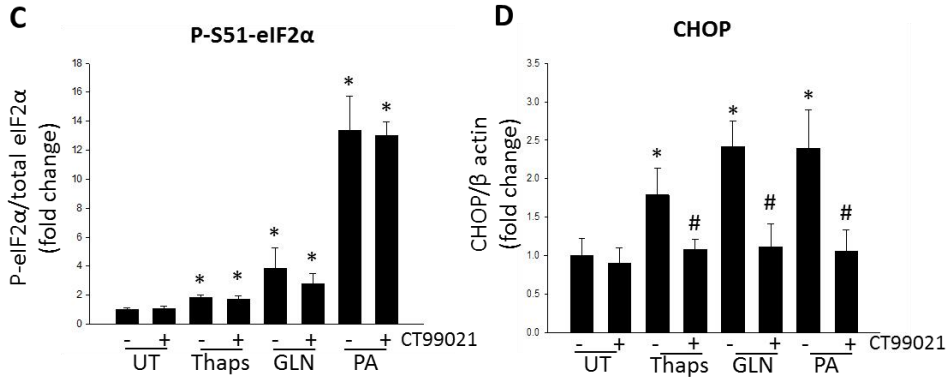
C
P-S51-eIF2α
P-eIF2α/total eIF2α (fold change)
D
CHOP
CHOP/β actin (fold change)
- + - + - + - +
UT Thaps GLN PA
CT99021

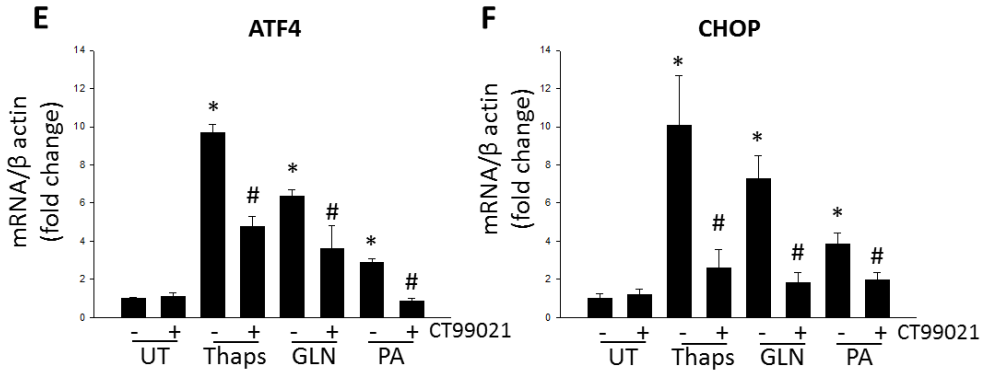
E
ATF4
mRNA/β actin (fold change)
F
CHOP
mRNA/β actin (fold change)
- + - + - + - +
UT Thaps GLN PA
CT99021

GSK3α/β inhibition is associated with attenuated CHOP expression in atherosclerotic macrophages

Having identified a role for GSK3α/β in PERK signaling *in vitro* we then asked if CHOP expression in macrophages within the atherosclerotic plaque could be attenuated by GSK3α/β inhibition. Five week old female ApoE$^{-/-}$ mice were placed on a high fat diet (HFD) containing 21% milk fat and 0.2% cholesterol for 20 weeks. A subset of mice were given a HFD supplemented with valproate (VPA, 625mg valproate/kg body weight), a small molecule shown to inhibit GSK3α/β both *in vitro* and *in vivo.*[7,30,34-36] We have previously reported that ApoE$^{-/-}$mice fed a HFD supplemented with VPA present with attenuated GSK3β activity in hepatic tissue and within the aortic wall and have significantly reduced atherosclerotic plaque volume (by ~10%) and necrotic core area (by ~27%) (Table 4.1).[7] Aortic sections were co-stained with a macrophage specific anti-Mac3 (CD107) antibody and an anti-KDEL antibody specific for GRP78 and 94. Serial sections were stained with appropriate pre-immune IgG antibodies to control for nonspecific staining (Supplementary Figure VI). Representative images (Figure 4.3A) and quantitation (Figure 4.3C) show no detectible alterations to KDEL staining pattern or intensity in the VPA-supplemented mice. Next, serial aortic sections were co-stained with anti-Mac3 and anti-CHOP antibodies. We observed a significant reduction in CHOP staining within macrophages of the atherosclerotic plaque in VPA-supplemented mice (Figure 4.3B and D).

Peritoneal macrophages were isolated from a separate group of ApoE$^{-/-}$ mice fed a HFD or a HFD supplemented with VPA for 3 weeks. Macrophages isolated from mice fed a HFD supplemented with VPA displayed significantly reduced CHOP protein and mRNA expression while GRP94 and GRP78 mRNA and protein levels were unchanged

relative to HFD fed mice (Figure 4.3E-H). These observations are consistent with our *in vitro* data showing that GSK3α/β does not regulate upstream, adaptive components of the UPR but does modulate distal components of the PERK signaling pathway.

Table 4.1. Metabolic parameters of ApoE$^{-/-}$ mice on a HFD with and without VPA supplementation.

Parameter	HFD	HFD+VPA
Body Weight, g	23.4±0.9	23.0±0.5
Atherosclerotic lesion volume, 10^{-3} mm^3	208±9.0	187±8.0*
Necrotic core volume, 10^{-3} mm^3	132±9.6	97±13.0*
Plasma		
VPA, µM	0	7.3±5.4
Glucose, mM	11.2±0.9	10.3±0.5
Cholesterol, mM	25.0±3.6	19.4±1.8

n=9-12 per treatment group. *p<0.05 relative to control mice fed the nonsupplemented diet.

Figure 4.3. CHOP expression is reduced in macrophages from ApoE$^{-/-}$ mice supplemented with valproate. Representative aortic sections from ApoE$^{-/-}$ mice fed a high fat diet (HFD) with or without supplementation with the GSK3α/β inhibitor valproate (VPA), as indicated. L indicates vessel lumen. Sections were co-stained with DAPI (blue) and antibodies against **A)** Mac3 (green) and KDEL (GRP78/94) (red) or **B)** Mac3 (green) and CHOP (red). Merged images are shown on the right. Arrows indicate positively stained macrophages. Florescence intensity of **C)** KDEL and **D)** CHOP was quantified. Peritoneal macrophages were isolated from ApoE$^{-/-}$ mice fed a HFD or a HFD supplemented with VPA. Total RNA was isolated from peritoneal macrophages and the expression level of **E)** GRP78 and **F)** CHOP were quantified by real time PCR. **G)** Whole cell protein lysates from peritoneal macrophages were resolved by SDS-PAGE and probed with antibodies against KDEL (GRP78 and GRP94), CHOP and β-actin. **H)** Immunoblots were quantified by densitometry. n=6-7, #$p<0.05$ relative to non-VPA supplemented group.

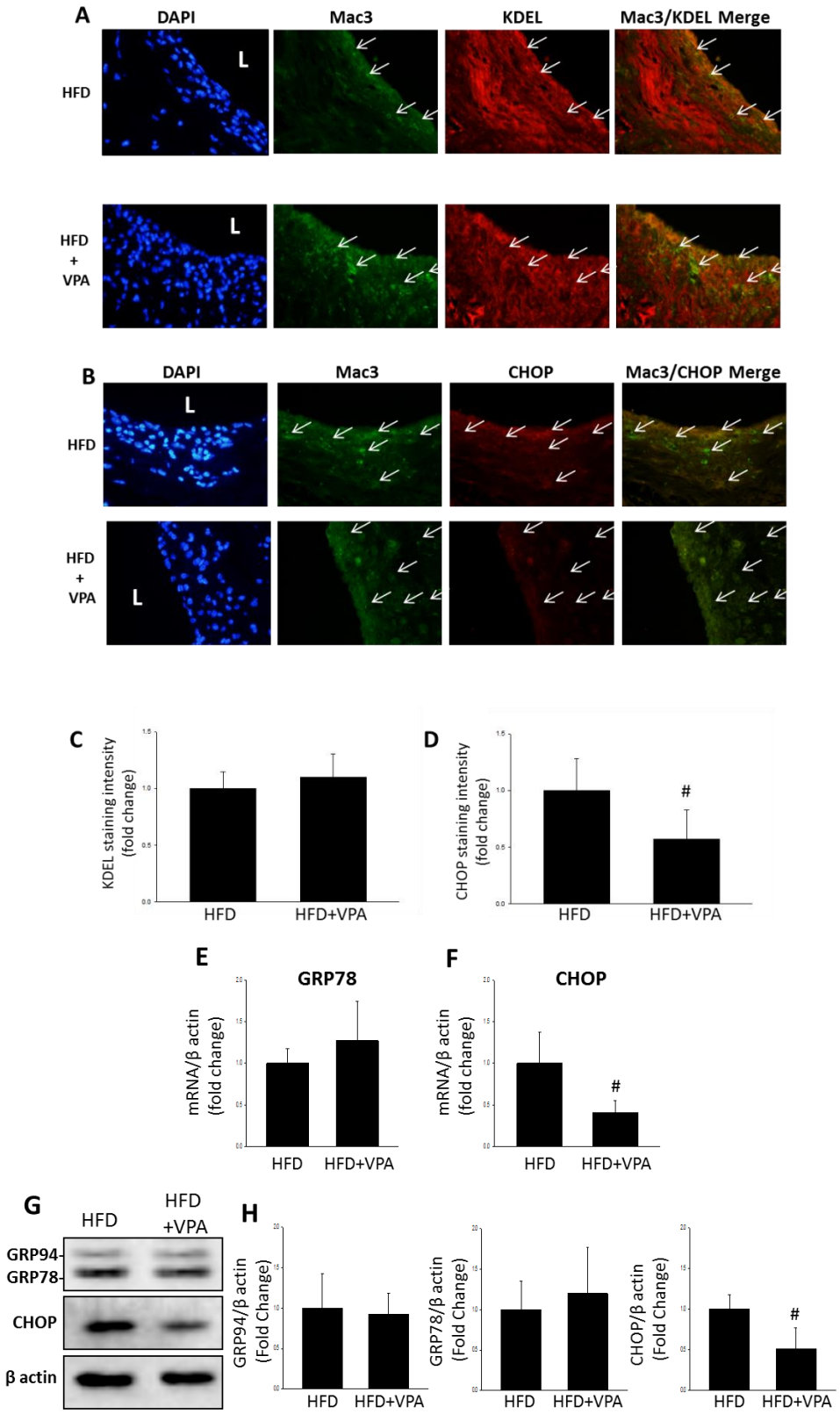
A
DAPI
Mac3
KDEL
Mac3/KDEL Merge
HFD
HFD + VPA
L
B
DAPI
Mac3
CHOP
Mac3/CHOP Merge
HFD
HFD + VPA
L
C
KDEL staining intensity (fold change)
HFD
HFD+VPA
D
CHOP staining intensity (fold change)
#
HFD
HFD+VPA
E
GRP78
mRNA/β actin (fold change)
HFD
HFD+VPA
F
CHOP
mRNA/β actin (fold change)
#
HFD
HFD+VPA
G
HFD
HFD +VPA
GRP94
GRP78
CHOP
β actin
H
GRP94/β actin (Fold Change)
HFD
HFD+VPA
GRP78/β actin (Fold Change)
HFD
HFD+VPA
CHOP/β actin (Fold Change)
#
HFD
HFD+VPA

GSK3α/β inhibition attenuates ER stress-induced lipid accumulation in macrophages

We hypothesize that ER stress may play a role in the dysregulated accumulation of lipids in atherosclerotic foam cells. Our data suggest that inhibition of GSK3α/β will modulate this response. To test this, cultured Thp-1 macrophages were challenged with ER stress-inducing agents in the presence or absence of CT99021. After 18 hours, the expression levels of selected transcripts involved in lipid biosynthesis and uptake were quantified by real time PCR. Results show that ER stress was associated with significantly enhanced expression of genes regulating lipid and cholesterol metabolism including fatty acid synthase (FAS), sterol regulatory element binding protein (SREBP)-1c, SREBP-2, 3-hydroxy-3-methylglutaryl-coenzyme A (HMGCoA) and low-density lipoprotein receptor (LDLR) (Figure 4.4). Inhibition of GSK3α/β activity by CT99021 significantly attenuated ER stress-induced FAS, SREBP-1c, SREBP-2, HMGCoA and LDLR expression (Figure 4.4). Transcript levels of genes involved in other metabolic pathways were not significantly affected by ER stress or GSK3α/β inhibition (Supplementary Figure VII).

To determine if these changes in gene expression affected lipid and cholesterol accumulation within macrophages, esterified and unesterified cholesterol levels were quantified. ER stress induction by Thaps, GLN and PA resulted in significant accumulation of both esterified and unesterified cholesterol (Figure 4.5A and B). GSK3α/β inhibition by CT99021, as well as two other GSK3α/β inhibitors, significantly attenuated the accumulation of free and esterified cholesterol in the macrophages (Figure 4.5A and B and Supplementary Figure VIII). Consistent with these findings, Oil red O staining showed increased lipid droplet formation in the macrophages exposed to

ER stress-inducing agents and siRNA-directed GSK3α/β knockdown attenuated this effect (Supplementary Figure IV).

The mechanism by which ER stress signaling through GSK3α/β promotes macrophage lipid accumulation and foam cell formation could involve altered lipoprotein uptake/efflux and/or altered intracellular lipid biosynthesis. To determine if ER stress signaling through GSK3α/β plays a role in uptake of modified LDL, Thp-1 macrophages were incubated with acetylated LDL (AcLDL) labeled with Alexa 488. Pretreatment with ER stress-inducing agents enhanced AcLDL uptake and this effect was blocked by GSK3α/β inhibition (Figure 4.5C and D). To examine the effect on lipid biosynthesis, macrophages were treated with ER stress-inducing agents and then cultured in the absence of lipoproteins. ER stress enhanced cellular unesterified cholesterol levels and this effect was attenuated by GSK3α/β inhibition (Supplementary Figure IX). Neither ER stress nor GSK3α/β inhibition significantly altered macrophage cholesterol ester levels. Taken together these data suggest that ER stress signaling through GSK3α/β plays a role in lipid uptake and biosynthesis.

Figure 4.4. GSK3α/β regulates lipid metabolism in macrophages. ER stress was induced in Thp-1 macrophages using 1μmol/L thapsigargin (Thaps), 5mmol/L glucosamine (GLN) or 600μmol/L palmitic acid (PA) treatment with or without GSK3α/β inhibition by 4μmol/L CT99021. The expression of **A)** sterol regulatory element binding protein (SREBP)-1C, **B)** SREBP-2, **C)** 3-hydroxy-3-methylglutaryl-coenzyme A (HMGCoA), **D)** low-density lipoprotein receptor (LDLR) and **E)** fatty acid synthase were determined by real time PCR. n=4, *$p<0.05$ relative to untreated cells, #$p<0.05$ relative to cells of the same treatment without CT99021.

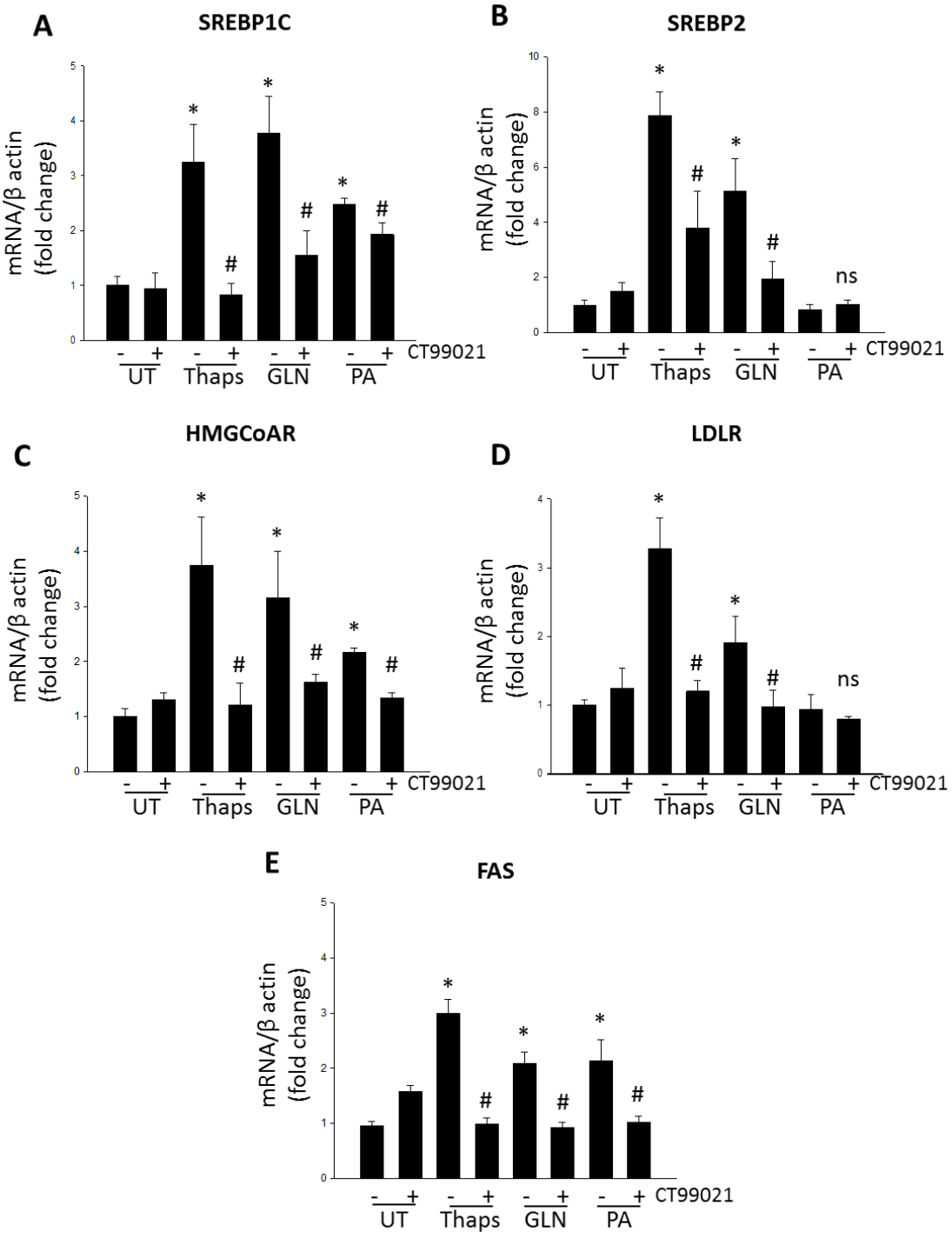
A
SREBP1C
mRNA/β actin (fold change)
B
SREBP2
mRNA/β actin (fold change)
ns
C
HMGCoAR
mRNA/β actin (fold change)
D
LDLR
mRNA/β actin (fold change)
ns
E
FAS
mRNA/β actin (fold change)
- + - + - + - + CT99021
UT Thaps GLN PA

Figure 4.5. GSK3α/β inhibition attenuates ER stress-induced cholesterol accumulation and AcLDL uptake. ER stress was induced in Thp-1 macrophages using 1μmol/L thapsigargin (Thaps), 5mmol/L glucosamine (GLN) or 600μmol/L palmitic acid (PA). GSK3α/β was inhibited by treating cells with 4μmol/L CT99021. Cellular **A)** free and **B)** esterified cholesterol levels were quantified. Thp-1 macrophages were treated with Thaps, GLN or PA, in the presence or absence of CT99021, and then exposed to Alexa fluor 488-AcLDL (7μg/ml). **C)** Representative images of AcLDL uptake are shown and **D)** quantified. n=4, *$p<0.05$ relative to untreated cells, #$p<0.05$ relative to cells of the same treatment without CT99021.

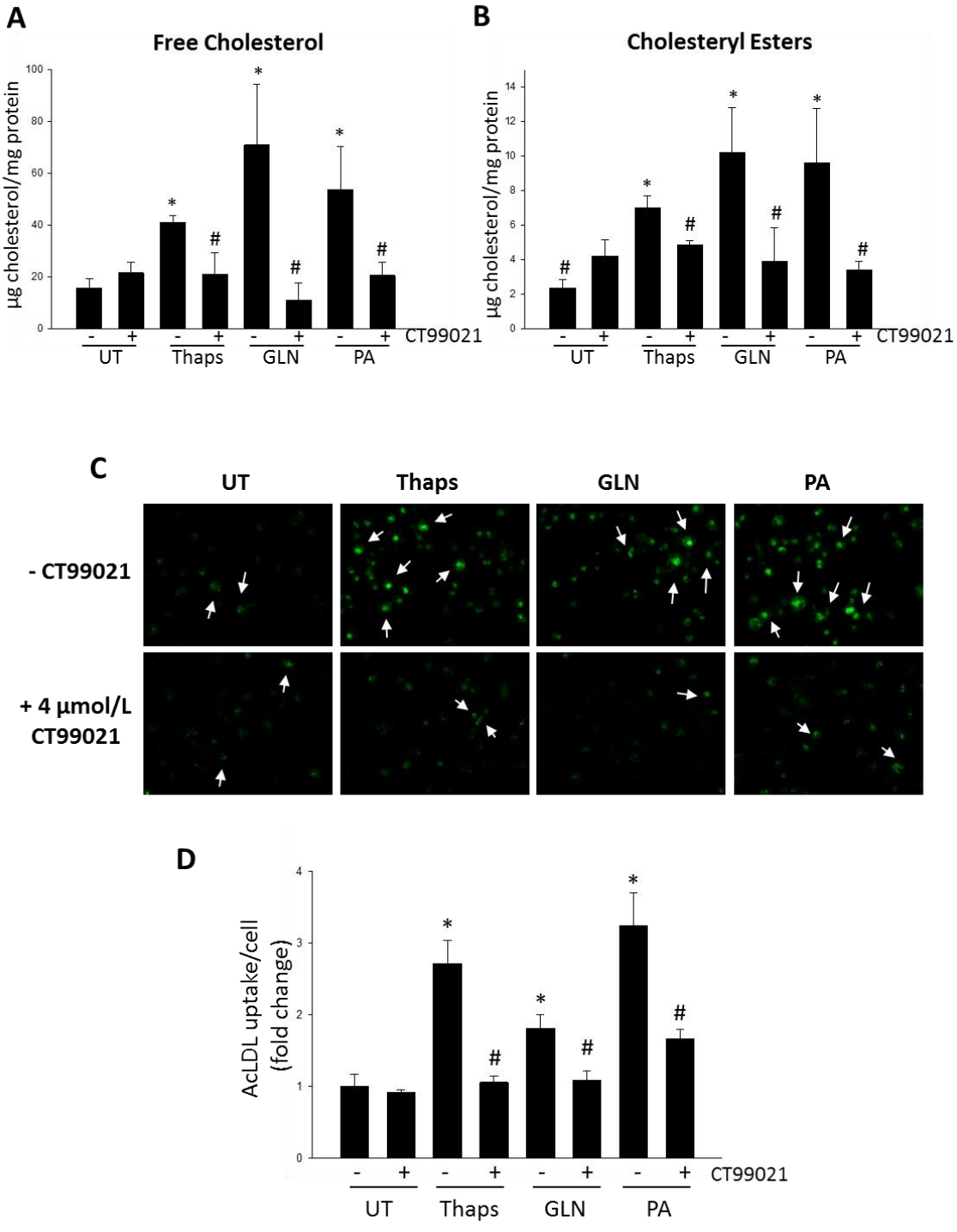
A
Free Cholesterol
µg cholesterol/mg protein
CT99021
UT
Thaps
GLN
PA
B
Cholesteryl Esters
µg cholesterol/mg protein
CT99021
UT
Thaps
GLN
PA
C
UT
Thaps
GLN
PA
- CT99021
+ 4 µmol/L CT99021
D
AcLDL uptake/cell (fold change)
CT99021
UT
Thaps
GLN
PA

PERK-GSK3α/β signaling regulates ER stress-induced foam cell formation in primary macrophages

To investigate the relevance of PERK-GSK3α/β signaling in primary macrophages, peritoneal macrophages were isolated from C57Bl6 mice. Mouse macrophages were cultured in the presence or absence of ER stress-inducing agents, Thaps, GLN or PA. Consistent with our findings in Thp-1 cells, ER stress increased intracellular lipid concentrations, as assessed by Oil Red O staining, relative to untreated controls (Figure 4.6A-C). Inhibition of PERK or GSK3α/β was sufficient to block ER stress-induced lipid accumulation and cells treated with either of these inhibitors had lipid concentrations similar to those observed in untreated cells (Figure 4.6A-C).

A constitutively active form of GSK3β, S9A-GSK3β, was overexpressed in primary macrophages using an adenovirus vector (Ad-S9A-GSK3β, 10 MOI) (Supplementary Figure X). As a control, cells were infected with an empty adenovirus (Ad-Null, 10 MOI).S9A-GSK3β overexpression resulted in significant lipid accumulation which was not detectibly altered by the presence or absence of ER stress (Figure 4.6D-F). PERK inhibition, which blocked ER stress-induced lipid accumulation (Figure 4.6B), did not alter the ability of SA9-GSK3β to increase macrophage lipid content (Figure 4.6E). Exposing the cells to CT99021 attenuated S9A-GSK3β-induced lipid accumulation (Figure 4.6F). Constitutive GSK3β activation also resulted in the induction of CHOP protein levels and significantly elevated mRNA expression in primary macrophages, even in the presence of the PERK inhibitor (Figure 4.6G-I). Together, these data are consistent with our hypothesis that ER stress signals though PERK-GSK3α/β to induce macrophage lipid accumulation and foam cell formation.

Figure 4.6. PERK-GSK3α/β signaling regulates foam cell formation in primary mouse macrophages. Thioglycolate elicited mouse peritoneal macrophages were isolated from female C57BL6 mice. Macrophages were exposed to using 1μmol/L thapsigargin (Thaps), 5mmol/L glucosamine (GLN) or 600μmol/L palmitic acid (PA) in the presence or absence of PERK inhibitor (3μmol/L) or CT99021 (4μmol/L). After treatment cells were stained with Oil Red O and DAPI. **A)** Representative images are shown and quantified **(B and C)**. Primary mouse macrophages were infected with adenovirus encoding constitutively active GSK3β (Ad-S9A-GSK3β) or an empty vector control (Ad-CMV-Null). ER stress was induced in the cells expressing GSK3β-S9A as above in the presence or absence of CT99021 or PERK inhibitor. Cells were stained with Oil Red O and DAPI. **D)** Representative images are shown and quantified **(E and F)**. Protein lysates from primary macrophages expressing GSK3β-S9A with or without being exposed to PERK inhibitor were resolved by SDS page and probed for CHOP and β actin. **G)** Representative blots are shown and **H)** quantified. **I)** CHOP mRNA expression was determined by quantitative RT-PCR in primary macrophages expressing S9A-GSK3β in the presence or absence of PERK inhibitor. n=4-5, *$p<0.05$ relative to untreated cells, #$p<0.05$ relative to cells of the same treatment without inhibitor.

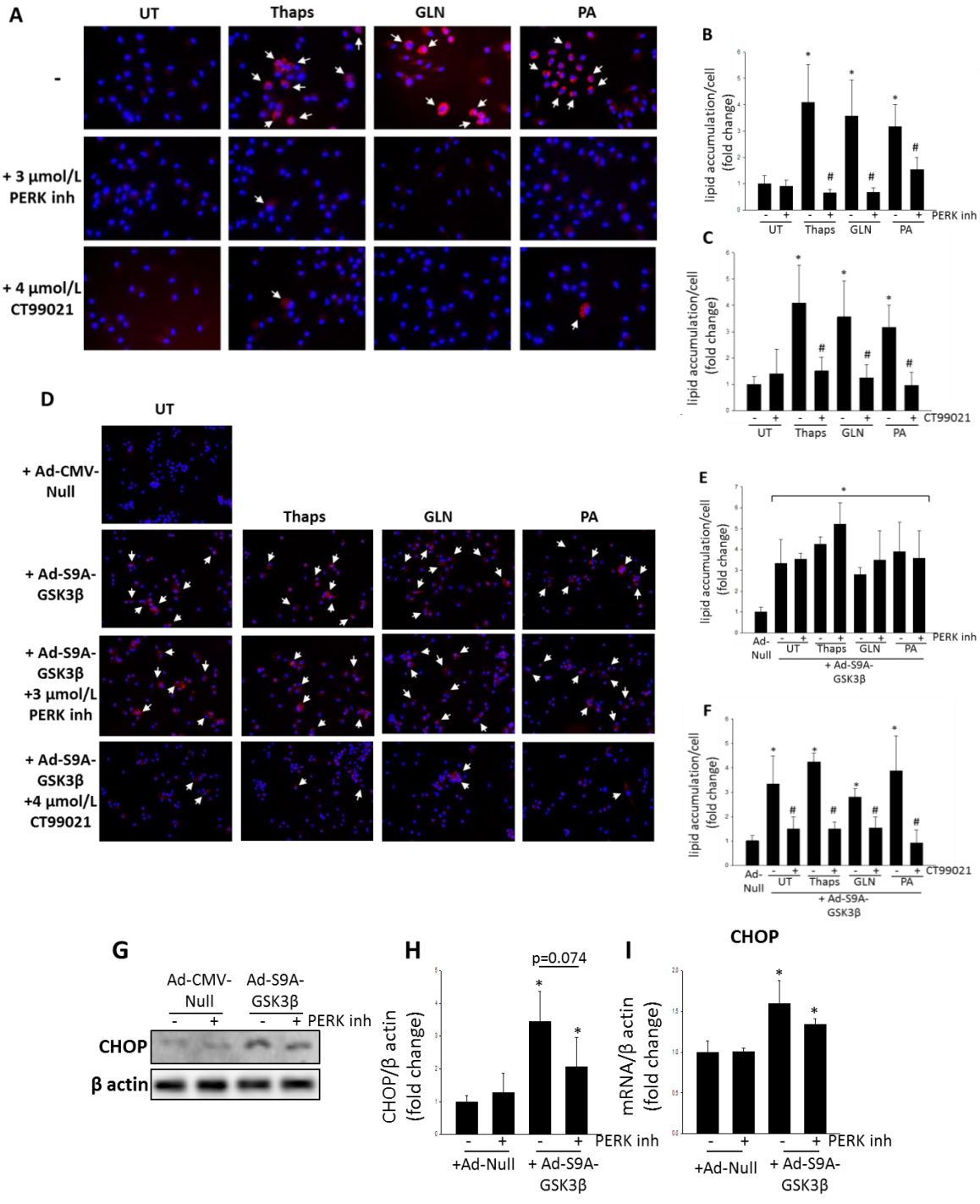
A
UT
Thaps
GLN
PA
-
+ 3 µmol/L PERK inh
+ 4 µmol/L CT99021
B
lipid accumulation/cell (fold change)
PERK inh
UT
Thaps
GLN
PA
C
lipid accumulation/cell (fold change)
CT99021
D
+ Ad-CMV-Null
+ Ad-S9A-GSK3β
+ Ad-S9A-GSK3β +3 µmol/L PERK inh
+ Ad-S9A-GSK3β +4 µmol/L CT99021
E
lipid accumulation/cell (fold change)
Ad-Null
+ Ad-S9A-GSK3β
F
lipid accumulation/cell (fold change)
G
Ad-CMV-Null
Ad-S9A-GSK3β
PERK inh
CHOP
β actin
H
p=0.074
CHOP/β actin (fold change)
+Ad-Null
+ Ad-S9A-GSK3β
I
CHOP
mRNA/β actin (fold change)

4.6 DISCUSSION

Recent evidence suggests a causative role for ER stress in the initiation, development and progression of atherosclerosis.[7, 13, 14, 30] The mechanistic details of how ER stress induces the pro-atherogenic process are poorly understood. We present data showing that the PERK branch of the UPR signals through GSK3α/β to promote macrophage foam cell formation. Our results suggest that GSK3α/β does not modulate the adaptive components of ER stress signaling including chaperone expression and translation attenuation in human macrophages. Rather, ER stress-induced GSK3α/β activation plays a role in regulating the distal components of the PERK pathway and is involved in the upregulation of transcription factors including ATF4 and CHOP. Inhibition or knockdown of PERK or GSK3α/β attenuates ER stress-induced macrophage lipid accumulation. Our results suggest that both lipid uptake and biosynthesis pathways may be affected however it is also possible that lipid efflux from macrophages is also regulated by GSK3α/β.[37] Constitutive GSK3β activation is able to overcome the effect of PERK inhibition and promotes lipid accumulation and foam cell formation. Constitutive GSK3β activation also induces CHOP protein and mRNA expression even when PERK is inhibited. Taken together, these results illuminate a novel signaling mechanism by which ER stress may promote lipid accumulation in macrophage foam cells by activation of the PERK-GSK3α/β pathway.

Multiple cardiovascular risk factors are capable of inducing ER stress in cell culture and animal models; however, the mechanisms by which individual risk factors promote ER stress are not fully understood. Elevated levels of ER stress have been observed in animal models of hyperglycemia, obesity and dyslipidemia.[6, 7, 30, 37] In a hyperglycemic state, glucosamine, a metabolite of glucose, accumulates within cells and

acts as a potent inducer of ER stress.[39-41] In addition, lipids such as palmitic acid and unesterified cholesterol, are thought to disturb ER function by disrupting the composition of the ER membrane.[11, 42] ER stress/UPR activation may be a central mechanism by which multiple cardiovascular risk factors promote atherosclerosis development. GSK3α/β is involved in a number of signaling networks and regulates many aspects of cell metabolism and physiology. The role of GSK3α/β in the regulation of inflammatory cytokines is relatively well established. For example, in monocytes and macrophages induction of nuclear factor-κB (NFκB) is mediated by GSK3α/β.[43] Interestingly, GSK3α/β appears to play a role in the regulation of interleukin-10 expression, an anti-inflammatory cytokine. In monocytes and macrophages, stimulation of the phosphatidylinositol-3 kinase (PI3K)/AKT pathway results in GSK3β inhibition, through phosphorylation of serine 9, and results in a significant increase in IL-10 expression.[44, 45] Moreover, GSK3α/β inhibition may also inhibit the expression of the pro-inflammatory cytokines IL-1β and IL-6.[44] To the best of our knowledge, we present the first evidence of a role for GSK3α/β in the regulation of lipid metabolism in macrophages. Together these findings may indicate that GSK3α/β has a role in regulating the differentiation between pro-inflammatory, lipid engorged foam cells and anti-inflammatory macrophages.

The involvement of ER stress signaling in metabolic disease has been well established and the PERK signaling branch of the UPR has been the focus of many studies. In both the ApoE and LDLR knockout mice, CHOP deficiency decreases atherosclerotic plaque size and decreases plaque complexity.[46] $ApoE^{-/-}CHOP^{-/-}$ and $LDLR^{-/-}CHOP^{-/-}$ mice fed a Western diet develop atherosclerotic plaques that are less necrotic and display decreased caspase 3 activation.[46] Similarly, Oyadomari *et al* examined a mouse model in which eIF2α phosphorylation was impaired by enhanced

GADD34 expression.[47] These mice had decreased signaling through the downstream components of the PERK pathway and displayed significantly reduced hepatic fat droplet and triglyceride deposition as well as dramatically improved glucose and insulin tolerance.[46] The authors characterized these mice further by observing reduced expression of many genes involved in lipid metabolism including SCD1, FAS and LPL.[47] Moreover, ATF4 knockout mice have decreased circulating serum triglycerides and free fatty acids along with decreased white adipose tissue size and reduced SCD1, FAS and SREBP1c expression.[48]

While our results show that the IRE1 and ATF6 pathways are not directly involved in ER stress signaling through GSK3α/β, other studies have suggested that the IRE1 and ATF6 do play a role in the regulation of lipid metabolism.[49-51] Although poorly defined, cross talk between UPR pathways appears to coordinate the appropriate response to an external stimulus and thus these pathways may collectively regulate lipid homeostasis.[52] These studies, along with the results presented here, suggest activation of the PERK branch of the UPR leads to increased lipid synthesis and uptake while attenuation of PERK signaling impairs lipid deposition.

Our investigations define an important role for GSK3α/β in the regulation of downstream components of the PERK signaling branch of the UPR. Moreover, PERK-GSK3α/β signaling may play a critical role in the regulation of macrophage lipid accumulation and foam cell formation *in vivo*. There are a number of important aspects of this pathway that remain to be investigated. For example, it will be important to understand the mechanism by which PERK regulates GSK3α/β and whether other signaling networks such as the PI3K/AKT, Wnt or MAPK pathways are involved. Secondly, we need to identify the direct targets of GSK3α/β and understand their roles in

the regulation of ATF4 and CHOP expression, as well as lipid metabolism. This will be a challenging task because of the number of putative GSK3α/β substrates that have already been identified.[53] It will also be interesting to determine the specific roles of GSK3α and GSK3β in this process. The delineation of these pathways may lead to the identification of novel targets for the development of future anti-atherogenic therapeutics. Our work presented here provides an initial step toward a clearer understanding of the mechanisms linking ER stress and pro-atherogenic processes.

4.7 REFERENCES FOR CHAPTER 4

1. Ross, R. Mechanisms of disease - atherosclerosis - an inflammatory disease. *N. Engl. J. Med*. 1999;340:115-126.
2. Glass CK, Witztum JL. Atherosclerosis: The road ahead. *Cell.*2001;104:503-516.
1. Yusuf S, Hawken S, Ounpuu S, Dans T, Avezum A, Lanas F, McQueen M, Budaj A, Pais P, Varigos J, Lisheng L, INTERHEART Study Investigators. Effect of potentially modifiable risk factors associated with myocardial infarction in 52 countries (the INTERHEART study): Case-control study. *Lancet.*2004;364:937-952.
2. Moore KJ, Tabas I. 2011. Macrophages in the pathogenesis of atherosclerosis. *Cell.*2001;145:341-355.
3. Schroder M,Kaufman R.The mammalian unfolded protein response. *Annu. Rev. Biochem*. 2005;74:739-789.
4. Khan MI, Pichna BA,Shi Y,Bowes AJ,Werstuck GH. Evidence supporting a role for endoplasmic reticulum stress in the development of atherosclerosis in a hyperglycaemic mouse model. *Antioxid. Redox Signal.*2009;11:2289-2298.
5. McAlpine CS,Bowes AJ,Khan MI,Shi Y,Werstuck GH.Endoplasmic reticulum stress and glycogen synthase kinase-3 beta activation in apolipoprotein E-deficient mouse models of accelerated atherosclerosis. *Arterioscler. Thromb. Vasc. Biol*.2012;32:82-91.
6. Werstuck GH,Lentz SR,Dayal S,Hossain GH,Sood SK,Shi YY, Zhou J, Maeda N,Krisans SK, Malinow MR,Austin RC.Homocysteine-induced endoplasmic reticulum stress causes dysregulation of the cholesterol and triglyceride biosynthetic pathways. *J. Clin. Invest.*2001;107:1263-1273.
7. Ozcan U, Cao Q, Yilmaz E,Lee AH,Iwakoshi NN,Ozdelen E,Tuncman G, Gorgun C,Glimcher JH,Hotamisligil GH.Endoplasmic reticulum stress links obesity, insulin action, and type 2 diabetes. *Science*. 2004;306:457-461.
8. Kelsen SG,Duan X,Ji R,Perez O,Liu C, Merali S. Cigarette smoke induces an unfolded protein response in the human lung - A proteomic approach. *Am. J. Respir. Cell Mol. Biol.*. 2008;38:541-550.

9. Li Y, Schwabe RF, DeVries-Seimon T,Yao PM,Gerbod-Giannone MC,Tall AR,Davis RJ,Flavell R,Brenner DA,Tabas I. Free cholesterol-loaded macrophages are an abundant source of tumor necrosis factor-alpha and interleukin-6: Model of NF-kappaB- and map kinase-dependent inflammation in advanced atherosclerosis. *J. Bio.l Chem*. 2005;280:21763-21772.
10. Karaskov E, Scott C,Zhang L,Teodoro T,Ravazzola M,Volchuk A.Chronic palmitate but not oleate exposure induces endoplasmic reticulum stress, which may contribute to INS-1 pancreatic beta-cell apoptosis. *Endocrinology.*2006;147:3398-3407.
11. Civelek M,Manduchi E,Riley RJ,Stoeckert CJ,Davies PF. Chronic endoplasmic reticulum stress activates unfolded protein response in arterial endothelium in regions of susceptibility to atherosclerosis. *Circ. Res.*2009;105:453-461.
12. Zhou J,Lhotak S,Hilditch BA,Austin RC.Activation of the unfolded protein response occurs at all stages of atherosclerotic lesion development in apolipoprotein E-deficient mice. *Circulation.*2005;111:1814-1821.
13. Erbay E,Babaev VR,Mayers JR,Makowski L,Charles KN,Snitow ME,Fazio S,Wiest MM, Watkins SM,Linton MF,Hotamisligil GS.Reducing endoplasmic reticulum stress through a macrophage lipid chaperone alleviates atherosclerosis. *Nat. Med*. 2009;15:1383-U5.
14. Shimano H,Horton J,Hammer R,Shimomura I,Brown M,Goldstein J. Overproduction of cholesterol and fatty acids causes massive liver enlargement in transgenic mice expressing truncated SREBP-1a. *J. Clin. Invest.*1996;98:1575-1584.
15. Jiang H,Wek S,McGrath B,Scheuner D,Kaufman R,Cavener D, Wek R. Phosphorylation of the a subunit of eukaryotic initiation factor 2 is required for activation of NF-kappa B in response to diverse cellular stresses. *Mol. Cell. Biol.*2003;23:5651-5663.
16. Hotamisligil GS. Endoplasmic reticulum stress and the inflammatory basis of metabolic disease. *Cell.*2010;140:900-917.
17. Zinszner H, Kuroda M,Wang X,Batchvarova N,Lightfoot R, Remotti H, Stevens J,Ron D.CHOP is implicated in programmed cell death in response to impaired function of the endoplasmic reticulum. *Genes Dev*.1998;12:982-995.
18. Morishima N,Nakanishi K,Takenouchi H,Shibata T,Yasuhiko Y. An endoplasmic reticulum stress-specific caspase cascade in apoptosis - cytochrome c-independent activation of caspase-9 by caspase-12. *J. Biol. Chem.*2002;277:34287-34294.
19. Doble BW,Woodgett JR. GSK-3: Tricks of the trade for a multi-tasking kinase. *J. Cell Sci*. 2003;116:1175-1186.
20. Meares GP,Jope RS.Resolution of the nuclear localization mechanism of glycogen synthase kinase-3 - functional effects in apoptosis. *J. Biol. Chem.*2007;282:16989-17001.
21. Bijur G,Jope R.Proapoptotic stimuli induce nuclear accumulation of glycogen synthase kinase-3 beta. *J. Biol. Chem.*2001;276:37436-37442.
22. Kerkela R,Kockeritz L,MacAulay K,Zhou J,Doble BW,Beahm C,Greytak S, Woulfe K,Trivedi CM,Woodgett JR,Epstein JA,Force T,Huggins GS.Deletion of GSK-3 beta in mice leads to hypertrophic cardiomyopathy secondary to cardiomyoblast hyperproliferation. *J. Clin. Invest.*2008;118:3609-3618.

23. Doble BW, Patel S,Wood GA,Kockeritz LK,Woodgett JR.Functional redundancy of GSK-3 alpha and GSK-3 beta in Wnt/beta-catenin signaling shown by using an allelic series of embryonic stem cell lines. *Developmental Cell.*2007;12:957-971.
24. MacAulay K,Doble BW,Patel S,Hansotia T, Sinclair EM,Drucker DJ,Nagy A,Woodgett JR. Glycogen synthase kinase 3alpha-specific regulation of murine hepatic glycogen metabolism. *Cell Metab.*2007;6:329-337.
25. Song L,De Sarno P,Jope R. Central role of glycogen synthase kinase-3 beta in endoplasmic reticulum stress-induced caspase-3 activation. *J. Biol. Chem.*2002;277:44701-44708.
26. Chen Y,Chen G,Fan Z,Luo J,Ke Z.GSK3 beta and endoplasmic reticulum stress mediate rotenone-induced death of SK-N-MC neuroblastoma cells. *Biochem. Pharmacol*.2008;76:128-138.
27. Hoeflich KP, Luo J,Rubie EA,Tsao MS,Jin O,Woodgett JR.Requirement for glycogen synthase kinase-3beta in cell survival and NF-kappaB activation. *Nature.*2000;406:86-90.
28. Bowes AJ,Khan MI,Shi Y,Robertson L,Werstuck GH. Valproate attenuates accelerated atherosclerosis in hyperglycemic ApoE-deficient mice: Evidence in support of a role for endoplasmic reticulum stress and glycogen synthase kinase-3 in lesion development and hepatic steatosis. *Am. J. Pathol.*2009;174:330-342.
29. Choi S,Jang H,Kang Y,Jung JG,Han SJ,Kim HJ,Kim DJ,Lee K.Atherosclerosis induced by a high-fat diet is alleviated by lithium chloride via reduction of VCAM expression in ApoE-deficient mice. *Vascular Pharmacology.*2010;53:264-272.
30. Bain J,Plater L,Elliott M,Shpiro N,Hastie CJ,Mclauchlan H,Klevernic I, Arthur JSC,Alessi DR,Cohen P. The selectivity of protein kinase inhibitors: A further update. *Biochem. J.*2007;408:297-315.
31. Kim AJ, Shi Y,Austin RC,Werstuck GH. Valproate protects cells from ER stress-induced lipid accumulation and apoptosis by inhibiting glycogen synthase kinase-3. *J. Cell. Sci.*2005;118:89-99.
32. Werstuck GH,Kim AJ,Brenstrum T,Ohnmacht SA,Panna E,Capretta A. Examining the correlations between GSK-3 inhibitory properties and anti-convulsant efficacy of valproate and valproate-related compounds. *Bioorg. Med. Chem. Lett.*2004;14:5465-5467.
33. Chen G,Huang LD,Jiang Ym,Manji HK.The mood-stabilizing agent valproate inhibits the activity of glycogen synthase kinase-3. *J. Neurochem.*1999;72:1327-1330.
34. De Sarno P, Li XH,Jope RS. Regulation of akt and glycogen synthase kinase-3 beta phosphorylation by sodium valproate and lithium. *Neuropharmacology.*2002;43:1158-1164.
35. Maitra U, Li L. Molecular mechanisms responsible for the reduced expression of cholesterol transporters from macrophages by low-dose endotoxin. *Arterioscler. Thromb. Vasc. Biol. 2013;*33:24-33.
36. Ai D,Baez JM,Jiang H,Conlon DM,Hernandez-Ono A,Frank-Kamenetsky M,Milstein S, Fitzgerald K,Murphy AJ,Woo CW,Strong A,Ginsberg HN,Tabas I,Rader DJ,Tall AR.Activation of ER stress and mTORC1 suppresses hepatic sortilin-1 levels in obese mice. *J. Clin. Invest.*2012;122:1677-1687.
37. Raciti GA,Iadicicco C,Ulianich L,Vind BF,Gaster M, Andreozzi F,Longo M, Teperino R,Ungaro P,Di Jeso B,Formisano P,Beguinot F,Miele C.Glucosamine-induced endoplasmic reticulum stress affects GLUT4 expression via activating

transcription factor 6 in rat and human skeletal muscle cells. *Diabetologia.*2010;53:955-965.
38. Sage AT,Walter LA,Shi Y,Khan MI,Kaneto H,Capretta A,Werstuck GH. Hexosamine biosynthesis pathway flux promotes endoplasmic reticulum stress, lipid accumulation, and inflammatory gene expression in hepatic cells. *Am. J. Physiol. Endocrinol. Metab.*2010;298:499-E511.
39. Beriault DR,Sharma S,Shi Y,Khan MI,Werstuck GH. Glucosamine-supplementation promotes endoplasmic reticulum stress, hepatic steatosis and accelerated atherogenesis in ApoE-/- mice. *Atherosclerosis.*2011;219:134-140.
40. Guo W,Wong S,Xie W,Lei T,Luo Z.Palmitate modulates intracellular signaling, induces endoplasmic reticulum stress, and causes apoptosis in mouse 3T3-L1 and rat primary preadipocytes. *Am.J. Physiol. Endocrinol. Metab.*2007;293:576-586.
41. Steinbrecher K,Wilson W, Cogswell P,Baldwin A. Glycogen synthase kinase 3 beta functions to specify gene-specific, NF-kappa B-dependent transcription. *Mol. Cell Biol.*2005;25:8444-8455.
42. Martin M,Rehani K,Jope R,Michalek S. Toll-like receptor-mediated cytokine production is differentially regulated by glycogen synthase kinase 3. *Nat. Immunol.*2005;6:777-784.
43. Pengal R, Ganesan L,Wei G,Fang H,Ostrowski M,Tridandapani S. Lipopolysaccharide-induced production of interleukin-10 is promoted by the serine/threonine kinase akt. *Mol. Immunol.*2006;43:1557-1564.
44. Thorp E,Li G,Seimon TA, Kuriakose G,Ron D,Tabas I. Reduced apoptosis and plaque necrosis in advanced atherosclerotic lesions of apoe-/- and ldlr-/- mice lacking CHOP. *Cell Metabolism.*2009;9:474-481.
45. Oyadomari S, Harding HP,Zhang Y,Oyadomari M,Ron D.Dephosphorylation of translation initiation factor 2 alpha enhances glucose tolerance and attenuates hepatosteatosis in mice. *Cell Metab*. 2008;7:520-532.
46. Wang C,Huang Z,Du Y,Cheng Y,Chen S,Guo F.ATF4 regulates lipid metabolism and thermogenesis. *Cell Res*.2010;20:174-184.
47. Lee A, Scapa EF, Cohen DE,Glimcher LH. Regulation of hepatic lipogenesis by the transcription factor XBP1. *Science.*2008;320:1492-1496.
48. Jo H,Shim J,Lee JH,Lee J,Kim JB. IRE-1 and HSP-4 contribute to energy homeostasis via fasting-induced lipases in C. elegans. *Cell Metab.*2009;9:440-448.
49. Yamamoto K,Takahara K,Oyadomari S,Okada T,Sato T,Harada A,Mori K. Induction of liver steatosis and lipid droplet formation in ATF6 alpha-knockout mice burdened with pharmacological endoplasmic reticulum stress. *Mol. Biol. Cell.*2010;21:2975-2986.
50. Lee A,Glimcher LH. Intersection of the unfolded protein response and hepatic lipid metabolism. *Cell Mol. Life Sci.*2009;66:2835-2850.
51. Frame S,Cohen PGSK3 takes centre stage more than 20 years after its discovery.*Biochem. J.*2001;359:1-16.

CHAPTER 5: Deletion of Myeloid GSK3α Attenuates Atherosclerosis and Promotes an M2 Macrophage Phenotype

Cameron S.McAlpine,[1,3] Aric Huang,[3] Abby Emdin,[3] Nicole S. Banko,[2,3] Daniel R. Beriault,[2,3] Yuanyuan Shi[1,3] and Geoff H.Werstuck[1,2,3]

Departments of [1]Medicine, [2]Biochemistry and Biomedical Sciences, and the [3]Thrombosis and Atherosclerosis Research Institute, McMaster University, Hamilton, Ontario, Canada

5.1 FOREWORD

This study investigates the tissue specific functions of GSK3α and GSK3β in atherosclerosis. We demonstrate that deletion of hepatic GSK3α or GSK3β does not alter liver lipid metabolism or atherosclerosis in high fat diet fed $LDLR^{-/-}$ mice. Deletion of myeloid GSK3α but not GSK3β reduces atherosclerosis and lesion complexity. Mechanistically, deletion of GSK3α attenuates M1 macrophage polarization and promotes M2 macrophage polarization by modulating STAT3 and STAT6 phosphorylation and activation.

This work was published in *Arteriosclerosis, Thrombosis and Vascular Biology*, volume 35, pages 1113-1122, May 2015. The experiments in this study were conducted by Cameron McAlpine with assistance from the co-authors. The manuscript was written by Cameron McAlpine in collaboration with Dr. Geoff Werstuck. The content of Chapter 5 is a direct representation of this publication. The complete reference is as follows: McAlpine CS, Huang A, Emdin A, Banko NS, Beriault DR, Shi Y and Werstuck GH. Deletion of myeloid GSK3α attenuates atherosclerosis and promotes an M2 macrophage phenoypte. *Arteriosclerosis, Thrombosis and Vascular Biology*. 2015;35:1113-1122.

5.2 ABSTRACT

Objective

Glycogen Synthase Kinase (GSK)-3α/β has been implicated in the pathogenesis of diabetes, cancer, Alzheimer's and atherosclerosis. The tissue and homolog specific functions of GSK3α and β in atherosclerosis are unknown. This study examines the effect of hepatocyte or myeloid cell deletion of GSK3α or GSK3β on atherosclerosis in $LDLR^{-/-}$ mice.

Approach and results

We ablated GSK3α or GSK3β expression in hepatic or myeloid cells of $LDLR^{-/-}$ mice and mice were fed a high fat diet for 10 weeks. GSK3α or GSK3β deficiency in hepatic or myeloid cells did not affect metabolic parameters, including plasma lipid levels. Hepatic deletion of GSK3α or GSK3β did not affect the development of atherosclerosis or hepatic lipid content. Myeloid deletion of GSK3α, but not GSK3β, reduced atherosclerotic lesion volume as well as lesion complexity. Mice lacking GSK3α in myeloid cells had a less inflammatory and more anti-inflammatory plasma cytokine profile. Macrophages within atherosclerotic lesions of myeloid GSK3α deficient mice, but not GSK3β deficient mice, displayed reduced expression of markers associated with M1 macrophage polarization and enhanced expression of the M2 markers. Finally, bone marrow derived macrophages were isolated and differentiated into classical M1 macrophages or alternative M2 macrophages *in vitro*. GSK3α deletion, but not GSK3β deletion, attenuated the expression of genes associated with M1 polarization while promoting the expression of genes associated with M2 polarization by modulating STAT3 and STAT6 activation.

Conclusions

Our findings suggest that deletion of myeloid GSK3α attenuates the progression of atherosclerosis by promoting an M2 macrophage phenotype.

5.3 INTRODUCTION

Atherosclerosis is the main underlying pathology of cardiovascular disease which accounts for the majority of deaths in developed nations.[1] Myeloid lineage cells are critical mediators in the development of atherosclerosis and account for the majority of a lesion's cellular bulk.[2] Within the atherosclerotic lesion, macrophages phagocytose modified lipid particles becoming lipid engorged foam cells. Foam cells exacerbate disease progression through the secretion of pro-inflammatory cytokines and growth factors. In advanced lesions, foam cells undergo apoptosis leading to the formation of a lipid rich, acellular and highly thrombotic necrotic core. The underlying molecular mechanisms that regulate myeloid cell behavior during atherosclerosis remain poorly defined.

Increasing evidence suggests myeloid cell subpopulations are heterogeneous and have distinctive phenotypes that play unique roles in disease states. Macrophages are often broadly classified as having a classical (M1) or an alternative (M2) phenotype. M1 macrophages, elicited by toll-like receptor (TLR) or interferon-γ receptor (IFNγR) stimulation, are the most prominent macrophages at sites of inflammation and exacerbate the inflammatory response through the secretion of pro-inflammatory cytokines and chemoatractants.[3, 4] M1 macrophages promote atherosclerotic lesion development and complexity.[5-7] M2 macrophages patrol tissue, perform reparative and immunoregulatory functions, efferocytose debris and are anti-atherogenic.[3, 4, 8] Other

macrophage subtypes have been identified in atherosclerotic lesions including M4, Mox and Mhem, however, their roles are less well characterized.[3, 5, 9, 10] Our understanding of the cellular signaling networks that regulate macrophage polarization in the context of atherosclerosis and the relative contribution of each phenotype to the progression and development of atherosclerosis is limited.

Glycogen synthase kinase (GSK)-3 α and β are homologous serine/threonine kinases encoded by separate genes.[11] GSK3α and GSK3β share 98% amino acid homology within their kinase domain but only 36% homology in the C terminal domain. GSK3α (51 kDa) is 5kDa larger than GSK3β (46kDa) due to an N-terminal glycine rich domain with an unknown function. Both GSK3α and GSK3β are ubiquitously expressed although expression levels vary greatly from tissue to tissue.GSK3α/β is found in the cytoplasm, endoplasmic reticulum (ER) and nucleus of most cells.[11] Originally described as a regulator of glycogen synthase and βcatenin, GSK3α/β is now recognized to be a target of a number of signaling networks including insulin/PI3K/AKT, MAPKs and ER stress.[11, 12] While GSK3α and GSK3β share a number of common substrates they are not redundant and appear to have distinct functions.[13-15] Whole body GSK3α-deficient mice are viable and develop normally while GSK3β deletion is embryonically lethal.[16-19] Recent evidence has suggested a role for GSK3α/β in atherosclerosis. In mouse models, pharmacological inhibition of GSK3α/β or whole body GSK3α deletion attenuates atherosclerotic lesion formation and the development of hepatic steatosis.[19-21] While suggestive of a role for GSK3α/β in atherosclerosis, the homolog and tissue specific function of GSK3α and GSK3β as well as the mechanism by which GSK3α/β regulates atherosclerosis are not known.

We have developed hepatocyte and myeloid cell specific GSK3α or GSK3β knockout LDLR$^{-/-}$ mice. Our results demonstrate that GSK3α and GSK3β play distinctive homolog and tissue specific roles during atherogenesis. Specifically, myeloid GSK3α, but not GSK3β, deletion promotes an M2 macrophage phenotype and attenuates high fat diet-induced atherosclerosis.

5.4 METHODS

An expanded methods section is available in Appendix 3

Mice

The Cre-loxP system was utilized to specifically ablate GSK3α or GSK3β expression in myeloid or hepatic cells of LDLR$^{-/-}$ mice. To generate mice lacking GSK3α or GSK3β in hepatic cells, LDLR$^{-/-}$ mice were crossed with GSK3α-floxed[22] or GSK3β-floxed[23] mice (resulting in LDLR$^{-/-}$GSK3β$^{fl/fl}$ and LDLR$^{-/-}$GSK3α$^{fl/fl}$ mice). Resultant mice were crossed with mice expressing Cre recombinase under the control of the hepatocyte specific albumin promoter (Alb). This breeding strategy resulted in LDLR$^{-/-}$ GSK3α$^{fl/fl}$AlbCre^{+} mice, referred to as LDLR$^{-/-}$ liver-specific GSK3α knockout (LLαKO) and LDLR$^{-/-}$GSK3β$^{fl/fl}$AlbCre^{+} mice, referred to as LDLR$^{-/-}$ liver-specific GSK3β knockout (LLβKO). Similarly, to generate mice lacking GSK3α or GSK3β in myeloid cells, LDLR$^{-/-}$ GSK3α$^{fl/fl}$ and LDLR$^{-/-}$GSK3β$^{fl/fl}$ mice were crossed with mice expressing Cre recombinase under the control of the myeloid cell specific lysozyme M promoter (LyzM). This breeding strategy resulted in LDLR$^{-/-}$GSK3α$^{fl/fl}$LyzMCre$^{+/-}$ mice, referred to as LDLR$^{-/-}$ myeloid-specific GSK3α knockout (LMαKO) and LDLR$^{-/-}$GSK3β$^{fl/fl}$LyzMCre$^{+/-}$ mice, referred to as LDLR$^{-/-}$ myeloid-specific GSK3β knockout (LMβKO). As controls, littermates lacking expression of the Cre recombinase were used and are referred to as

Lαfl/fl (LDLR$^{-/-}$GSK3α$^{fl/fl}$) and Lβfl/fl (LDLR$^{-/-}$GSK3β$^{fl/fl}$). All mice have a C57Bl/6 genetic background (>99.9%). Genotypes were determined by PCR (Supplementary Figure IA). All mice were fed a high fat diet (HFD, 21% milk fat, 0.2% cholesterol, Harlan Teklad, TD97363) for 10 weeks beginning at 5 weeks of age. GSK3α$^{-/-}$ mice were used for bone marrow transplantation (BMT) experiments.[16, 19] Briefly, 5 week old recipient mice were irradiated and then injected with bone marrow (3X10^6 cells) from donor mice. Recipient mice were then fed a HFD for 10 weeks. All mice had unlimited access to food and water and were maintained on a 12 hour light/dark cycle. All animal experiments were conducted with approval of the McMaster University Animal Research Ethics Board.

5.5 RESULTS

Hepatic or myeloid cell specific GSK3α or β knockout LDLR$^{-/-}$ mice are viable and develop normally

Tissue specific ablation of GSK3α or GSK3βprotein expression was confirmed by immunoblot (Figure 5.1A). LLαKO and LLβKO mice have no detectible expression of hepatic GSK3α or GSK3β protein respectively, but retain GSK3α/β expression in all other tissues including heart, quadriceps muscle and brain. Similarly, LMαKO and LMβKO mice have no detectible expression of macrophage GSK3α or GSK3β protein respectively but retain GSK3α/β expression in all other tissues. There was no detectable compensation in the expression of the retained homolog when GSK3α or GSK3β was deleted in hepatic or myeloid cells (Figure 5.1B). All mice are viable, fertile, born at expected Mendelian frequencies and do not display any overt phenotype. All mouse strains have similar body weights to littermate controls (Table 5.1 and 5.2, Supplementary Figure IB).

Figure 5.1. Characterization of hepatic and myeloid cell specific GSK3α and GSK3β knockout LDLR$^{-/-}$ mice. A) Whole tissue lysates from indicated tissues of LLαKO, LLβKO, LMαKO and LMβKO mice and littermate controls were resolved by SDS PAGE and probed for GSK3α and GSK3β protein. Immunoblots confirm tissue specific ablation of GSK3α or GSK3β in hepatic or myeloid tissue. **B)** Quantified GSK3α and GSK3β protein levels in liver tissue and macrophages determined by densitometry analysis. Data is shown as a fold change relative to the corresponding homolog in the same tissue of the control mice. ns = not significant, n=4, *p<0.05

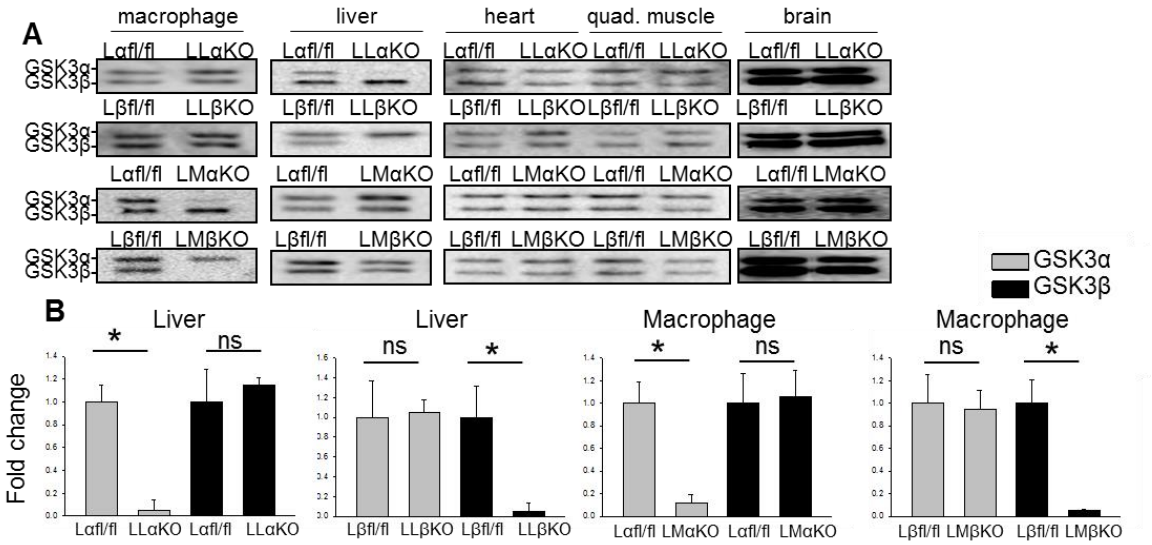
A
macrophage
liver
heart
quad. muscle
brain
GSK3α
GSK3β
Lαfl/fl LLαKO
Lβfl/fl LLβKO
Lαfl/fl LMαKO
Lβfl/fl LMβKO
GSK3α
GSK3β
B
Liver
Liver
Macrophage
Macrophage
Fold change
*
ns
Lαfl/fl LLαKO Lαfl/fl LLαKO
Lβfl/fl LLβKO Lβfl/fl LLβKO
Lαfl/fl LMαKO Lαfl/fl LMαKO
Lβfl/fl LMβKO Lβfl/fl LMβKO

Table 5.1. Metabolic parameters of LLαKO, LLβKO and control mice. n=12

	Lαfl/fl	LLαKO	Lβfl/fl	LLβKO
Fasting Plasma Concentration (mmol/L)				
Glucose	7.4±0.7	7.0±1.4	7.2±1.2	6.9±1.1
Cholesterol	24.6±5.4	26.9±5.3	27.4±5.2	30.8±6.7
Triglyceride	2.2±0.3	2.1±0.6	2.4±0.3	2.3±0.4
Adipose weight (g)	0.23±0.13	0.25±0.14	0.22±0.1	0.23±0.11
Liver weight (g)	1.10±0.19	1.14±0.18	1.03±0.24	1.06±0.14
Body weight (g)	22.2±1.5	23.7±2.7	23.8±2.3	24.3±2.2

Table 5.2. Metabolic parameters of LMαKO, LMβKO and control mice. n=12

	Lαfl/fl	LMαKO	Lβfl/fl	LMβKO
Fasting Plasma Concentration (mmol/L)				
Glucose	7.7±1.5	7.4±1	6.8±1.3	7.5±0.8
Cholesterol	25.2±5.2	26.5±5.7	27±4.9	28±4.7
Triglyceride	2.1±0.4	2.3±0.5	2.5±0.2	2.3±0.3
Adipose weight (g)	0.24±0.12	0.25±0.12	0.23±0.11	0.21±0.09
Liver weight (g)	1.05±0.18	1.10±0.22	1.13±0.27	1.14±0.31
Body weight (g)	23.3±1.8	24.0±1.4	23.8±1.7	25.2±2.4

Hepatic GSK3α or GSK3β deletion does not impact atherosclerosis

To determine the effect of hepatic GSK3α or GSK3β deletion on atherosclerosis at the aortic root, female LLαKO and LLβKO mice and Lαfl/fl and Lβfl/fl controls were placed on a high fat diet (HFD, 21% milk fat and 0.2%cholesterol) for 10 weeks beginning at 5 weeks of age. Metabolic parameters including plasma cholesterol, plasma triglyceride, blood glucose, liver weight and adipose weight were not altered in HFD fed LLαKO and LLβKO mice relative to controls (Table 5.1). Analysis of atherosclerotic lesions at the aortic root revealed no change in lesion area, lesion volume or necrotic core volume in LLαKO and LLβKO mice relative to Lαfl/fl and Lβfl/fl controls (Supplementary Figure IIA-C and F-I). Hepatic GSK3α or GSK3β deletion did not impact plasma IL-6, TNFα or IL-10 levels (Supplementary Figure IIE and J). Similar effects were observed in male mice (Supplementary Figure III). These data suggest that modulation of hepatic GSK3α or βactivity does not affect atherosclerosis.

Hepatic GSK3α or GSK3β deletion does not impact hepatic lipid content

GSK3α/β signaling plays an important role in the regulation of cellular lipid metabolism.[12, 19, 20, 24] However, the homolog specific functions of GSK3α and GSK3β in hepatic lipid metabolism have not been determined. We therefore analyzed lipid metabolism in the liver of HFD fed LLαKO and LLβKO mice. Relative to Lαfl/fl and Lβfl/fl controls, LLαKO and LLβKO mice do not display altered liver neutral lipid, cholesterol or triglyceride content (Figure 5.2A-D and F-I). Moreover, hepatic GSK3α or GSK3β deletion did not result in altered plasma lipid profiles (Figure 5.2E and J). Lastly, liver expression of genes involved in lipid homeostasis including SREBP1c, SREBP2,

HMGCoA, FAS, SR-A, SR-B1, ABCA1 and ABCG1 were unaffected by hepatic GSK3α or GSK3β deletion in mice fed a HFD (Supplementary Figure IV).

Figure 5.2. Hepatic and plasma lipids in female LLαKO and LLβKO mice.

Representative images of hepatic tissue sections from LLαKO mice **(A)**, LLβKO mice **(F)** and control mice stained with Oil Red O and Hematoxylin. **(B and G)** Quantification of Oil Red O stained area. Cholesterol **(C and H)** and triglyceride **(D and I)** levels within hepatic tissue of LLαKO, LLβKO and control mice **(E and J)**.Plasma lipid profiles of LLαKO mice, LLβKO and control mice. n=6-10, *$p<0.05$

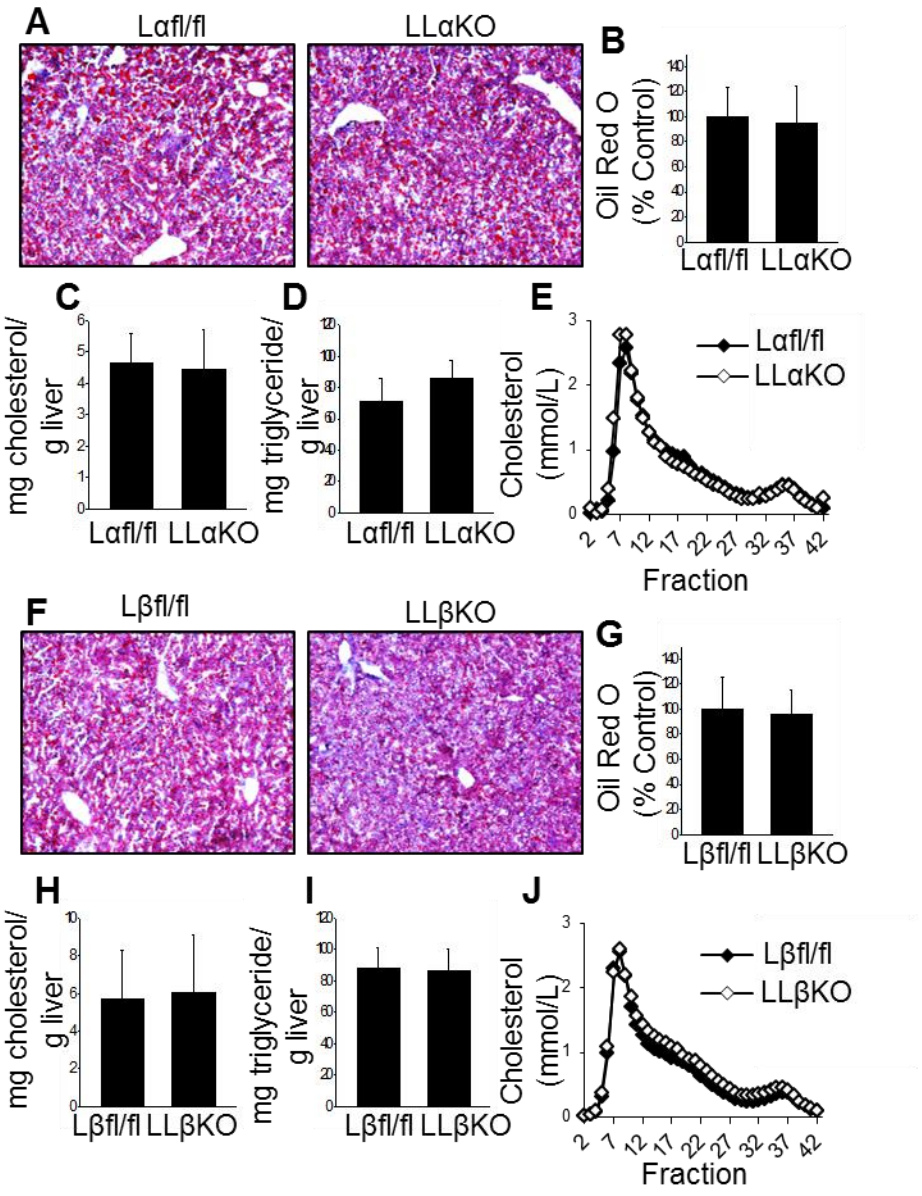
A
Lαfl/fl
LLαKO
B
Oil Red O (% Control)
Lαfl/fl LLαKO
C
mg cholesterol/ g liver
Lαfl/fl LLαKO
D
mg triglyceride/ g liver
Lαfl/fl LLαKO
E
Cholesterol (mmol/L)
Lαfl/fl
LLαKO
Fraction
F
Lβfl/fl
LLβKO
G
Oil Red O (% Control)
Lβfl/fl LLβKO
H
mg cholesterol/ g liver
Lβfl/fl LLβKO
I
mg triglyceride/ g liver
Lβfl/fl LLβKO
J
Cholesterol (mmol/L)
Lβfl/fl
LLβKO
Fraction

Myeloid GSK3α deletion attenuates atherosclerosis

To determine the role of GSK3α in myeloid cells during atherogenesis, LMαKO and Lαfl/fl control mice were placed on a HFD. After 10 weeks of HFD feeding, myeloid cell ablation of GSK3α did not significantly alter plasma cholesterol, triglyceride or glucose concentrations, or affect liver or adipose weight (Table 5.2). Furthermore, myeloid GSK3α deletion did not impact hepatic lipid content or plasma lipid profiles relative to controls (Supplementary Figure VA-E). LMαKO mice did, however, have significantly reduced atherosclerotic lesion area, lesion volume and necrotic core volume relative to Lαfl/fl controls (Figure 5.3A-D). Myeloid GSK3α deletion also reduced lesion collagen content, fibrous cap thickness and smooth muscle content, suggestive of less complex and less advanced lesions (Supplementary Figure VIA-E). Recent evidence suggests that GSK3α/β plays a role in the regulation of inflammatory cytokine expression.[19, 25, 26] To investigate this further we analyzed the plasma cytokine profile in LMαKO mice. After 10 weeks of HFD LMαKO mice displayed reduced plasma levels of the pro-inflammatory cytokines IL-6 and TNFα, and increased plasma levels of the anti-inflammatory cytokine IL-10 (Figure 5.3E). Similar effects were observed in male LMαKO mice (Supplementary Figure VIIA-C).

Whole body GSK3α deficiency attenuates atherosclerosis in HFD fed $LDLR^{-/-}$ mice.[19] To investigate the role of myeloid GSK3α in an alternate model of experimental atherosclerosis, $LDLR^{-/-}$ mice were irradiated and transplanted with $LDLR^{-/-}GSK3\alpha^{-/-}$or $LDLR^{-/-}GSK3\alpha^{+/+}$ (control) bone marrow. We found that atherosclerosis was attenuated in $LDLR^{-/-}$ mice receiving $LDLR^{-/-}GSK3\alpha^{-/-}$bone marrow relative to controls (Supplementary Figure VIIIA-C).Conversely, transplantation of $LDLR^{-/-}$ bone marrow into $LDLR^{-/-}GSK3\alpha^{-/-}$ mice enhanced atherosclerotic lesion formation relative to control $LDLR^{-}$

$^{-/-}$GSK3α$^{-/-}$ mice transplanted with LDLR$^{-/-}$GSK3α$^{-/-}$ bone marrow (Supplementary Figure VIIID-F). All bone marrow transplantation models displayed unaltered metabolic parameters (Supplementary Table I).

Figure 5.3. Atherosclerosis in female LMαKO mice. A) Representative aortic root sections from HFD fed LMαKO and Lαfl/fl littermate control mice stained with hematoxylin and eosin (H&E), Masons Trichrome or Oil Red O. **B)** Quantification of atherosclerotic lesion area at the aortic sinus and ascending aorta of LMαKO and control mice. Quantification of atherosclerotic lesion volume **(C)** and necrotic core volume **(D)**. n=10-12, *p<0.05. **E)** Plasma levels of IL-6, TNFα and IL-10 after 10 weeks of HFD. n=6-8, *p<0.05

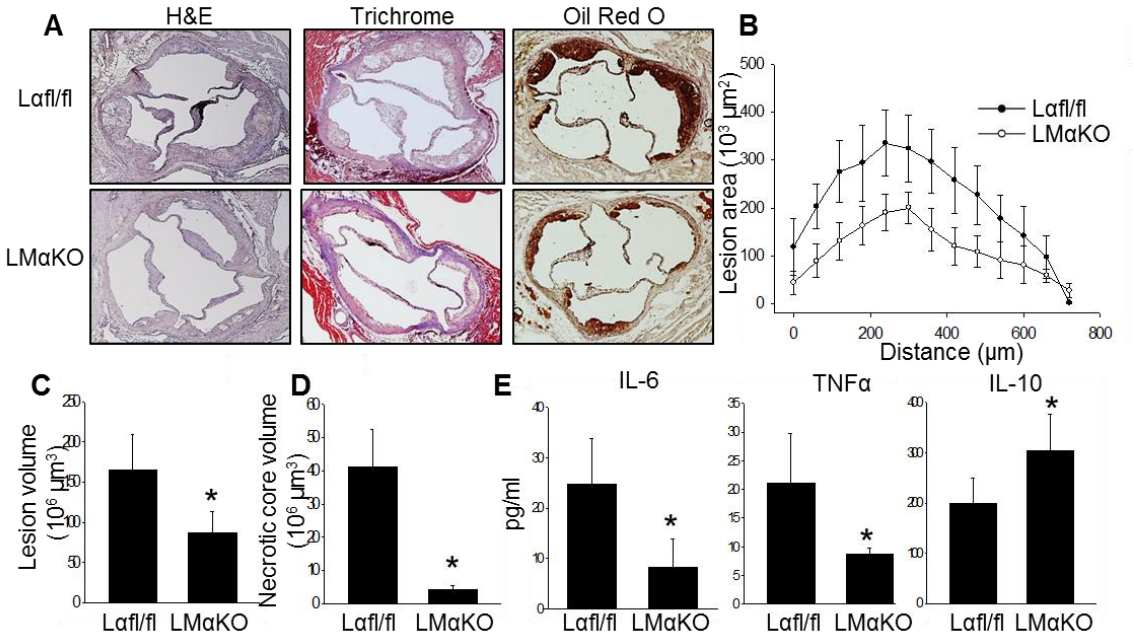
A
H&E
Trichrome
Oil Red O
Lαfl/fl
LMαKO
B
Lesion area (10³ µm²)
Distance (µm)
Lαfl/fl
LMαKO
C
Lesion volume (10⁶ µm³)
D
Necrotic core volume (10⁶ µm³)
E
IL-6
TNFα
IL-10
pg/ml
Lαfl/fl
LMαKO

Myeloid GSK3β deletion does not alter atherosclerosis

Myeloid GSK3β deletion did not affect plasma cholesterol, triglyceride or glucose concentration, or alter liver or adipose weight (Table 5.2). Moreover, LMβKO mice display similar levels of hepatic lipids and an unaltered plasma lipid profile relative to Lβfl/fl controls (Supplementary Figure VF-J). At the aortic root, myeloid GSK3β deletion did not impact atherosclerotic lesion area or volume (Figure 5.4A-C). LMβKO mice did, however, have reduced necrosis within their atherosclerotic lesion (Figure 5.4D). Myeloid GSK3β deficiency did not alter lesion fibrous cap thickness, collagen content or smooth muscle cell content (Supplementary Figure VIF-J). After 10 weeks of HFD the only detected difference in the plasma cytokine profile of LMβKO mice was a decrease in IL-6 with no change in TNFα or IL-10 levels (Figure 5.4E). Similar effects were observed in male LMβKO mice (Supplementary Figure VIID-F).

Figure 5.4. Atherosclerosis in female LMβKO mice. A) Representative aortic root sections from HFD fed LMβKO and Lβfl/fl littermate control mice stained with hematoxylin and eosin (H&E), Masons Trichrome or Oil Red O. **B)** Quantification of atherosclerotic lesion area at the aortic sinus and ascending aorta of LMβKO and control mice . Quantification of atherosclerotic lesion volume **(C)** and necrotic core volume **(D)**. n=10-12, *p<0.05. **E)** Plasma levels of IL-6, TNFα and IL-10 after 10 weeks of HFD. n=6-8, *p<0.05

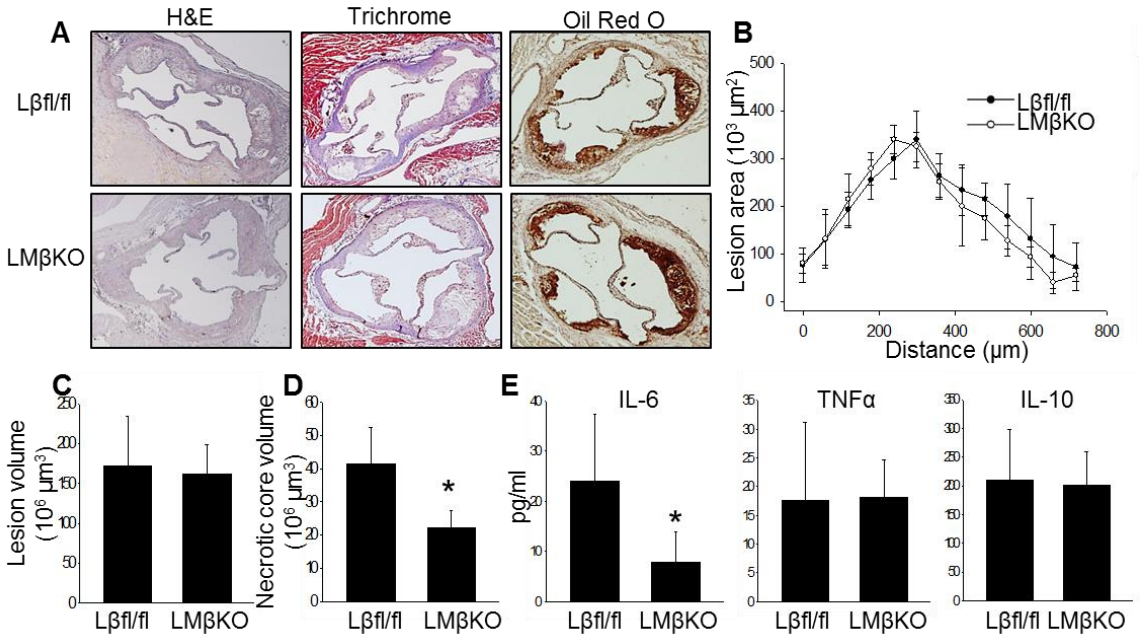
A
H&E
Trichrome
Oil Red O
Lβfl/fl
LMβKO
B
Lesion area (10³ µm²)
Distance (µm)
Lβfl/fl
LMβKO
C
Lesion volume (10⁶ µm³)
D
Necrotic core volume (10⁶ µm³)
E
IL-6
pg/ml
TNFα
IL-10
Lβfl/fl
LMβKO

GSK3α deletion promotes M2 macrophage polarization

We examined the possible effects of myeloid GSK3α or GSK3β deficiency on monocyte subsets and macrophage phenotype. We first established that myeloid GSK3α or GSK3β deletion does not alter the number of monocytes in whole blood (Supplementary Figure IXA). Next, $Cd115^{+}Cd11b^{+}$ monocytes were gated from whole blood of LMαKO, LMβKO and control mice; and Ly6Cexpression was determined by flow cytometry. Myeloid deletion of GSK3α or GSK3β did not impact the proportion of $Ly6C^{hi}$, $Ly6C^{int}$ or $Ly6C^{lo}$monocyte populations, suggesting that GSK3α/β does not play a role in the differentiation of these monocyte subsets (Supplementary Figure IXB).

We next investigated the effect of GSK3α or GSK3β deletion on macrophage polarization within atherosclerotic lesions. Analysis of the entire length of the lesion revealed that $Mac3^{+}$ macrophages from lesions of LMαKO mice displayed decreased expression of the M1 markers, fatty acid binding protein (FABP)-4 and CD36, and increased expression of the M2 markers Arginasae (Arg)-1 and peroxisome proliferator-activated receptor gama coactivator (Pgc)-1 (Figure 5.5).[27] $Mac3^{+}$ cells within the atherosclerotic lesions of LMβKO mice showed no change in the expression of M1 markers and an increase in the expression of the M2 marker Pgc1, but not Arg1 (Figure 5.5).

To further investigate the role of GSK3α and GSK3β in macrophage polarization, bone marrow was isolated from LMαKO, LMβKO and control mice. Cells were exposed to 10ng/ml MCSF for 5 days to induce differentiation into unstimulated, M0, bone marrow derived macrophages (BMDMs). BMDMs were then polarized into classical M1 macrophages by exposure to 10ng/ml LPS for 6 hours or polarized into alternative M2 macrophages by exposure to 10ng/ml IL-4 for 24 hours. Total RNA was isolated from the

cells and the transcript expression of genes suggestive of M1 or M2 polarization was determined. GSK3α-deficient macrophages treated with LPS had significantly decreased expression of the M1 markers TNFα, IL-6, CD36, FABP4, IL-1β and IL-12 (Figure 5.6A).[27] Similarly treated GSK3β-deficient macrophages had decreased expression of FABP4, IL-1β and IL-12 (Figure 5.6A). GSK3α-deficient macrophages had elevated levels of the M2 markers IL-10, Arg1, Fizz1, Ym1, Mgl-2 and Pgc1β, when exposed to IL-4 (Figure 5.6B).[27] Similarly treatedGSK3β-deficient macrophages had elevated expression of Arg1 only, relative to controls (Figure 5.6B).

Signal transducer and activator of transcription (STAT) proteins regulate transcription of the M1 and M2 gene programs (reviewed by Biswas and Mantovani[28]). In M1 polarized cells STAT1 becomes phosphorylated and promotes the transcription of the M1 gene program.[29-31] As a negative feedback mechanism, STAT3 is also phosphorylated in M1 cells and suppresses P-STAT1 activity by forming STAT3:STAT1 heterodimers.[32-35] Exposing macrophages to IL-4 results in the phosphorylation of STAT6 and the transcription of the M2 gene program.[36-38] We investigated the effect of GSK3α or GSK3β deletion on STAT phosphorylation/activation. Exposure of BMDMs to LPS resulted in the phosphorylation and activation of STAT1 and STAT3 (Figure 5.6C and D). GSK3α or GSK3β deletion did not alter P-Tyr701-STAT1 levels (Figure 5.6C and D). GSK3α deletion, but not GSK3β deletion, promoted P-Tyr705-STAT3 in LPS treated macrophages (Figure 5.6C and D). Polarization of BMDMs into M2 macrophages by IL-4 induced STAT6 phosphorylation and deletion of GSK3α, but not GSK3β, promoted P-Tyr641-STAT6 relative to controls (Figure 5.6C and D). Together, these data suggest that myeloid GSK3α deficiency enhances the M2 macrophage phenotype through increased STAT3 and STAT6 phosphorylation and activation.

Figure 5.5. M1 and M2 polarization of lesional macrophages of female LMαKO and LMβKO mice. Atherosclerotic lesions of LMαKO, LMβKO and control mice were probed with specific antibodies against the macrophage marker Mac3 and co-probed with antibodies against the M1 markers FABP4 **(A)** or CD36 **(B)**. FABP4 and CD36 staining intensity within the atherosclerotic lesions (outlined) was quantified relative to controls. Atherosclerotic lesions were stained for the M2 markers Arg1 **(C)** or Pgc1 **(D)**. Arg1 and Pgc1 staining intensity within the atherosclerotic lesion (outlined) was quantified relative to controls. n=6, *p<0.05

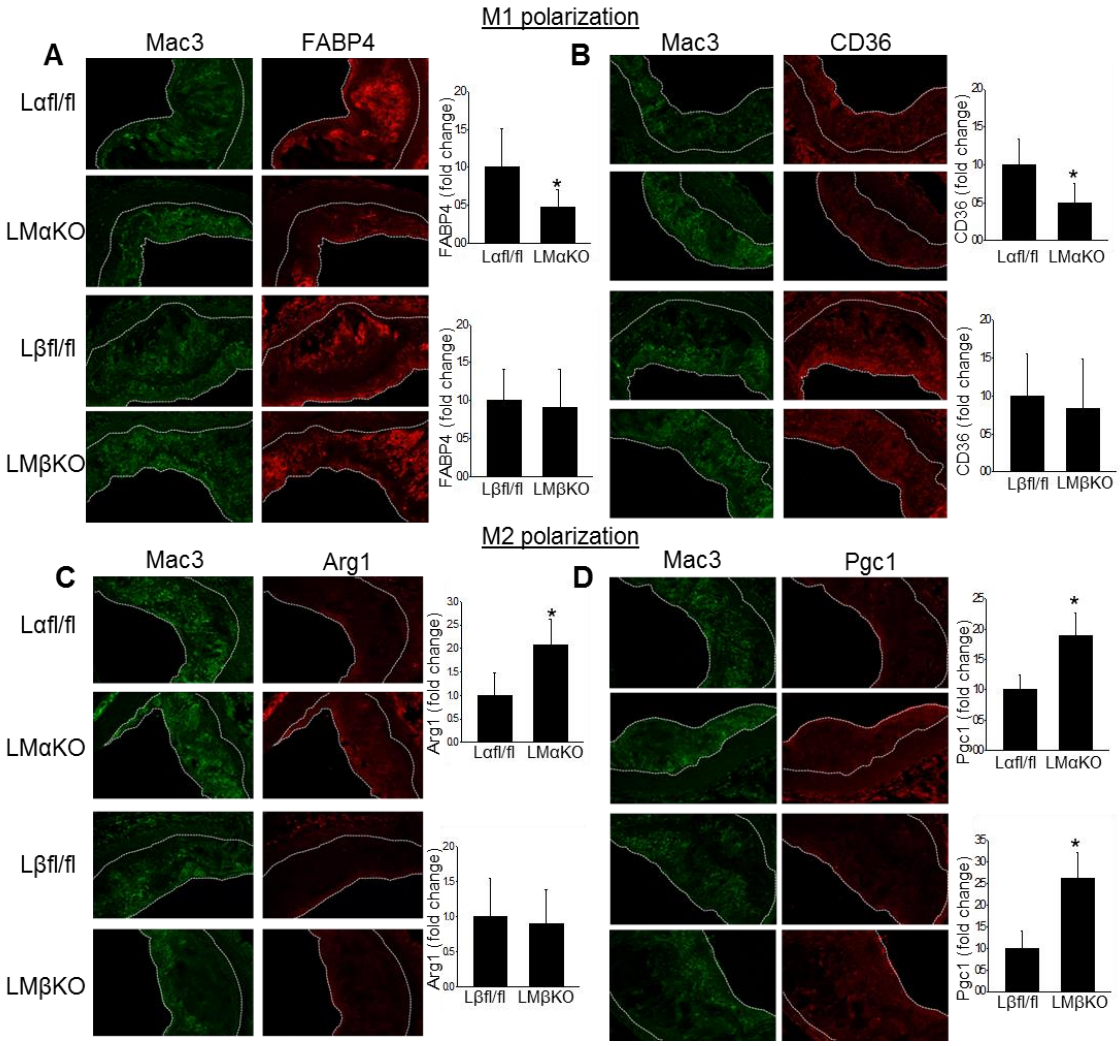
M1 polarization
A
Mac3
FABP4
Lαfl/fl
LMαKO
Lβfl/fl
LMβKO
FABP4 (fold change)
Lαfl/fl LMαKO
Lβfl/fl LMβKO
B
Mac3
CD36
CD36 (fold change)
Lαfl/fl LMαKO
Lβfl/fl LMβKO
M2 polarization
C
Mac3
Arg1
Arg1 (fold change)
Lαfl/fl LMαKO
Lβfl/fl LMβKO
D
Mac3
Pgc1
Pgc1 (fold change)
Lαfl/fl LMαKO
Lβfl/fl LMβKO

Figure 5.6. M1 and M2 macrophage polarization of GSK3α- or GSK3β-deficient BMDMs. Bone marrow derived macrophages (BMDMs) were isolated from female LMαKO, LMβKO and control mice and exposed to 10 ng/ml LPS for 6 hours to induce M1 polarization or 10 ng/ml IL-4 for 24 hours to induced M2 polarization. Transcript expression of genes associated with M1 and M2 macrophage polarization were determined by RT-PCR. **A)** M1 polarization markers included TNFα, IL-6, CD36, FABP4, IL-1β and IL-12. **B)** M2 polarization markers included IL-10, Arg1, Fizz1, Ym1, Mgl-2 and Pgc1β. **C)** Cell lysates were resolved by SDS PAGE and immunoblots were probed for P-STAT1, P-STAT3 and P-STAT6; total STAT1, STAT3 and STAT6; and βactin. **D)** Densitometry analysis of STAT phosphorylation in BMDMs. n=4-5, *$p<0.05$

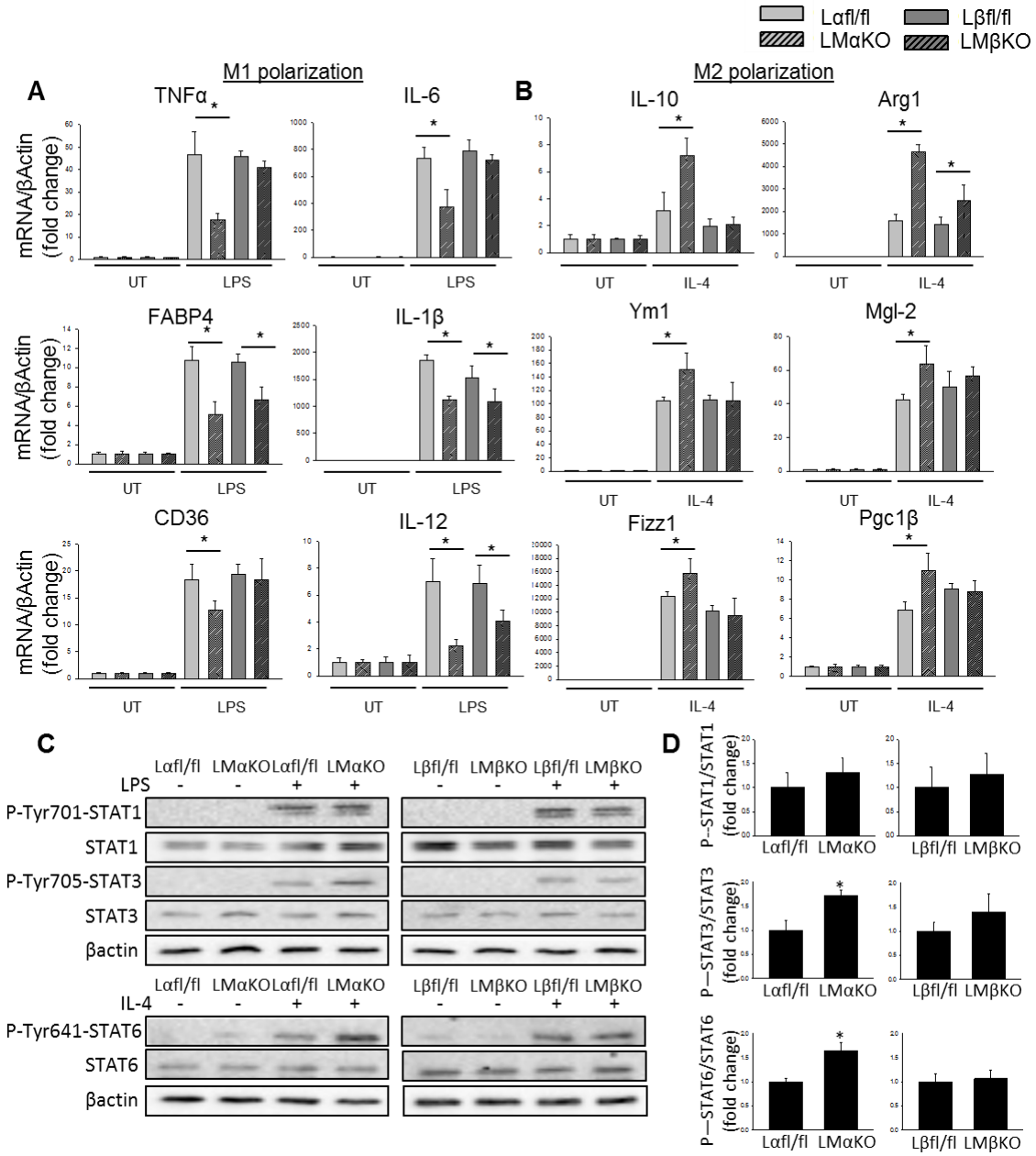
Lαfl/fl
LMαKO
Lβfl/fl
LMβKO
A
M1 polarization
TNFα
IL-6
B
M2 polarization
IL-10
Arg1
FABP4
IL-1β
Ym1
Mgl-2
CD36
IL-12
Fizz1
Pgc1β
mRNA/βActin (fold change)
UT
LPS
IL-4
C
LPS
IL-4
P-Tyr701-STAT1
STAT1
P-Tyr705-STAT3
STAT3
P-Tyr641-STAT6
STAT6
βactin
D
P–STAT1/STAT1 (fold change)
P—STAT3/STAT3 (fold change)
P—STAT6/STAT6 (fold change)

5.6 DISCUSSION

Here we present the first evidence for tissue and homolog specific functions of GSK3α/β in atherosclerosis. Myeloid GSK3α deletion, but not GSK3β deletion, attenuated atherosclerosis in HFD LDLR$^{-/-}$ mice and promoted an anti-inflammatory cytokine profile. Bone marrow from LDLR$^{-/-}$ (GSK3α$^{+/+}$) mice enhanced atherosclerotic lesion formation when transplanted into LDLR$^{-/-}$GSK3α$^{-/-}$ mice. Moreover, macrophage GSK3α deletion suppressed M1 polarization and promoted M2 polarization in both cultured macrophages and macrophages within the atherosclerotic lesion. Hepatic deletion of GSK3α or GSK3β did not alter liver lipid levels, plasma lipid profiles or atherosclerosis at the aortic root. Together, these data highlight a critical and specific role for myeloid GSK3α in atherosclerosis progression and macrophage phenotype.

Signaling through GSK3α/β is important in the regulation of liver glucose and lipid metabolism. Systemic inhibition of GSK3α/β improves glucose tolerance and insulin sensitivity in multiple rodent models of diabetes.[39, 40] We have previously shown that systemic inhibition of GSK3α/β or whole body deletion of GSK3α attenuates hepatic steatosis.[19, 20] Herein, we present data that hepatocyte or myeloid cell specific deletion of GSK3α or β does not alter plasma or liver lipid levels. Similarly, hepatocyte specific deletion of GSK3α or GSK3β does not alter glucose or insulin metabolism, tolerance or signaling.[22, 23] These observations may be explained by the high degree of homology and substrate similarity between GSK3α and GSK3β and suggest functional redundancy in lipid metabolism within hepatic cells. Moreover, these observations may be indicative of the complex coordination between liver endothelial cells, Kupffer cells and hepatocytes in the regulation of liver lipid metabolism. Indeed, depletion of Kupffer cells attenuates hepatic steatosis and improves insulin sensitivity.[41-43] Together, these results

suggest functional GSK3α/β signaling in multiple cell types coordinate glucose, insulin and lipid metabolism in the liver.

Prior to this study, investigations into the role of GSK3α/β in animal models of atherosclerosis used non-specific inhibitors or whole body genetic deletion.[19-21] These studies were unable to differentiate whether GSK3α/β's role in atherosclerosis was due to alterations in peripheral tissue, such as the liver or adipose, or local alterations within the vessel wall. In this report we clearly show that GSK3α plays a local role in myeloid cells within the aortic wall during atherosclerosis development. In support of our results from the LMαKO mice, we observe that transplantation of $LDLR^{-/-}$ ($GSK3\alpha^{+/+}$) bone marrow into $LDLR^{-/-}GSK3\alpha^{-/-}$mice restores atherosclerotic lesion formation. This is a critical observation as $LDLR^{-/-}GSK3\alpha^{-/-}$ mice transplanted with $LDLR^{-/-}$ bone marrow lack GSK3α expression in other cell types important to atherosclerosis progression including endothelial cells and smooth muscle cells and further suggests GSK3α's function in atherosclerosis is myeloid cell specific. However, as in liver pathology, cross-talk between cell types within the lesion is important during atherosclerosis development.[44] Our observations of reduced collagen deposition, fibrous cap thickness and smooth muscle cell content in the lesions of LMαKO mice, suggestive of less complex and less advanced lesions, is consistent with this hypothesis.

Recent studies have implicated a role for GSK3α/β signaling in macrophage function.[12, 19, 25, 26] We have extended these findings and present the first evidence suggesting GSK3α regulates macrophage, but not monocyte, polarization. While deletion of GSK3α does not impact $Ly6C^{hi/int/lo}$ monocyte populations, it does shift macrophage polarization towards an M2 phenotype and away from an M1 phenotype. This shift along the macrophage spectrum towards an M2 phenotype may explain the

anti-inflammatory cytokine profile and attenuated atherosclerosis observed in LMαKO mice. Indeed, deletion of STAT1, a key promoter of M1 genes, attenuates atherosclerosis while IL-13 deletion inhibits M2 polarization and promotes atherosclerosis.[7, 8, 45] Moreover, during regression of atherosclerotic lesions macrophages switch from an M1 phenotype to an M2 phenotype.[46, 47] Mhem and Mox macrophages also play functional roles in atherosclerosis progression however their contributions are less well characterized.

Together our data are consistent with a model in which pro-atherogenic stimuli signal through macrophage GSK3α to promote lesion growth and development. The factors that lie directly upstream of GSK3α have yet to be identified. Our previous results have suggested that endoplasmic reticulum stress activates GSK3α/β via induction of the PERK pathway.[12, 20] Recently, the serine/threonine kinase AKT has been shown to modulate atherosclerosis and macrophage polarization.[48] This is intriguing as AKT is activated by ER stress and is a known regulator of GSK3α/β. The factors lying directly downstream of GSK3α are also not known. Herein we present evidence for STAT3 and STAT6 being targets of GSK3α signaling. Increased P-STAT3in GSK3α-null M1 cells and increased P-STAT6 in GSK3α-null M2 cells underscores the role of GSK3α activation in shifting macrophages towards the M1 phenotype and promoting atherosclerosis. Furthermore, GSK3α/β is an established regulator of NF-κB which also influences macrophage phenotype.[17, 49] The identification of the factors directly upstream and downstream of GSK3α in JAK/STAT signaling and their impact on M1 and M2 polarization is a critical next step.

The therapeutic potential of small molecule inhibitors of GSK3α/β has been limited by our lack of understanding of its homolog specific functions. Our results

suggest that specific targeting of GSK3α may have a number of clinical advantages as an anti-atherogenic therapy. First, modulating specific macrophage subpopulations in the vessel wall may alter local macrophage behavior while retaining systemic functions. Further, the inhibition of GSK3α specifically would be predicted to have fewer side effects, because GSK3β signaling would be maintained.

In summary, we present the first evidence for tissue and homolog specific functions of GSK3α/β in atherosclerosis. We demonstrate that myeloid cell GSK3α signaling regulates atherosclerosis development and macrophage polarization.

5.7 REFERENCES FOR CHAPTER 5

1. Yusuf S, Hawken S, Ounpuu S, et al. Effect of potentially modifiable risk factors associated with myocardial infarction in 52 countries (the INTERHEART study): case-control study. *Lancet*. 2004;364:937-952.
2. Hansson G, Libby P. The immune response in atherosclerosis: a double-edged sword. *Nat Rev Immunol*. 2006;6:508-519.
3. Mantovani A, Garlanda C, Locati M. Macrophage Diversity and Polarization in Atherosclerosis A Question of Balance. *Arteriosclerosis Thrombosis and Vascular Biology*. 2009;29:1419-1423.
4. Leitinger N, Schulman IG. Phenotypic Polarization of Macrophages in Atherosclerosis.*ArterioscIerThrombVasc Biol*. 2013;33:1120-1126.
5. Khallou-Laschet J, Varthaman A, Fornasa G, et al. Macrophage Plasticity in Experimental Atherosclerosis. *Plos One*. 2010;5:e8852.
6. Lim W, Timmins JM, Seimon TA, et al. Signal transducer and activator of transcription-1 is critical for apoptosis in macrophages subjected to endoplasmic reticulum stress in vitro and in advanced atherosclerotic lesions in vivo. *Circulation*. 2008;117:940-951.
7. Agrawal S, Febbraio M, Podrez E, Cathcart MK, Stark GR, Chisolm GM. Signal transducer and activator of transcription 1 is required for optimal foam cell formation and atherosclerotic lesion development. *Circulation*. 2007;115:2939-2947.
8. Cardilo-Reis L, Gruber S, Schreier SM, et al. Interleukin-13 protects from atherosclerosis and modulates plaque composition by skewing the macrophage phenotype. *EMBO Mol Med*. 2012;4:1072-1086.
9. Kadl A, Meher AK, Sharma PR, et al. Identification of a Novel Macrophage Phenotype That Develops in Response to Atherogenic Phospholipids via Nrf2. *Circ Res*. 2010;107:737-U155.
10. De Paoli F, Staels B, Chinetti-Gbaguidi G. Macrophage Phenotypes and Their Modulation in Atherosclerosis.*Circ J*. 2014;78:1775-1781.

11. Doble BW, Woodgett JR. GSK-3: tricks of the trade for a multi-tasking kinase. *J Cell Sci*. 2003;116:1175-1186.
12. McAlpine CS, Werstuck GH. PKR-Like Endoplasmic Reticulum Kinase and Glycogen Synthase Kinase-3alpha/beta Regulate Foam Cell Formation.*J Lipid Res.* 2014;55:2320-2333.
13. Doble BW, Patel S, Wood GA, Kockeritz LK, Woodgett JR. Functional redundancy of GSK-3 alpha and GSK-3 beta in Wnt/beta-catenin signaling shown by using an allelic series of embryonic stem cell lines. *Developmental Cell*. 2007;12:957-971.
14. WANG Q, PARK I, FIOL C, ROACH P, DEPAOLIROACH A. Isoform Differences in Substrate Recognition by Glycogen-Synthase Kinase-3-Alpha and Kinase-3-Beta in the Phosphorylation of Phosphatase Inhibitor-2. *Biochemistry (N Y)*. 1994;33:143-147.
15. Soutar MPM, Kim W, Williamson R, et al. Evidence that glycogen synthase kinase-3 isoforms have distinct substrate preference in the brain. *J Neurochem*. 2010;115:974-983.
16. MacAulay K, Doble BW, Patel S, et al. Glycogen synthase kinase 3alpha-specific regulation of murine hepatic glycogen metabolism. *Cell Metab*. 2007;6:329-337.
17. Hoeflich K, Luo J, Rubie E, Tsao M, Jin O, Woodgett J. Requirement for glycogen synthase kinase-3 beta in cell survival and NF-kappa B activation. *Nature*. 2000;406:86-90.
18. Kerkela R, Kockeritz L, MacAulay K, et al. Deletion of GSK-3 beta in mice leads to hypertrophic cardiomyopathy secondary to cardiomyoblasthyperproliferation. *J Clin Invest*. 2008;118:3609-3618.
19. Banko N, McAlpine CS, Venegas-Pino DE, et al. Glycogen Synthase Kinase (GSK)-3alpha deficiency attenuates atherosclerosis and hepatic steatosis in high fat diet fed $LDLR^{-/-}$ mice. *American Journal of Physiology*. 2014;184:3394-3404.
20. McAlpine CS, Bowes AJ, Khan MI, Shi Y, Werstuck GH. Endoplasmic Reticulum Stress and Glycogen Synthase Kinase-3 beta Activation in Apolipoprotein E-Deficient Mouse Models of Accelerated Atherosclerosis.*ArterioscIerThrombVasc Biol*. 2012;32:82-U204.
21. Choi S, Jang H, Kang Y, et al. Atherosclerosis induced by a high-fat diet is alleviated by lithium chloride via reduction of VCAM expression in ApoE-deficient mice. *Vascular Pharmacology*. 2010;53:264-272.
22. Patel S, Macaulay K, Woodgett JR. Tissue-specific analysis of glycogen synthase kinase-3alpha (GSK-3alpha) in glucose metabolism: effect of strain variation. *PLoS One*. 2011;6:e15845.
23. Patel S, Doble BW, MacAulay K, Sinclair EM, Drucker DJ, Woodgett JR. Tissue-specific role of glycogen synthase kinase 3beta in glucose homeostasis and insulin action. *Mol Cell Biol*. 2008;28:6314-6328.
24. Bowes AJ, Khan MI, Shi Y, Robertson L, Werstuck GH. Valproate attenuates accelerated atherosclerosis in hyperglycemic apoE-deficient mice: evidence in support of a role for endoplasmic reticulum stress and glycogen synthase kinase-3 in lesion development and hepatic steatosis. *Am J Pathol*. 2009;174:330-342.
25. Hu X, Paik P, Chen J, et al. IFN-gamma suppresses IL-10 production and synergizes with TLR2 by regulating GSK3 and CREB/AP-1 proteins. *Immunity*. 2006;24:563-574.

26. Antoniv TT, Ivashkiv LB. Interleukin-10-induced gene expression and suppressive function are selectively modulated by the PI3K-Akt-GSK3 pathway. *Immunology*. 2011;132:567-577.
27. Byles V, Covarrubias AJ, Ben-Sahra I, et al. The TSC-mTOR pathway regulates macrophage polarization. *Nat Commun*. 2013;4:2834.
28. Biswas SK, Mantovani A. Macrophage plasticity and interaction with lymphocyte subsets: cancer as a paradigm. *Nat Immunol*. 2010;11:889-896.
29. Toshchakov V, Jones B, Perera P, et al. TLR4, but not TLR2, mediates IFN-beta-induced STAT1 alpha/beta-dependent gene expression in macrophages. *Nat Immunol*. 2002;3:392-398.
30. Kovarik P, Stoiber D, Novy M, Decker T. Stat1 combines signals derived from IFN-gamma and LPS receptors during macrophage activation. *EMBO J*. 1998;17:3660-3668.
31. Ohmori Y, Hamilton T. Requirement for STAT1 in LPS-induced gene expression in macrophages. *J Leukoc Biol*. 2001;69:598-604.
32. Riley J, Takeda K, Akira S, Schreiber R. Interleukin-10 receptor signaling through the JAK-STAT pathway - Requirement for two distinct receptor-derived signals for anti-inflammatory action. *J Biol Chem*. 1999;274:16513-16521.
33. Matsukawa A, Kudo S, Maeda T, et al. Stat3 in resident macrophages as a repressor protein of inflammatory response. *J Immunol*. 2005;175:3354-3359.
34. Ho H, Ivashkiv L. Role of STAT3 in type I interferon responses - Negative regulation of STAT1-dependent inflammatory gene activation. *J Biol Chem*. 2006;281:14111-14118.
35. Shen Y, Devgan G, Darnell J, Bromberg J. Constitutively activated Stat3 protects fibroblasts from serum withdrawal and UV-induced apoptosis and antagonizes the proapoptotic effects of activated Stat1. *ProcNatlAcadSci U S A*. 2001;98:1543-1548.
36. Welch J, Escoubet-Lozach L, Sykes D, Liddiard K, Greaves D, Glass C. T(H)2 cytokines and allergic challenge induce YM1 expression in macrophages by a STAT6-dependent mechanism. *J Biol Chem*. 2002;277:42821-42829.
37. Van den Bossche J, Bogaert P, van Hengel J, et al. Alternatively activated macrophages engage in homotypic and heterotypic interactions through IL-4 and polyamine-induced E-cadherin/catenin complexes. *Blood*. 2009;114:4664-4674.
38. Sinha P, Clements V, Ostrand-Rosenberg S. Interleukin-13-regulated M2 macrophages in combination with myeloid suppressor cells block immune surveillance against metastasis. *Cancer Res*. 2005;65:11743-11751.
39. Frame S, Zheleva D. Targeting glycogen synthase kinase-3 in insulin signalling. *Expert OpinTher Targets*. 2006;10:429-444.
40. Wagman A, Johnson K, Bussiere D. Discovery and development of GSK3 inhibitors for the treatment of type 2 diabetes. *Curr Pharm Des*. 2004;10:1105-1137.
41. Huang W, Metlakunta A, Dedousis N, et al. Depletion of Liver Kupffer Cells Prevents the Development of Diet-Induced Hepatic Steatosis and Insulin Resistance. *Diabetes*. 2010;59:347-357.
42. Stienstra R, Saudale F, Duval C, et al. Kupffer Cells Promote Hepatic Steatosis Via Interleukin-1 beta-Dependent Suppression of Peroxisome Proliferator-Activated Receptor alpha Activity. *Hepatology*. 2010;51:511-522.

43. Neyrinck A, Taper H, Gevers V, Declerck B, Delzenne M. Inhibition of Kupffer cell activity induces hepatic triglyceride synthesis in fasted rats, independent of lipopolysaccharide challenge. *J Hepatol*. 2002;36:466-473.
44. Sahar S, Dwarakanath R, Reddy M, Lanting L, Todorov I, Natarajan R. Angiotensin II enhances interleukin-18 mediated inflammatory gene expression in vascular smooth muscle cells - A novel cross-talk in the pathogenesis of atherosclerosis. *Circ Res*. 2005;96:1064-1071.
45. Lim W, Timmins JM, Seimon TA, et al. Signal transducer and activator of transcription-1 is critical for apoptosis in macrophages subjected to endoplasmic reticulum stress in vitro and in advanced atherosclerotic lesions in vivo. *Circulation*. 2008;117:940-951.
46. Feig JE, Vengrenyuk Y, Reiser V, et al. Regression of Atherosclerosis Is Characterized by Broad Changes in the Plaque Macrophage Transcriptome. *PLoS One*. 2012;7:e39790.
47. Hewing B, Parathath S, Mai CK, Fiel MI, Guo L, Fisher EA. Rapid regression of atherosclerosis with MTP inhibitor treatment. *Atherosclerosis*. 2013;227:125-129.
48. Babaev VR, Hebron KE, Wiese CB, et al. Macrophage deficiency of Akt2 reduces atherosclerosis in LDLR null mice. *J Lipid Res.*2014;55:2296-2308.
49. Schwabe R, Brenner D. Role of glycogen synthase kinase-3 in TNF-alpha-induced NF-kappa B activation and apoptosis in hepatocytes. *Am J Physiol - Gastroint Liver Physiol*. 2002;283:G204-G211.

CHAPTER 6: General Discussion

The clinical outcomes of atherosclerosis, including myocardial infarction and stroke, are an increasing health burden. Despite the wide use of statins (inhibitors of cholesterol synthesis) the prevalence of atherosclerosis and CVD continue to rise and remain the primary cause of death globally.[3] The goal of this research project was to identify and characterize novel molecular and cellular mechanisms in atherosclerosis that could be targeted therapeutically. A working model of ER stress and GSK3α/β mediated atherosclerosis is presented in Figure 6.1.

Prior to the investigations presented in this thesis a role for GSK3α/β in atherosclerosis was suggested, but poorly understood.[123, 153, 154] Therefore, we sought to delineate the role of GSK3α/β signaling using multiple animal models of experimental atherosclerosis. As presented in Chapter 3, three different ApoE$^{-/-}$ mouse models of accelerated atherosclerosis were established involving hyperglycemia, hyperhomocysteinemia and relative dyslipidemia. Each condition enhanced ER stress levels in hepatic tissue and in the aortic wall, and accelerated the development of atherosclerosis at the aortic sinus. Furthermore, pro-atherogenic conditions enhanced GSK3β activity in the liver by promoting Tyr216 phosphorylation. A subset of mice from each group was supplemented with the GSK3α/β inhibitor valproate. Valproate supplementation inhibited GSK3β activity, increased Ser9 phosphorylation and attenuated atherosclerosis but did not alter ER stress levels. This study is the first to demonstrate a function for GSK3α/β signaling in multiple murine models of accelerated atherosclerosis.

Figure 6.1. Working Model. Working model of macrophage endoplasmic reticulum (ER) stress and glycogen synthase kinase (GSK)-3α/β mediated atherosclerosis. In macrophages, multiple cardiovascular risk factors induce ER stress which promotes the upregulation of chaperones and foldases along with the attenuation of translation. Downstream of these adaptive mechanisms, protein kinase R-like endoplasmic reticulum kinase (PERK) signaling activates GSK3α/β. Subsequently, GSK3α and/or GSK3β mediate distal pro-atherogenic ER stress responses including foam cell formation, C/EBP homologous protein (CHOP) expression and inflammation

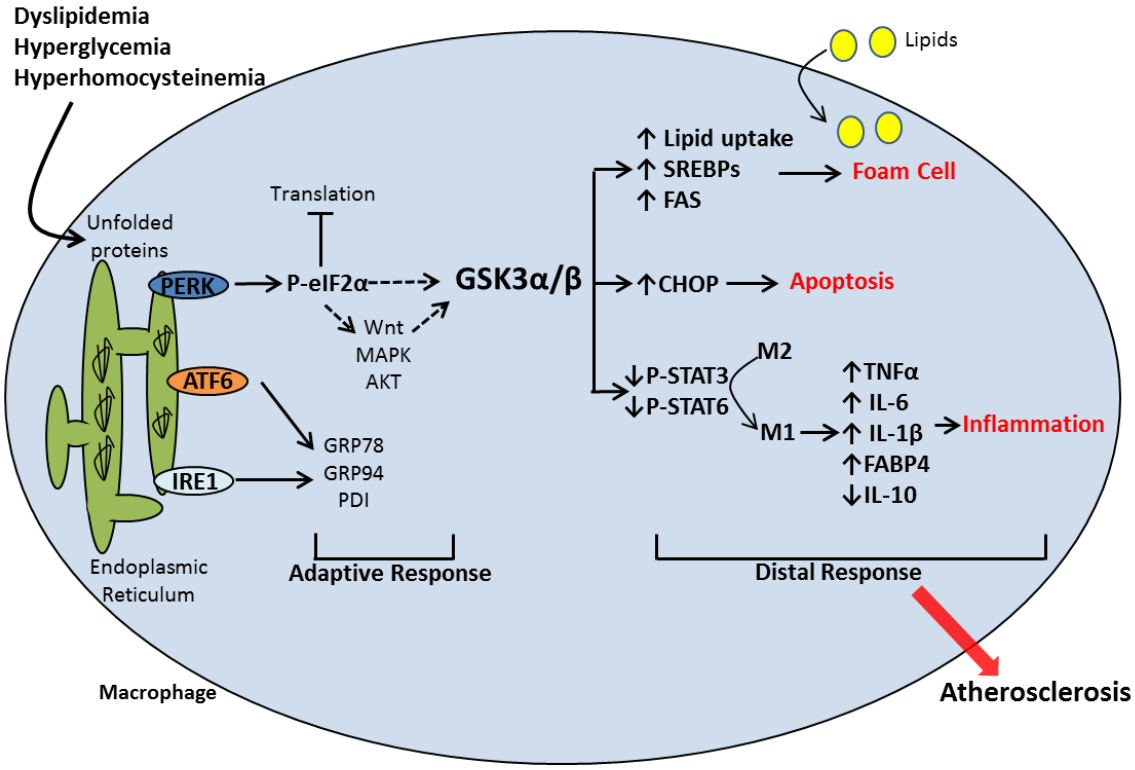
Dyslipidemia
Hyperglycemia
Hyperhomocysteinemia
Lipids
↑ Lipid uptake
↑ SREBPs
↑ FAS
Foam Cell
Translation
Unfolded proteins
PERK
P-eIF2α
GSK3α/β
↑CHOP
Apoptosis
Wnt
MAPK
AKT
M2
↓P-STAT3
↓P-STAT6
↑TNFα
↑ IL-6
M1
↑ IL-1β
Inflammation
↑FABP4
↓IL-10
ATF6
GRP78
GRP94
PDI
IRE1
Endoplasmic Reticulum
Adaptive Response
Distal Response
Macrophage
Atherosclerosis

Valproate (valproic acid or 2-propylpentanoic acid) is a small branched fatty acid clinically prescribed as an anti-convulsant and a mood stabilizer.[155] The molecular mechanisms that confer its clinical and therapeutic efficacy are unclear. Exposure of neuronal cells to valproate induces the upregulation of cellular chaperones protecting them from cytotoxicity and ER stress.[156-158] Further, valproate acts as an inhibitor of histone deacetylases (HDACs).[159, 160] Histones undergo a dynamic process of acetylation and deacetylation which impacts gene transcription by altering the ability of transcription factors to bind to DNA.[161] Valproate is also a direct and indirect inhibitor of GSK3α and GSK3β.[73, 162-164] Due to GSK3α/β's diverse role in cellular metabolism including glucose regulation, lipid metabolism and apoptosis, we anticipate that valproate's anti-atherogenic effects are conferred by its ability to inhibit GSK3α/β. In fact, HDAC inhibition has been shown to exacerbate atherosclerosis.[165] In response to atherogenic stimulus and/or valproate supplementation, modulation of GSK3β's activity appears to result from changes in its phosphorylation state. This suggests that, in these animal models, valproate is altering GSK3α/β activity, at least partially, through an indirect mechanism. Indeed, valproate has been demonstrated to modulate AKT and ERK signaling independent of its effects on GSK3α/β.[166, 167] Our early *in vivo* observations of GSK3α/β inhibition by valproate attenuating atherosclerosis were recently corroborated by Choi *et al.* who observed that a structurally distinct GSK3α/β inhibitor, lithium, reduced atherosclerosis in HFD fed ApoE$^{-/-}$ mice.[168]

To establish a direct role for GSK3α/β in atherosclerosis, our group recently analyzed the effect of whole body GSK3α deletion in LDLR$^{-/-}$ mice.[67] HFD fed GSK3α$^{-/-}$ LDLR$^{-/-}$ and GSK3α$^{+/-}$LDL$^{-/-}$ mice have significantly reduced atherosclerotic lesion size (70% and 50% respectively) relative to LDLR$^{-/-}$ controls. This study was the first to

investigate the role of GSK3α/β in atherosclerosis by genetic manipulation. Along with the results presented in Chapter 3, these observations suggest an important function for GSK3α/β signaling in the progression of atherosclerosis. The molecular mechanisms by which GSK3α/β regulates pro-atherogenic processes, however, remained elusive.

In Chapter 3, we observed increased ER stress associated with increased GSK3β activity and that inhibition of GSK3α/β activity reduces atherosclerosis without altering ER stress levels. These observations suggested that GSK3α/β is a target of UPR signaling and that UPR-GSK3α/β mediates pro-atherogenic responses. This association, however, had yet to be shown directly. Further, the specific UPR pathway (PERK, IRE1 or ATF6, see Figure 1.2) that targets and modulates GSK3α/β activity during ER stress signaling had not been identified.

In Chapter 4, we investigated ER stress and GSK3α/β signaling in macrophage foam cell formation. In these experiments we relied on a highly specific GSK3α/β inhibitor, CT99021, along with siRNA directed GSK3α/β knockdown.[169] In macrophages, ER stress enhanced GSK3α/β activity in a PERK, but not IRE1 or ATF6, dependent manner. GSK3α/β knockdown or inhibition did not impact chaperone expression or the attenuation of translation, which are adaptive, pro-survival, components of the ER stress response. Inhibition of GSK3α/β signaling did, however, attenuate the expression of CHOP and ATF4, which are distal, pro-apoptotic, components of the PERK branch of the UPR. GSK3α/β inhibition attenuated ER stress induced lipid synthesis and uptake in macrophages. Moreover, constitutive GSK3β activation enhanced foam cell formation even in the presence of a PERK inhibitor. These results defined a novel signaling pathway in which GSK3α/β is a distal component of the PERK branch of the UPR and that PERK-GSK3α/β signaling regulates macrophage lipid metabolism and foam cell

formation. The targets directly upstream and downstream of GSK3α/β in PERK signaling have not been identified. Intriguingly, many kinase signaling pathways that target GSK3α/β, including PI3K/AKT, Wnt and JNK, have also been linked to PERK signaling.[170-172]

Over the past decade a critical role for UPR signaling in metabolic diseases, including atherosclerosis, has emerged.[28] Atherosclerosis is a complicated multifactorial disease and many chemically and biologically diverse risk factors promote a similar disease pathology. The molecular mechanism by which multiple risk factors promote disease progression is not well understood. We present data in Chapter 3 and 4 that suggest a critical role for ER stress in the progression of atherosclerosis. Our observations support the hypothesis of UPR activation being a unifying molecular mechanism of atherosclerosis development. Multiple risk factors as diverse as dyslipidemia and hyperglycemia induce the UPR and UPR activation promotes many atherogenic processes including foam cell formation, apoptosis and inflammation.[28] This central hypothesis, however, should be tested further. The chemical chaperone 4PBA resolves ER stress and attenuates atherosclerosis progression in HFD fed ApoE$^{-/-}$ and LDLR$^{-/-}$ mice.[66, 173] Moreover, our group has observed that 4PBA treatments can regress lesions in HFD fed LDLR$^{-/-}$ mice (unpublished data). Testing the ability of 4PBA to attenuate and regress atherosclerosis in multiple animal models of metabolic dysfunction, including hyperglycemia and hypercholesterolemia, is a critical next step.

The specific UPR branches (IRE1, ATF6 and PERK) that contribute to the pathologies of atherosclerosis and metabolic dysfunction have only begun to be investigated. IRE1 alternatively splices the transcript encoding XBP resulting in the translation of a functional transcription factor that binds directly to the promoter/enhancer

region of SREBP2 and FAS, enhancing their expression.[174] Further, IRE1β deficiency in ApoE$^{-/-}$ mice increases plasma triglyceride and cholesterol levels, due to increased lipid absorption from the gut, and as a consequence, accelerates atherosclerosis.[175] Both ATF6 and SREBP2 are activated by the same proteolytic machinery and ATF6 has been linked to SREBP2 activation.[176] Moreover, ER stress induction in macrophages promotes lipid uptake through the upregulation of CD36 and this is at least partially mediated by ATF6 signaling.[177] Similar results have been found in animal models as ATF6 deletion increases hepatic cholesterol and triglyceride levels.[178] Finally, and as presented in Chapter 4 of this thesis, PERK signaling plays a central role in metabolism. Oyadomari and colleagues demonstrated that inhibition of PERK signaling in mice by reduced eIF2α phosphorylation attenuated hepatic lipid accumulation and improved glucose and insulin tolerance.[179] In another model of attenuated PERK signaling, Wang *et al.* demonstrated that ATF4 deficient mice have reduced plasma triglyceride levels along with reduced FAS and lipoprotein lipase (LPL) expression.[180] Lastly, CHOP deletion in both ApoE$^{-/-}$ and LDLR$^{-/-}$ mice attenuates atherosclerosis.[87] The work presented in Chapter 4 extends our understanding of PERK signaling in metabolic disease and suggests that GSK3α/β is a downstream target.

Increasing evidence suggests that sustained inflammation, due to improper resolution, is the underlying stimulus of atherosclerosis progression. Multiple cardiovascular risk factors including hyperglycemia and dyslipidemia are associated with a state of chronic inflammation.[181, 182] Interestingly, a functional role for ER stress has been implicated in the inflammatory response; the induction of ER stress activates NF-κB and enhances the expression of TNFα, IL-6 and MCP-1.[183, 184] Furthermore, inflammation can itself impair ER homeostasis.[185] A link between ER stress and

inflammation has been extended to macrophage polarization - our group has demonstrated that ER stress promotes IL-6 expression and suppresses IL-10 expression in macrophages.[67, 186] Moreover, the UPR mediates STAT phosphorylation and activation.[149] The mechanism by which ER stress regulates the inflammatory process, and macrophage polarization in particular, is not well understood and worthy of further investigation. For example, does ER stress alone promote a specific macrophage phenotype or does ER stress induce macrophage phenotypic switching in pre-polarized cells? If ER stress does play a significant role in macrophage polarization, is the attenuation or regression of atherosclerosis in mice by 4PBA due to a transition from an M1 to an M2 phenotype? These questions will have to be addressed experimentally and may illuminate novel roles of ER stress in atherosclerosis.

Data presented in this thesis supports the hypothesis that GSK3α/β is a downstream target of ER stress signaling. GSK3α/β inhibition by valproate in animals or CT99021 and siRNA in cell culture does not impact the adaptive and restorative components of ER stress response, including the expression of the chaperones GRP78/94, the foldase PDI and the attenuation of translation by eIF2α phosphorylation. Rather; GSK3α/β appears to mediate the distal and maladaptive components of the ER stress response, including the induction of the pro-apoptotic factor CHOP and the dysregulation of lipid metabolism. The “multiple hit” hypothesis of ER stress signaling suggests that a second “hit” of ER stress, either a second inducer or prolonged UPR activation, is required for the induction of distal ER stress pathways.[30, 31] Our observations suggest GSK3α/β may act as a mediator or “gate-keeper” between the adaptive pro-survival and the distal, maladaptive and pro-atherogenic ER stress responses. This theory, however, needs to be tested further. For example, a time course

experiment monitoring GSK3α/β activation as well as adaptive and apoptotic pathways during initial and prolonged UPR activation could be conducted. Another possibility is to monitor GSK3α/β activation during a mild ER stress response followed by augmentation with a second more potent ER stress inducing agent, such as enhanced cholesterol trafficking from the plasma membrane to the ER.[49, 51, 84]

The results from Chapter 3 and 4 have a number of limitations. First, GSK3α/β inhibitors, including valproate, lithium and CT99021, are unable to distinguish between the GSK3α and GSK3β homologs. While our lab's observation of smaller atherosclerotic lesions in GSK3α$^{-/-}$LDLR$^{-/-}$ mice illuminated a role for GSK3α in atherosclerosis, the role of GSK3β was unknown and could not be investigated using a similar model due to the embryonic lethality of whole body GSK3β deficiency.[93, 95] Lastly, the use of inhibitors and whole body genetic knockouts impose systemic effects and the tissue specific functions of GSK3α/β in atherosclerosis were unknown. Does GSK3α or β mediate atherosclerosis by altering metabolism in the liver or modulating cell function within the aortic wall? To overcome these limitations and to answer these questions, we developed hepatocyte or myeloid cell specific GSK3α or GSK3β knockout LDLR$^{-/-}$ mice.

As presented in Chapter 5, LDLR$^{-/-}$ mice lacking GSK3α or GSK3β in hepatocytes or myeloid cells are viable, fertile, born at expected frequencies and do not display any overt phenotype. When placed on a HFD all mouse models display unaltered metabolic parameters. Hepatocyte GSK3α or GSK3β deletion did not impact atherosclerosis at the aortic root or lipid levels in the liver. Importantly, myeloid GSK3α deletion, but not myeloid GSK3β deletion, attenuated atherosclerosis. Myeloid GSK3α deficient mice displayed a more anti-inflammatory and less pro-inflammatory plasma cytokine profile. Mechanistically, GSK3α deletion, more so than GSK3β deletion,

suppressed M1 macrophage polarization and promoted M2 macrophage polarization by modulating STAT3 and STAT6 phosphorylation and activation. This study demonstrates that GSK3α mediates atherosclerosis by altering myeloid cell behaviour and phenotype within the aortic wall and is the first to describe homolog and tissue specific functions of GSK3α and GSK3β in atherosclerosis and metabolic dysfunction.

GSK3α and GSK3β transcript and protein are expressed in all tissues in both mice and humans.[187, 188] The level of total GSK3α/β, however, can vary from tissue to tissue - GSK3α/β mRNA and protein is expressed at higher levels in the brain relative to other tissues.[187, 188] Generally, the GSK3α and GSK3β homologs are expressed at comparable levels in most tissues, however, slight differences have been noted. For example, GSK3α is expressed at higher levels than GSK3β in testis and in the heart of neonatal mice.[187, 188] In agreement with previous reports, this thesis presents evidence that GSK3α and GSK3β protein are expressed at similar levels in murine hepatocytes and macrophages.[126, 189, 190] The relative expression of GSK3α and GSK3β in other myeloid cells has not been fully investigated. Recent evidence, however, suggests GSK3α is expressed at much higher levels than GSK3β in neutrophils.[190] This observation is important to consider when interpreting the role of myeloid GSK3α and/or β during atherosclerosis. Despite their ubiquitous expression, GSK3α and GSK3β are functionally and physiologically distinct.

The majority of investigations into GSK3α/β focus solely on the β homolog. This bias arose for a number of reasons. First, the kinase domain of GSK3α and GSK3β are 98% identical, therefore their activity, regulation and signaling was assumed to be highly similar despite significant variability in their C and N terminal domains. Second, early reports suggested GSK3β and not GSK3α was responsible for βcatenin phosphorylation

during Wnt signaling. [191, 192] In these studies, however, the relative expression of GSK3α and GSK3β in the *Drosophila* model was not measured. More recent evidence overwhelmingly indicates GSK3α and GSK3β are redundant in Wnt/βcatenin signaling.[92] While GSK3α/β redundancy may exist in Wnt signaling, GSK3α and GSK3β are not functionally identical. Whole body GSK3α deficient mice are viable and do not display any overt phenotype while GSK3β$^{-/-}$ mice die in mid-gestation at day E15.5.[67, 93-95] The lethality of GSK3β deficiency was attributed to hypertrophic cardiomyopathy and indeed GSK3β, but not GSK3α, is required for proper cardiomyocyte differentiation and development.[93, 193, 194] Further evidence of unique physiological functions of GSK3α and GSK3β comes from analysis of liver and smooth muscle cell specific knockout mice. Liver specific deletion of GSK3α or GSK3β does not alter glucose or insulin tolerance or, as presented within this thesis, lipid metabolism in a HFD model.[189, 190] However, smooth muscle cell deletion of GSK3β but not GSK3α improves glucose and insulin tolerance.[189, 190] Along with the data presented herein, these studies point to both common and unique physiological functions of GSK3α and GSK3β.

Emerging evidence suggests that GSK3α and GSK3β are uniquely regulated by subcellular localization. While GSK3α and GSK3β are present in all organelles including at high levels in the cytoplasm, the level of GSK3β is higher than GSK3α in mitochondria.[195] Further, the nuclear levels of GSK3α and GSK3β are dynamic and altered by extracellular stimuli and cellular condition. For example, the nuclear accumulation of GSK3β is at least partially dependent on its association with FRAT, a protein that shuttles GSK3β to the nucleus upon PI3K/AKT activation.[196-198] The role of FRAT in the localization of GSK3α has not been explored. GSK3α has a glycine-rich N-terminus extension not found in GSK3β which may mediate its distinct pattern of nuclear

localization.[90, 199] Consistent with this idea, shuttling of GSK3α to the nucleus upon increased cytoplasmic calcium concentration is blocked by deletion of its unique N-terminus.[199]

This thesis presents evidence for homolog specific roles of GSK3α and GSK3β in atherosclerosis and macrophage behaviour. We observe that myeloid GSK3α deficiency, but not GSK3β deficiency, attenuates atherosclerosis. Whether this observation is due to the unique regulation of GSK3α by its N-terminus is worthy of further investigation. For example, does ER stress induction or lipid loading of macrophages alter the nuclear level of GSK3α or GSK3β? What is the role of GSKα's N-terminus and FRAT in GSK3α and GSK3β localization in macrophages? Does the nuclear level of GSK3α or GSK3β impact macrophage phenotype?

Interestingly, a unique role for GSK3α and GSK3β has also been suggested in the polarization of $CD4^+$ T cells.[200] In cultured lymphocytes, inhibition of GSK3α/β by lithium or CT99021 prevents the polarization of $CD4^+$ T cells into IFN-γ producing Th1 cells.[200] This effect is specific to the polarization of Th1 cells as GSK3α/β inhibition does not alter Th17 or Th2 cell polarization. Moreover, when probing GSK3α and GSK3β homolog specific functions, the authors noted that deletion of GSK3α, but not GSK3β, attenuated Th1 cell polarization. These observations are consistent with our observations of GSK3α mediating macrophage M1 polarization.

Recent studies have presented evidence that GSK3α/β mediates cytokine production and expression.[122, 125] The work herein extends these findings and demonstrates macrophage GSK3α is not only a mediator of cytokine expression but also a mediator of macrophage function. The upstream regulators and downstream targets of GSK3α in immune response are beginning to emerge. Recently, Babaev *et al*.

demonstrated that bone marrow deficiency of AKT, an upstream regulator of GSK3α/β, modulates atherosclerosis development and macrophage polarization.[201] Downstream, this thesis presents data that the STAT family of transcription factors are regulated by GSK3α in macrophages. A role for GSK3α/β signaling in the regulation of STAT phosphorylation has also been suggested by a number of other groups.[124-126, 200, 202] In classically activated M1 macrophages, STAT1 phosphorylation and activation promotes the transcription of the M1 gene program. Meanwhile, STAT3 is also activated in M1 cells and functions as a negative feedback mechanism inhibiting STAT1 by forming STAT3:STAT1 heterodimers and by upregulating SOCS and SHIP.[203-208] GSK3α deletion increases STAT3 phosphorylation in BMDMs exposed to LPS which underscores our observations of suppressed M1 gene expression in these cells. The mechanism by which GSK3α regulates STAT3 is unclear and may be indirect. Binding of IL-6 or IL-10, components of the M1 program, to their receptors induces STAT3 phosphorylation through JAK2.[122, 125] Therefore, alterations to STAT3 phosphorylation by GSK3α may be an indirect consequence of alterations to IL-6 or IL-10 production. STAT6 is phosphorylated upon stimulation of the IL-4 receptor and leads to the upregulation of the M2 gene program.[209-211] In IL-4 treated macrophages GSK3α deletion promotes M2 gene expression by increasing P-Tyr641-STAT6. Together, modulation of STAT3 and STAT6 phosphorylation by GSK3α signaling may underlie our observations of reduced inflammation and attenuated atherosclerosis in LMαKO mice. Whether STATs are direct GSK3α substrates is unclear. GSK3α and GSK3β are poor tyrosine kinases and display higher affinity for serine and threonine residues.[90] The phosphorylation sites of STAT proteins are predominantly tyrosine residues making it unlikely that they are direct GSK3α substrates. Moreover, we observe an increase in STAT3 and STAT6

phosphorylation with GSK3α deletion. Further investigations are needed to delineate direct upstream and downstream targets of GSK3α and β in JAK/STAT signaling and their role in the regulation of macrophage phenotype, particularly in the context of atherosclerosis.

Functionally, M1 macrophages propagate atherosclerosis by secreting pro-inflammatory cytokines and mediators. Deletion of STAT1 attenuates the M1 program and reduces atherosclerosis in multiple mouse models.[149, 150] Meanwhile M2 macrophages are associated with the resolution of inflammation and attenuated lesion growth. Deletion of IL-13 or IL-10, stimulators of M2 macrophages, skews cells towards an M1 phenotype and aggravates atherosclerosis.[148, 212] Furthermore, during lesion regression macrophages switch from an M1 phenotype to an M2 phenotype.[151, 152] Along with the data presented herein, these studies suggest that promoting an M2 macrophage phenotype may be an innovative and intriguing anti-atherogenic therapy. This notion, however, is complicated by recent evidence suggesting there are multiple M2 macrophage subtypes, each with unique functionality. Exposing macrophages to IL-4, as was done in this thesis, elicits M2a macrophages which express higher levels of mannose receptor (CD206) and pro-fibrotic factors such as fibronectin, insulin-like growth factor (IGF) and transforming growth factor (TGF)β and are therefore often referred to as “wound healing macrophages”.[213] M2b macrophages, elicited by co-stimulation with a TLR agonist (such as LPS) and IL-4 or IL-13, attenuate the inflammatory response to a greater degree than other M2 subtypes and produce moderate amounts of IL-6 and TNFα.[213] IL-10 induces M2c macrophages which have a high capacity for efferocytosis.[213] Lastly, co-treatment with TLR and adenosine A_{2A} receptor agonists gives rise to M2d macrophages which promote vascularization by

producing high levels of VEGF.[135] If promoting these M2 macrophage phenotypes is a viable clinical goal, further investigations into the role of each M2 subtype in atherosclerotic lesion progression and regression is necessary. Moreover, a library of specific and reliable markers for each M2 subpopulation should be developed. It also should be noted that much of our understanding of macrophage polarization comes from experiments performed on murine cells. Further analysis into the polarization of human macrophages is needed.

One limitation of the work presented herein is an inability to directly compare GSK3α$^{-/-}$, GSK3β$^{-/-}$ and wildtype (LDLR$^{-/-}$) macrophages within the same atherosclerotic lesion. This limitation could be overcome by conducting chimeric bone marrow transplant experiments. Briefly, LDLR$^{-/-}$ mice would be irradiated and injected with a 50:50 mix of GSK3α$^{-/-}$ (from LMαKO mice) and LDLR$^{-/-}$ bone marrow; or GSK3β$^{-/-}$ (from LMβKO mice) and LDLR$^{-/-}$ bone marrow; or GSK3α$^{-/-}$ and GSK3β$^{-/-}$ bone marrow. Mice would then be placed on a HFD. This experiment would allow us to directly compare the consequence of GSK3α or GSK3β deletion on macrophage function, behaviour and phenotype within the same atherosclerotic lesion. For example, does having only 50% of monocytes/macrophages deficient in GSK3α sufficient to attenuate atherosclerosis? Do GSK3α deficient monocytes infiltrate the vessel wall to a lesser degree than their GSK3β$^{-/-}$ or wildtype (LDLR$^{-/-}$) counterparts? What is the proportion of GSK3α$^{-/-}$ (GSK3β$^{+/+}$) and GSK3β$^{-/-}$ (GSK3α$^{+/+}$) macrophages within the lesion? Do GSK3α$^{-/-}$ macrophages have an M2 phenotype while GSK3β$^{-/-}$ and LDLR$^{-/-}$ macrophages have an M1 phenotype and does this impact their location within the lesion? These are critical questions which must be answered to fully understand the role of myeloid GSK3α/β signaling in atherosclerosis.

Clinically, GSK3α/β is an attractive therapeutic target. A number of clinical investigations have shown that epileptic patients given valproate have significantly reduced risk of myocardial infarction and stroke even when compared to other anti-epileptic therapies.[214-216] The data presented here suggests targeting GSK3α specifically may offer even more clinical benefit. GSK3α specific inhibition may be able to retain the adaptive components of UPR signaling while preventing its detrimental distal effects. GSK3α inhibition may give the cell more time to recover from the stress before initiating pro-apoptotic and pro-inflammatory pathways. Moreover, targeting specific macrophage subtypes within the vessel wall may offer local anti-atherogenic and immune resolving properties while retaining systemic leukocyte function. Lastly, targeting GSK3α specifically would predict to have fewer side effects as GSK3β activity would be maintained. The first step in developing a GSK3α specific small molecule inhibitor is determining its crystal structure. To date, only the crystal structure of GSK3β has been resolved.[217, 218] Along with the development and validation of a GSK3α specific inhibitor further investigations into GSK3α and GSK3β's role in atherosclerosis progression and particularly regression are needed.

Atherosclerosis has been detected in children as young as two years old and generally, CVD symptoms do not arise until lesions are large and advanced or have ruptured.[219] Therefore, clinically relevant anti-atherogenic interventions must focus on the regression of established lesions. Our group has recently begun to investigate the role of GSK3α/β in lesion regression. In preliminary studies, we have observed lesion regression in HFD fed $LDLR^{-/-}$ mice that are switched to a diet containing valproate after lesion establishment (unpublished data). This work could be extended further to investigate the role of GSK3α and GSK3β in myeloid cells during lesion regression.

These studies would involve a myeloid cell-specific tamoxifen inducible Cre recombination system. This would require mice with mutated Gly525Arg mouse estrogen receptor (Mer) sequences inserted into the coding region of the Cre recombinase gene under the control of the Lysozyme M promoter. In this way, the Mer-Cre-Mer fusion protein, which has an inactive Cre domain and is not responsive to estrogen, will be expressed specifically in myeloid cells. These mice will be crossed with $LDLR^{-/-}$ mice and mice expressing either $GSK3\alpha^{fl/fl}$ or $GSK3\beta^{fl/fl}$. The resultant $LDLR^{-/-}GSK3\alpha^{fl/fl}$LyzMmer-cre-mer and $LDLR^{-/-}GSK3\beta^{fl/fl}$LyzMmer-cre-mer mice will be fed a HFD and after lesion development mice will be injected with tamoxifen or saline. Tamoxifen induces the nuclear translocation of the Mer-Cre-Mer protein complex allowing it to excise exon 2 of GSK3α or GSK3β. The impact of myeloid cell-specific GSK3α or GSK3β deletion on lesion regression and M1/M2 macrophage phenotypic switching can then be determined.

Summary and significance

Atherosclerosis is the major underlying pathology of CVD which is the number one cause of mortality worldwide. In order to develop targeted and effective therapeutics the molecular and cellular mechanisms that underlie the disease must be understood. The data presented in this thesis demonstrates a critical role for GSK3α/β and ER stress signaling in atherosclerosis. Specifically, the results suggest that 1) GSK3α/β inhibition attenuates atherosclerosis in multiple mouse models, 2) PERK-GSK3α/β signaling regulates macrophage foam cell formation and 3) myeloid cell GSK3α signaling mediates atherosclerosis and macrophage phenotype. These observations have extended our understanding of atherosclerosis progression and have illuminated innovative anti-atherogenic targets.

References for General Introduction and General Discussion

1. World Health Organization. Global status report on noncommunicable diseases 2010 - Description of the global burden of NCDs, their risk factors and determinants. 2011.
2. Public Health Agency of Canada. Tracking Heart Disease and Stroke in Canada. 2009.
3. Yusuf S, Hawken S, Ounpuu S, et al. Effect of potentially modifiable risk factors associated with myocardial infarction in 52 countries (the INTERHEART study): case-control study. *Lancet*. 2004;364:937-952.
4. Tuncman G, Erbay E, Hom X, et al. A genetic variant at the fatty acid-binding protein aP2 locus reduces the risk for hypertriglyceridemia, type 2 diabetes, and cardiovascular disease. *Proc Natl Acad Sci U S A*. 2006;103:6970-6975.
5. FROSST P, BLOM H, MILOS R, et al. A Candidate Genetic Risk Factor for Vascular-Disease - a Common Mutation in Methylenetetrahydrofolate Reductase. *Nat Genet*. 1995;10:111-113.
6. Koenig W, Sund M, Frohlich M, et al. C-reactive protein, a sensitive marker of inflammation, predicts future risk of coronary heart disease in initially healthy middle-aged men - Results from the MONICA (Monitoring Trends and Determinants in Cardiovascular Disease) Augsburg Cohort Study, 1984 to 1992. *Circulation*. 1999;99:237-242.
7. Ridker P, Hennekens C, Buring J, Rifai N. C-reactive protein and other markers of inflammation in the prediction of cardiovascular disease in women. *N Engl J Med*. 2000;342:836-843.
8. Ross R. Mechanisms of disease - Atherosclerosis - An inflammatory disease. *N Engl J Med*. 1999;340:115-126.
9. Libby P, Ridker P, Maseri A. Inflammation and atherosclerosis. *Circulation*. 2002;105:1135-1143.
10. Robbins CS, Chudnovskiy A, Rauch PJ, et al. Extramedullary Hematopoiesis Generates Ly-6C(high) Monocytes That Infiltrate Atherosclerotic Lesions. *Circulation*. 2012;125:364-U415.
11. Cybulsky M, Iiyama K, Li H, et al. A major role for VCAM-1, but not ICAM-1, in early atherosclerosis. *J Clin Invest*. 2001;107:1255-1262.
12. Gu L, Okada Y, Clinton S, et al. Absence of monocyte chemoattractant protein-1 reduces atherosclerosis in low density lipoprotein receptor-deficient mice. *Mol Cell*. 1998;2:275-281.
13. Amorino G, Hoover R. Interactions of monocytic cells with human endothelial cells stimulate monocytic metalloproteinase production. *Am J Pathol*. 1998;152:199-207.
14. Haghighat A, Weiss D, Whalin MK, Cowan DP, Taylor WR. Granulocyte colony-stimulating factor and granulocyte macrophage colony-stimulating factor exacerbate atherosclerosis in apolipoprotein E-deficient mice. *Circulation*. 2007;115:2049-2054.
15. Tabas I, Glass CK. Anti-Inflammatory Therapy in Chronic Disease: Challenges and Opportunities. *Science*. 2013;339:166-172.

16. Blann A, Seigneur M, Adams R, McCollum C. Neutrophil elastase, von Willebrand factor, soluble thrombomodulin and percutaneous oxygen in peripheral atherosclerosis. *Eur J Vasc Endovasc Surg*. 1996;12:218-222.
17. Ostos M, Recalde D, Zakin M, Scott-Algara D. Implication of natural killer T cells in atherosclerosis development during a LPS-induced chronic inflammation. *FEBS Lett*. 2002;519:23-29.
18. Zhou X, Stemme S, Hansson G. Evidence for a local immune response in atherosclerosis - CD4(+) T cells infiltrate lesions of apolipoprotein-E-deficient mice. *Am J Pathol*. 1996;149:359-366.
19. To K, Agrotis A, Besra G, Bobik A, Toh B. NKT Cell Subsets Mediate Differential Proatherogenic Effects in ApoE(-/-) Mice. *Arterioscler Thromb Vasc Biol*. 2009;29:671-U121.
20. Robbins CS, Hilgendorf I, Weber GF, et al. Local proliferation dominates lesional macrophage accumulation in atherosclerosis. *Nat Med*. 2013;19:1166-1172.
21. Lane A, Graham L, Cook M, et al. Cytokine Production by Cholesterol-Loaded Human Peripheral Monocyte-Macrophages - the Effect on Fibrinogen Messenger-Rna Levels in a Hepatoma Cell-Line (Hepg2). *Biochim Biophys Acta*. 1991;1097:161-165.
22. Veerman KJ, Venegas-Pino DE, Shi Y, Khan MI, Gerstein HC, Werstuck GH. Hyperglycaemia is associated with impaired vasa vasorum neovascularization and accelerated atherosclerosis in apolipoprotein-E deficient mice. *Atherosclerosis*. 2013;227:250-258.
23. Newby AC. Metalloproteinase Expression in Monocytes and Macrophages and its Relationship to Atherosclerotic Plaque Instability. *Arterioscler Thromb Vasc Biol*. 2008;28:2108-U20.
24. AMENTO E, EHSANI N, PALMER H, LIBBY P. Cytokines and Growth-Factors Positively and Negatively Regulate Interstitial Collagen Gene-Expression in Human Vascular Smooth-Muscle Cells. *Arterioscler Thromb*. 1991;11:1223-1230.
25. Thim T, Hagensen MK, Bentzon JF, Falk E. From vulnerable plaque to atherothrombosis. *J Intern Med*. 2008;263:506-516.
26. Ron D, Walter P. Signal integration in the endoplasmic reticulum unfolded protein response. *Nat Rev Mol Cell Biol*. 2007;8:519-529.
27. Nikawa J, Yamashita S. Ire1 Encodes a Putative Protein-Kinase Containing a Membrane-Spanning Domain and is Required for Inositol Phototrophy in Saccharomyces-Cerevisiae. *Mol Microbiol*. 1992;6:1441-1446.
28. Hotamisligil GS. Endoplasmic reticulum stress and the inflammatory basis of metabolic disease. *Cell*. 2010;140:900-917.
29. Chan C, Kok K, Tang HV, Wong C, Jin D. Internal ribosome entry site-mediated translational regulation of ATF4 splice variant in mammalian unfolded protein response. *Biochim Biophys Acta-Mol Cell Res*. 2013;1833:2165-2175.
30. Tabas I, Ron D. Integrating the mechanisms of apoptosis induced by endoplasmic reticulum stress. *Nat Cell Biol*. 2011;13:184-190.
31. Tabas I. The role of endoplasmic reticulum stress in the progression of atherosclerosis. *Circ Res*. 2010;107:839-850.
32. Lee A, Glimcher LH. Intersection of the unfolded protein response and hepatic lipid metabolism. *Cell Mol Life Sci*. 2009;66:2835-2850.
33. Ron D, Walter P. Signal integration in the endoplasmic reticulum unfolded protein response. *Nat Rev Mol Cell Biol*. 2007;8:519-529.

34. Austin RC, Lentz SR, Werstuck GH. Role of hyperhomocysteinemia in endothelial dysfunction and atherothrombotic disease. *Cell Death Differ*. 2004;11 Suppl 1:S56-64.
35. Robertson LA, Kim AJ, Werstuck GH. Mechanisms linking diabetes mellitus to the development of atherosclerosis: a role for endoplasmic reticulum stress and glycogen synthase kinase-3. *Can J Physiol Pharmacol*. 2006;84:39-48.
36. Seimon T, Tabas I. Mechanisms and consequences of macrophage apoptosis in atherosclerosis. *J Lipid Res*. 2009;50:S382-S387.
37. Werstuck GH, Khan MI, Femia G, et al. Glucosamine-induced endoplasmic reticulum dysfunction is associated with accelerated atherosclerosis in a hyperglycemic mouse model. *Diabetes*. 2006;55:93-101.
38. Werstuck G, Lentz S, Dayal S, et al. Homocysteine-induced endoplasmic reticulum stress causes dysregulation of the cholesterol and triglyceride biosynthetic pathways. *J Clin Invest*. 2001;107:1263-1273.
39. Ozcan U, Cao Q, Yilmaz E, et al. Endoplasmic reticulum stress links obesity, insulin action, and type 2 diabetes. *Science*. 2004;306:457-461.
40. Jorgensen E, Stinson A, Shan L, Yang J, Gietl D, Albino AP. Cigarette smoke induces endoplasmic reticulum stress and the unfolded protein response in normal and malignant human lung cells. *BMC Cancer*. 2008;8:229.
41. Laing S, Wang G, Briazova T, et al. Airborne particulate matter selectively activates endoplasmic reticulum stress response in the lung and liver tissues. *Am J Physiol -Cell Physiol*. 2010;299:C736-C749.
42. Li Y, Schwabe R, DeVries-Seimon T, et al. Free cholesterol-loaded macrophages are an abundant source of tumor necrosis factor-alpha and interleukin-6. *J Biol Chem*. 2005;280:21763-21772.
43. Gwiazda KS, Yang TB, Lin Y, Johnson JD. Effects of palmitate on ER and cytosolic Ca2+ homeostasis in beta-cells. *Am J Physiol -Endocrinol Metab*. 2009;296:E690-E701.
44. Ursini F, Davies K, Maiorino M, Parasassi T, Sevanian A. Atherosclerosis: another protein misfolding disease? *Trends Mol Med*. 2002;8:370-374.
45. Gargalovic PS. Atherogenesis on the Chopping Block. *Cell Metab*. 2009;9:399-401.
46. Das SK, Chu WS, Mondal AK, et al. Effect of pioglitazone treatment on endoplasmic reticulum stress response in human adipose and in palmitate-induced stress in human liver and adipose cell lines. *Am J Physiol -Endocrinol Metab*. 2008;295:E393-E400.
47. Ota T, Gayet C, Ginsberg HN. Inhibition of apolipoprotein B100 secretion by lipid-induced hepatic endoplasmic reticulum stress in rodents. *J Clin Invest*. 2008;118:316-332.
48. Hotamisligil GS. Endoplasmic Reticulum Stress and the Inflammatory Basis of Metabolic Disease. *Cell*. 2010;140:900-917.
49. Feng B, Yao P, Li Y, et al. The endoplasmic reticulum is the site of cholesterol-induced cytotoxicity in macrophages. *Nat Cell Biol*. 2003;5:781-792.
50. Fu S, Yang L, Li P, et al. Aberrant lipid metabolism disrupts calcium homeostasis causing liver endoplasmic reticulum stress in obesity. *Nature*. 2011;473:528-531.
51. Li Y, Ge M, Ciani L, et al. Enrichment of endoplasmic reticulum with cholesterol inhibits sarcoplasmic-endoplasmic reticulum calcium ATPase-2b activity in parallel with increased order of membrane lipids - Implications for depletion of

endoplasmic reticulum calcium stores and apoptosis in cholesterol-loaded macrophages. *J Biol Chem*. 2004;279:37030-37039.
52. Lander H, Tauras J, Ogiste J, Hori O, Moss R, Schmidt A. Activation of the receptor for advanced glycation end products triggers a p21(ras)-dependent mitogen-activated protein kinase pathway regulated by oxidant stress. *J Biol Chem*. 1997;272:17810-17814.
53. Soro-Paavonen A, Watson AMD, Li J, et al. Receptor for advanced glycation end products (RAGE) deficiency attenuates the development of atherosclerosis in diabetes. *Diabetes*. 2008;57:2461-2469.
54. Park' L, Raman K, Lee K, et al. Suppression of accelerated diabetic atherosclerosis by the soluble receptor for advanced glycation endproducts. *Nat Med*. 1998;4:1025-1031.
55. Hofmann M, Lalla E, Lu Y, et al. Hyperhomocysteinemia enhances vascular inflammation and accelerates atherosclerosis in a murine model. *J Clin Invest*. 2001;107:675-683.
56. Smedsrod B, Melkko J, Araki N, Sano H, Horiuchi S. Advanced glycation end products are eliminated by scavenger-receptor-mediated endocytosis in hepatic sinusoidal Kupffer and endothelial cells. *Biochem J*. 1997;322:567-573.
57. Li Y, Mitsuhashi T, Wojciechowicz D, et al. Molecular identity and cellular distribution of advanced glycation endproduct receptors: Relationship of p60 to OST-48 and p90 to 80K-H membrane proteins. *Proc Natl Acad Sci U S A*. 1996;93:11047-11052.
58. Thomson MJ, Puntmann V, Kaski J. Atherosclerosis and oxidant stress: The end of the road for antioxidant vitamin treatment? *Cardiovasc Drugs Ther*. 2007;21:195-210.
59. Gerstein H, Yusuf S, Mann J, et al. Effects of ramipril on cardiovascular and microvascular outcomes in people with diabetes mellitus: results of the HOPE study and MICRO-HOPE substudy. *Lancet*. 2000;355:253-259.
60. Srinivasan V, Tatu U, Mohan V, Balasubramanyam M. Molecular convergence of hexosamine biosynthetic pathway and ER stress leading to insulin resistance in L6 skeletal muscle cells. *Mol Cell Biochem*. 2009;328:217-224.
61. Khan MI, Pichna BA, Shi Y, Bowes AJ, Werstuck GH. Evidence supporting a role for endoplasmic reticulum stress in the development of atherosclerosis in a hyperglycaemic mouse model. *Antioxid Redox Signal*. 2009;11:2289-2298.
62. Sage AT, Walter LA, Shi Y, et al. Hexosamine biosynthesis pathway flux promotes endoplasmic reticulum stress, lipid accumulation, and inflammatory gene expression in hepatic cells. *Am J Physiol Endocrinol Metab*. 2010;298:E499-511.
63. Beriault DR, Sharma S, Shi Y, Khan MI, Werstuck GH. Glucosamine-supplementation promotes endoplasmic reticulum stress, hepatic steatosis and accelerated atherogenesis in apoE-/- mice. *Atherosclerosis*. 2011;219:134-140.
64. Zhou J, Lhotak S, Hilditch BA, Austin RC. Activation of the unfolded protein response occurs at all stages of atherosclerotic lesion development in apolipoprotein E-deficient mice. *Circulation*. 2005;111:1814-1821.
65. Oezcan U, Yilmaz E, Oezcan L, et al. Chemical chaperones reduce ER stress and restore glucose homeostasis in a mouse model of type 2 diabetes. *Science*. 2006;313:1137-1140.

66. Erbay E, Babaev VR, Mayers JR, et al. Reducing endoplasmic reticulum stress through a macrophage lipid chaperone alleviates atherosclerosis. *Nat Med*. 2009;15:1383-U5.
67. Banko N, McAlpine CS, Venegas-Pino DE, et al. Glycogen Synthase Kinase (GSK)-3alpha deficiency attenuates atherosclerosis and hepatic steatosis in high fat diet fed LDLR$^{-/-}$ mice. *American Journal of Physiology*. 2014;184:3394-3404
68. Civelek M, Manduchi E, Riley RJ, Stoeckert CJ,Jr, Davies PF. Chronic endoplasmic reticulum stress activates unfolded protein response in arterial endothelium in regions of susceptibility to atherosclerosis. *Circ Res*. 2009;105:453-461.
69. Pahl H, Baeuerle P. A Novel Signal-Transduction Pathway from the Endoplasmic-Reticulum to the Nucleus is Mediated by Transcription Factor Nf-Kappa-B. *EMBO J*. 1995;14:2580-2588.
70. Li YK, Schwabe RF, DeVries-Seimon T, et al. Free cholesterol-loaded macrophages are an abundant source of tumor necrosis factor-alpha and interleukin-6. *J Biol Chem*. 2005;280:21763-21772.
71. Urano F, Wang X, Bertolotti A, et al. Coupling of stress in the ER to activation of JNK protein kinases by transmembrane protein kinase IRE1. *Science*. 2000;287:664-666.
72. Nishitoh H, Matsuzawa A, Tobiume K, et al. ASK1 is essential for endoplasmic reticulum stress-induced neuronal cell death triggered by expanded polyglutamine repeats. *Genes Dev*. 2002;16:1345-1355.
73. Kim AJ, Shi Y, Austin RC, Werstuck GH. Valproate protects cells from ER stress-induced lipid accumulation and apoptosis by inhibiting glycogen synthase kinase-3. *J Cell Sci*. 2005;118:89-99.
74. Kammoun HL, Chabanon H, Hainault I, et al. GRP78 expression inhibits insulin and ER stress-induced SREBP-1c activation and reduces hepatic steatosis in mice. *J Clin Invest*. 2009;119:1201-1215.
75. Shank K, Su P, Brglez I, Boss W, Dewey R, Boston R. Induction of lipid metabolic enzymes during the endoplasmic reticulum stress response in plants. *Plant Physiol*. 2001;126:267-277.
76. Lee J, Ye J. Proteolytic activation of sterol regulatory element-binding protein induced by cellular stress through depletion of Insig-1. *J Biol Chem*. 2004;279:45257-45265.
77. Granados DP, Tanguay P, Hardy M, et al. ER stress affects processing of MHC class I-associated peptides. *BMC Immunol*. 2009;10:10.
78. de Almeida SF, Fleming JV, Azevedo JE, Carmo-Fonseca M, de Sousa M. Stimulation of an unfolded protein response impairs MHC class I expression. *J Immunol*. 2007;178:3612-3619.
79. Yang L, Jhaveri R, Huang J, Qi Y, Diehl AM. Endoplasmic reticulum stress, hepatocyte CD1d and NKT cell abnormalities in murine fatty livers. *Lab Invest*. 2007;87:927-937.
80. Zhu S, Chen M, Jongstra-Bilen J, Cybulsky MI. GM-CSF regulates intimal cell proliferation in nascent atherosclerotic lesions. *J Exp Med*. 2009;206:2141-2149.
81. Liu Y, Saini A, Cohen D, Ooi B. Modulation of Macrophage Proliferation by Hyperglycemia. *Mol Cell Endocrinol*. 1995;114:187-192.
82. Berridge M. Calcium Signaling and Cell-Proliferation. *Bioessays*. 1995;17:491-500.

83. Hotamisligil GS. Endoplasmic reticulum stress and atherosclerosis. *Nat Med*. 2010;16:396-399.
84. Li Y, Schwabe RF, DeVries-Seimon T, et al. Free cholesterol-loaded macrophages are an abundant source of tumor necrosis factor-alpha and interleukin-6: model of NF-kappaB- and map kinase-dependent inflammation in advanced atherosclerosis. *J Biol Chem*. 2005;280:21763-21772.
85. Seimon TA, Obstfeld A, Moore KJ, Golenbock DT, Tabas I. Combinatorial pattern recognition receptor signaling alters the balance of life and death in macrophages. *Proc Natl Acad Sci U S A*. 2006;103:19794-19799.
86. Karaskov E, Scott C, Zhang L, Teodoro T, Ravazzola M, Volchuk A. Chronic palmitate but not oleate exposure induces endoplasmic reticulum stress, which may contribute to INS-1 pancreatic beta-cell apoptosis. *Endocrinology*. 2006;147:3398-3407.
87. Thorp E, Li G, Seimon TA, Kuriakose G, Ron D, Tabas I. Reduced Apoptosis and Plaque Necrosis in Advanced Atherosclerotic Lesions of Apoe-/- and Ldlr-/- Mice Lacking CHOP. *Cell Metabolism*. 2009;9:474-481.
88. Kaidanovich-Beilin O, Woodgett JR. GSK-3: Functional Insights from Cell Biology and Animal Models. - *Front Mol Neurosci.2011 Nov 16;4:40.doi: 10.3389/fnmol.2011.00040.eCollection 2011.*
89. Jope RS, Johnson GV. The glamour and gloom of glycogen synthase kinase-3. *Trends Biochem Sci*. 2004;29:95-102.
90. Doble BW, Woodgett JR. GSK-3: tricks of the trade for a multi-tasking kinase. *J Cell Sci*. 2003;116:1175-1186.
91. Mukai F, Ishiguro K, Sano Y, Fujita S. Alternative splicing isoform of tau protein kinase I/glycogen synthase kinase 3 beta. *J Neurochem*. 2002;81:1073-1083.
92. Doble BW, Patel S, Wood GA, Kockeritz LK, Woodgett JR. Functional redundancy of GSK-3 alpha and GSK-3 beta in Wnt/beta-catenin signaling shown by using an allelic series of embryonic stem cell lines. *Developmental Cell*. 2007;12:957-971.
93. Kerkela R, Kockeritz L, MacAulay K, et al. Deletion of GSK-3 beta in mice leads to hypertrophic cardiomyopathy secondary to cardiomyoblast hyperproliferation. *J Clin Invest*. 2008;118:3609-3618.
94. MacAulay K, Doble BW, Patel S, et al. Glycogen synthase kinase 3alpha-specific regulation of murine hepatic glycogen metabolism. *Cell Metab*. 2007;6:329-337.
95. Hoeflich KP, Luo J, Rubie EA, Tsao MS, Jin O, Woodgett JR. Requirement for glycogen synthase kinase-3beta in cell survival and NF-kappaB activation. *Nature*. 2000;406:86-90.
96. Brady M, Bourbonais F, Saltiel A. The activation of glycogen synthase by insulin switches from kinase inhibition to phosphatase activation during adipogenesis in 3T3-L1 cells. *J Biol Chem*. 1998;273:14063-14066.
97. Dent P, Campbell D, HUBBARD M, COHEN P. Multisite Phosphorylation of the Glycogen-Binding Subunit of Protein Phosphatase-1g by Cyclic Amp-Dependent Protein-Kinase and Glycogen-Synthase Kinase-3. *FEBS Lett*. 1989;248:67-72.
98. Stambolic V, Woodgett J. Mitogen Inactivation of Glycogen-Synthase Kinase-3-Beta in Intact-Cells Via Serine-9 Phosphorylation. *Biochem J*. 1994;303:701-704.
99. Sutherland C, Cohen P. The Alpha-Isoform of Glycogen-Synthase Kinase-3 from Rabbit Skeletal-Muscle is Inactivated by P70 S6 Kinase Or Map Kinase-Activated Protein Kinase-1 In-Vitro. *FEBS Lett*. 1994;338:37-42.

100. Kim L, Liu J, Kimmel A. The novel tyrosine kinase ZAK1 activates GSK3 to direct cell fate specification. *Cell*. 1999;99:399-408.
101. Lochhead PA, Kinstrie R, Sibbet G, Rawjee T, Morrice N, Cleghon V. A chaperone-dependent GSK3 beta transitional intermediate mediates activation-loop autophosphorylation. *Mol Cell*. 2006;24:627-633.
102. Cole A, Frame S, Cohen P. Further evidence that the tyrosine phosphorylation of glycogen synthase kinase-3 (GSK3) in mammalian cells is an autophosphorylation event. *Biochem J*. 2004;377:249-255.
103. Poirier V, Bach H, Av-Gay Y. Mycobacterium tuberculosis Promotes Anti-apoptotic Activity of the Macrophage by PtpA Protein-dependent Dephosphorylation of Host GSK3 alpha. *J Biol Chem*. 2014;289:29376-29385.
104. Thornton TM, Pedraza-Alva G, Deng B, et al. Phosphorylation by p38 MAPK as an alternative pathway for GSK3 beta inactivation. *Science*. 2008;320:667-670.
105. Ding Q, Xia W, Liu J, et al. Erk associates with and primes GSK-3 beta for its inactivation resulting in upregulation of beta-catenin. *Mol Cell*. 2005;19:159-170.
106. Bhat R, Shanley J, Correll M, et al. Regulation and localization of tyrosine(216) phosphorylation of glycogen synthase kinase-3 beta in cellular and animal models of neuronal degeneration. *Proc Natl Acad Sci U S A*. 2000;97:11074-11079.
107. Franca-Koh J, Yeo M, Fraser E, Young N, Dale T. The regulation of glycogen synthase kinase-3 nuclear export by Frat/GBP. *J Biol Chem*. 2002;277:43844-43848.
108. Diehl J, Cheng M, Roussel M, Sherr C. Glycogen synthase kinase 3 beta regulates cyclin D1 proteolysis and subcellular localization. *Genes Dev*. 1998;12:3499-3511.
109. Bijur G, Jope R. Proapoptotic stimuli induce nuclear accumulation of glycogen synthase kinase-3 beta. *J Biol Chem*. 2001;276:37436-37442.
110. Sutherland C. What Are the bona fide GSK3 Substrates? *Int J Alzheimers Dis*. 2011;2011:505607.
111. Cohen P, FAU - Nimmo HG, Nimmo HG, FAU - Proud CG, Proud CG. How does insulin stimulate glycogen synthesis? - *Biochem Soc Symp.1978;(43):69-95.*
112. Logan C, Nusse R. The Wnt signaling pathway in development and disease. *Annu Rev Cell Dev Biol*. 2004;20:781-810.
113. Thornton TM, Pedraza-Alva G, Deng B, et al. Phosphorylation by p38 MAPK as an alternative pathway for GSK3 beta inactivation. *Science*. 2008;320:667-670.
114. Frame S, Cohen P. GSK3 takes centre stage more than 20 years after its discovery. *Biochem J*. 2001;359:1-16.
115. Takada Y, Fang X, Jamaluddin M, Boyd D, Aggarwal B. Genetic deletion of glycogen synthase kinase-3 beta abrogates activation of I kappa B alpha kinase, JNK, Akt, and p44/p42 MAPK but potentiates apoptosis induced by tumor necrosis factor. *J Biol Chem*. 2004;279:39541-39554.
116. Song L, De Sarno P, Jope R. Central role of glycogen synthase kinase-3 beta in endoplasmic reticulum stress-induced caspase-3 activation. *J Biol Chem*. 2002;277:44701-44708.
117. Qu L, Huang S, Baltzis D, et al. Endoplasmic reticulum stress induces p53 cytoplasmic localization and prevents p53-dependent apoptosis by a pathway involving glycogen synthase kinase-3 beta. *Genes Dev*. 2004;18:261-277.

118. Srinivasan S, Ohsugi M, Liu Z, Fatrai S, Bernal-Mizrachi E, Permutt M. Endoplasmic reticulum stress-induced apoptosis is partly mediated by reduced insulin signaling through phosphatidylinositol 3-kinase/Akt and increased glycogen synthase kinase-3 beta in mouse insulinoma cells. *Diabetes*. 2005;54:968-975.
119. Srinivasan S, Ohsugi M, Liu Z, Fatrai S, Bernal-Mizrachi E, Permutt M. Endoplasmic reticulum stress-induced apoptosis is partly mediated by reduced insulin signaling through phosphatidylinositol 3-kinase/Akt and increased glycogen synthase kinase-3 beta in mouse insulinoma cells. *Diabetes*. 2005;54:968-975.
120. Meares GP, Zmijewska AA, Jope RS. HSP105 interacts with GRP78 and GSK3 and promotes ER stress-induced caspase-3 activation. *Cell Signal*. 2008;20:347-358.
121. Shi Y, Gerritsma D, Bowes AJ, Capretta A, Werstuck GH. Induction of GRP78 by valproic acid is dependent upon histone deacetylase inhibition. *Bioorg Med Chem Lett*. 2007;17:4491-4494.
122. Beurel E, Michalek SM, Jope RS. Innate and adaptive immune responses regulated by glycogen synthase kinase-3 (GSK3). *Trends Immunol*. 2010;31:24-31.
123. Bowes AJ, Khan MI, Shi Y, Robertson L, Werstuck GH. Valproate attenuates accelerated atherosclerosis in hyperglycemic apoE-deficient mice: evidence in support of a role for endoplasmic reticulum stress and glycogen synthase kinase-3 in lesion development and hepatic steatosis. *Am J Pathol*. 2009;174:330-342.
124. Martin M, Rehani K, Jope R, Michalek S. Toll-like receptor-mediated cytokine production is differentially regulated by glycogen synthase kinase 3. *Nat Immunol*. 2005;6:777-784.
125. Beurel E, Jope RS. Glycogen synthase kinase-3 promotes the synergistic action of interferon-gamma on lipopolysaccharide-induced IL-6 production in RAW264.7 cells. *Cell Signal*. 2009;21:978-985.
126. Beurel E, Jope RS. Differential regulation of STAT family members by glycogen synthase kinase-3. *J Biol Chem*. 2008;283:21934-21944.
127. Geissmann F, Manz MG, Jung S, Sieweke MH, Merad M, Ley K. Development of Monocytes, Macrophages, and Dendritic Cells. *Science*. 2010;327:656-661.
128. Geissmann F, Jung S, Littman D. Blood monocytes consist of two principal subsets with distinct migratory properties. *Immunity*. 2003;19:71-82.
129. Biswas SK, Mantovani A. Macrophage plasticity and interaction with lymphocyte subsets: cancer as a paradigm. *Nat Immunol*. 2010;11:889-896.
130. De Paoli F, Staels B, Chinetti-Gbaguidi G. Macrophage Phenotypes and Their Modulation in Atherosclerosis. *Circ J*. 2014;78:1775-1781.
131. Xuan W, Qu Q, Zheng B, Xiong S, Fan G. The chemotaxis of M1 and M2 macrophages is regulated by different chemokines. *J Leukoc Biol*. 2015;97:61-69.
132. Shechter R, Miller O, Yovel G, et al. Recruitment of Beneficial M2 Macrophages to Injured Spinal Cord Is Orchestrated by Remote Brain Choroid Plexus. *Immunity*. 2013;38:555-569.
133. Vats D, Mukundan L, Odegaard JI, et al. Oxidative metabolism and PGC-1 beta attenuate macrophage-mediated inflammation. *Cell Metab*. 2006;4:13-24.

134. Lacy-Hulbert A, Moore KJ. Designer macrophages: Oxidative metabolism fuels inflammation repair. *Cell Metab*. 2006;4:7-8.
135. Colin S, Chinetti-Gbaguidi G, Staels B. Macrophage phenotypes in atherosclerosis. *Immunol Rev*. 2014;262:153-166.
136. Nielsen MJ, Moller HJ, Moestrup SK. Hemoglobin and Heme Scavenger Receptors. *Antioxid Redox Signal*. 2010;12:261-273.
137. Gleissner CA, Shaked I, Little KM, Ley K. CXC Chemokine Ligand 4 Induces a Unique Transcriptome in Monocyte-Derived Macrophages. *J Immunol*. 2010;184:4810-4818.
138. Hansson G, Libby P. The immune response in atherosclerosis: a double-edged sword. *Nat Rev Immunol*. 2006;6:508-519.
139. Swirski FK, Nahrendorf M. Leukocyte Behavior in Atherosclerosis, Myocardial Infarction, and Heart Failure. *Science*. 2013;339:161-166.
140. Murphy AJ, Akhtari M, Tolani S, et al. ApoE regulates hematopoietic stem cell proliferation, monocytosis, and monocyte accumulation in atherosclerotic lesions in mice. *J Clin Invest*. 2011;121:4138-4149.
141. Swirski FK, Nahrendorf M, Etzrodt M, et al. Identification of Splenic Reservoir Monocytes and Their Deployment to Inflammatory Sites. *Science*. 2009;325:612-616.
142. Swirski FK, Libby P, Aikawa E, et al. Ly-6C(hi) monocytes dominate hypercholesterolemia-associated monocytosis and give rise to macrophages in atheromata. *J Clin Invest*. 2007;117:195-205.
143. Johnson JL, Newby AC. Macrophage heterogeneity in atherosclerotic plaques. *Curr Opin Lipidol*. 2009;20:370-378.
144. DeVries-Seimon T, Li YK, Yao PM, et al. Cholesterol-induced macrophage apoptosis requires ER stress pathways and engagement of the type A scavenger receptor. *J Cell Biol*. 2005;171:61-73.
145. Leitinger N, Schulman IG. Phenotypic Polarization of Macrophages in Atherosclerosis. *Arterioscler Thromb Vasc Biol*. 2013;33:1120-1126.
146. Stoger JL, Gijbels MJJ, van der Velden S, et al. Distribution of macrophage polarization markers in human atherosclerosis. *Atherosclerosis*. 2012;225:461-468.
147. Chinetti-Gbaguidi G, Baron M, Bouhlel MA, et al. Human Atherosclerotic Plaque Alternative Macrophages Display Low Cholesterol Handling but High Phagocytosis Because of Distinct Activities of the PPAR gamma and LXR alpha Pathways. *Circ Res*. 2011;108:985-995.
148. Cardilo-Reis L, Gruber S, Schreier SM, et al. Interleukin-13 protects from atherosclerosis and modulates plaque composition by skewing the macrophage phenotype. *EMBO Mol Med*. 2012;4:1072-1086.
149. Lim W, Timmins JM, Seimon TA, et al. Signal transducer and activator of transcription-1 is critical for apoptosis in macrophages subjected to endoplasmic reticulum stress in vitro and in advanced atherosclerotic lesions in vivo. *Circulation*. 2008;117:940-951.
150. Agrawal S, Febbraio M, Podrez E, Cathcart MK, Stark GR, Chisolm GM. Signal transducer and activator of transcription 1 is required for optimal foam cell formation and atherosclerotic lesion development. *Circulation*. 2007;115:2939-2947.

151. Feig JE, Vengrenyuk Y, Reiser V, et al. Regression of Atherosclerosis Is Characterized by Broad Changes in the Plaque Macrophage Transcriptome. *PLoS One*. 2012;7:e39790.
152. Hewing B, Parathath S, Mai CK, Fiel MI, Guo L, Fisher EA. Rapid regression of atherosclerosis with MTP inhibitor treatment. *Atherosclerosis*. 2013;227:125-129.
153. Kim A, Shi Y, Austin R, Werstuck G. Valproate protects cells from ER stress-induced lipid accumulation and apoptosis by inhibiting glycogen synthase kinase-3. *J Cell Sci*. 2005;118:89-99.
154. Werstuck GH, Kim AJ, Brenstrum T, Ohnmacht SA, Panna E, Capretta A. Examining the correlations between GSK-3 inhibitory properties and anti-convulsant efficacy of valproate and valproate-related compounds. *Bioorg Med Chem Lett*. 2004;14:5465-5467.
155. Chapman A, Keane P, Meldrum B, Simiand J, Vernieres J. Mechanism of Anti-Convulsant Action of Valproate. *Prog Neurobiol*. 1982;19:315-359.
156. Marinova Z, Ren M, Wendland JR, et al. Valproic acid induces functional heat-shock protein 70 via Class I histone deacetylase inhibition in cortical neurons: a potential role of Sp1 acetylation. *J Neurochem*. 2009;111:976-987.
157. Nuutinen T, Suuronen T, Kauppinen A, Salminen A. Valproic acid stimulates clusterin expression in human astrocytes: Implications for Alzheimer's disease. *Neurosci Lett*. 2010;475:64-68.
158. Shi Y, Gerritsma D, Bowes AJ, Capretta A, Werstuck GH. Induction of GRP78 by valproic acid is dependent upon histone deacetylase inhibition. *Bioorg Med Chem Lett*. 2007;17:4491-4494.
159. Gottlicher M, Minucci S, Zhu P, et al. Valproic acid defines a novel class of HDAC inhibitors inducing differentiation of transformed cells. *EMBO J*. 2001;20:6969-6978.
160. Phiel C, Zhang F, Huang E, Guenther M, Lazar M, Klein P. Histone deacetylase is a direct target of valproic acid, a potent anticonvulsant, mood stabilizer, and teratogen. *J Biol Chem*. 2001;276:36734-36741.
161. Haberland M, Montgomery RL, Olson EN. The many roles of histone deacetylases in development and physiology: implications for disease and therapy. *Nat Rev Genet*. 2009;10:32-42.
162. Chen Z, Haegeli V, Yu H, Strickland S. Cortical deficiency of laminin gamma 1 impairs the AKT/GSK-3 beta signaling pathway and leads to defects in neurite outgrowth and neuronal migration. *Dev Biol*. 2009;327:158-168.
163. Chen G, Huang L, Jiang Y, Manji H. The mood-stabilizing agent valproate inhibits the activity of glycogen synthase kinase-3. *J Neurochem*. 1999;72:1327-1330.
164. Werstuck G, Kim A, Brenstrum T, Ohnmacht S, Panna E, Capretta A. Examining the correlations between GSK-3 inhibitory properties and anti-convulsant efficacy of valproate and valproate-related compounds. *Bioorg Med Chem Lett*. 2004;14:5465-5467.
165. Choi J, Nam K, Kim J, et al. Trichostatin A exacerbates atherosclerosis in low density lipoprotein receptor-deficient mice. *Arterioscler Thromb Vasc Biol*. 2005;25:2404-2409.
166. De Sarno P, Li XH, Jope RS. Regulation of Akt and glycogen synthase kinase-3 beta phosphorylation by sodium valproate and lithium. *Neuropharmacology*. 2002;43:1158-1164.

167. Hao Y, Creson T, Zhang L, et al. Mood stabilizer valproate promotes ERK pathway-dependent cortical neuronal growth and neurogenesis. *J Neurosci*. 2004;24:6590-6599.
168. Choi S, Jang H, Kang Y, et al. Atherosclerosis induced by a high-fat diet is alleviated by lithium chloride via reduction of VCAM expression in ApoE-deficient mice. *Vascular Pharmacology*. 2010;53:264-272.
169. Bain J, Plater L, Elliott M, et al. The selectivity of protein kinase inhibitors: a further update. *Biochem J*. 2007;408:297-315.
170. Blaustein M, Perez-Munizaga D, Alejandro Sanchez M, et al. Modulation of the Akt Pathway Reveals a Novel Link with PERK/eIF2 alpha, which Is Relevant during Hypoxia. *PLoS One*. 2013;8:e69668.
171. Mounir Z, Krishnamoorthy JL, Wang S, et al. Akt Determines Cell Fate Through Inhibition of the PERK-eIF2 alpha Phosphorylation Pathway. *Sci Signal*. 2011;4:ra62.
172. Demay Y, Perochon J, Szuplewski S, Mignotte B, Gaumer S. The PERK pathway independently triggers apoptosis and a Rac1/Slpr/JNK/Dilp8 signaling favoring tissue homeostasis in a chronic ER stress Drosophila model. *Cell Death Dis*. 2014;5:e1452.
173. Engin F, Hotamisligil GS. Restoring endoplasmic reticulum function by chemical chaperones: an emerging therapeutic approach for metabolic diseases. *Diabetes Obes Metab*. 2010;12:108-115.
174. Ning J, Hong T, Ward A, et al. Constitutive Role for IRE1 alpha-XBP1 Signaling Pathway in the Insulin-Mediated Hepatic Lipogenic Program. *Endocrinology*. 2011;152:2247-2255.
175. Iqbal J, Queiroz J, Li Y, Jiang X, Ron D, Hussain MM. Increased Intestinal Lipid Absorption Caused by Ire1 beta Deficiency Contributes to Hyperlipidemia and Atherosclerosis in Apolipoprotein E-Deficient Mice. *Circ Res*. 2012;110:1575-1584.
176. Zeng L, Lu M, Mori K, et al. ATF6 modulates SREBP2-mediated lipogenesis. *EMBO J*. 2004;23:950-958.
177. Yao S, Miao C, Tian H, et al. Endoplasmic Reticulum Stress Promotes Macrophage-derived Foam Cell Formation by Up-regulating Cluster of Differentiation 36 (CD36) Expression. *J Biol Chem*. 2014;289:4032-4042.
178. Yamamoto K, Takahara K, Oyadomari S, et al. Induction of Liver Steatosis and Lipid Droplet Formation in ATF6 alpha-Knockout Mice Burdened with Pharmacological Endoplasmic Reticulum Stress. *Mol Biol Cell*. 2010;21:2975-2986.
179. Oyadomari S, Harding HP, Zhang Y, Oyadomari M, Ron D. Dephosphorylation of translation initiation factor 2 alpha enhances glucose tolerance and attenuates hepatosteatosis in mice. *Cell Metab*. 2008;7:520-532.
180. Wang C, Huang Z, Du Y, Cheng Y, Chen S, Guo F. ATF4 regulates lipid metabolism and thermogenesis. *Cell Res*. 2010;20:174-184.
181. Wellen K, Hotamisligil G. Inflammation, stress, and diabetes. *J Clin Invest*. 2005;115:1111-1119.
182. Esteve E, Ricart W, Fernandez-Real J. Dyslipidemia and inflammation: an evotutionary conserved mechanism. *Clin Nutr*. 2005;24:16-31.

183. Hotamisligil G, Shargill N, Spiegelman B. Adipose Expression of Tumor-Necrosis-Factor-Alpha - Direct Role in Obesity-Linked Insulin Resistance. *Science*. 1993;259:87-91.
184. Yoshida H, Okada T, Haze K, et al. ATF6 activated by proteolysis binds in the presence of NF-Y (CBF) directly to the cis-acting element responsible for the mammalian unfolded protein response. *Mol Cell Biol*. 2000;20:6755-6767.
185. Zhang X, Zhang G, Zhang H, Karin M, Bai H, Cai D. Hypothalamic IKK beta/NF-kappa B and ER stress link overnutrition to energy imbalance and obesity. *Cell*. 2008;135:61-73.
186. Oh J, Riek AE, Weng S, et al. Endoplasmic Reticulum Stress Controls M2 Macrophage Differentiation and Foam Cell Formation. *J Biol Chem*. 2012;287:11629-11641.
187. Lau K, Miller C, Anderton B, Shaw P. Expression analysis of glycogen synthase kinase-3 in human tissues. *J Pept Res*. 1999;54:85-91.
188. Calamai A, Cullen A, Ettarh R. Glycogen synthase kinase 3 expression in murine tissues. *J Anat*. 2011;218:469-469.
189. Patel S, Macaulay K, Woodgett JR. Tissue-specific analysis of glycogen synthase kinase-3alpha (GSK-3alpha) in glucose metabolism: effect of strain variation. *PLoS One*. 2011;6:e15845.
190. Patel S, Doble BW, MacAulay K, Sinclair EM, Drucker DJ, Woodgett JR. Tissue-specific role of glycogen synthase kinase 3beta in glucose homeostasis and insulin action. *Mol Cell Biol*. 2008;28:6314-6328.
191. Ruel L, Bourouis M, Heitzler P, Pantesco V, Simpson P. Drosophila Shaggy Kinase and Rat Glycogen-Synthase Kinase-3 have Conserved Activities and Act Downstream of Notch. *Nature*. 1993;362:557-560.
192. Siegfried E, Chou T, Perrimon N. Wingless Signaling Acts through Zeste-White 3, the Drosophila Homolog of Glycogen-Synthase Kinase-3, to Regulate Engrailed and Establish Cell Fate. *Cell*. 1992;71:1167-1179.
193. Lee H, Tsai J, Liao P, et al. Glycogen synthase kinase 3 alpha and 3 beta have distinct functions during cardiogenesis of zebrafish embryo. *BMC Dev Biol*. 2007;7:93.
194. Cho J, Rameshwar P, Sadoshima J. Distinct Roles of Glycogen Synthase Kinase (GSK)-3 alpha and GSK-3 beta in Mediating Cardiomyocyte Differentiation in Murine Bone Marrow-derived Mesenchymal Stem Cells. *J Biol Chem*. 2009;284:36647-36658.
195. Hoshi M, Sato M, Kondo S, et al. Different Localization of Tau-Protein-Kinase-i Glycogen-Synthase Kinase-3-Beta from Glycogen-Synthase Kinase-3-Alpha in Cerebellum Mitochondria. *J Biochem*. 1995;118:683-685.
196. Bechard M, Trost R, Singh AM, Dalton S. Frat Is a Phosphatidylinositol 3-Kinase/Akt-Regulated Determinant of Glycogen Synthase Kinase 3 beta Subcellular Localization in Pluripotent Cells. *Mol Cell Biol*. 2012;32:288-296.
197. Bechard M, Dalton S. Subcellular Localization of Glycogen Synthase Kinase 3 beta Controls Embryonic Stem Cell Self-Renewal. *Mol Cell Biol*. 2009;29:2092-2104.
198. Meares GP, Jope RS. Resolution of the nuclear localization mechanism of glycogen synthase kinase-3 - Functional effects in apoptosis. *J Biol Chem*. 2007;282:16989-17001.

199. Azoulay-Alfaguter I, Yaffe Y, Licht-Murava A, et al. Distinct Molecular Regulation of Glycogen Synthase Kinase-3 alpha Isozyme Controlled by Its N-terminal Region Functional Role in Calcium/Calpain Signaling. *J Biol Chem*. 2011;286:13470-13480.
200. Beurel E, Kaidanovich-Beilin O, Yeh W, et al. Regulation of Th1 Cells and Experimental Autoimmune Encephalomyelitis by Glycogen Synthase Kinase-3. *J Immunol*. 2013;190:5000-5011.
201. Babaev VR, Hebron KE, Wiese CB, et al. Macrophage deficiency of Akt2 reduces atherosclerosis in LDLR null mice. *J Lipid Res.*2014;55:2296-2308.
202. Hu X, Paik P, Chen J, et al. IFN-gamma suppresses IL-10 production and synergizes with TLR2 by regulating GSK3 and CREB/AP-1 proteins. *Immunity*. 2006;24:563-574.
203. Riley J, Takeda K, Akira S, Schreiber R. Interleukin-10 receptor signaling through the JAK-STAT pathway - Requirement for two distinct receptor-derived signals for anti-inflammatory action. *J Biol Chem*. 1999;274:16513-16521.
204. Fujiwara Y, Komohara Y, Kudo R, et al. Oleanolic acid inhibits macrophage differentiation into the M2 phenotype and glioblastoma cell proliferation by suppressing the activation of STAT3. *Oncol Rep*. 2011;26:1533-1537.
205. de Jonge W, van der Zanden E, O The F, et al. Stimulation of the vagus nerve attenuates macrophage activation by activating the Jak2-STAT3 signaling pathway. *Nat Immunol*. 2005;6:844-851.
206. Matsukawa A, Kudo S, Maeda T, et al. Stat3 in resident macrophages as a repressor protein of inflammatory response. *J Immunol*. 2005;175:3354-3359.
207. Ho H, Ivashkiv L. Role of STAT3 in type I interferon responses - Negative regulation of STAT1-dependent inflammatory gene activation. *J Biol Chem*. 2006;281:14111-14118.
208. Shen Y, Devgan G, Darnell J, Bromberg J. Constitutively activated Stat3 protects fibroblasts from serum withdrawal and UV-induced apoptosis and antagonizes the proapoptotic effects of activated Stat1. *Proc Natl Acad Sci U S A*. 2001;98:1543-1548.
209. Welch J, Escoubet-Lozach L, Sykes D, Liddiard K, Greaves D, Glass C. T(H)2 cytokines and allergic challenge induce YM1 expression in macrophages by a STAT6-dependent mechanism. *J Biol Chem*. 2002;277:42821-42829.
210. Van den Bossche J, Bogaert P, van Hengel J, et al. Alternatively activated macrophages engage in homotypic and heterotypic interactions through IL-4 and polyamine-induced E-cadherin/catenin complexes. *Blood*. 2009;114:4664-4674.
211. Sinha P, Clements V, Ostrand-Rosenberg S. Interleukin-13-regulated M2 macrophages in combination with myeloid suppressor cells block immune surveillance against metastasis. *Cancer Res*. 2005;65:11743-11751.
212. Caligiuri G, Rudling M, Ollivier V, et al. Interleukin-10 deficiency increases atherosclerosis, thrombosis, and low-density lipoproteins in apolipoprotein E knockout mice. *Mol Med*. 2003;9:10-17.
213. Mosser DM, Edwards JP. Exploring the full spectrum of macrophage activation. *Nature Reviews Immunology*. 2008;8:958-969.
214. Olesen JB, Hansen PR, Abildstrom SZ, et al. Valproate attenuates the risk of myocardial infarction in patients with epilepsy: a nationwide cohort study. *Pharmacoepidemiol Drug Saf*. 2011;20:146-153.

215. Olesen JB, Abildstrom SZ, Erdal J, et al. Effects of epilepsy and selected antiepileptic drugs on risk of myocardial infarction, stroke, and death in patients with or without previous stroke: a nationwide cohort study. *Pharmacoepidemiol Drug Saf*. 2011.
216. Dregan A, Charlton J, Wolfe CDA, Gulliford MC, Markus HS. Is Sodium Valproate, an HDAC inhibitor, associated with reduced risk of stroke and myocardial infarction? A nested case-control study. *Pharmacoepidemiol Drug Saf*. 2014;23:759-767.
217. ter Haar E, Coll J, Austen D, Hsiao H, Swenson L, Jain J. Structure of GSK3 beta reveals a primed phosphorylation mechanism. *Nat Struct Biol*. 2001;8:593-596.
218. Dajani R, Fraser E, Roe S, et al. Crystal structure of glycogen synthase kinase 3 beta: Structural basis for phosphate-primed substrate specificity and autoinhibition. *Cell*. 2001;105:721-732.
219. Berenson G, Srinivasan S, Bao W, et al. Association between multiple cardiovascular risk factors and atherosclerosis in children and young adults. *N Engl J Med*. 1998;338:1650-1656.

APPENDIX 1: Supplemental Material for Chapter 3

Foreword

Appendix 1 is a direct representation of the supplemental material published in *Arteriosclerosis Thrombosis and Vascular Biology*, volume 32, pages 82-91, January 2012. The experiments were conducted by Cameron McAlpine with assistance from the co-authors. The full reference is as follows:

McAlpine CS, Bowes AJ, Khan MI, Shi Y, Werstuck GH. Endoplasmic reticulum stress and glycogen synthase kinase-3β activation in apolipoprotein E-deficient mouse models of accelerated atherosclerosis. *Arteriosclerosis Thrombosis and Vascular Bioogy*. 2012;32:82-91.

Supplementary Figure I. Plasma Lipid Profiles. Plasma lipid profiles of control, hyperhomocysteinemic (HH), hyperglycemic (HG), and high fat diet fed (HF) mice with (+V) or without valproate-supplementation. Values represent the average cholesterol concentration in 3 independent plasma samples from each group after plasma fractionation by FPLC.

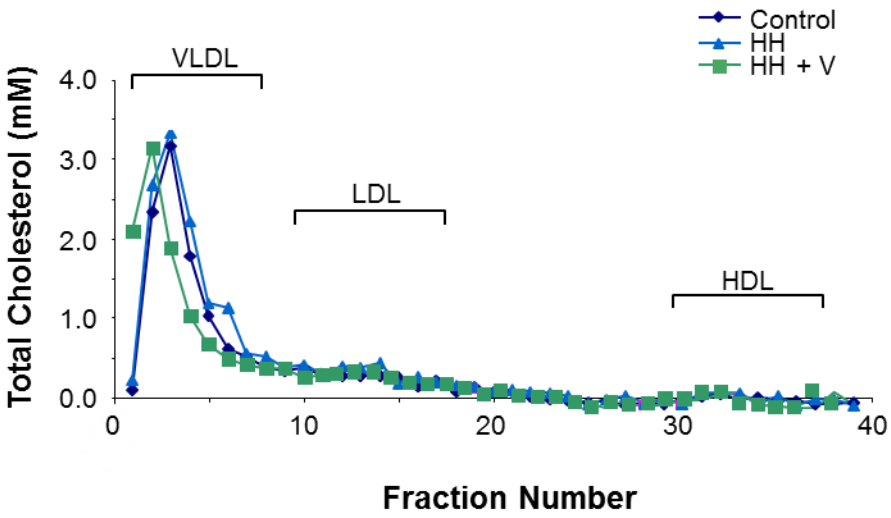
Control
HH
HH + V
VLDL
LDL
HDL
Total Cholesterol (mM)
4.0
3.0
2.0
1.0
0.0
0
10
20
30
40
Fraction Number

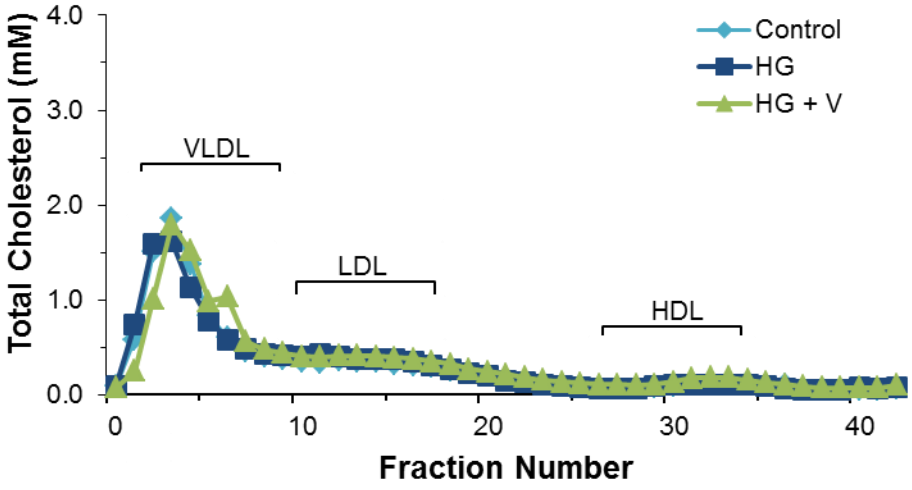
Control
HG
HG + V
VLDL
LDL
HDL
Total Cholesterol (mM)
4.0
3.0
2.0
1.0
0.0
0
10
20
30
40
Fraction Number

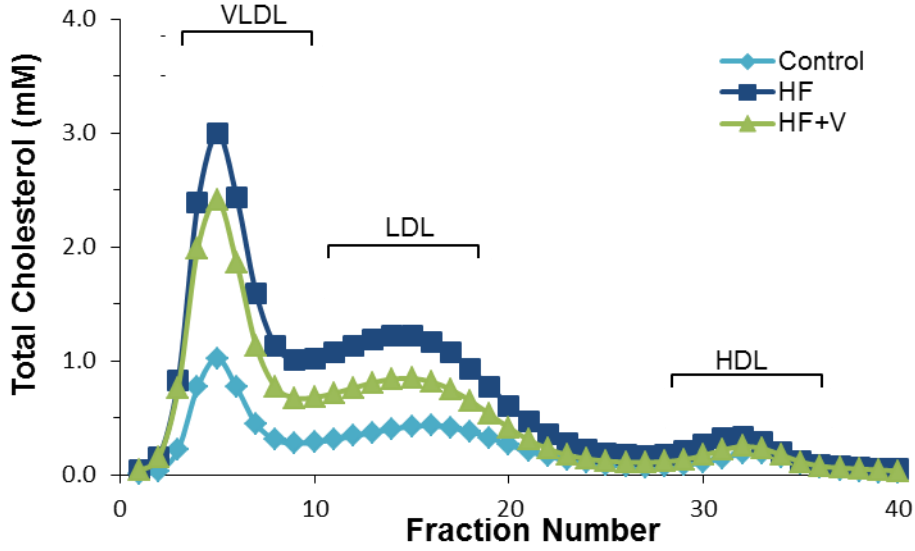
Control
HF
HF+V
VLDL
LDL
HDL
Total Cholesterol (mM)
4.0
3.0
2.0
1.0
0.0
0
10
20
30
40
Fraction Number

Supplementary Figure II. The effect of valproate-supplementation on lesion area in the aortas of high fat fed mice. A) Representative mounts of Sudan IV stained aortas of 24 week old C, HF and HF valproate-supplemented mice. **B)** Quantification of the lesion area as a percentage of aorta surface area. *P<0.05 relative to control mice fed the non-supplemented (control) diet. #P<0.05 relative to the same group fed control diet, n=5-6/group.

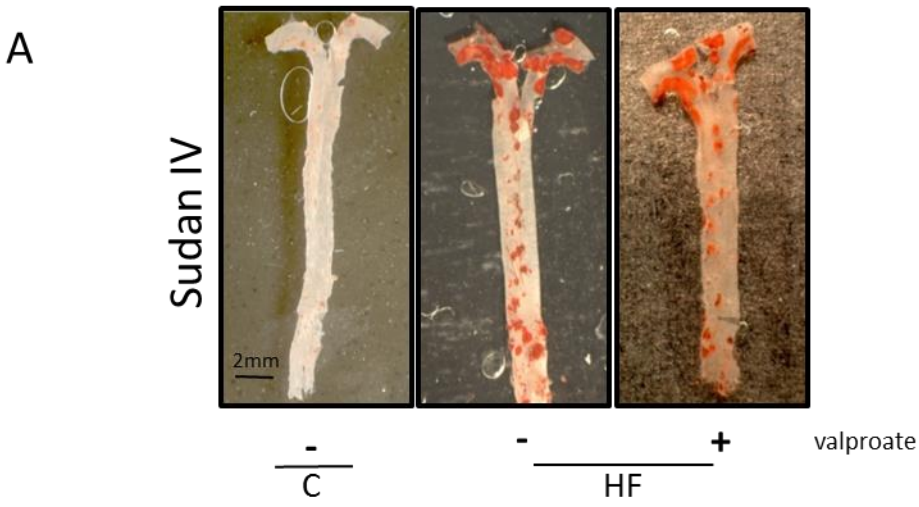
A
Sudan IV
2mm
-
C
-
+
HF
valproate

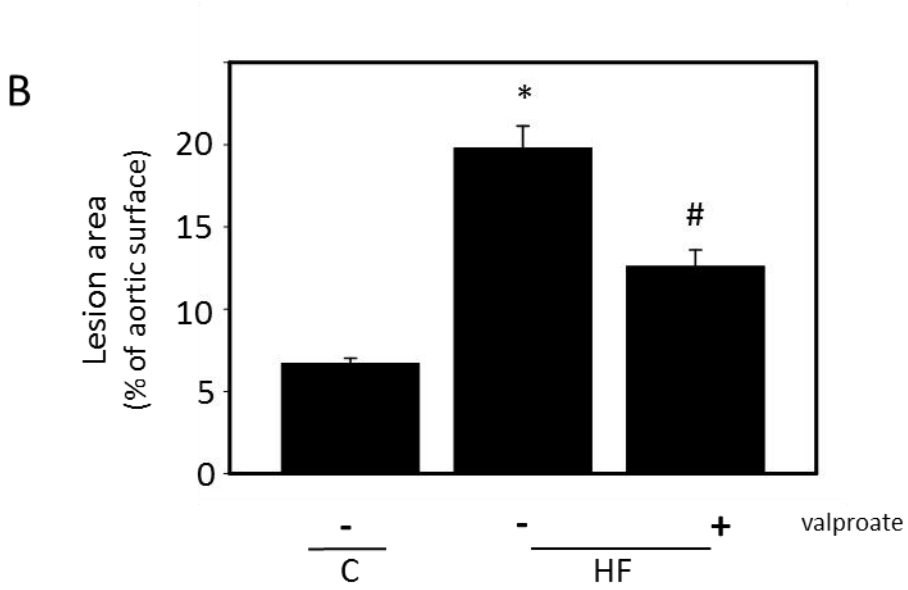
B
Lesion area
(% of aortic surface)
0
5
10
15
20
*
#
-
C
-
+
HF
valproate

Supplementary Figure III. ER stress induced neutral lipid accumulation in HepG2 and the effect of GSK3 inhibition. HepG2 cells were treated with 8μg/ml tunicamycin or 250μM palmitic acid in the presence or absence of 2mM valproate or 200μM GSK3β Inhibitor II for 6 hours. Cells were stained with Oil Red O and imaged. Proportion of stained lipids was quantified using Image J, normalized to the number of cells and presented relative to untreated controls. n=3, *P<0.05 relative to untreated controls, #P<0.05 relative to no inhibitor within same group.

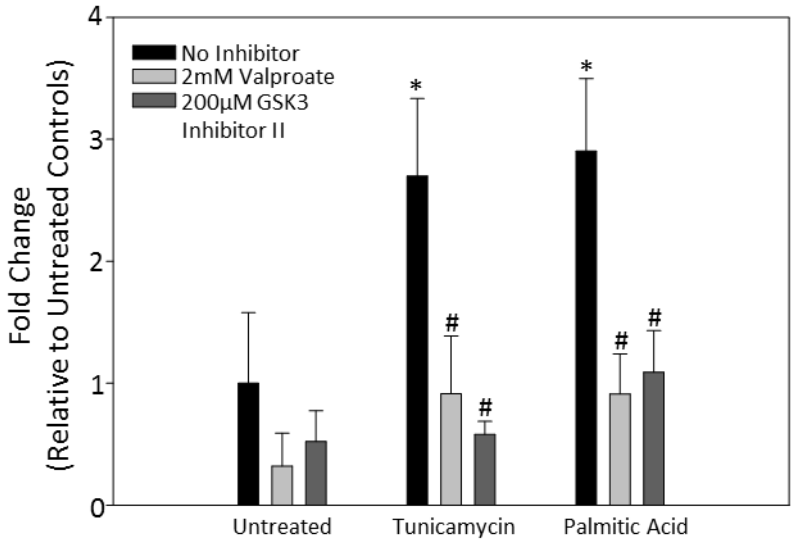
No Inhibitor
2mM Valproate
200µM GSK3 Inhibitor II
Fold Change (Relative to Untreated Controls)
0
1
2
3
4
*
*
#
#
#
#
Untreated
Tunicamycin
Palmitic Acid

APPENDIX 2: Supplemental Material for Chapter 4

Foreword

Appendix 2 is a direct representation of the supplemental material published in *Journal of Lipid Research*, volume 55, pages 2320-2333, November 2014. The experiments were conducted by Cameron McAlpine.The full reference is as follows:

McAlpine CS, Werstuck GH. Protein kinase R-like endoplasmic reticulum kase and glycogen synthase kinase-3α/β regulate foam cell formation. *J Lipid Res.* 2014;55:2320-2333.

Supplementary Table I. Sequences of real time PCR primers.

Primer Name	Primer Sequences (5'-3')	Product Size (bp)
GRP78 (human)	Fwd: CGA GGA GGA GGA CAA GAA GG Rev: CAC CTT GAA CGG CAA GAA CT	**86**
GRP78 (mouse)	Fwd: ACC TGG GTG GGG AAC ACT TT Rev: TCT TCA AAT TTG GCC CGA GT	**212**
GRP94	Fwd: TGG GAA GAG GTT CCA GAA TG Rev: GTT GCC AGA CCA TCC GTA CT	**219**
Calreticulin	Fwd: AAA TGA GAA GAG CCC CGT TCT TCC T Rev: AAG CCA CAG GCC TGA GAT TTC ATC T	**115**
PDI	Fwd: AAG CTC AGC AAA GAC CCA AA Rev: CAC TTA ATT CAC GGC CAC CT	**159**
ATF4	Fwd: CTC CGG GAC AGA TTG GAT GTT Rev: GGC TGC TTA GTC TCC TGG AC	**153**
CHOP (human)	Fwd: TGC CTT TCT CTT CGG ACA CT Rev: TGT GAC CTC TGC TGG TTC TG	**202**
CHOP (mouse)	Fwd: GTC CCT AGC TTG GCT GAC AGA Rev: TGG AGA GCG AGG GCT TTG	**140**
FAS	Fwd: AAG GAC CTG TCT AGG TTT GAT GC Rev: TGG CTT CAT AGG TGA CTT CCA	**105**
SREBP2	Fwd: CAA GAT GCA CAA GTC TGG CG Rev: GCT TCA GCA CCA TGT TCT CCT G	**100**
SREBP1c	Fwd: CGA CAT CGA AGA CAT GCT TCA Rev: GGA AGG CTT CAA GAG AGG AGC	**138**
HMGCoA	Fwd: CTG TCA TTC CAG CCA AGG TTG Rev: GTC CAC AGG CAA TGT AGA TGG	**167**
GLUD	Fwd: CCG TTA CAG CAC TGA TGT GAG Rev: TGG TGA ACC TCC TTG TGA TCT	**169**
Citrate Synthase	Fwd: TGC TTC CTC CAC GAA TTT GAA A Rev: CCA CCA TAC ATC ATG TCC ACA G	**131**
βActin (human)	Fwd: ACC GAG CGC GGC TAC AG Rev: CTT AAT GTG ACG CAC GAT TTC C	**50**
βActin (mouse)	Fwd: GGC ACC ACA CCT TCT ACA ATG Rev: GGG GTG TTG AAG GTC TCA AAC	**92**

Supplementary Figure I. Validation of cholesterol assay (Sigma Aldrich cat#MAK043). Colorimetric assay conducted according to manufacturers instructions on cholesterol standard.

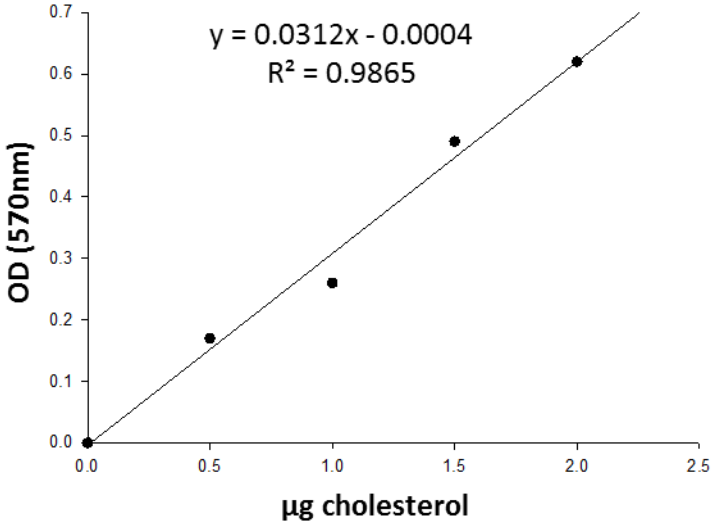
y = 0.0312x - 0.0004
R² = 0.9865
OD (570nm)
µg cholesterol
0.0
0.1
0.2
0.3
0.4
0.5
0.6
0.7
0.0
0.5
1.0
1.5
2.0
2.5

Supplementary Figure II. CT99021 inhibits GSK3α and GSK3β kinase activity. GSK3α and GSK3β were immunoprecipitated from whole cell Thp-1 macrophage lysates. **A)** Kinase activity was determined in the presence or absence of 0.5μmol/L CT99021. **B)** Whole cell lysates from Thp-1 macrophages treated in the presence or absence of 4μmol/L CT99021 were resolved by SDS page and probed for β catenin to demonstrate GSK3α/β inhibition. n=3 #$p<0.05$ relative to cells of the same treatment without GSK3α/β inhibition

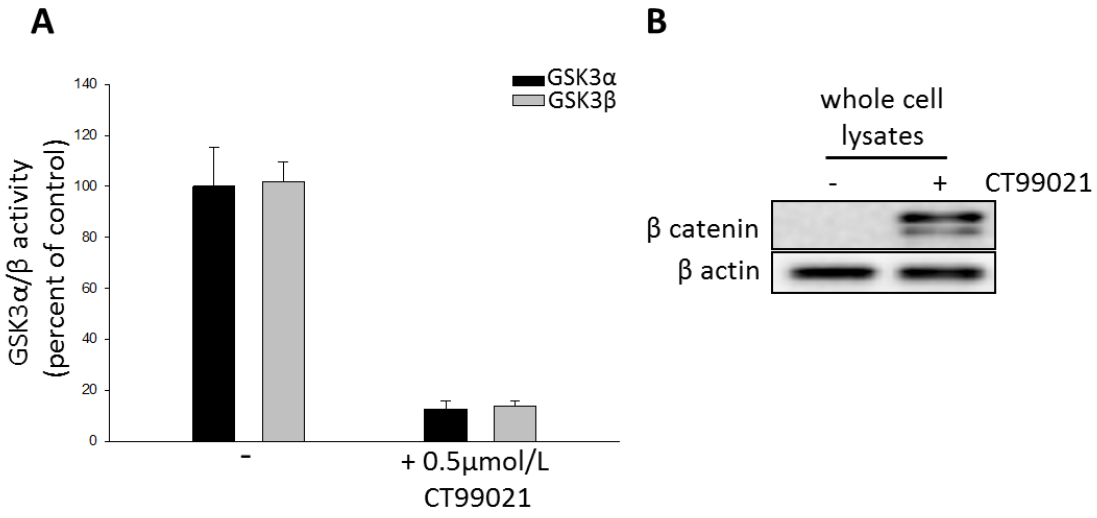
A
GSK3α
GSK3β
GSK3α/β activity
(percent of control)
140
120
100
80
60
40
20
0
-
+ 0.5µmol/L
CT99021
B
whole cell
lysates
-
+
CT99021
β catenin
β actin

Supplementary Figure III. Apoptosis does not induce foam cell formation. A) Thp1 derived macrophages were exposed to the ER stress-inducing agents thapsigargin (Thaps, 1µmol/L), glucosamine (GLN, 5mmol/L) or palmitic acid (PA, 600µmol/L) with or without pretreatment with CT99021. Cell viability was determined after 18 hours. **B)** Thp1 derived macrophages were exposed to 0, 1, 1.5 or 2 µM Doxorubicin (Dox) for 6 hours and stained with Oil Red O, arrows indicate positive staining. **C)** Quantification of Oil Red O staining.**D)** Dox exposure induced apoptosis and reduced viability of Thp1 macrophages n=3, #$p<0.05$ relative to untreated cells.

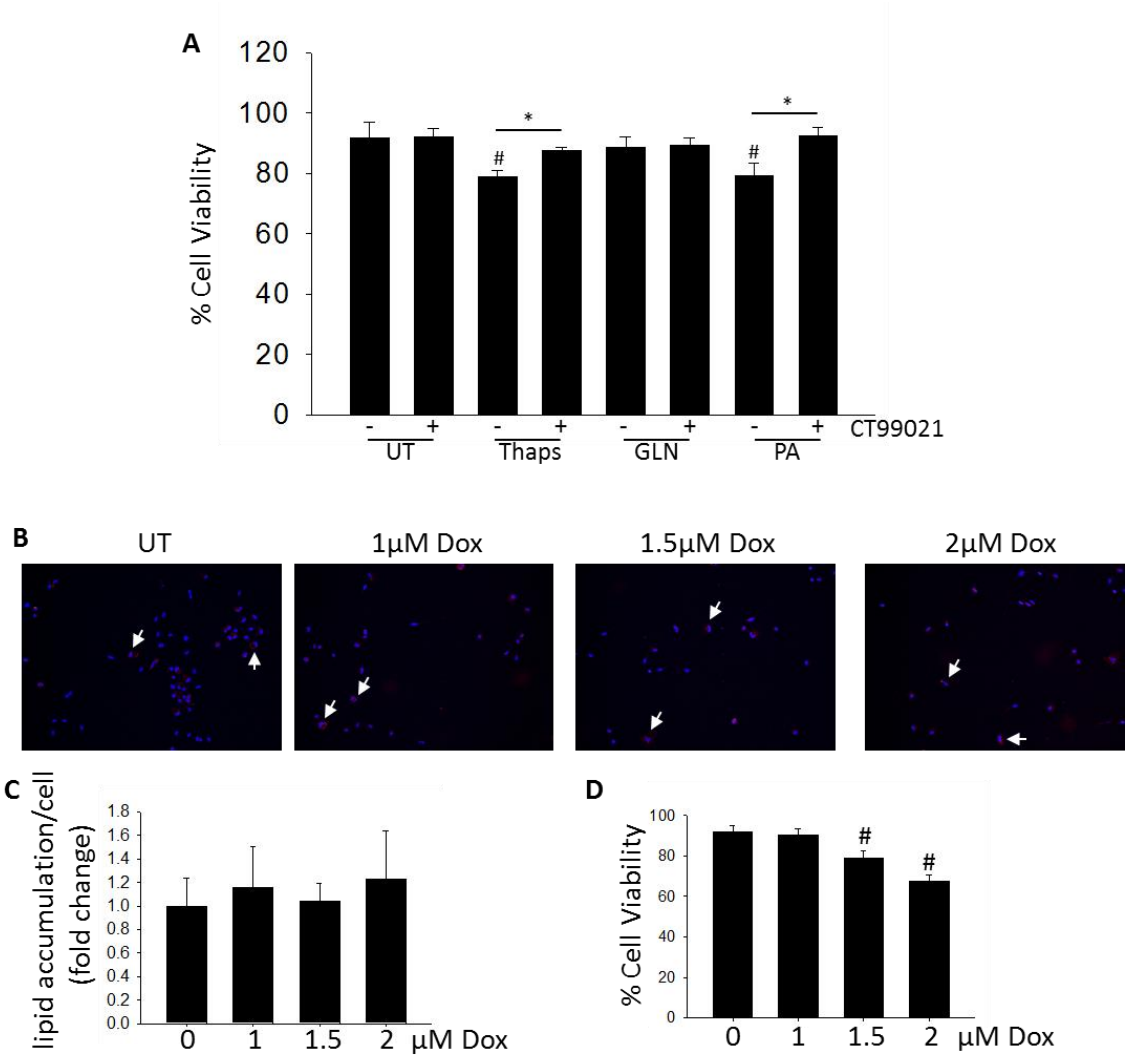
A
120
100
80
60
40
20
0
% Cell Viability
*
*
#
#
- + - + - + - + CT99021
UT
Thaps
GLN
PA
B
UT
1μM Dox
1.5μM Dox
2μM Dox
C
lipid accumulation/cell (fold change)
1.8
1.6
1.4
1.2
1.0
0.8
0.6
0.4
0.2
0.0
0 1 1.5 2 μM Dox
D
% Cell Viability
100
80
60
40
20
0
#
#
0 1 1.5 2 μM Dox

Supplementary Figure IV. Knockdown of GSK3α/β by siRNA attenuates ER stress-induced CHOP expression and lipid accumulation. Thp1 derived macrophages were exposed to 50nmol/L scramble or GSK3α/β siRNA.**A)** Knockdown of GSK3α/β protein levels was confirmed by SDS PAGE. Cells were subsequently treated with the ER stress-inducing agents thapsigargin (Thaps, 1μmol/L), glucosamine (GLN, 5mmol/L) or palmitic acid (PA, 600μmol/L) for 18 hours. **B)** Whole cell lysates were resolved by SDS PAGE and probed with antibodies against GRP78 and CHOP. Immunoblots were quantified by densitometry **(C and D)**. Cells were stained with Oil Red O and DAPI and representative images are shown **(E)** and quantified **(F)**. n=4 *$p<0.05$ relative to scramble siRNA, untreated cells, #$p<0.05$ relative to cells of the same treatment without GSK3α/β siRNA

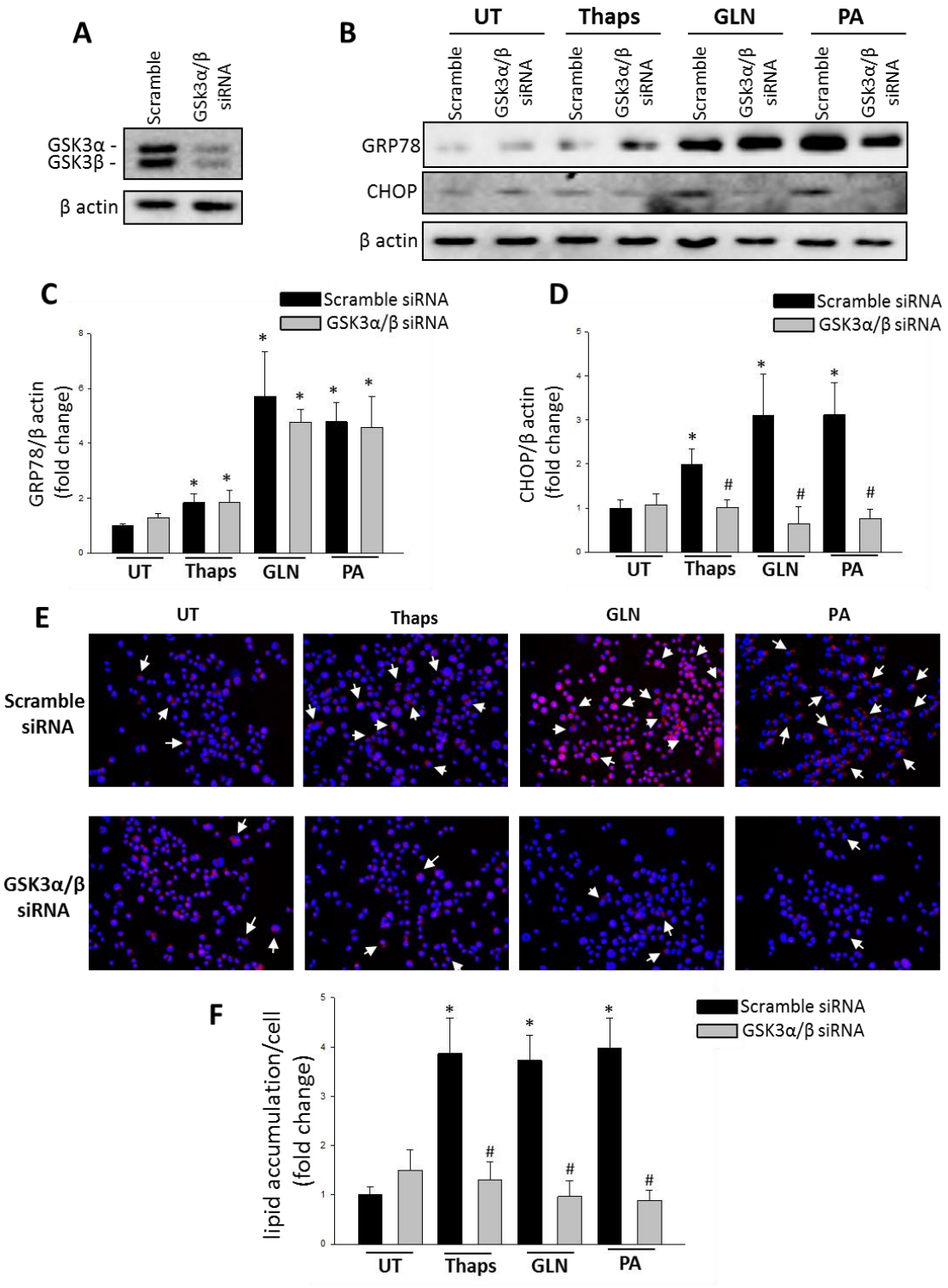
A
Scramble
GSK3α/β siRNA
GSK3α -
GSK3β -
β actin
B
UT
Thaps
GLN
PA
Scramble
GSK3α/β siRNA
GRP78
CHOP
β actin
C
Scramble siRNA
GSK3α/β siRNA
GRP78/β actin (fold change)
UT
Thaps
GLN
PA
D
Scramble siRNA
GSK3α/β siRNA
CHOP/β actin (fold change)
UT
Thaps
GLN
PA
E
UT
Thaps
GLN
PA
Scramble siRNA
GSK3α/β siRNA
F
Scramble siRNA
GSK3α/β siRNA
lipid accumulation/cell (fold change)
UT
Thaps
GLN
PA

Supplementary Figure V. PERK inhibitor (GSK2606414) attenuates PERK signaling. Whole well lysates from Thp-1 derived macrophages treated with 1μM thapsigargin (Thaps) in the presence or absence of 3μmol/L GSK2606414 (PERK Inhibitor) were resolved by SDS-PAGE and probed for CHOP to demonstrate PERK inhibition.

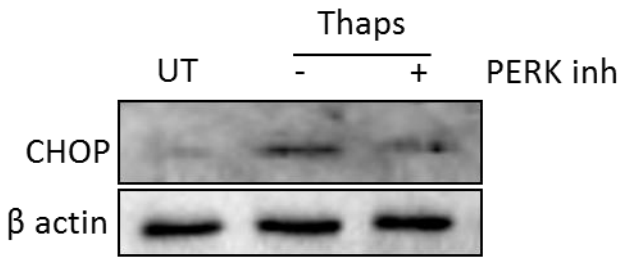
Thaps
UT
-
+
PERK inh
CHOP
β actin

Supplementary Figure VI. IgG control antibodies. Aortic sections were exposed to **A)** pre-immune rat or mouse IgG antibodies to control for non specific binding of antibodies against Mac3 and KDEL respectively and **B)** rabbit IgG antibodies to control for non specific binding of antibodies against CHOP.

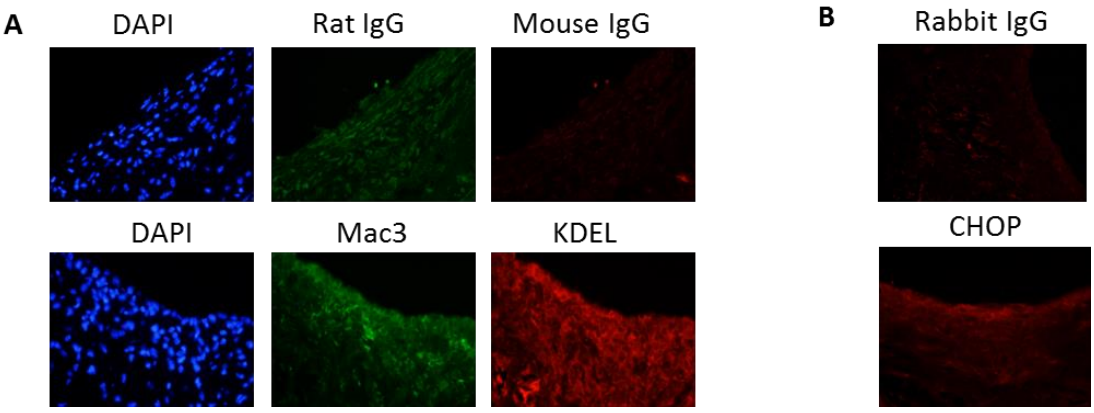
A
DAPI
Rat IgG
Mouse IgG
DAPI
Mac3
KDEL
B
Rabbit IgG
CHOP

Supplementary Figure VII. ER stress and CT99021 do not impact the expression of glutamate dehydrogenase or citrate synthase. Thp1 derived macrophages were exposed to the ER stress-inducing agents thapsigargin (Thaps, 1μmol/L), glucosamine (GLN, 5mmol/L) or palmitic acid (PA, 600μmol/L) for 18 hours with or without pretreatment with CT99021. The mRNA expression of **A)** Glutamate Dehydrogenase and **B)** Citrate Synthase was determined by real time PCR. n=3, ns = not significant.

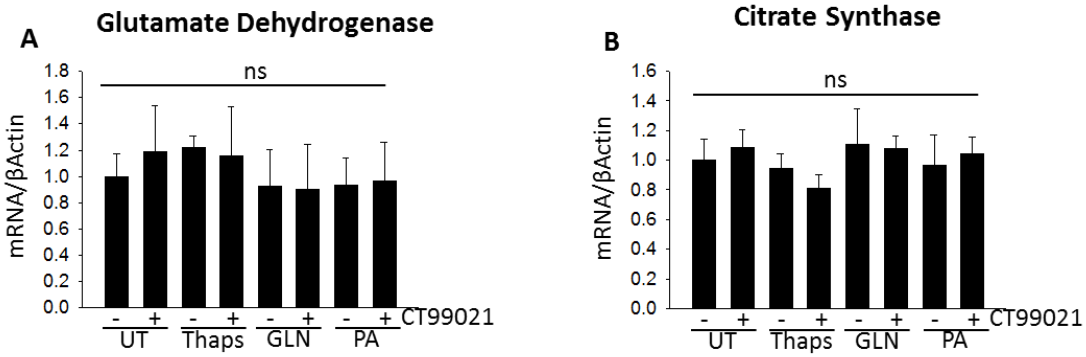
A
Glutamate Dehydrogenase
mRNA/βActin
ns
1.8
1.6
1.4
1.2
1.0
0.8
0.6
0.4
0.2
0.0
- + - + - + - + CT99021
UT
Thaps
GLN
PA
B
Citrate Synthase
mRNA/βActin
ns
1.6
1.4
1.2
1.0
0.8
0.6
0.4
0.2
0.0
- + - + - + - + CT99021
UT
Thaps
GLN
PA

Supplementary Figure VIII. ER stress-induced cholesterol accumulation is attenuated by different GSK3α/β inhibitors. ER stress was induced in Thp-1 macrophages using 1μmol/L thapsigargin (Thaps), 5mmol/L glucosamine (GLN) or 600μmol/L palmitic acid (PA). GSK3α/β was inhibited by treating cells with 4μmol/L CT99021 (CT), or 250μmol/L GSK3 inhibitor II (Inh2), or 2mmol/L valproate (VPA). Free **(A)** and esterified **(B)** cholesterol levels were determined, as indicated. n=3-4, *$p<0.05$ relative to untreated cells, #$p<0.05$ relative to cells of the same treatment without GSK3α/β inhibition.

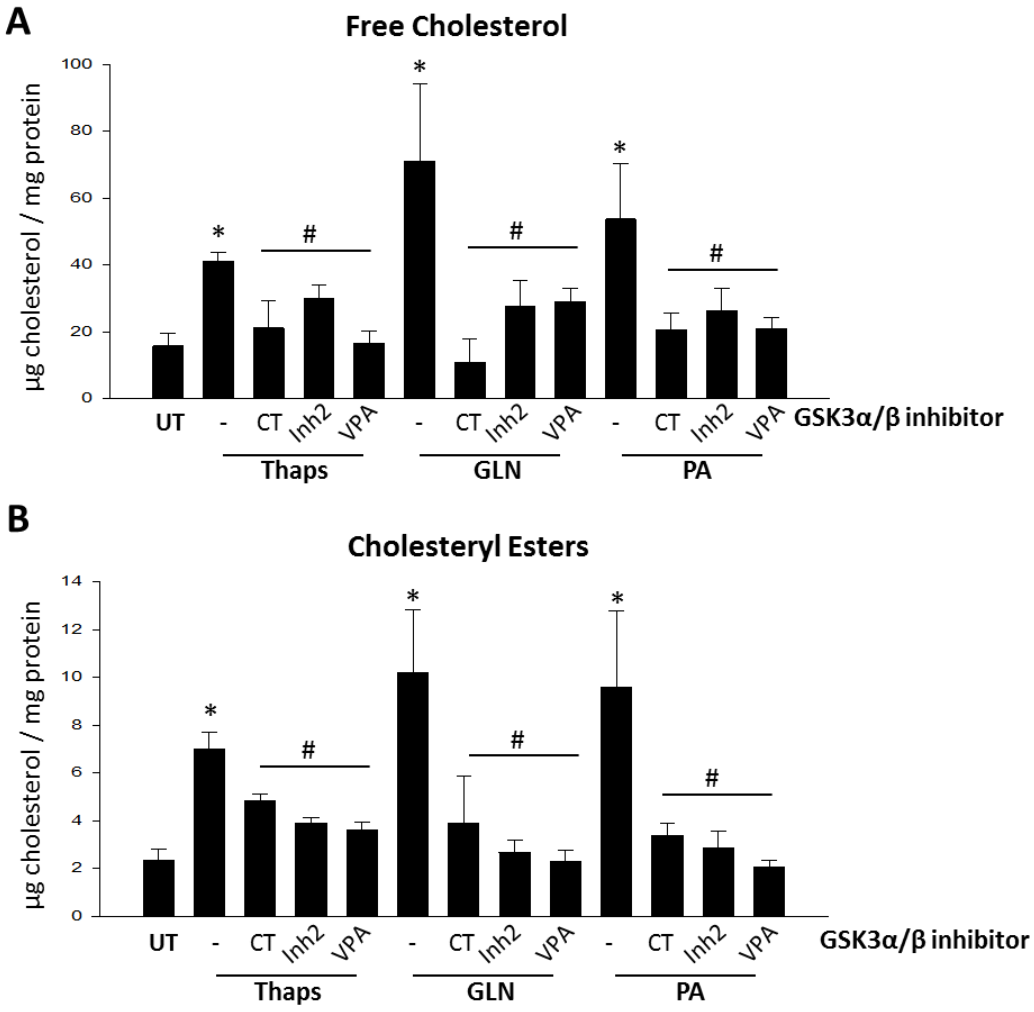
A
Free Cholesterol
µg cholesterol / mg protein
100
80
60
40
20
0
UT
-
CT
Inh2
VPA
Thaps
GLN
PA
GSK3α/β inhibitor
B
Cholesteryl Esters
µg cholesterol / mg protein
14
12
10
8
6
4
2
0
UT
-
CT
Inh2
VPA
Thaps
GLN
PA
GSK3α/β inhibitor

Supplementary Figure IX. GSK3α/β inhibition attenuates free cholesterol synthesis in macrophages cultured in lipoprotein-deficient media. ER stress was induced in Thp-1 macrophages cultured in lipoprotein free media using 1μmol/L thapsigargin (Thaps), 5mmol/L glucosamine (GLN) or 600μmol/L palmitic acid (PA). GSK3α/β was inhibited by treating cells with 4μmol/L CT99021. Free **(A)** and esterified **(B)** cholesterol levels were determined. n=3-4, *$p<0.05$ relative to untreated cells, #$p<0.05$ relative to cells of the same treatment without CT99021.

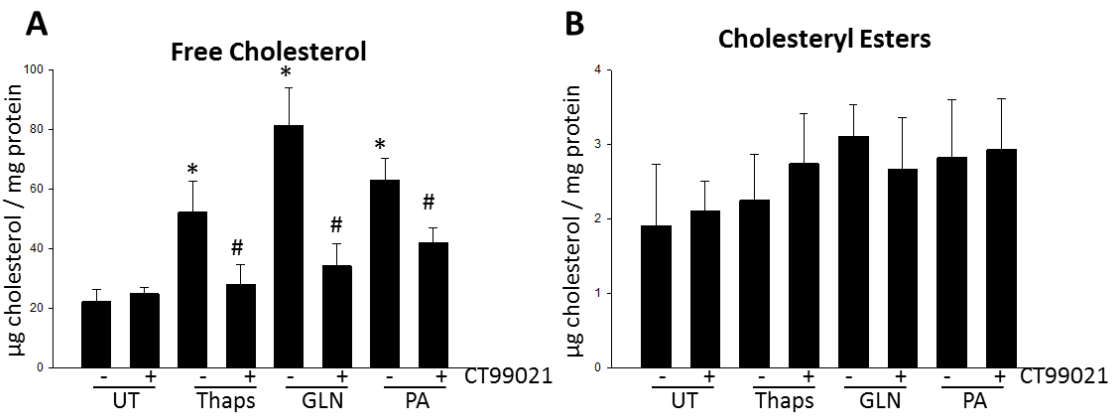
A
Free Cholesterol
µg cholesterol / mg protein
100
80
60
40
20
0
*
*
*
#
#
#
- + - + - + - + CT99021
UT Thaps GLN PA
B
Cholesteryl Esters
µg cholesterol / mg protein
4
3
2
1
0
- + - + - + - + CT99021
UT Thaps GLN PA

Supplementary Figure X. Adenovirus directed overexpression of GSK3β. Primary mouse macrophages were infected with control adenovirus (Ad-Null) or adenovirus encoding constitutively active GSK3β (Ad-S9A-GSK3β) at 10 MOI. **A)** Protein lysates were resolved by SDS-PAGE immunostained for GSK3β and β actin as indicated and **B)** quantified. Similarly, primary mouse macrophages were infected with Ad-Null or adenovirus encoding GFP (Ad-GFP) at 10 MOI. **C)** Bright field and florescent images were captured and the percentage of cell expressing GFP was quantified. Quantification indicates 65.7±3.6% of cells are infected with the adenovirus. n=3 *$p<0.05$ relative to Ad-Null

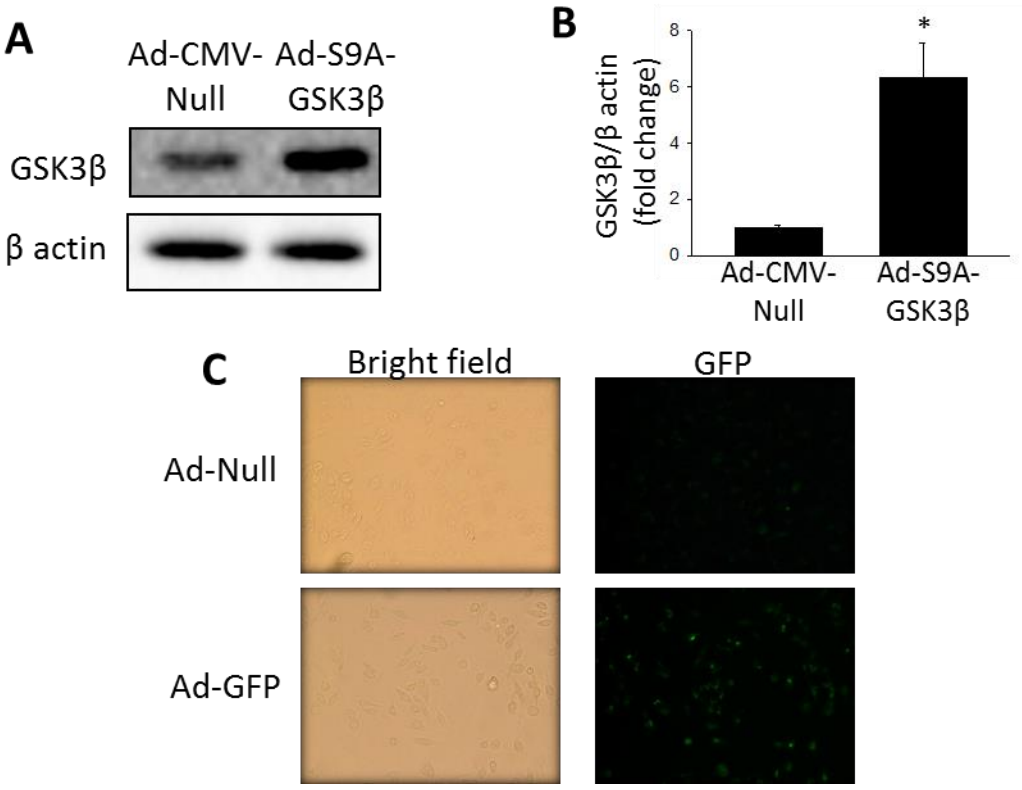
A
Ad-CMV-Null
Ad-S9A-GSK3β
GSK3β
β actin
B
GSK3β/β actin (fold change)
8
6
4
2
0
*
Ad-CMV-Null
Ad-S9A-GSK3β
C
Bright field
GFP
Ad-Null
Ad-GFP

APPENDIX 3: Supplemental Material for Chapter 5

Foreword

Appendix 3 is a direct representation of the supplemental material published in *Arteriosclerosis, Thrombosis and Vascular Biology*, volume 35, pages 1113-1122, May 2015. The experiments were conducted by Cameron McAlpine with assistance from the co-authors.The full reference is as follows:

McAlpine CS, Huang A, Emdin A, Banko NS, Beriault DR, Shi Y and Werstuck GH. Deletion of myeloid GSK3α attenuates atherosclerosis and promotes an M2 macrophage phenoypte. *Arteriosclerosis, Thrombosis and Vascular Biology*. 2015;35:1113-1122.

Supplemental Materials and Methods

Mouse models

All animal experiments were conducted with approval of the McMaster University Animal research Ethics Board. LDLR$^{-/-}$mice (B6.129S7-*Ldlr*^{tm1Her}/J), AlbCre mice (B6N.Cg-TgAlb-cre^{21Mgn}/J) and LyzMCre (B6.129P2-Lyz2$^{tm(cre)Ifo}$/J) mice were purchased from Jackson Labs. Floxed GSK3α, floxed GSK3β and GSK3α$^{-/-}$ mice were a generous gifts from Dr. Bradley Doble (McMaster University) and Dr. Jim Woodgett (University of Toronto).[1-4] All mice were backcrossed >10 times onto a C57Bl6 background. Genotype was determined by PCR (Supplementary Figure 1). Tissue specific GSK3α or GSK3β knockout LDLR$^{-/-}$ mice were placed on a high fat diet (HFD) containing 21% milk fat, 0.2% cholesterol (42% kcal from fat)(Harlan Teklad, TD97363) at 5 weeks of age and sacrificed at 15 weeks of age. For bone marrow transplantation experiments, 5 weeks old recipient mice were irradiated with 12Gy of γ-irradiation from a ^{137}C source using a Gammacel 3000 small animal irradiator. Irradiated mice received bone marrow (3X10^{6} cells) injected by i.v. and were left to recover for 4 weeks before being switched to a HFD for 10 weeks (from 9 to 19 weeks of age). All mice had unlimited access to food and water. Body weights were monitored and fasted blood glucose and lipid levels were quantified as previously described.[5]Pooled plasma from at least 5 animals of each group was fractioned using fast performance liquid chromatography with the FRAC-950 FPLC (Amersham Pharmacia Biotech) and cholesterol concentration was measured using the infinity cholesterol reagent (Thermo Scientific). Plasma IL-6, TNFα and IL-10 was quantified by ELISA (eBioScience). Monocyte concentration in whole blood was determined using a Hemavet 950 Multi Species Hematology System (Drew Scientific).

Plasma and tissue cholesterol and triglyceride levels were determined using infinity reagent (Thermo Scientific).

Tissue collections and analysis

After 10 weeks of HFD feeding mice were anesthetized (isoflourane) and harvested at 15 weeks (tissue specific knockout mice) or 19 weeks (bone marrow transplant mice) of age. Vasculature was flushed with saline and perfusion fixed with 10% neutral buffer formalin. Hearts, aortas and liver were collected for further analysis. Hearts and aortas were imbedded in paraffin and serial 5μm sections of the aortic root were collected. Sections were stained with Harris hematoxylin and eosin (Sigma) and Masons Trichrome (Sigma). On a separate subset of mice, hearts, aortas and liver were imbedded in optical cutting temperature (OCT) compound (Tissue-Tek) and frozen. OCT imbedded frozen tissue was serial sectioned at 10μm and stained with Oil Red O and Mayer's Hematoxylin (Sigma). Images were collected using a Leitz LABORLUX S microscope connected to a DP71 Olympus camera and lesion area was quantified using Image J 1.43M software as previously described.[6] Briefly, for atherosclerotic lesion area, volume and necrotic core volume paraffin imbedded sections stained with H&E were used. Sections 60μm apart spanning the entire length of the lesion were used. Fibrous cap thickness was determined throughout the length of the lesion using ImageJ software. Average fibrous cap thickness is presented. Lesion collagen content was determined by quantifying collagen stained area using ImageJ software and is presented relative to total lesion area.

Immunoblot

Total protein lysates were prepared from flash frozen tissue solubilized in 4x SDS-PAGE sample buffer (0.5M Tris-HCl pH6.8, glycerol and 10% SDS) and quantified by Bradford assay. 30μg of total protein was separated by SDS-PAGE under reducing conditions and transferred to nitrocellulose membranes. Membranes were incubated with antibodies overnight at 4˚C. Antibodies used include GSK3α/β, P-701-STAT1, STAT1, P-705-STAT3, STAT3, STAT 6 (Cell Signaling) and P-641-STAT6 (BD Biosciences). Membranes were then exposed to the appropriate horseradish peroxidase secondary antibody (Life Technologies) for 1 hr at room temperature and developed using Immobilon Western Chemiluminescent horseradish peroxidase substrate (Millipore). Densitometry analysis of bands was conducted using Image Lab software (Invitrogen).

Bone marrow derived macrophage isolation and polarization

Bone marrow was isolated from tibias and femurs of mice and cultured in DMEM (Life Technologies) containing 10% fetal bovine serum. Bone marrow was exposed to 10ng/ml mouse macrophage colony stimulating factor (MCSF) for 5 days producing unstimulated (M0) bone marrow derived macrophages (BMDMs). BMDMs were then polarized into M1 macrophages by exposure to 10ng/ml LPS for 6 hours or M2 macrophages by exposure to 10ng/ml IL-4 for 24 hours.

Gene expression

Total RNA was isolated from BMDMs or hepatic tissue using the RNeasy Mini Kit (Qiagen). RNA concentration and purity was determined by measuring the absorbance

at 260nm/280nm. RT-PCR was performed using 2µg of total RNA transcribed using the High Capacity cDNA Reverse Transcription kit (Applied Biosystems). Amplification of PCR products was carried out using a GeneAmp 7300 sequence detection system (Applied Biosystems) and SYBR Green qPCRSuperMix (Invitrogen). PCR reactions were performed in technical triplicates and biological quadruplets using primers sequences indicated in Supplemental Table II. RT-PCR results were analyzed using Data Assist 3.0 software (Applied Biosystems).

Flow cytometry

Blood was collected via the tail vein and Ly6C expression was determined using a BD LSR II flow cytometer. Using forward scatter and side scatter plots, red blood cell and dead cells were excluded from analysis. $CD115^+$ and $CD11b^+$ monocytes were identified using PE- and FITC- conjugated antibodies (BD Pharmingen). Ly6C expression was then determined in the monocyte population using an APC-conjugated antibody (BD Pharmingen).

Immunoflorescence

Paraffin imbedded serial sections (4µm) were immunostained using primary antibodies against Mac3 (BD Transductions), αactin (Santa Cruz), FABP4 (Cell Signaling), CD36 (Santa Cruz), Arg1 (Santa Cruz) and Pgc1 (Santa Cruz). Serial sections were stained with pre-immune IgG, in place of primary antibodies, to control for non-specific staining (Supplementary Figure X). Appropriate secondary antibodies (BD transductions) conjugated to a florophore were used for detection. Images were collected using a Leitz LABORLUX S microscope connected to a DP71 Olympus camera. Immunofluorescent staining intensity was quantified using Image J 1.43M software. Briefly, 12 aortic sections from each animal (n=5-6 mice per group) representing the entire length of the lesion were stained and imaged. Mac3+ stained area was excised from each image and FABP4, CD36, Arg1 and Pgc1staining intensity above background within the Mac3+ area of the atherosclerotic lesion was determined over a fixed threshold. For αactin staining the entire lesion area was excised from the image and similarly quantified. The staining intensity of the 12 aortic sections from each animal was averaged to provide a staining intensity for each animal. Data shown represent average staining intensity for each animal within the group.

Statistical analysis

All data is expressed as mean±SD of independent biological experiments. The number of biological replicates is indicated in the figure legends. An unpaired Student *t* test or a 1-way ANOVA test was used to determine statistical significance. A value of $P<0.05$ was considered statistically significant.

Supplementary References

1. Patel S, Doble BW, MacAulay K, Sinclair EM, Drucker DJ, Woodgett JR. Tissue-specific role of glycogen synthase kinase 3beta in glucose homeostasis and insulin action. *Mol Cell Biol*. 2008;28:6314-6328.

2. Patel S, Macaulay K, Woodgett JR. Tissue-specific analysis of glycogen synthase kinase-3alpha (GSK-3alpha) in glucose metabolism: effect of strain variation. *PLoS One*. 2011;6:e15845.
3. MacAulay K, Doble BW, Patel S, et al. Glycogen synthase kinase 3alpha-specific regulation of murine hepatic glycogen metabolism. *Cell Metab*. 2007;6:329-337.
4. Banko N, McAlpine CS, Venegas-Pino DE, et al. Glycogen Synthase Kinase (GSK)-3alpha deficiency attenuates atherosclerosis and hepatic steatosis in high fat diet fed $LDLR^{-/-}$ mice. *American Journal of Physiology*. 2014;184:3394-3404.
5. Werstruck G, Khan M, Femia G, et al. Glucosamine-induced endoplasmic reticulum dysfunction is associated with accelerated atherosclerosis in a hyperglycemic mouse model. *Diabetes*. 2006;55:93-101.
6. Venegas-Pino DE, Banko N, FAU - Khan MI, et al. Quantitative analysis and characterization of atherosclerotic lesions in the murine aortic sinus. *J Vis Exp,* 2013;82:50933.

Supplementary Table I. Metabolic parameters of bone marrow transplanted mice fed a HFD.
n=5

	LDLR$^{-/-}$ → LDLR$^{-/-}$	**LDLR$^{-/-}$GSK3α$^{-/-}$ → LDLR$^{-/-}$**	**LDLR$^{-/-}$ GSK3α$^{-/-}$ → LDLR$^{-/-}$ GSK3α$^{-/-}$**	**LDLR$^{-/-}$ → LDLR$^{-/-}$ GSK3α$^{-/-}$**
Fasting Plasma Concentration (mmol/L)				
Glucose	9.6±0.3	9.9±1.2	8.5±0.8	8.5±0.4
Cholesterol	30.4±0.6	29.7±4.2	32.2±2.4	25.3±2.5
Triglyceride	3.4±0.1	3.2±0.4	4.0±0.7	2.4±0.6
Adipose weight (g)	0.20±0.05	0.21±0.02	0.24±0.03	0.25±0.05
Liver weight (g)	1.04±0.03	0.90±0.03	0.99±0.03	0.90±0.05

Supplementary Table II. RT-PCR Primer Sequences.

Gene	Primer Sequence
TNFα	Fwd: TCT CAG CCT CTT CTC ATT CCT GCT Rev: AGA ACT GAT GAG AGG GAG GCC ATT
IL-6	Fwd: ACA AAG CCA GAG TCC TTC AGA GAG Rev: TTG GAT GGT CTT GGT CCT TAG CCA
CD36	Fwd: TCA TGC CAG TCG GAG ACA TGC TTA Rev: ACC TGT CTG TAC ACA GTG GTG CCT
FABP4	Fwd: ATG AAA TCA CCG CAG ACG ACA GGA Rev: TGT GGT CGA CTT TCC ATC CCA CTT
IL-1β	Fwd: CTG CTT CCA AAC CTT TGA CC Rev: AG CTT CTC CAG AGC CAC AAT
IL-12p35	Fwd: TGC CCT CCT AAA CCA CCT CAG TTT Rev: TTT CTC TGG CCG TCT TCA CCA TGT
IL-10	Fwd: GCT CTT ACT GAC TGG CAT GAG Rev: CGC AGC TCT AGG AGC ATG TG
Arg1	Fwd: ACC TGG CCT TTG TTG ATG TCC CTA Rev: AGA GAT GCT TCC AAC TGC CAG ACT
Fizz1	Fwd: TCC AGC TGA TGG TCC CAG TGA ATA Rev: ACA AGC ACA CCC AGT AGC AGT CAT
Ym1	Fwd: AGA AGG GAG TTT CAA ACC T Rev: GTC TTG CTC ATG TGT GTA AGT GA
Mgcl-2	Fwd: GCA TGA AGG CAG CTG CTA TTG GTT Rev: TAG GCC CAT CCA GCT AAG CAC ATT
Pgc1β	Fwd: CTT CCG TTG GCC CAG ATA C Rev: CTG CTG GGC CTC TTT CAG TA
HMGCoA	Fwd:GTC CCT AGC TTG GCT GAC AGA Rev: TGG AGA GCG AGG GCT TTG
SREBP2	Fwd: GCG TTC TGG AGA CCA TGG A Rev:ACA AAG TTG CTC TGA AAA CAA ATC A
SREBP1c	Fwd: GGA GCC ATG GAT TGC ACA TT Rev:GCT TCC AGA GAG GAG GCC AG
FAS	Fwd:GCT GCG GAA ACT TCA GGA AAT Rev:AGA GAC GTG TCA CTC CTG GAC TT
SR-A	Fwd:TGA ACG AGA GGA TGC TGA CTG Rev:GGA GGG GCC ATT TTT AGT GC
SR-B1	Fwd:GGC TGC TGT TTG CTG CG Rev:GCT GCT TGA TGA GGG AGG G
ABCA1	Fwd:GGT TTG GAG ATG GTT ATA CAA TAG TTG T Rev:TTC CCG GAA ACG CAA GTC
ABCG1	Fwd:AGG TCT CAG CCT TCT AAA GTT CCT C Rev:TCT CTC GAA GTG AAT GAA ATT TAT CG
βactin	Fwd: GGC ACC ACA CCT TCT ACA ATG Rev: GGG GTG TTG AAG GTC TCA AAC

Supplementary Figure I. **PCR and body weight analysis of mouse models. A)** Genotyping of LLαKO, LLβKO, LMαKO and LMβKO mice. Lane (a) indicates $LDLR^{-/-}$ (~320bp band), lane (b) indicates $GSK3\alpha^{fl/fl}$ (750bp band)or $GSK3\beta^{fl/fl}$ (685bp band), and lane (c) indicates expression of the appropriate Cre recombinase (100bp band for AlbCre and 700bp + 350bp bands for $LyzCre^{+}$ and wildtype respectively). **B)** Body weight analysis of female mice on a HFD. n=8-9

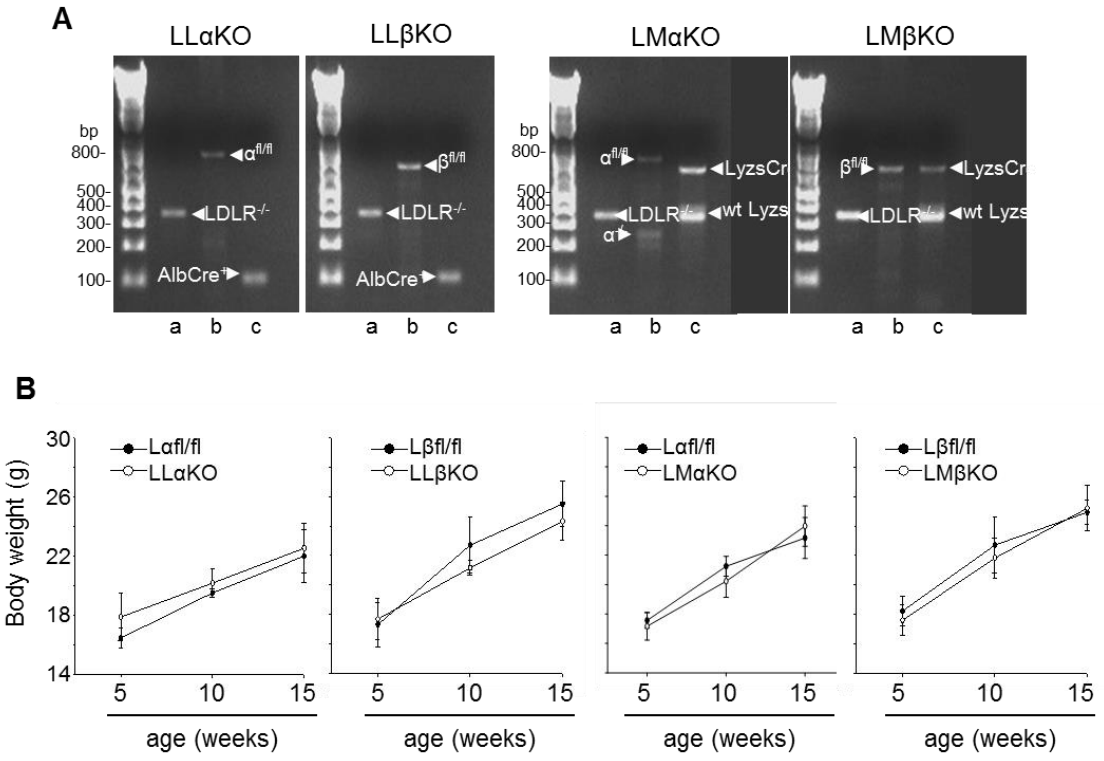
A
LLαKO
LLβKO
LMαKO
LMβKO
bp
800-
500-
400-
300-
200-
100-
αfl/fl
βfl/fl
LDLR-/-
AlbCre+
LyzsCr
wt Lyzs
a b c
B
Body weight (g)
30
26
22
18
14
Lαfl/fl
LLαKO
Lβfl/fl
LLβKO
LMαKO
LMβKO
5 10 15
age (weeks)

Supplementary Figure II. **Atherosclerosis in female LLαKO and LLβKO mice.** Representative aortic root sections from HFD fed LLαKO and Lαfl/fl control mice **(A)** or LLβKO and Lβfl/fl control mice **(F)** stained with hematoxylin and eosin (H&E), Masons Trichrome or Oil Red O. Quantification of atherosclerotic lesion area at the aortic sinus and ascending aorta of LLαKO mice **(B)**, LLβKO mice **(G)** and corresponding controls. Quantification of atherosclerotic lesion volume and necrotic core volume of LLαKO **(C and D)** and LLβKO **(H and I)** mice and corresponding controls. n=10-12. **(E and J)** Plasma levels of IL-6, TNFα and IL-10 after 10 weeks of HFD. n=5-8

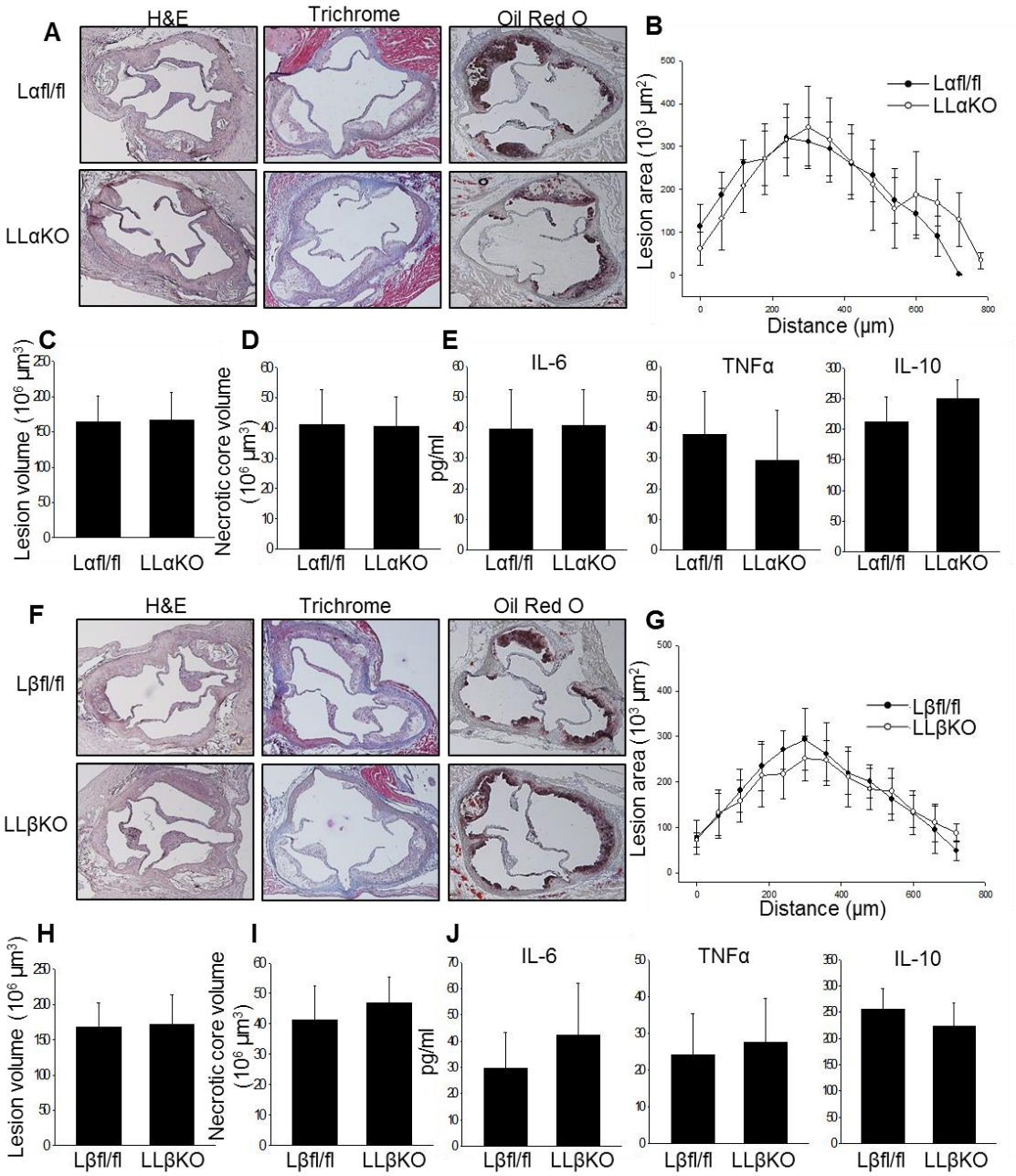
A
H&E
Trichrome
Oil Red O
Lαfl/fl
LLαKO
B
Lαfl/fl
LLαKO
Lesion area (10³ µm²)
Distance (µm)
C
Lesion volume (10⁶ µm³)
Lαfl/fl
LLαKO
D
Necrotic core volume (10⁶ µm³)
E
IL-6
pg/ml
TNFα
IL-10
F
Lβfl/fl
LLβKO
G
H
I
J

Supplementary Figure III. Atherosclerosis in male LLαKO and LLβKO mice.

Representative images of hematoyxylin and eosin stained aortic root sections from male LLαKO **(A)**, LLβKO **(D)** and control mice fed a HFD for 10 weeks. Quantification of atherosclerotic lesion area beginning at the aortic root **(B and E)** and lesion volume **(C and F)** of male mice. n=5

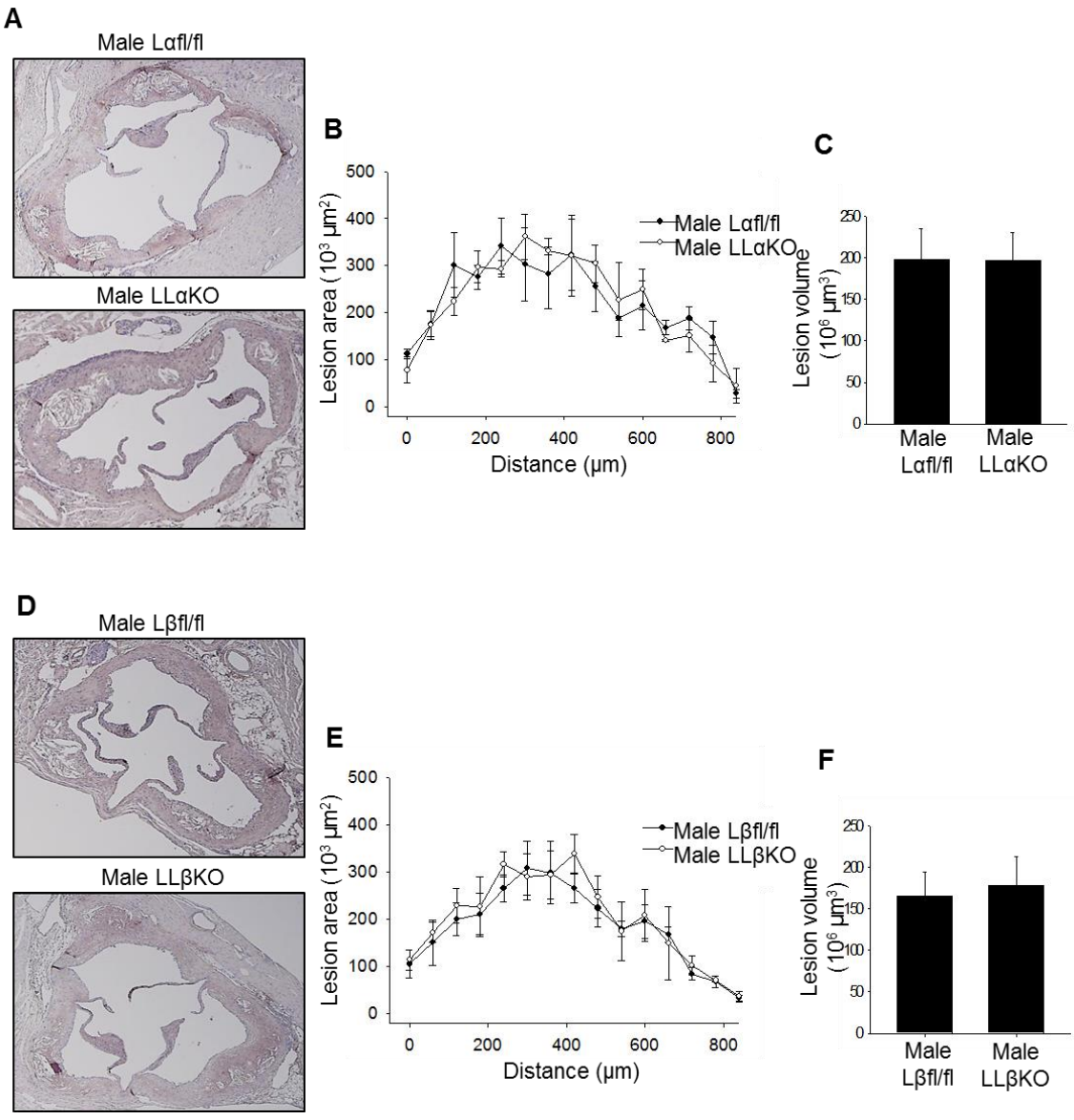
A
Male Lαfl/fl
Male LLαKO
B
Lesion area (10³ µm²)
Distance (µm)
Male Lαfl/fl
Male LLαKO
C
Lesion volume (10⁶ µm³)
Male Lαfl/fl
Male LLαKO
D
Male Lβfl/fl
Male LLβKO
E
Lesion area (10³ µm²)
Distance (µm)
Male Lβfl/fl
Male LLβKO
F
Lesion volume (10⁶ µm³)
Male Lβfl/fl
Male LLβKO

Supplementary Figure IV. Metabolic gene expression in liver of female LLαKO and LLβKO mice. Transcript expression of lipid metabolism genes in the liver of LLαKO, LLβKO and littermate controls fed a HFD. Genes include sterol regulatory element binding protein (SREBP)1c, SREBP2, HMGCoA, fatty acid synthase (FAS), scavenger receptor (SR)-A, SR-B1, ABCA1 and ABCG1. n=8

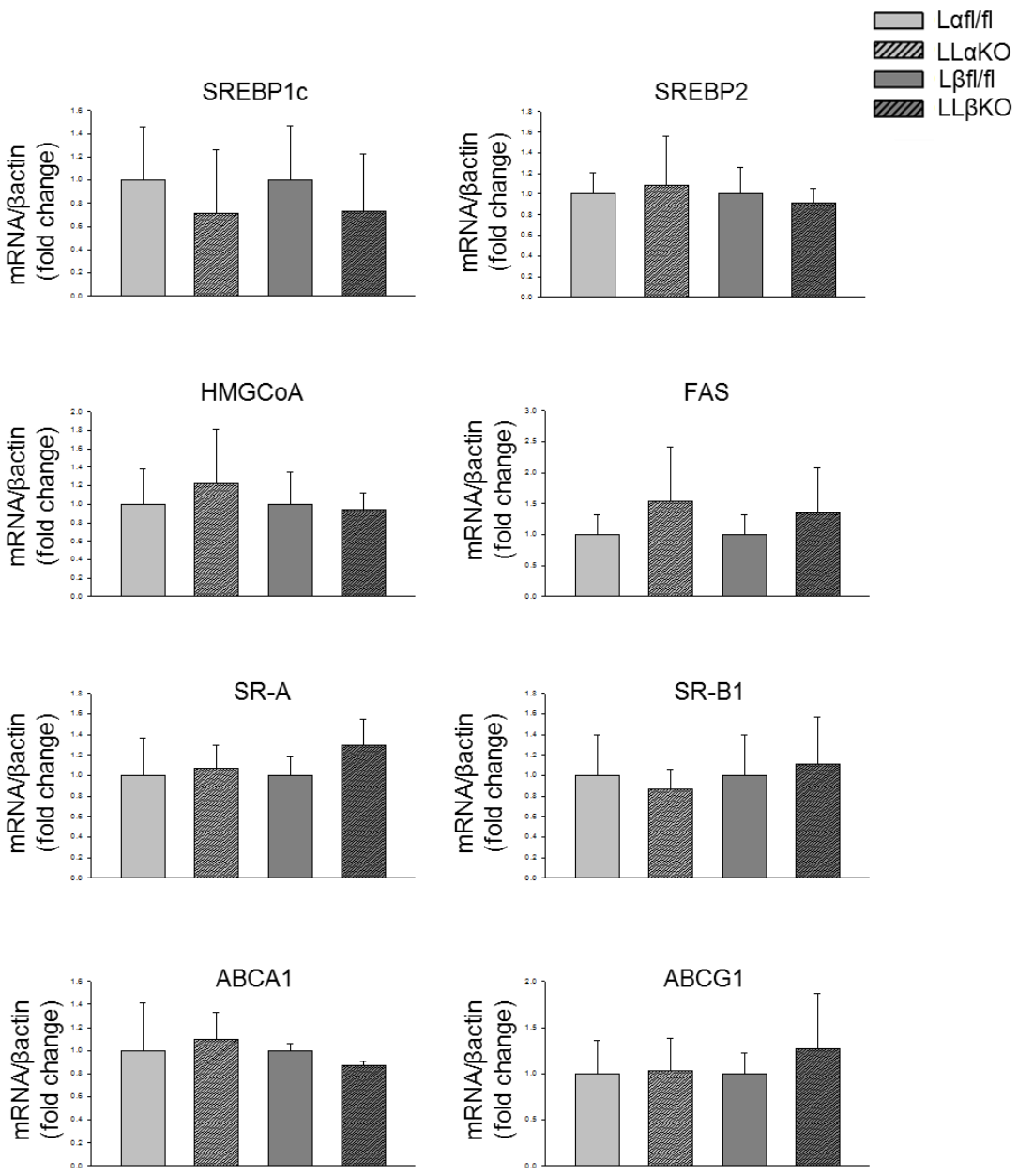
Lαfl/fl
LLαKO
Lβfl/fl
LLβKO
SREBP1c
SREBP2
HMGCoA
FAS
SR-A
SR-B1
ABCA1
ABCG1
mRNA/βactin
(fold change)

Supplementary Figure V. Hepatic lipids in female LMαKO and LMβKO mice.

Representative images of hepatic tissue stained with Oil Red O and Hematoxylin from LMαKO **(A)**, LMβKO **(F)** and control mice. Quantification of Oil Red O stained area in LMαKO **(B)**, LMβKO **(G)** and control mice. Cholesterol **(C and G)** and triglyceride **(D and H)** levels within hepatic tissue of LMαKO, LMβKO and control mice. Plasma lipid profiles of LMαKO **(E)**, LMβKO **(J)** and control mice. n=5-10

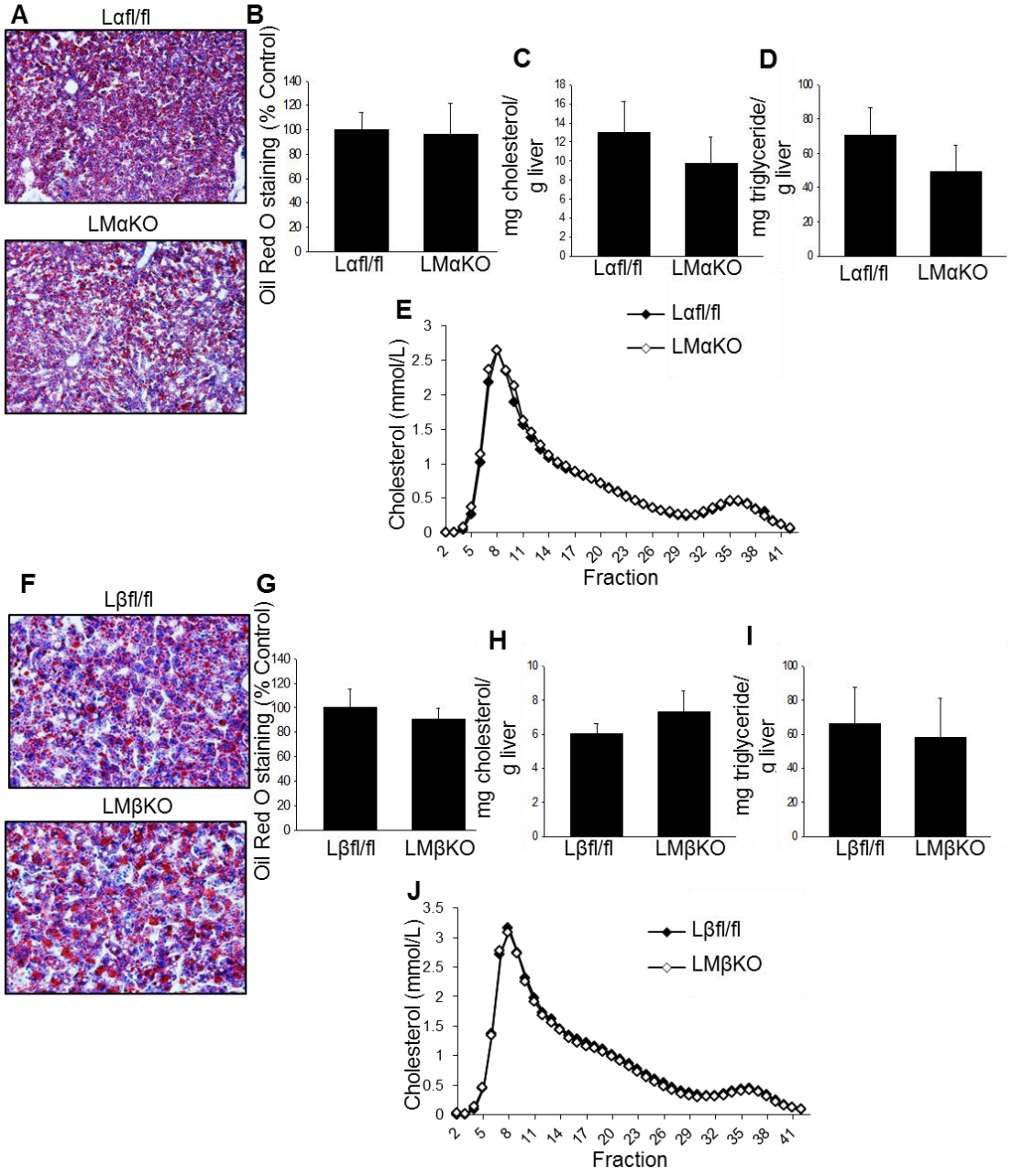
A
Lαfl/fl
LMαKO
B
Oil Red O staining (% Control)
Lαfl/fl
LMαKO
C
mg cholesterol/ g liver
Lαfl/fl
LMαKO
D
mg triglyceride/ g liver
Lαfl/fl
LMαKO
E
Lαfl/fl
LMαKO
Cholesterol (mmol/L)
Fraction
F
Lβfl/fl
LMβKO
G
Oil Red O staining (% Control)
Lβfl/fl
LMβKO
H
mg cholesterol/ g liver
Lβfl/fl
LMβKO
I
mg triglyceride/ g liver
Lβfl/fl
LMβKO
J
Lβfl/fl
LMβKO
Cholesterol (mmol/L)
Fraction

Supplementary Figure VI. Lesion characterization in female LMαKO and LMβKO mice. Aortic root sections from LMαKO, LMβKO and control mice stained with Maisons trichrome **(A and F)**. Fibrous cap thickness **(B and G)** and collagen contentrelative to lesion area **(C and H)** were quantified. **(D and I)** Aortic root sections from LMαKO, LMβKO and control mice stained with the smooth muscle cell marker alpha actin. **(E and J)** Alpha actin staining intensity within the atherosclerotic lesions was quantified. n=6 *p<0.05

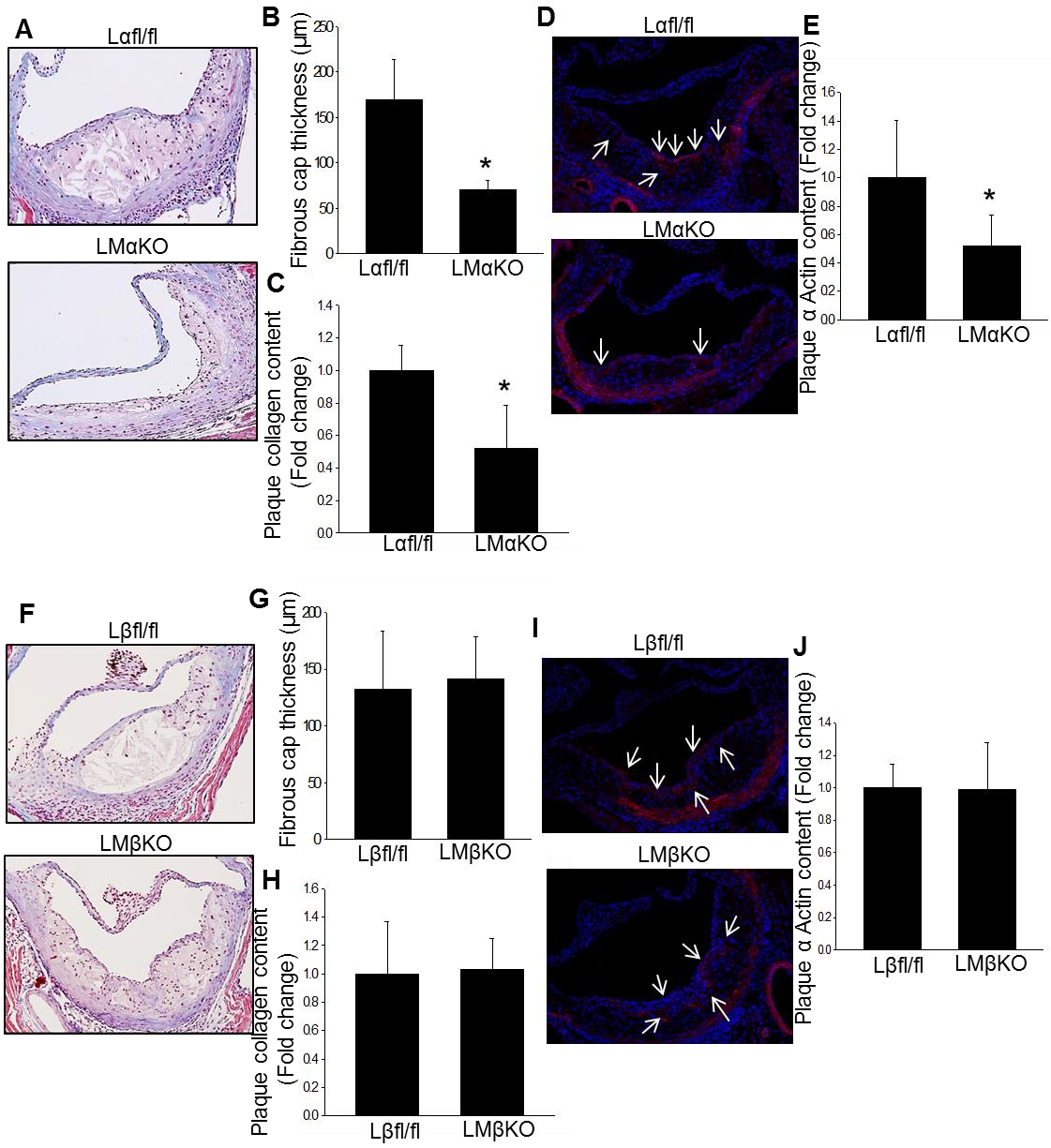
A
Lαfl/fl
LMαKO
B
Fibrous cap thickness (µm)
Lαfl/fl
LMαKO
C
Plaque collagen content (Fold change)
Lαfl/fl
LMαKO
D
Lαfl/fl
LMαKO
E
Plaque α Actin content (Fold change)
Lαfl/fl
LMαKO
F
Lβfl/fl
LMβKO
G
Fibrous cap thickness (µm)
Lβfl/fl
LMβKO
H
Plaque collagen content (Fold change)
Lβfl/fl
LMβKO
I
Lβfl/fl
LMβKO
J
Plaque α Actin content (Fold change)
Lβfl/fl
LMβKO

Supplementary Figure VII. Atherosclerosis in male LMαKO and LMβKO mice. Representative images of hematoyxylin and eosin stained aortic root sections from male LMαKO **(A)**, LMβKO **(D)** and control mice fed a HFD for 10 weeks. Quantification of atherosclerotic lesion area beginning at the aortic root **(B and E)** and lesion volume **(C and F)** of male mice. n=5, *p<0.05

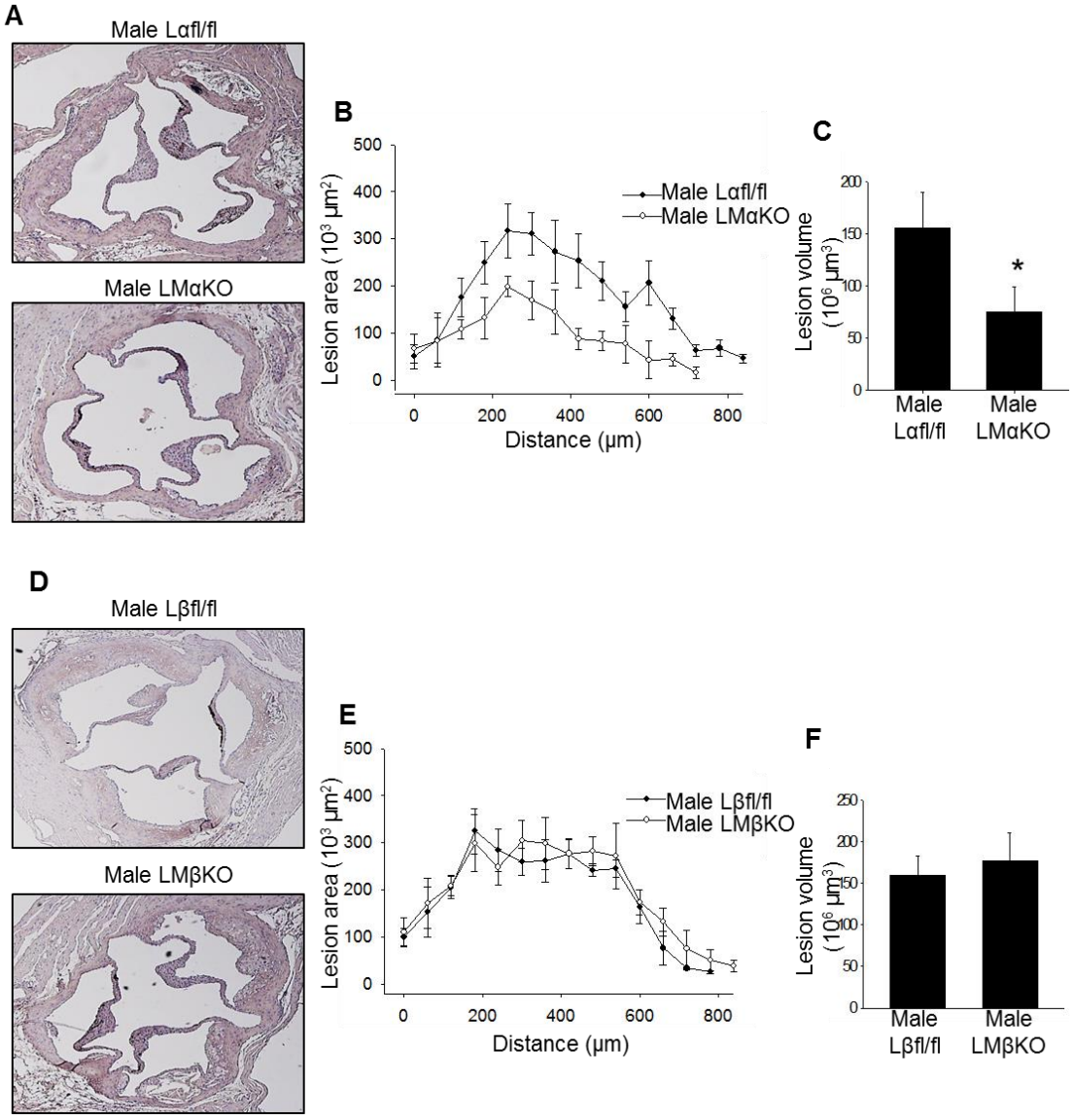
A
Male Lαfl/fl
Male LMαKO
B
Lesion area (10^3 µm^2)
Male Lαfl/fl
Male LMαKO
Distance (µm)
C
Lesion volume (10^6 µm^3)
*
Male Lαfl/fl
Male LMαKO
D
Male Lβfl/fl
Male LMβKO
E
Lesion area (10^3 µm^2)
Male Lβfl/fl
Male LMβKO
Distance (µm)
F
Lesion volume (10^6 µm^3)
Male Lβfl/fl
Male LMβKO

Supplementary Figure VIII. Atherosclerosis in female bone marrow transplanted mice. A) Representative images of aortic root sections stained with hematoxylin and eosin from $LDLR^{-/-}$ mice transplanted with $LDLR^{-/-}$ or $LDLR^{-/-}GSK3\alpha^{-/-}$ bone marrow and fed a HFD for 10 weeks. **B)** Quantification of lesion area at the aortic root. **C)** Quantification of lesion volume. **D)** Representative images of hematoxylin and eosin stained aortic root sections from $LDLR^{-/-}GSK3\alpha^{-/-}$ mice transplanted with $LDLR^{-/-}GSK3\alpha^{-/-}$ or $LDLR^{-/-}$ bone marrow and fed a HFD for 10 weeks. **E)** Quantification of lesion area at the aortic root. **F)** Quantification of lesion volume. n=5, *$p<0.05$

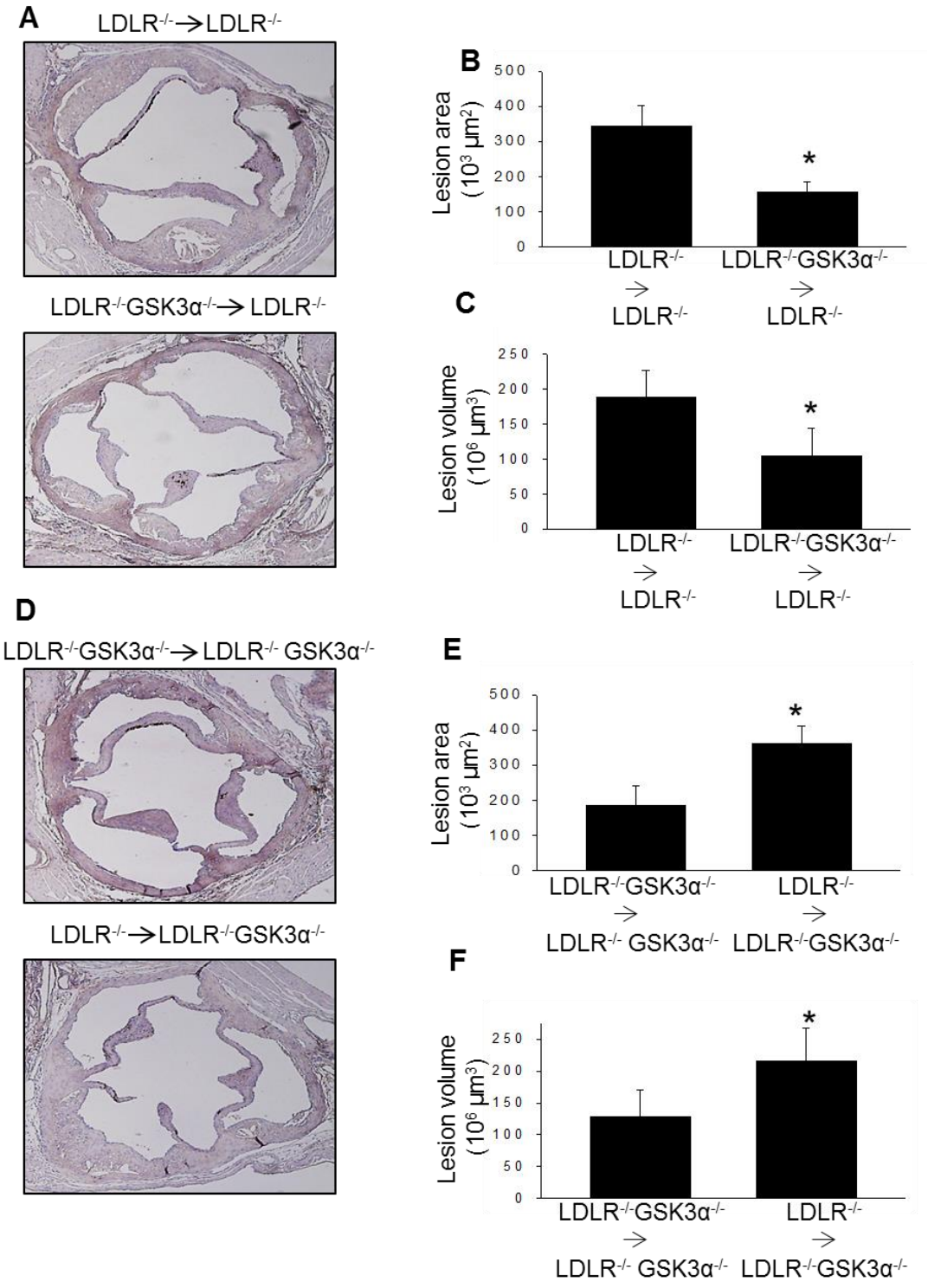
A
LDLR-/-→LDLR-/-
LDLR-/-GSK3α-/-→ LDLR-/-
B
Lesion area (10³ µm²)
500
400
300
200
100
0
*
LDLR-/-
→
LDLR-/-
LDLR-/-GSK3α-/-
→
LDLR-/-
C
Lesion volume (10⁶ µm³)
250
200
150
100
50
0
*
LDLR-/-
→
LDLR-/-
LDLR-/-GSK3α-/-
→
LDLR-/-
D
LDLR-/-GSK3α-/-→ LDLR-/- GSK3α-/-
LDLR-/-→LDLR-/-GSK3α-/-
E
Lesion area (10³ µm²)
500
400
300
200
100
0
*
LDLR-/-GSK3α-/-
→
LDLR-/- GSK3α-/-
LDLR-/-
→
LDLR-/-GSK3α-/-
F
Lesion volume (10⁶ µm³)
250
200
150
100
50
0
*
LDLR-/-GSK3α-/-
→
LDLR-/- GSK3α-/-
LDLR-/-
→
LDLR-/-GSK3α-/-

Supplementary Figure IX. Ly6C expression on monocytes from female LMαKO and LMβKO mice. **A)** Number of monocyte in the blood of LMαKO, LMβKO and control mice fed a HFD for 5 weeks. **B)** $Cd115^{+}Cd11b^{+}Ly6C^{lo}$, $Cd115^{+}Cd11b^{+}Ly6C^{int}$ and $Cd115^{+}Cd11b^{+}Ly6C^{lo}$ monocyte levels in the blood of LMαKO, LMβKO and control mice fed a HFD for 5 weeks. n=8-10

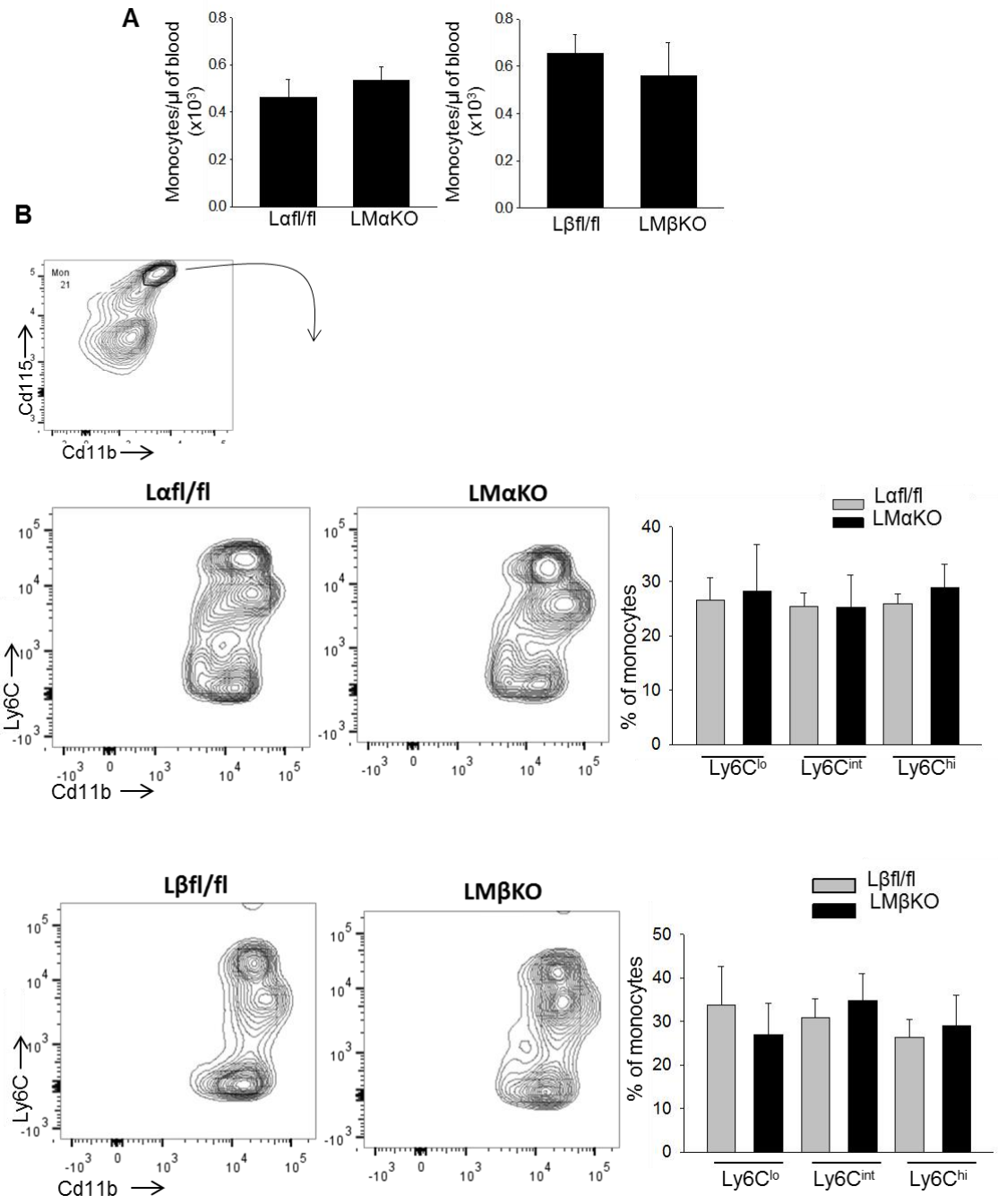
A
Monocytes/µl of blood (x10³)
0.8
0.6
0.4
0.2
0.0
Lαfl/fl
LMαKO
Monocytes/µl of blood (x10³)
Lβfl/fl
LMβKO
B
Mon
21
Cd115
Cd11b
Lαfl/fl
LMαKO
Ly6C
Cd11b
Lαfl/fl
LMαKO
% of monocytes
Ly6C^lo
Ly6C^int
Ly6C^hi
Lβfl/fl
LMβKO
Ly6C
Cd11b
Lβfl/fl
LMβKO
% of monocytes
Ly6C^lo
Ly6C^int
Ly6C^hi

Supplementary Figure X. Representative images of control Igg immunoflorescent staining and specific antibody staining.

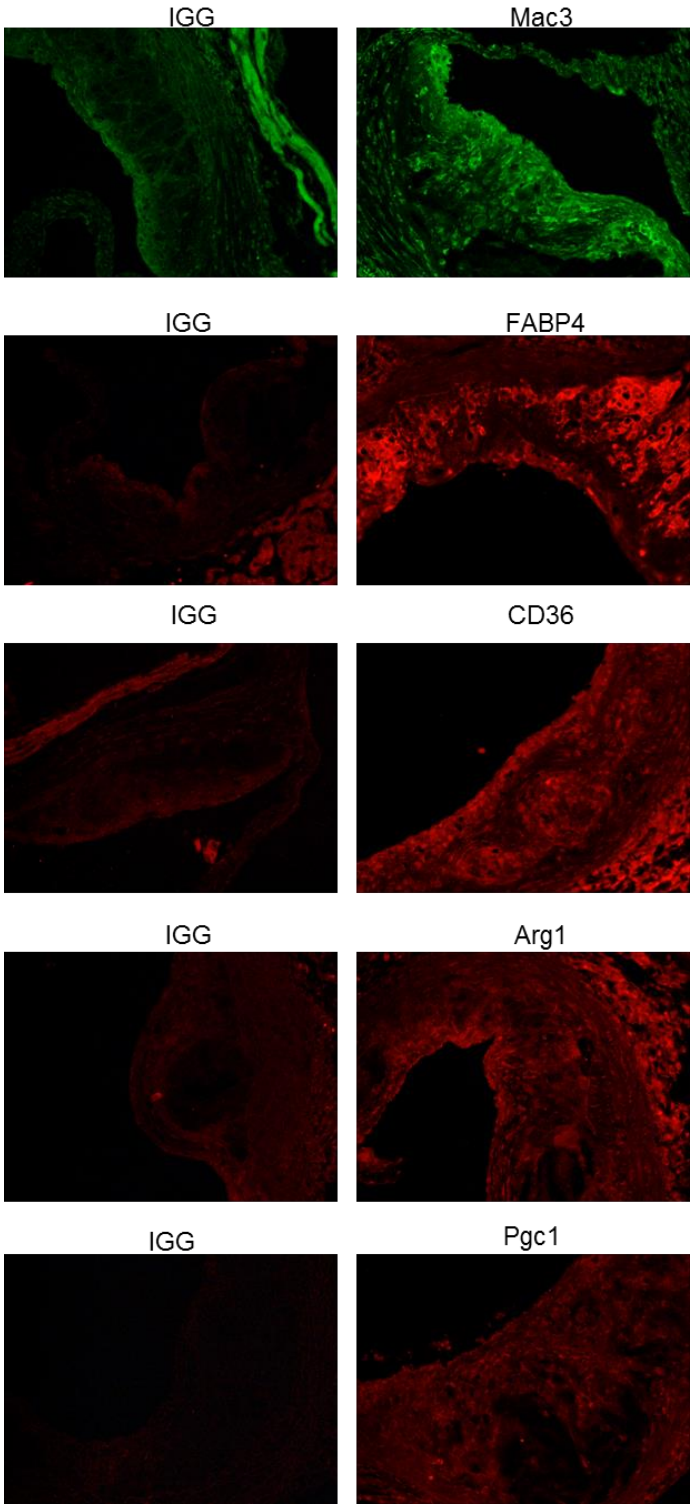
IGG
Mac3
IGG
FABP4
IGG
CD36
IGG
Arg1
IGG
Pgc1